

**SYNTHESIS, THERMODYNAMIC AND KINETIC STUDIES OF NOVEL
DIARYLAMINE ANTIOXIDANTS**

&

**DEVELOPMENT OF A FLUORESCENT PROBE FOR QUANTIFYING
HYDROPEROXIDES AND MEASURING H-ATOM TRANSFER KINETICS WITH
PEROXYL RADICALS**

By

Jason John Hanthorn

A thesis submitted to the Graduate Program in Chemistry

in conformity with the requirements for the

Degree of Doctor of Philosophy

Queen's University

Kingston, Ontario, Canada

May 2012

Copyright © Jason John Hanthorn, 2012

Abstract

Diarylamines (Ar_2NH) and phenols (ArOH) comprise the bulk of radical-trapping antioxidant (RTA) additives to petroleum-derived products, owing to their ability to slow hydrocarbon autoxidation through rate-controlling inhibition reactions. While much work has been done to optimize and understand structure-activity relationships of phenolic antioxidants, optimization of highly-reactive diarylamine antioxidants has been comparatively difficult due to their propensity to undergo one-electron oxidation with molecular oxygen. Recently, it was demonstrated that incorporation of nitrogen atoms into the aromatic ring of phenolic antioxidants greatly improves their stability to one-electron oxidation without compromising their antioxidant efficacy. Given these results, it was our supposition that this approach could be extended to the development of highly reactive diarylamine RTAs.

Herein we describe the synthesis of a small library of pyridine- and pyrimidine-containing diarylamines and characterize their thermodynamic properties (standard potentials (E°) and N-H bond dissociation enthalpies) as well as their kinetic properties (rate constants for reactions with peroxy and alkyl radicals) – demonstrating that the approach of N-atom incorporation is also very effective at increasing diarylamines' stability to one-electron oxidation without compromising their antioxidant efficacy. In fact, the diarylamines described herein are among the best peroxy-radical trapping antioxidants known, having inhibition rate constants ca. 200-fold greater than the current industry standard. Through a series of mechanistic studies (measuring Arrhenius parameters, kinetic solvent effects, deuterium kinetic isotope effects and transition state calculations) we have provided strong evidence that reactions between electron-rich diarylamines and peroxy radicals occur by a proton-coupled electron transfer (PCET) mechanism.

The reaction of diarylamines with peroxy radicals at elevated temperatures (>160 °C) is highly relevant industrially, as this reflects the operating environment of lubricants in engine applications. At these temperatures, diarylamines are known to react catalytically as peroxy trapping RTAs, although the mechanism has yet to be fully elucidated for this important chemistry. Current methods of studying high temperature oxidations suffer from time-consuming and/or air-sensitive analytical methods (e.g. iodometry, GC analysis). To enable rapid, accurate mechanistic studies at high temperature, we have improved the analytical component by developing a fluorescent dye that can be applied in an assay to determine hydroperoxide concentrations in solution in real-time.

Acknowledgements

I have been very fortunate over the past years to work with a number of colleagues who loved to embrace the “work hard/play hard” mentality. I was going to do an elaborate acknowledgements section as a tribute to these people that I have become good friends with over the years, but I realized that doing so could only get us all into trouble. With that in mind, I will keep this short.

Thank you to Andrew “mustard” Fraser and Kevin “Ricky” Fowler from the Baird lab, Ben and Vivian “Bivian” Glasspoole and Phil Lynett - people who helped me take many years off my life in the process of doing my PhD. There are too many other names to mention here, but I have to give a shout out to Johan Brinkhorst, the man who left an indelible mark on Chernoff for his legendary nights, but also a person who taught me a great deal of chemistry in my early years.

A huge thank you to Derek Pratt for being everything a person could ask for in a supervisor – super knowledgeable and enthusiastic about chemistry while maintaining a good perspective on what is really important in life. I learned an awful lot in my years working with Derek, and not just chemistry. If I have imparted any wisdom on you over the years, Derek, I hope it’s that you never forget to use the stairs.

Finally, I need to give a huge shout out to my family. A big thank you to my parents Dianne and Glenn for “encouraging” me to go to university and for providing nothing but love and support for the past 29 years. An extremely big thank you to my loving wife Emily who has not only supported me throughout my graduate career, but has been extremely understanding when it comes to some of the poor decisions made by me, my friends and my boss (in many combinations). You’re the best part of my life. Lastly, I want to give a super big shout out to Leroy – the greatest dog in the world and the best friend a guy could ask for.

Statement of Originality

I hereby certify that all of the work described within this thesis is the original work of the author, with the following exceptions: All of the computational calculations throughout this thesis were performed by Derek A. Pratt. All of the N-H bond dissociation enthalpies (Chapters 3 and 7) and the inhibited autoxidation data presented in Chapter 7 were obtained by our collaborators Dr. Luca Valgimigli and Dr. Riccardo Amoroti (University of Bologna). The inhibited autoxidation data provided in Chapter 5 was obtained by fellow graduate student Evan Haidasz.

Jason Hanthorn

2012

Table of Contents

Abstract.....	ii
Acknowledgements.....	iv
Statement of Originality.....	v
Table of Contents.....	vi
List of Schemes.....	xi
List of Figures.....	xv
List of Tables.....	xx
List of Abbreviations.....	xxii

Chapter 1	Background and Significance.....	1
1.1	Lipid Peroxidation.....	3
1.2	Inhibited Autoxidation – Antioxidants.....	11
1.3	Techniques for Measuring Peroxyl Radical Kinetics.....	15
1.3.1	Electron Paramagnetic Resonance.....	16
1.3.2	Laser Flash Photolysis (LFP).....	16
1.3.3	Rotating Sector Method.....	17
1.3.4	Radical Clocks.....	18
1.4	Phenolic Antioxidants.....	23
1.4.1	Bond Dissociation Enthalpies.....	24
1.4.2	Sterics.....	26
1.4.3	Kinetic Solvent Effects and Reaction Mechanisms.....	27
1.5	Aromatic Amine Antioxidants.....	31
1.5.1	The Fate of Diarylaminy Radical – Potential Catalytic Inhibition.....	35
1.6	Improving Antioxidant Activity.....	37
1.7	Research Objectives.....	40
1.7.1	Air-Stable Diarylamine Antioxidants.....	40
1.7.2	Development of a New Peroxyester-Based Peroxyl Radical Clock And Extending Peroxyl Radical Clock Methodology.....	43

1.7.3	Design and Application of a Fluorescent Dye for Rapid, High Throughput Quantification of Hydroperoxides.....	43
1.7.4	Development of a New Precursor for Transient Absorption Kinetic Studies of Fast Peroxyl Radical Reactions.....	45
1.8	References.....	46
Chapter 2	Preparation of Highly-Reactive Pyridine- and Pyrimidine-Containing Diarylamine antioxidants.....	55
2.1	Preface.....	55
2.2	Introduction.....	56
2.3	Results and Discussion.....	59
2.3.1	Preparation of 3-Pyridyl and 5-pyrimidyl Bromides.....	59
2.3.2	Preparation of 3-aminopyridines and 5-aminopyrimidines.....	61
2.3.3	Preparation of Diarylamines.....	63
2.3.4	Determining the Optimal Palladium Pre-catalyst.....	68
2.4	Conclusions.....	71
2.5	Experimental Section.....	72
2.5.1	General.....	72
2.5.2	Cu-Catalyzed Benzylamination of Pyri(mi)dyl Bromides.....	72
2.5.3	Direct Amination of Pyri(mi)dyl Bromides.....	75
2.5.4	Deprotection of <i>N</i> -benzylamines.....	77
2.5.5	General Procedure for Synthesis of Diarylamines.....	77
2.6	References.....	90
Chapter 3	The Reactivity of Air-Stable Pyridine- and Pyrimidine-Containing Diarylamine Antioxidants.....	93
3.1	Preface.....	93
3.2	Introduction.....	94

3.3	Results.....	97
3.3.1	Calculated BDEs and IPs of Heterocycle-Containing Diarylamines.....	97
3.3.2	Synthesis of Pyridine and Pyrimidine-Based Diarylamines.....	99
3.3.3	Electrochemistry.....	100
3.3.4	Kinetics of Reactions with Peroxyl Radicals.....	101
3.3.5	N-H Bond Dissociation Enthalpies.....	105
3.3.6	Mechanistic Studies.....	107
3.3.7	Kinetics of Reactions with Alkyl Radicals.....	109
3.4	Discussion.....	110
3.5	Conclusions.....	126
3.6	Experimental Section.....	126
3.6.1	General.....	126
3.6.2	Electrochemistry.....	127
3.6.3	Peroxyl Radical Kinetics.....	127
3.6.4	Alkyl Radical Kinetics.....	127
3.6.5	Electrochemical Data.....	128
3.6.6	Peroxyl Radical Kinetic Data.....	143
3.6.7	Alkyl Radical Kinetic Data.....	156
3.7	References.....	159
Chapter 4	Peroxyesters as Precursors to Peroxyl Radical Clocks.....	163
4.1	Preface.....	163
4.2	Introduction.....	164
4.3	Results.....	167
4.3.1	Synthesis of Peroxyester 3 and Its Derived Products.....	167
4.3.2	Calibration of Peroxyl Radical Clock Derived from 4.3	169
4.3.3	Representative Clocking Experiments Using Peroxyester 3	171

4.3.4	Origin of Carbonyl-Containing Products.....	173
4.3.5	Temperature Dependence on Beta-Fragmentation.....	176
4.3.6	Kinetic Isotope Effect Measurements.....	177
4.4	Discussion.....	179
4.5	Conclusion.....	185
4.6	Experimental Details.....	186
4.6.1	Synthesis of Peroxyester 4.3	186
4.6.2	Calibration Experiments to Determine k_{β}	187
4.6.3	Clocking Experiments.....	187
4.7	References.....	188
Chapter 5:	Development of a Fluorescent Probe for Quantifying Hydroperoxides and Measuring H-Atom Transfer Kinetics with Peroxyl Radicals.....	192
5.1	Introduction.....	192
5.2	Results and Discussion.....	197
5.3	Conclusions.....	208
5.4	Supporting Information.....	208
5.4.1	Inhibited Autoxidation of 7-dehydrocholesterol.....	208
5.4.2	High-temperature Inhibited Autoxidation of Hexadecane.....	209
5.4.3	Preparation and Characterization of Phosphine Dyes.....	209
5.5	References.....	218
Chapter 6	Development of a New Precursor for Transient Absorption Kinetic Studies of Fast Peroxyl Radical Reactions.....	222
6.1	Reactivity of α -tocopherol (α -TOH).....	222

6.2	Temperature Dependence on Reactions of α -TOH with Radicals.....	224
6.2.1	Arrhenius Parameters for Reactions of α -TOH and Alkyl Radicals.....	225
6.2.2	Arrhenius Parameters for Reactions of α -TOH and Aryloxy Radicals.....	226
6.2.3	Arrhenius Parameters for Reactions of α -TOH and Alkoxy Radicals.....	226
6.2.4	Arrhenius Parameters for Reactions of α -TOH and Peroxy Radicals.....	227
6.3	Project Objectives.....	228
6.4	Results and Discussion.....	229
6.5	Conclusions and Future Directions.....	243
6.6	Experimental Section.....	244
6.7.1	General.....	244
6.7.2	Synthetic Procedures and Characterization.....	244
6.7	References.....	251
Chapter 7	Summary and Prospective.....	255
7.1	Summary.....	255
7.2	Prospective.....	267
7.3	References.....	276

List of Schemes

Scheme 1.1.	General schemes depicting radical chain reactions found industrially in radical polymerization and biologically in lipid peroxidation.....	1
Scheme 1.2.	Industrial synthesis of phenol and acetone via the Hock process.....	2
Scheme 1.3.	Degradation pathway of superoxide <i>in vivo</i>	2
Scheme 1.4.	Mechanism of uninhibited lipid (L) peroxidation.....	6
Scheme 1.5.	Products of methyl linoleate free radical oxidation.....	7
Scheme 1.6.	Mechanism of peroxidation of linoleic acid and its esters.....	8
Scheme 1.7	Reaction pathways for peroxy radical formed at the 11-position of arachidonic acid leading to cyclized products that can react further to generate multiple products.....	10
Scheme 1.8	Important reactions and relative rate constants required for effective peroxy trapping antioxidants.....	12
Scheme 1.9	<i>5-exo-trig</i> cyclization of the 5-hexen-1-yl radical used as an alkyl radical clock.....	18
Scheme 1.10	Kinetic scheme describing the first peroxy radical clock based on product distribution of linoleate oxidation in the presence of an antioxidant (α -TOH shown).....	20
Scheme 1.11	Kinetic scheme depicting the peroxy radical clock based on the product distribution arising from oxidation of allylbenzene in the presence of an antioxidant (A-H).....	22

Scheme 1.12	A peroxyester as a precursor to a peroxy radical clock.....	23
Scheme 1.13	Hydrogen-atom transfer (HAT) and a kinetic solvent effect.....	28
Scheme 1.14	Sequential proton-loss electron transfer (SPLET).....	29
Scheme 1.15	Reaction between a phenol and a peroxy radical proceeding via hydrogen-atom transfer (HAT, A) or proton-coupled electron transfer (PCET, B).....	31
Scheme 1.16	Mechanism for catalytic inhibition by Ar ₂ NH and Ar ₂ NO• proposed by Korcek <i>et al.</i>	36
Scheme 1.17	Reaction pathways for diphenylamine showing both the desired radical trapping pathway and the undesired one-electron oxidations with molecular oxygen or hydroperoxides yielding ROS that can initiate peroxidation.....	38
Scheme 2.1	Non-transition metal catalyzed methods of preparing diarylamines.....	58
Scheme 2.2	Library approach to heterocyclic diarylamines.....	59
Scheme 2.3	Preparation of relevant pyri(mi)dyl halides.....	61
Scheme 2.4	Proposed origin of the induction periods observed in reactions shown in Figure 1: competition between reversible formation of the Lewis-base (B) coordination complex of 65 and irreversible reductive elimination of the Cp and Cinn ligands of 65 in the presence of XPhos to form the catalytically active Pd(XPhos) ₂	70
Scheme 3.1	Competing antioxidant and proantioxidant reactions of electron- rich diphenylamine antioxidants.....	95

Scheme 3.2	Synthetic approach to substituted diarylamines (A-D = CH or N; R = H, Alkyl, Alkoxy or <i>N,N</i> -dialkylamino).....	99
Scheme 3.3	Reaction scheme illustrating the application of the peroxy- radical clock methodology. R = naphthyl.....	101
Scheme 3.4	Reaction scheme illustrating the application of the alkyl- radical clock methodology.....	109
Scheme 3.5	Kinetic solvent effect on the reaction of diarylamines with peroxy radicals.....	118
Scheme 3.6	The polar effect in the reaction of phenols with alkyl radicals.....	123
Scheme 4.1	Kinetic scheme describing the allylbenzene-based peroxy radical clock.....	165
Scheme 4.2	Decomposition of a peroxyester under thermalytic or photolytic conditions.....	166
Scheme 4.3	Synthesis of (<i>E</i>)- <i>tert</i> -butyl 4-(naphthalen-2-yl)but-eneperoxoate.....	167
Scheme 4.4	Synthesis of conjugated and non-conjugated products used as GC standards....	168
Scheme 4.5	Synthesis of conjugated and non-conjugated cinnamyl- derived hydroperoxides.....	174
Scheme 4.6	Decomposition pathways for peroxyester 4.3	182
Scheme 5.1	Preparation of reduced (5.8) and oxidized (5.9) phosphine dyes.....	195
Scheme 6.1	(A) Photolysis of dicumylketone under aerobic conditions to generate cumyl peroxy which is trapped by α -tocopherol. Reaction kinetics are monitored by watching the growth of α -tocoperoxy radical at 420 nm. (B) Photolysis of di- <i>tert</i> -butylperoxide in the presence of a trialkylamine to generate an α -aminoalkyl-peroxy radical that is trapped by α -tocopherol. Reaction kinetics are monitored by watching the decay of the α -aminoalkyl-peroxy radical at ca. 380-420 nm (380 nm for Et ₃ N as shown).....	224

Scheme 6.2	Photolysis of dicumylketone to generate cumylperoxyl radicals and their trapping by α -tocopherol.....	229
Scheme 6.3	Photolysis of azocumene at 355 nm in the presence of oxygen to generate two cumylperoxyl radicals.....	231
Scheme 6.4	Synthetic route to prepare azocumene.....	232
Scheme 6.5	Decomposition and isomerization pathways for azocumene.....	234
Scheme 6.6	Undesired cyclization reaction when preparing symmetrical sulfonamides via sulfuryl chloride or when preparing unsymmetrical sulfonamides using chlorosulfonyl isocyanate and <i>tert</i> -butylamine.....	237
Scheme 6.7	Synthesis of β -amino carbonyl compounds 6.5 and 6.6	238
Scheme 6.8	Possible competing reaction pathways from excited ketones 6.5 and 6.6	239
Scheme 6.9	Photolysis of di- <i>tert</i> -butylperoxide, followed by H-atom abstraction from a benzylic acetal in the presence of oxygen to produce a peroxyl radical having calculated absorbance in the 350-400 nm range.....	240
Scheme 6.10	Synthesis of acetal compounds 6.7 and 6.8	240
Scheme 6.11	Synthesis of <i>para</i> -brominated cumylsulfonamide 6.10	241
Scheme 6.12	Decomposition of Barton ester to generate a cumylperoxyl radical and a 2-thiopyridyl radical.....	242
Scheme 6.13	Synthesis of PTOC (Barton) ester 6.12	242
Scheme 7.1	Synthetic approach to substituted diarylamines (A-D = CH or N; R = H, Alkyl, Alkoxy or <i>N,N</i> -dialkylamino).....	257
Scheme 7.2	Proposed mechanisms by Valgimigli <i>et al.</i> and Korcek <i>et al.</i> to explain the catalytic reactivity (i.e. large stoichiometric factors)	

	observed for diarylamines reacting at high temperatures with peroxy radicals.....	272
Scheme 7.3	Synthetic route to prepare 3.12 cost-effectively on a multi-gram scale.....	275

List of Figures

Figure 1.1	Profiles of oxygen-uptake during peroxidation of a substrate in the absence of an inhibitor or with either a retarder or an antioxidant.....	15
Figure 1.2	Termination rate constants ($2k_t$) for a series of <i>para</i> -substituted phenols.....	27
Figure 1.3	Reaction between a phenol and a peroxy radical proceeding via hydrogen-atom transfer (HAT, A) or proton-coupled electron transfer (PCET, B).....	31
Figure 1.4	Calculated bond dissociation enthalpies (BDEs) and ionization potentials (IPs) in kcal/mol for a series of phenols with increasing nitrogen content.....	39
Figure 1.5	Calculated BDEs and IPs for a series of substituted pyri(mi)dinols in kcal/mol. k/k_{Toc} = rate of peroxy radical trapping relative to α -tocopherol ($k_{\text{inh}} = 3.2 \times 10^6 \text{ M}^{-1}\text{s}^{-1}$).....	40
Figure 1.6	Target molecules showing different possible substitution patterns.....	41
Figure 2.1	Target diarylamines.....	58
Figure 2.2	Comparative reaction profiles for a series of cross-coupling reactions where either 2.65 or $\text{Pd}_2(\text{dba})_3$ was used a pre-catalyst.....	69
Figure 3.1	(A) Cyclic voltammogram obtained for 20-22 in MeCN at 25 °C vs. Ag/AgNO_3 . (B) Differential pulse voltammograms obtained for	

	15-17 in MeCN at 25 °C vs. Ag/AgNO ₃ . For both (A) and (B) only the first oxidations are shown for clarity.....	100
Figure 3.2	Double reciprocal plot of clock product ratios (scheme 3) vs. 1/[28] (■) and 1/[16] (●) in chlorobenzene at 37 °C used to obtain $k_H = 2.1(\pm 0.4) \times 10^5 \text{ M}^{-1}\text{s}^{-1}$ and $k_H = 1.4(\pm 1.0) \times 10^6 \text{ M}^{-1}\text{s}^{-1}$ respectively.....	104
Figure 3.3	(A) (top) EPR spectrum of an equilibrated mixture of the diarylaminy radical derived from 31 and 3,5-di- <i>tert</i> -butylphenoxy radical in benzene at 298 K and. (bottom) the associated simulated spectrum for a 100:6.3 ratio of the two equilibrating radicals. (B) (top) EPR spectrum of an equilibrated mixture of the diarylaminy radical derived from 12 and 3,5-di- <i>tert</i> -butylphenoxy radical in benzene at 298 K and. (bottom) the associated simulated spectrum for a 100:1 ratio of the two equilibrating radicals.....	106
Figure 3.4	Rate constants for the reaction of diarylamines 12 (■) and 14 (●) with peroxy radicals as a function the H-bond accepting ability (β_H^2) of the solvent. Solvents used in the correlation (and their corresponding β_H^2 parameter) are chlorobenzene (0.09), benzene (0.14), anisole (0.26), MeCN (0.42) and EtOAc (0.45).....	107
Figure 3.5	Temperature dependence of the rate constants for reactions of diarylamines 2 (■), 18 (●) and 24 (▲) with peroxy radicals in chlorobenzene in the range of 37-95 °C.....	108
Figure 3.6	Plots of $\log k_H$ for peroxy trapping vs. N-H BDEs of diarylamines (■) and O-H BDEs of some 4-substituted phenols (▲), 2,6-dimethyl-4-substituted phenols (●) and 2,6-di- <i>tert</i> -butyl-4-substituted phenols.....	116
Figure 3.7	Calculated transition state structures for the formal H-atom transfer from diphenylamine (A) and phenol (B) to the methyl peroxy radical.....	120

Figure 3.8	Correlations of the second-order rate constants ($\log k_H$) vs. N-H BDEs for diarylamines (■) and O-H BDEs of phenols (●), <i>ortho</i> -methylated phenols (▲), <i>ortho-tert</i> -butylated phenols (▼) and pyrimidinols (◆).....	122
Figure 3.9	Correlation between N-H BDEs and $\log k_H$ for reaction of diarylamines, phenothiazines and phenoxazines for reaction with primary alkyl radicals (▲) and peroxy radicals (■). Data for diarylamines was obtained at 298 K while phenothiazines/phenoxazines were measured at 323 K.....	125
Figure 4.1	Representative gas chromatograms (GC-FID) in the retention time range of product elution following the incubation of perester 4.3 with 1.0 M α -TOH (A) and 0.03 M α -TOH (B) for 4 hours at 37°C in chlorobenzene. The peak labelled * is observed in most chromatograms and could not be identified; however the peak area does not change as a function of antioxidant concentration and therefore appears not to be relevant in our kinetic analysis.....	170
Figure 4.2	Ratio of non-conjugated ([4.4] + [4.5]) to conjugated ([4.6] + [4.7]) oxidation products formed in the decomposition of 4.3 as a function of [α -TOH, 4.8] following incubation for 12 hours at 37°C in benzene.....	170
Figure 4.3	Representative double-reciprocal plot used to obtain inhibition rate constants. Shown is data obtained for 2,4,6-trimethylphenol (4.9) in chlorobenzene at 37°C.....	172
Figure 4.4	Stacked plot of gas chromatograms (GC-FID) showing product distribution (phenyl analogs of 4.4 , 4.5 , 4.6 and 4.7) arising from hydroperoxide decomposition (5 mM) in the presence of various	

additives (50 mM) incubated at 37°C in chlorobenzene.

Initial ratio of conjugated/non-conjugated products (**4.15/4.16**) was 4:1175

Figure 4.5 Temperature dependence of the β -fragmentation of the non-conjugated peroxy radical derived from **4.3**, which yields $E_a = 9.6(\pm 0.9)$ kcal/mol and $\log A = 12.8(\pm 0.6)$. Corresponding oxygen partition coefficients (α) for each temperature are given in brackets next to each data point.....176

Figure 4.6 Kinetic isotope effect on the product distribution arising from the decomposition of **4.3** in the presence of 2,2,5,7,8-pentamethyl-6-chromanol (**4.17**) and either 1% D₂O (■) or 1% H₂O (●), which yield $k_H = 5.0 \times 10^6 \text{ M}^{-1}\text{s}^{-1}$ and $k_D = 2.4 \times 10^6 \text{ M}^{-1}\text{s}^{-1}$ for $k_H/k_D = 2.1$177

Figure 5.1 Simplified energy diagrams depicting the relative energies of the HOMO/LUMO of the fluorophore and the HOMO energy of the donor involved in a photoinduced electron transfer. An asterisk (*) denotes the fluorophore in an excited state.....196

Figure 5.2 Structures synthesized and evaluated for their potential application as fluorescent dyes for the quantitation of hydroperoxides.....198

Figure 5.3 Excitation and emission spectra of **5.8** and **5.9** (excitation $\lambda_{\text{max}} = 343 \text{ nm}$, emission $\lambda_{\text{max}} = 422 \text{ nm}$) taken in methanol.....201

Figure 5.4 Representative initial rates for reactions of **5.8** (20 μM) with tetralin hydroperoxide (150 μM – 775 μM) in methanol and the resulting plot of the initial rates vs. [ROOH] used to determine

the pseudo-first order rate constant, $k_{\text{obs}} = 1.9 \times 10^{-4} \text{ s}^{-1}$, which was used to obtain the second order rate constant of $k = 9.5 \text{ M}^{-1}\text{s}^{-1}$202

Figure 5.5 Inhibited autoxidation of 7-dehydrocholesterol with 4 μM of **5.10** (■) used to determine $k_{\text{H}} = 1.2 \times 10^6 \text{ M}^{-1}\text{s}^{-1}$ in 1,2-dichlorobenzene. Also shown is the corresponding uninhibited autoxidation of 7-dehydrocholesterol (●).....205

Figure 5.6 (left) Inhibited autoxidation of hexadecane at 160 °C in the presence of 1 mM BHT (●), shown with uninhibited autoxidation (■); (right) Inhibited autoxidation of hexadecane at 160 °C in the presence of 1 mM 4,4'-dioctyldiphenylamine (▲), shown with uninhibited autoxidation (■).....206

Figure 6.1 LFP traces for growth of α -TOH (recorded at 420 nm), initiated by photolysis of azocumene (5 mM) in oxygenated chlorobenzene in the presence of 40 mM α -TOH (black) and 120 mM α -TOH (red).....233

Figure 7.1 Diarylamine decomposition in the presence of a hydroperoxide. Data are presented for diarylamines **3.13** (●), **3.16** (◆) and **3.18** (■) (0.2 M) incubated at 80 °C with one equivalent of *tert*-butylhydroperoxide (0.2 M) in 1,2-dichlorobenzene using biphenyl as an internal standard and analyzed by gas chromatography.....268

Figure 7.2 (Left) Oxygen consumption during the oxidation of styrene (6.5 M) in chlorobenzene initiated by AIBN (25 mM) at 30°C without inhibitors (dashed line) or in the presence of pentamethylchromanol (PMC, 1.9 μM blue); **3.18** (1.4 μM , red); **3.16** (1.9 μM , black); **3.14** (1.3 μM , green). (Right) Plot of $\log k_{\text{H}}$ obtained by inhibited autoxidation vs. N-H BDEs. Correlation gives: $\log k_{\text{H}} = -0.53(\text{N-H BDE}) + 51.2$ ($r^2 = 0.98$).....271

List of Tables

Table 2.1	Copper-catalyzed amination of 2-substituted 5-bromopyridines and 5-bromopyrimidines.....	63
Table 2.2	<i>N,N</i> -Dialkylamino-substituted diarylamines prepared by palladium-catalyzed cross-couplings of aryl bromides and aryl amines.....	65
Table 2.3	Alkyl-substituted diarylamines prepared by palladium-catalyzed cross-couplings of aryl bromides and aryl amines.....	66
Table 2.4	Alkoxy-substituted diarylamines prepared by palladium-catalyzed cross-couplings of aryl bromides and aryl amines.....	67
Table 3.1	CBS-QB3 Calculated gas phase N-H bond dissociation enthalpies (BDEs) and ionization potentials (IPs) for a series of heteroatom-containing diphenylamines in kcal/mol.....	98
Table 3.2	Calculated N-H bond dissociation enthalpies (BDEs) and ionization potentials (IPs) for a series of diphenylamines incorporating heteroatoms at the 3- and 5-positions. Values are in kcal/mol.....	98
Table 3.3	Reactivity of Disubstituted Alkylated Diarylamines Towards Peroxyls and Corresponding Oxidation Potentials.....	102
Table 3.4	Reactivity of Disubstituted <i>N,N</i> -Dialkylaminated Diarylamines Towards Peroxyls and Corresponding Oxidation Potentials.....	103
Table 3.5	Reactivity of Disubstituted Alkoxyated Diarylamines Towards Peroxyls and Corresponding Oxidation Potentials.....	103
Table 3.6	Reactivity of Mono-Substituted Diarylamines Towards Peroxyl Radicals and Associated One-Electron Oxidation Potentials.....	104
Table 3.7	N-H Bond dissociation enthalpies of representative diarylamines measured by the radical equilibration EPR technique in benzene at 298 K. Values in kcal/mol.....	106

Table 3.8	Arrhenius parameters for the reactions of selected diarylamines with secondary peroxy radicals derived from rate constants measured from 37 to 95 °C in chlorobenzene.....	109
Table 3.9	Second-order rate constants for the reactions of selected diarylamines with primary alkyl radicals in chlorobenzene at 25 °C.....	110
Table 3.10	Reaction constants (ρ^+) from plots of $\log k_H$ vs. $\Sigma\sigma_P^+$ for the reactions of substituted diarylamines containing either phenyl, 3-pyridyl or 5-pyrimidyl rings.....	114
Table 4.1	β -Fragmentation rate constants and oxygen partition coefficients of the non-conjugated peroxy radical derived from 4.3 as a function of solvent. Inhibition rate constants used in the determination of k_β and α are given for reference.....	171
Table 4.2	Rate constants for reactions of 4.9-4.14 with peroxy radicals generated from perester 4.3 at 37 °C in chlorobenzene. Literature values obtained by inhibited autoxidation of styrene at the given temperatures are shown for comparison.....	173
Table 4.3	Deuterium kinetic isotope effects (k_H/k_D) on the reactions of a representative group of phenols with peroxy radicals determined by the peroxy radical clock methodology with perester 4.3 at 37 °C. Values obtained by inhibited autoxidation of styrene and the methyl linoleate-based peroxy radical clock are presented alongside for comparison.....	178
Table 7.1	Inhibition rate constants and stoichiometric factors obtained by inhibited autoxidation of styrene or cumene at 30 °C, shown with corresponding N-H BDEs.....	263

List of Abbreviations

α -TOH	α -tocopherol
AA	arachidonic acid
AIBN	azobisisobutyronitrile
BDE	bond dissociation enthalpy
BHA	butylated hydroxyanisole (2,6-di- <i>tert</i> -butyl-4-methoxyphenol)
BHT	butylated hydroxytoluene (2,6-di- <i>tert</i> -butyl-4-methylphenol)
CV	cyclic voltammetry
DFT	density functional theory
7-DHC	7-dehydrocholesterol
DIBAL	diisobutylaluminum hydride
DKIE	deuterium kinetic isotope effect
DPA	diphenylamine
DPV	differential pulse voltammetry
DMAc	<i>N,N</i> -dimethylacetamide
DMF	<i>N,N</i> -dimethylformamide
DMSO	dimethylsulfoxide
EDG	electron-donating group
EPR	electron paramagnetic resonance
EWG	electron-withdrawing group
FID	flame ionization detector

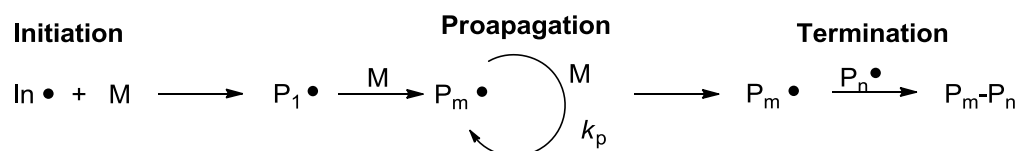
GC	gas chromatography
HAT	hydrogen-atom transfer
HB	hydrogen bond
HBA	hydrogen bond acceptor
HBD	hydrogen bond donor
HMDS	hexamethyldisilazane
HOMO	highest occupied molecular orbital
HPLC	high-pressure liquid chromatography
IP	ionization potential
KSE	kinetic solvent effect
LA	linoleic acid
LDL	low-density lipoprotein
LFP	laser flash photolysis
LUMO	lowest unoccupied molecular orbital
MeOAMVN	2,2'-azobis(4-methoxy-2,4-dimethylvaleronitrile)
MSE	molecule stabilization enthalpy
NBS	N-bromosuccinamide
Nd:YAG	neodymium-doped yttrium aluminum garnet (laser)
NHE	normal hydrogen electrode
PCC	pyridinium chlorochromate
PCET	proton-coupled electron transfer

PDT	photodynamic therapy
PET	photoinduced electron transfer
PMC	2,2,5,7,8-pentamethyl-6-chromanol
ROS	reactive oxygen species
RTA	radical trapping antioxidant
RSE	radical stabilization enthalpy
SOMO	singly-occupied molecular orbital
SPLET	sequential proton-loss electron transfer
TFA	trifluoroacetic acid
THF	tetrahydrofuran
TMP	2,4,6-trimethylphenol
TSE	total stabilization enthalpy

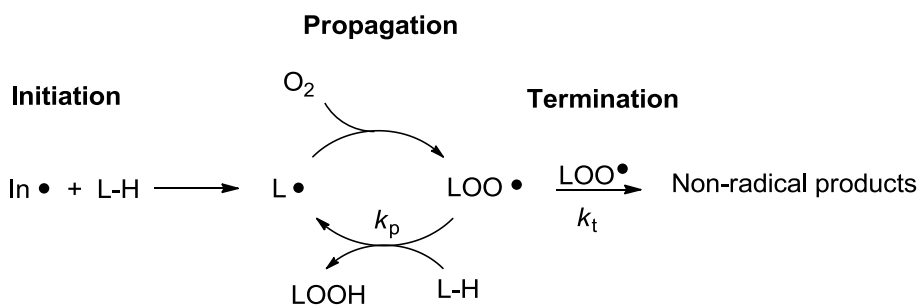
CHAPTER 1: BACKGROUND AND SIGNIFICANCE

Radical chain reactions are ubiquitous in nature and industry, and a great deal of research effort has been dedicated to understanding and controlling these processes. Many of the synthetic materials developed over the last half century are derived from radical polymerization processes (Scheme 1.1) and many radical reactions occurring within eukaryotic organisms have been implicated in the onset and development of disease and aging.

Radical Polymerization



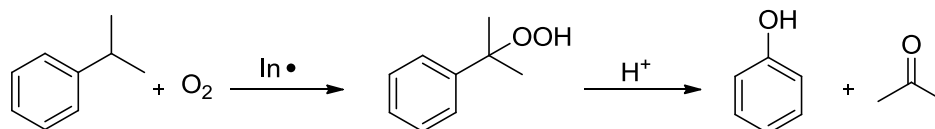
Lipid Peroxidation



Scheme 1.1. General schemes depicting radical chain reactions found industrially in radical polymerization and biologically in lipid peroxidation (M = monomer, P = polymer and L = lipid).

Lipid peroxidation (autoxidation, Scheme 1.1) is the major cause of the irreversible deterioration of all biological and hydrocarbon materials. Although many important chemicals

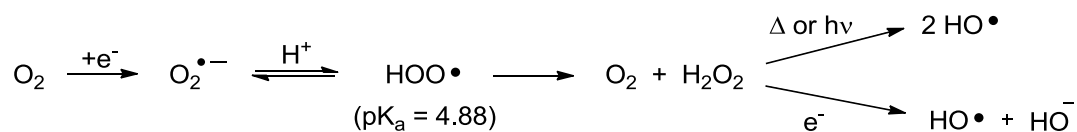
are synthesized from the oxidations of organic compounds by molecular oxygen; for example phenol is produced by the oxidation of cumene in the Hock process.¹



Scheme 1.2. Industrial synthesis of phenol and acetone via the Hock process.

At the same time, oxygen is responsible for the oxidative degradation and deterioration of essentially all petroleum-derived products, from plastics (e.g. polyethylene, polypropylenes, etc.) to rubbers, oils and fuels, as well as the hydrocarbons of living organisms. This is reflected in “the paradox of aerobic life,” which states that higher eukaryotic aerobic organisms cannot exist without oxygen, yet oxygen is inherently dangerous to their existence.²

The reason for such a paradox is the electronic configuration of molecular oxygen – having two unpaired electrons and existing in the ground state as a triplet, it is unable to react readily with other molecules due to spin-restrictions. However, by adding a single electron and removing the spin restriction, oxygen’s reactivity is dramatically increased. Under certain conditions, oxygen can undergo one-electron reduction to form reactive oxygen species (ROS) such as superoxide ($\text{O}_2^{\bullet-}$), which can undergo further reactions to yield hydroperoxyl ($\text{HOO}\cdot$), hydrogen peroxide (H_2O_2) or a hydroxyl radical ($\text{HO}\cdot$).³



Scheme 1.3. Degradation pathways of superoxide *in vivo* leading to ROS.

Superoxide has an important biological role as part of the immune system as it is the precursor to stronger oxidants, such as hydroperoxyl and hydroxyl radicals, which are used to kill invading microorganisms. In the cell, superoxide is toxic because of its ability to oxidize and reduce metal ions attached to biological targets, thereby degrading the invading target through electron transfer reactions.⁴ Additionally, the degradation products of superoxide – hydrogen peroxide and its further decomposition to hydroxyl radicals – are highly toxic, as hydroxyl radicals will react unselectively with any biomolecule nearby. The formation of superoxide and oxidants derived therefrom also arise during the incomplete reduction of oxygen to water as part of aerobic respiration. As such, nearly all organisms living in the presence of oxygen contain isoforms of superoxide dismutase (SOD) – the enzyme responsible for scavenging adventitious superoxide.

In addition to superoxide and ROS derived from superoxide, there are many other processes occurring within the body capable of initiating a radical chain process; metal ions (primarily Fe^{2+}) and hydroperoxides can generate reactive radicals via the Fenton reaction.⁵ Initiating radicals can also be produced by the reaction of metal ions with peroxynitrite (from $\text{NO}\cdot$ precursor) or as by-products of several enzymes, including xanthine oxidase and nitropropane dioxygenase.³ Reactive oxygen species can also result from incomplete reduction of molecular oxygen by the mitochondrial electron transport chain.

1.1 Lipid Peroxidation

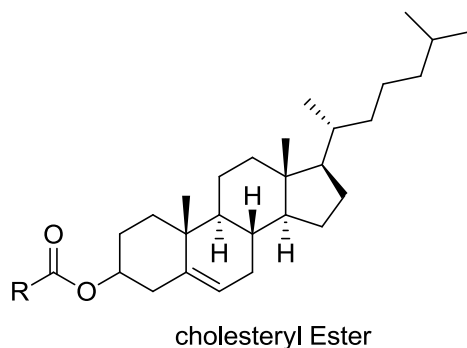
The unsaturation of biological lipids makes them relatively susceptible to autoxidation, and as such the study of lipid autoxidation (also commonly referred to as lipid peroxidation) has

received particular attention over the years.⁶⁻⁸ Since lipids are the key component of cellular membranes and also contribute to the regulation of many biological activities of cells, their oxidation has many implications in human health and disease; oxidation processes act as modulators of enzymes and have been shown to function as cell signalling molecules and regulators of several cellular processes, including gene regulation.⁹ Cyclooxygenases and lipoxygenases are important enzymes that perform lipid oxidation in a controlled manner to synthesize essential cell-signalling molecules that include prostaglandins and leukotrienes, which mediate cell homeostasis, as well as stimuli responsive actions such as pain, inflammation and pyresis.¹⁰

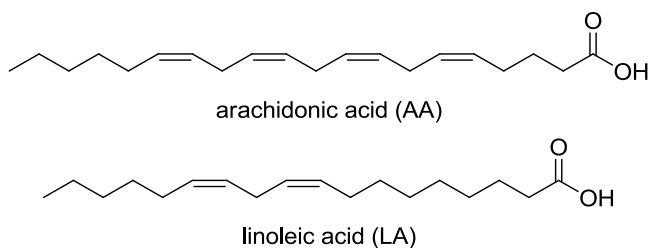
ROS-initiated lipid peroxidation can result in the formation of a number of cytotoxic compounds,¹⁰ including α,β -unsaturated aldehydes which are formed by oxidative cleavage of unsaturated lipid hydroperoxides. Well known examples include acrolein, malondialdehyde and 4-hydroxy-2-nonenal, and the cytotoxicity of these compounds stems from the fact that they are excellent Michael acceptors capable of undergoing unwanted reactions with nucleophiles present in the cell (e.g. amines or thiols). Of particular concern is the reaction of these α,β -unsaturated aldehydes with DNA because they can form DNA adducts that may lead to replication errors or block replication, which can give rise to mutations and perhaps cancer. Likewise, reactions of electrophilic carbonyls with nucleophilic sites on proteins can lead to protein misfolding or aggregation.^{11,12} When the human body's natural defenses against autoxidation (antioxidants, *vide infra*) are unable to effectively inhibit the formation of reactive oxygen species, the body is said to be under oxidative stress – a condition believed to be central in the aging process.¹³ A significant amount of recent literature has been focused on the role that lipid peroxidation plays

in the promotion of many diseases, including cancer, diabetes, Alzheimer's disease, Parkinson's disease and in particular, atherosclerosis.^{3,14}

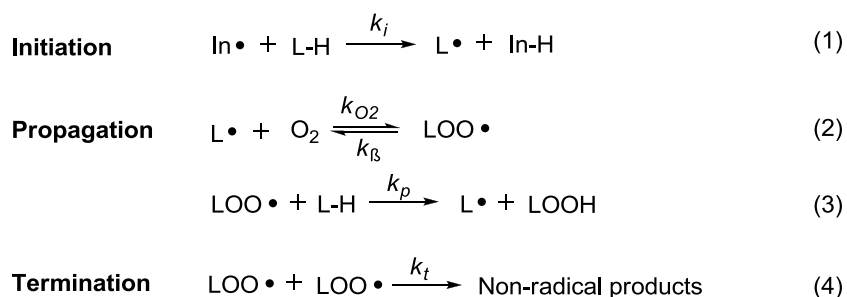
In Western Society, atherosclerosis remains the leading cause of death. So called "fatty streaks," primarily composed of peroxidized low-density lipoprotein (LDL) deposited on arterial walls are the first visible signs of atherosclerosis. Cholesterol is insoluble in blood, so it must be transported throughout the circulatory system within lipoproteins. The low-density lipoproteins, also known as "bad cholesterol," are one of the major carriers of cholesterol in blood. The neutral "lipid core" of an LDL particle is composed of triglycerides, small amounts of other fatty compounds and cholesteryl esters of polyunsaturated fatty acids.²



Cholesteryl esters represent the form in which cholesterol is transferred inside the LDL particle, and the two fatty acids which primarily form cholesteryl esters are linoleic acid (LA, C18:2, ~80%) and arachidonic acid (AA, C20:4, ~20%), both having *cis*-geometry around all double bonds.²



The autoxidation of polyunsaturated fatty acids and esters proceeds by a radical chain sequence as shown in Scheme 1.4. The first step is the abstraction of a hydrogen atom by an initiator ($\text{In}\cdot$) to form a carbon centred radical ($\text{L}\cdot$), which then reacts with O_2 at or near the diffusion controlled rate ($k_{\text{O}_2} \approx 10^{10} \text{ M}^{-1}\text{s}^{-1}$) to give a lipid peroxy radical ($\text{LOO}\cdot$).^{15,16} Oxygen addition is reversible for many stabilized carbon-centred radicals¹⁷ and the rate constant for the reverse reaction, k_{B} , is also shown. Generated peroxy radicals can then propagate the chain by abstracting a hydrogen atom from another lipid at a much slower rate ($k_{\text{p}} = 62 \text{ M}^{-1}\text{s}^{-1}$ for LA and $k_{\text{p}} = 197 \text{ M}^{-1}\text{s}^{-1}$ for AA)¹⁸ to yield a hydroperoxide (LOOH) and another lipid carbon-centred radical ($\text{L}\cdot$) that can continue the chain. Termination occurs when two lipid peroxy radicals react to give non-radical products by so-called Russell termination.¹⁹ Although the rate constant for the termination step ($k_{\text{t}} \approx 10^7\text{-}10^8 \text{ M}^{-1}\text{s}^{-1}$) is very large, the overall $[\text{LOO}\cdot]$ is very low, so many LOOH can be formed from just one initiation event.

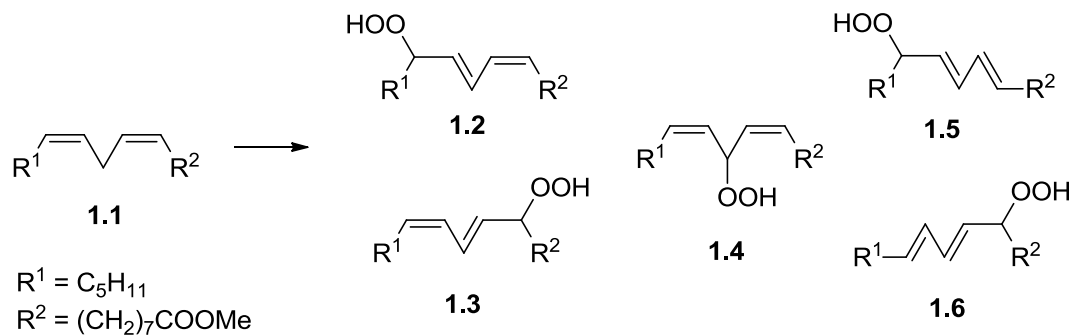


Scheme 1.4. Mechanism of uninhibited lipid (L-H) peroxidation.²⁰

The above description of free radical oxidation is based on the assumption that ground state molecular oxygen, $^3\text{O}_2$, is the reagent involved in the oxidation reactions. It is also possible

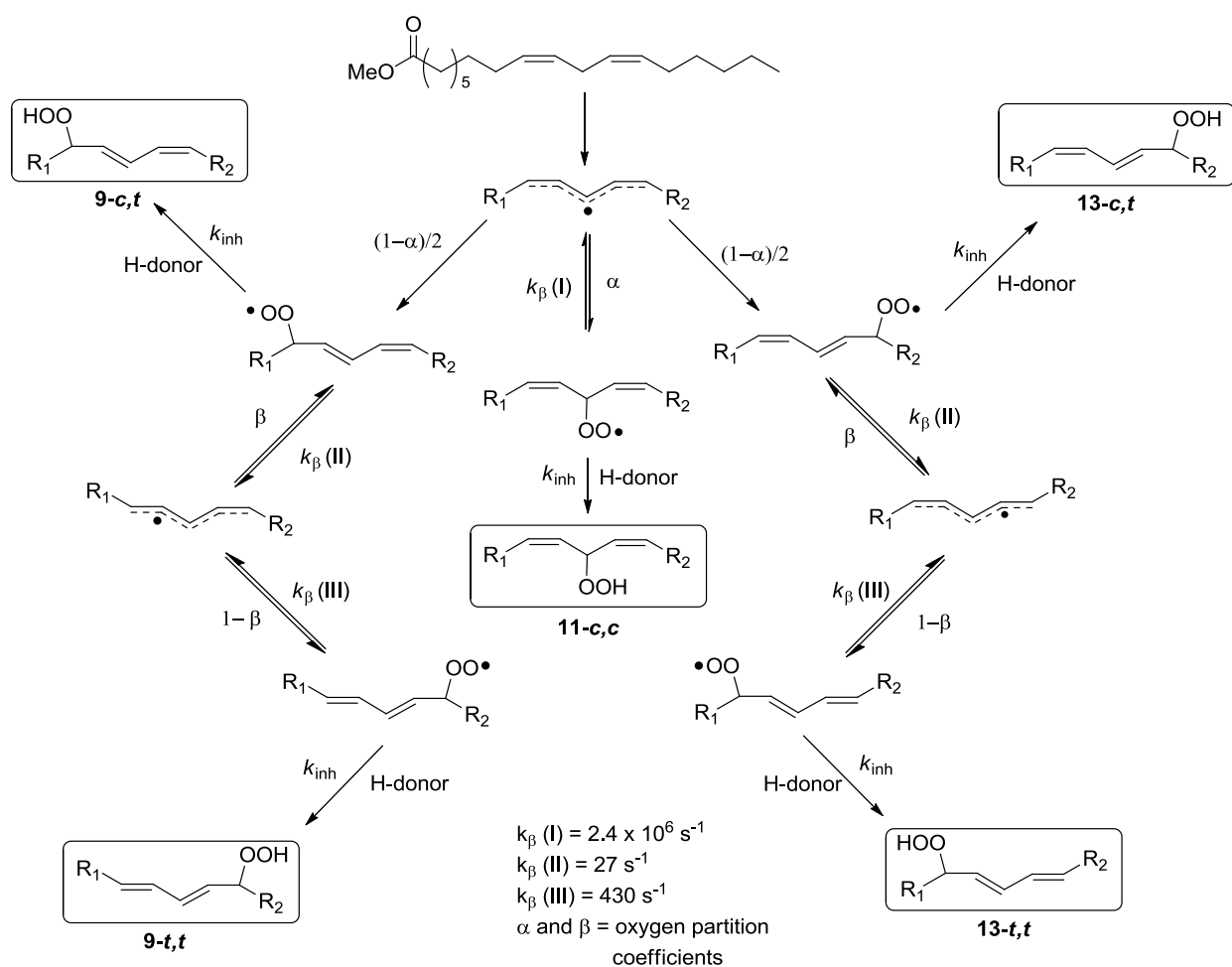
to generate hydroperoxides with no radical intermediates via type II photosensitized oxidation.²¹ This occurs when a photoexcitable compound (sensitizer) converts $^3\text{O}_2$ to singlet molecular oxygen, $^1\text{O}_2$, by energy transfer (ca. 22 kcal/mol).²² Although singlet oxygen is not generated readily *in vivo* (generally a photosensitizer pigment is required, such as chlorophyll in plants), singlet oxygen is the reactive oxygen species responsible for the cytotoxic effects of photodynamic therapy (PDT),²³ a treatment used clinically to treat a wide range of medical conditions including malignant cancers.

The products obtained from the free radical chain oxidation of diene fatty acids or esters are primarily diene hydroperoxides (Scheme 1.5). For example, autoxidation of methyl linoleate **1.1** leads to the formation of five major hydroperoxides:⁶ Two *trans,cis* dienes, **1.2** and **1.3**, are formed as the major products when millimolar concentrations of a good H-donor are present and two *trans,trans* dienes, **1.5** and **1.6**, are formed in the absence of H-donors via the β -fragmentation and rearrangement of the intermediate peroxy radicals.²⁴ A fifth, non-conjugated hydroperoxide **1.4** has also been observed from methyl linoleate oxidations to which ~ 0.1 M α -tocopherol, a very good H-donor, *vide infra*, was added.²⁵



Scheme 1.5. Products of methyl linoleate free radical oxidation.

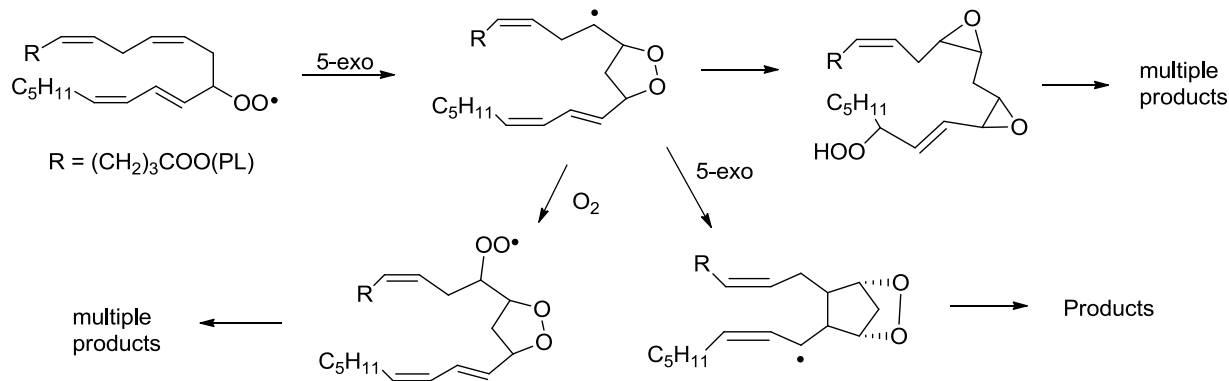
The observed product distribution when a diene fatty acid autoxidizes is dependent on the rate constants that govern the competing processes: the k_{β} values for each intermediate peroxy radical (their relative propensity to fragment back to a carbon-centred radical and oxygen), and the k_p of the substrate and/or the k_{inh} of an antioxidant if one is present in the medium – either of which can trap an intermediate peroxy radical as a hydroperoxide by donating a hydrogen atom.



Scheme 1.6. Mechanism of peroxidation of linoleic acid and its esters.

In the absence of an antioxidant, the major products observed are the *trans, trans*-diene hydroperoxides, arising from the isomerization of the *trans, cis*-diene peroxy radical following β -fragmentation. If there is a good H-atom donor (antioxidant) present in the medium, the intermediate *trans, cis*-diene peroxy radicals are trapped before they can fragment, preventing their isomerization and giving *trans, cis*-diene hydroperoxides as the major products. It has been shown that in the presence of very good H-atom donors (e.g. α -tocopherol, $k_{\text{inh}} = 3 \times 10^6 \text{ M}^{-1}\text{s}^{-1}$),²⁶ the non-conjugated diene peroxy radical can be trapped to yield a bis-allylic hydroperoxide (**11-c,c** in Scheme 1.6). Trapping this product requires high concentrations of a good antioxidant in order to compete with the very rapid β -fragmentation ($k_{\beta} = 2 \times 10^6 \text{ s}^{-1}$)²⁵ of the non-conjugated diene peroxy radical.

As the number of homoconjugated double bonds within a lipid increases, the lipid peroxidation product distributions become more complex. For example, the products of linoleate peroxidation (shown above in Scheme 1.6) are far less in number than those observed for arachidonate, which has 4-contiguous *cis*-alkene bonds. Oxidation products of compounds such as arachidonate have multiple reaction pathways available, including the 5-*exo*-cyclization as shown in Scheme 1.7 to give a cyclized peroxide that itself has multiple pathways available following cyclization.²⁷



Scheme 1.7. Reaction pathways for peroxy radical formed at the 11-position of arachadonate leading to cyclized products that can then react further to generate more products.²⁷

When comparing substrates on the basis of oxidizability, it would be expected that oxidation occurs more rapidly with substrates having weaker C-H bonds. In the propagation step of autoxidation, a peroxy radical is the abstracting radical and the O-H BDEs of hydroperoxides are relatively independent of structure (~ 88 kcal/mol),²⁵ leaving the C-H BDEs of the substrate as the determinant in the rate of H-abstraction. Both linoleic acid and arachidonic acid have bis-allylic positions (C-H BDEs ~ 73 kcal/mol) and will undergo much faster autoxidation compared to substrates such as oleic acid, which have only allylic positions (C-H BDEs ~ 84 kcal/mol).²⁰ Theoretical and experimental results confirm that molecules having low C-H BDEs have relatively high rates of hydrogen abstraction by peroxy radicals, and since H-abstractions are usually the rate-determining step for autoxidation (Scheme 1.4), there is a direct correlation between C-H BDE and k_p . By plotting the experimental rates of hydrogen atom transfer versus the DFT-calculated C-H BDEs of the hydrocarbon precursor, Pratt *et al.* were able to derive an equation (5) that can be used to predict propagation rates which are often difficult to obtain experimentally.¹⁷

$$\log k_p = -0.219(\text{C-H BDE}) + 18.9 \quad (5)$$

Similarly, the distribution of products obtained from lipid peroxidation (Scheme 1.5) correlates to the susceptibility of the intermediate peroxy radicals to undergo β -fragmentation and is therefore dependent on the C-OO• BDE. There is a correlation between calculated C-OO• BDEs and C-H BDEs derived from analogous structures given that the same carbon radicals are formed upon bond breaking and consequently both k_p and k_β values are correlated. Using calculated BDEs and experimental data, a relationship between C-OO• BDEs and k_β has been proposed (6).¹⁷

$$\log k_\beta = -0.46(\text{C-OO• BDE}) + 9.8 \quad (6)$$

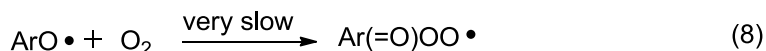
1.2 Inhibited Autoxidation - Antioxidants

Many substances can reduce the rate of autoxidation, acting as either retarders or antioxidants. Mechanistic studies have allowed the classification of antioxidants into two general classes: preventative and chain-breaking.²⁸ Preventative antioxidants reduce the initiation rate of free radical oxidation by quenching the source of initiating radicals, such as those that destroy hydroperoxides or H₂O₂ and those that quench ¹O₂. One series of preventative antioxidants found in living organisms are the superoxide dismutases that remove O₂^{•-} by catalyzing its conversion to hydrogen peroxide and molecular oxygen. The large quantities of H₂O₂ produced are then degraded either by catalases to water and oxygen or by glutathione peroxidases, which catalyze a redox reaction between H₂O₂ and glutathione (GSH) to produce water, GSSG and peroxiredoxins.³

Chain-breaking antioxidants function by ‘scavenging’ the peroxy radicals responsible for chain propagation. Although alkyl radicals are also chain-propagating, they react with molecular oxygen so rapidly that trapping them is generally unimportant. (However, alkyl radicals are the key chain-carrying radicals in free radical polymerization, so antioxidant reactions with R• have been well studied). The most common chain-breaking antioxidants found *in vivo* and industrially are H-atom donors such as phenols, non-tertiary aromatic amines and organosulfur compounds. These compounds inhibit chain-propagation by transferring a hydrogen atom to chain carrying peroxy (ROO•) radicals as shown in reaction 7 for a phenolic antioxidant (ArOH).



For efficient phenolic antioxidants, the resulting aryloxy radical is resonance-stabilized and usually unreactive toward molecular oxygen or the substrate, thus inhibiting the chain-propagated oxidation. The resulting aryloxy radical is destroyed by a bimolecular self-reaction or by reaction with another peroxy (ROO•) radical.



Scheme 1.8. Important reactions and relative rate constants required for effective peroxy trapping antioxidants.

Reactions 7 and 11 illustrate how one molecule of antioxidant is capable of ‘neutralizing’ two peroxy radicals. Using the simplified behavior of ArO• above and assuming quasi-

stationary state conditions, the rate of inhibited autoxidation under steady state rate of initiation (R_i) and low [ROOH] is given by:

$$R_{O_2} = \frac{k_p[RH]R_i}{nk_H[ArOH]} \quad (12)$$

where R_{O_2} equals the rate of oxygen consumption, k_p represents the propagation rate constant (Eq. 3), k_H is the inhibition rate constant (Eq. 7) and n is the stoichiometric factor of ArOH. The stoichiometric factor of ArOH is calculated by:²⁹

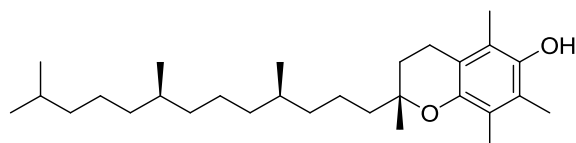
$$n = \frac{R_i \times \tau}{[ArOH]_0} \quad (13)$$

where τ and $[ArOH]_0$ are the induction period and the initial concentration of the antioxidant, respectively. The product $R_i \times \tau$ gives the moles per litre of peroxy radicals released by the initiator in a given time, τ . Therefore, the value of n represents the number of oxidative chains that can be terminated by 1 molecule of the antioxidant. Experimental evidence confirms that the rate of inhibited oxidation conforms to equation 12, but only during the early stages of oxidation.^{20,28}

Equation 12 implies that in order for a compound to be an effective antioxidant, its inhibition rate constant, k_H , must be several orders of magnitude greater than the propagation rate constant, k_p . This then implies that the effectiveness of a compound to perform as an antioxidant is not an absolute property of ArOH, but actually depends on the substrate undergoing free-radical chain oxidation. Antioxidants that are effective inhibitors for highly oxidizable (high k_p) substrates are characterized by having large rate constants for H-donation, k_H . Alternatively, substrates that react slowly with $ROO\cdot$ (low k_p) can be effectively protected by weaker

antioxidants having rate constants for H-donation, k_H , much lower than the most potent antioxidants.²⁸

If the rate of inhibition is less than several orders of magnitude larger than the rate of propagation, the compound will act as a retarder with no clear induction period. Effective antioxidants such as α -tocopherol, the most potent form of vitamin E



($k_H = 3.2 \times 10^6 \text{ M}^{-1}\text{s}^{-1}$ at 25°C in benzene),²⁶ are characterized by a defined induction period, τ (equation 13), measurable by rate of oxygen uptake.²⁹ Figure 1.1 shows the possible oxygen uptake profiles (oxygen is consumed to form $\text{ROO}\cdot$) that can result from substrate peroxidation and it can be seen that although retarders decrease the rate of oxygen uptake as they are slowly consumed, they are not as efficient as true chain-breaking antioxidants. Under retarding conditions, equation 12 no longer applies and more complicated equations have been derived by Denisov *et al.*³⁰ and Ruberto *et al.*³¹ to describe these systems that will not be discussed here.

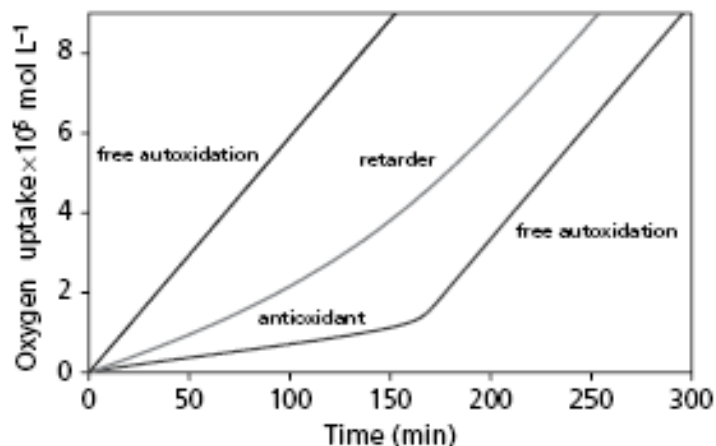


Figure 1.1. Profiles of oxygen-uptake during peroxidation of a substrate in the absence of an inhibitor or with either a retarder or an antioxidant.²⁸

1.3 Techniques for Measuring Peroxyl Radical Kinetics

Although there is no general method for measuring rate constants of radical reactions, there are many specialized methods available for measuring these rates and they can be classified as either direct or indirect. Direct methods such as flash photolysis, electron paramagnetic resonance (EPR) or the rotating sector method generally require specialized equipment and user expertise. Indirect methods are known as ‘radical clock’ reactions and involve a competition between a unimolecular reaction with a known rate constant and a bimolecular reaction with an unknown rate constant. A brief description of each technique is given below outlining their applications and inherent limitations.

1.3.1 Electron Paramagnetic Resonance

Peroxyl radical kinetics can be measured using EPR spectroscopy by measuring the decay traces of intermediate peroxyl radicals formed *in situ* by UV irradiation. A mechanical shutter is used to temporarily interrupt the irradiating light to allow for monitoring of the time course of EPR signal intensity. However, EPR spectroscopy can only be applied to systems where the balance between radical decay and radical generation is such that the concentration of radicals remains above the detection limit of the spectrometer. For this reason, EPR studies at room temperature are uncommon and cryogenic temperatures are usually required. This technique was recently applied by Valgimigli *et al.* to measure acid-accelerated inhibition rate constants between cumylperoxyl radicals and substituted phenols.³² The cumylperoxyl radicals were generated by photolysis of di-*tert*-butylperoxide in the presence of cumene and an appropriate phenol in oxygenated propionitrile at 193-213 K.

1.3.2 Laser Flash Photolysis (LFP)

Laser flash photolysis enables the near-instantaneous formation of transient radical species and monitoring of their decay (or growth) over extremely short timescales. Typically, lasers having nanosecond, picosecond or femtosecond pulse widths are used and the transient species is observed by optical absorption. One of the major limitations of LFP is that the emission wavelength of the laser is generally fixed (although high intensity pulses can be frequency doubled) and this limits the number of photoexcitable molecules that are compatible with a given laser. For example, azo-compounds can be excited at 355 nm (Nd:YAG), but ketones (e.g. Norrish fragmentation) generally require laser wavelengths below 266 nm.

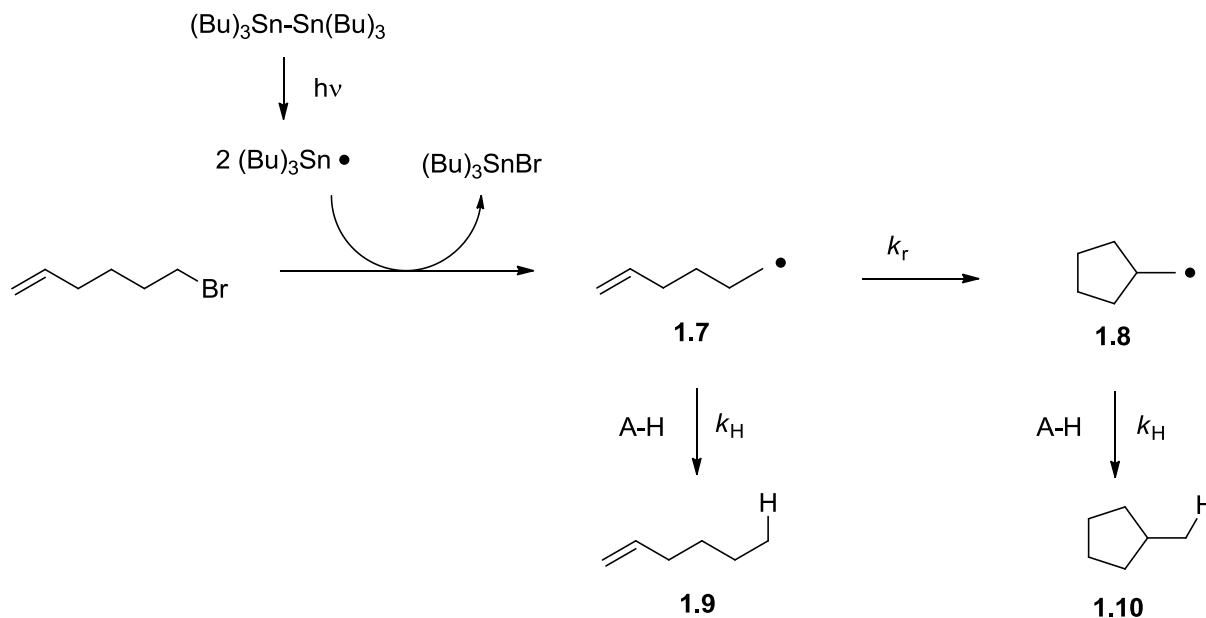
Peroxyl radicals generally do not absorb light at wavelengths above 250 nm, making it difficult to monitor their decay in a typical LFP experiment. For this reason it is often easier to measure the growth of a radical product formed in the reaction with peroxyl radicals (e.g. α -tocopheroxy radical has absorbance at 420 nm). In 2008, Lalevee *et al.* showed that α -aminoalkylperoxyl radicals can be easily observed in LFP experiments, and their rate of decay can be used to measure inhibition rate constants with phenols.³³ These α -aminoalkylperoxyl radicals have absorbances that are red-shifted to ca. 380-420 nm (depending on the alkyl substituents) due to hyperconjugation of the nitrogen lone pair with the π -orbital of the radical centre.³⁴

1.3.3 Rotating Sector Method

The rotating sector method involves initiating a chain reaction by photolysis of an initiator and periodically interrupting the beam of light hitting the sample. Using intermittent light allows evaluation of the rate constant for the chain termination process and thus the lifetime of the kinetic chain. The use of this technique is obviously limited to processes that can be initiated photochemically and are terminated by radical-radical reactions. Additionally, the radical chain must be reasonably long (>5 links) and it is therefore necessary that the propagation step(s) be fairly rapid. This technique has proven very effective for kinetic studies of autoxidation and radical polymerization, but due to the limitations discussed above the technique is not amenable to all radical-radical reactions (i.e. those where it would be difficult to make into the rate-determining propagation step of a chain reaction).

1.3.4 Radical Clocks

Radical clocks offer an indirect method for measuring radical-molecule reaction kinetics by utilizing a competition between a unimolecular reaction with a known rate constant and a bimolecular reaction with an unknown rate constant.³⁵ One of the best studied and utilized radical clocks is the 5-hexenyl radical cyclization, used to determine the rate of hydrogen abstraction from a substrate by a carbon-centred radical. The approach (Scheme 1.9) typically uses a tin radical (from photolysis of a di-tin reagent) to abstract bromine from 6-bromo-1-hexene to generate a primary alkyl radical (**1.7**) that can either rearrange to a methylcyclopentyl radical (k_r) or be trapped by a substrate A-H (k_H) as hexane.



Scheme 1.9. 5-*exo-trig* cyclization of the 5-hexen-1-yl radical (**1.7**) used as an alkyl radical clock.

The kinetic analysis is very simple:

$$\frac{d[\mathbf{1.9}]}{dt} = k_{\text{H}}[\text{A-H}][\mathbf{1.7}] \quad \text{and} \quad \frac{d[\mathbf{1.10}]}{dt} = k_{\text{r}}[\mathbf{1.7}]$$

The product ratio $[\mathbf{1.9}]/[\mathbf{1.10}]$ is directly proportional to the unknown rate constant, k_{H}

$$\frac{[\mathbf{1.9}]}{[\mathbf{1.10}]} = \frac{k_{\text{H}}[\text{A-H}]}{k_{\text{r}}} \quad \text{and therefore:} \quad k_{\text{H}} = \frac{k_{\text{r}}}{[\text{A-H}]} \frac{[\mathbf{1.9}]}{[\mathbf{1.10}]}$$

This approach is very well suited to measuring rates of hydrogen abstraction by alkyl radicals because there are a vast number of well-studied carbon-skeleton rearrangements of alkyl radicals in the literature. These unimolecular reactions have known rate constants that range from ca. $10^{-1} - 10^{13} \text{ M}^{-1}\text{s}^{-1}$ and allow for matching the ‘clock’ to the rate of the bimolecular reaction of interest.³⁵

Although the reduction of alkyl radicals by antioxidants (primarily phenols and diarylamines) are very important chain-breaking reactions in radical polymerizations (and thus understanding kinetics of these reactions is important in designing better inhibitors or stabilizers), the inhibition of alkyl radicals is only relevant in applications where low partial pressures of oxygen exist. This is because under normal atmospheric conditions, alkyl radicals will react with molecular oxygen at diffusion-controlled rates to produce peroxy radicals. Therefore, the more biologically and industrially relevant reaction for radical-trapping antioxidants is the reduction of peroxy radicals.



coefficient – as the concentration of antioxidant is increased, the yield of hydroperoxide **1.12** increases until the partition limit is reached. Analysis of the mechanism in Scheme 1.10 leads to equation 15:

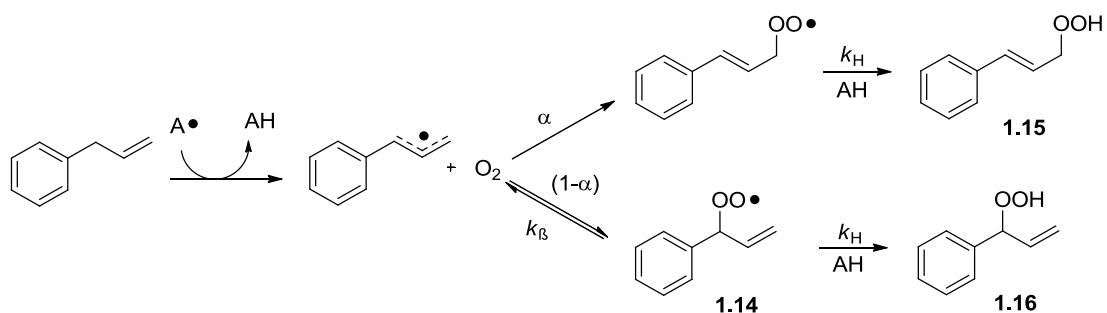
$$\frac{[\mathbf{1.12}]}{[\mathbf{1.11}+\mathbf{1.13}]} = \frac{k_{\text{H}}[\alpha\text{-TOH}]}{k_{\text{H}}[\alpha\text{-TOH}]+k_{\beta}} \cdot \frac{\alpha}{1-\alpha} \quad (15)$$

Therefore, the β -fragmentation of the non-conjugated 11-peroxyl radical can be used as a radical clock to measure H-atom transfers occurring at a similar rate. The rate of β -fragmentation (k_{β}) was determined to be $k_{\beta} = 1.9 \times 10^6 \text{ s}^{-1}$ by measuring linoleate product ratios vs. α -TOH concentration, which has an inhibition rate constant $k_{\text{H}} = 3.8 \times 10^6 \text{ M}^{-1}\text{s}^{-1}$ at 310 K and determining k_{β} by least-squares analysis. At low concentrations of antioxidant equation 15 can be simplified to equation 16:

$$\frac{[\mathbf{1.12}]}{[\mathbf{1.11}+\mathbf{1.13}]} = \frac{k_{\text{H}}[\alpha\text{-TOH}]}{k_{\beta}} \cdot \frac{\alpha}{1-\alpha} \quad (16)$$

Under these conditions the product ratios are expected to be linearly correlated to the concentration of the antioxidant, with the slope equal to $(k_{\text{H}}/k_{\beta}) \cdot (\alpha/(1-\alpha))$.

Although the linoleate clocks proved very effective for measuring H-atom transfer kinetics of very good antioxidants ($k_{\text{H}} \cong 10^6 \text{ M}^{-1}\text{s}^{-1}$), its β -fragmentation rate ($k_{\beta} = 1.9 \times 10^6 \text{ s}^{-1}$) is too fast to accurately measure inhibition rate constants for less potent antioxidants. To bridge the gap and facilitate ‘clocking’ less efficacious antioxidants, Porter *et al.* developed a peroxyl radical clock based on the oxidation of allylbenzene.³⁷ The unimolecular reaction in competition with H-atom transfer for the allylbenzene clock is the β -fragmentation of a non-conjugated (with respect to the alkene) peroxyl radical (**1.14**) shown in Scheme 1.11.

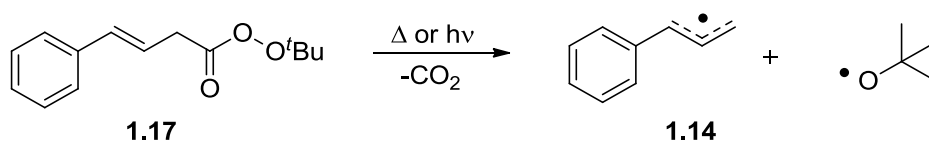


Scheme 1.11. Kinetic scheme depicting the peroxy radical clock based on the product distribution arising from oxidation of allylbenzene in the presence of an antioxidant (AH).

The conjugated peroxy radical does not undergo β -fragmentation at an appreciable rate and so inhibition rate constants can be determined by measuring the ratio of the conjugated/non-conjugated hydroperoxides. The rate of β -fragmentation was determined to be $k_{\beta} = 1.4 \times 10^5 \text{ s}^{-1}$,³⁷ again using α -TOH as an antioxidant with a known inhibition rate constant (*vide supra*).

Although the approach is effective for measuring rates of H-atom transfer from many phenols to peroxy radicals in benzene, a major limitation of this method is that it requires the antioxidant-derived radical ($A\bullet$) to abstract a hydrogen atom from allylbenzene to propagate the chain reaction. This becomes problematic if the antioxidant gives rise to either persistent (e.g. BHT, *vide supra*) or highly stabilized (e.g. 6-amino-3-pyridinols)³⁸ radicals that cannot efficiently propagate the chain. To offset low propagation rate constants – even for the most ideal A-H – a high concentration of oxidizable substrate (e.g. 2.6 M allylbenzene) must be used to ensure enough oxidation products are formed for reproducible analysis. A consequence of using such high concentrations of oxidizable substrate is that it precludes accurate kinetic or mechanistic studies in any solvent other than benzene.

In 2008, Jha and Pratt described the synthesis and utility of the homoconjugated peroxyester **1.17**,³⁹ which serves as a precursor to the same delocalized allylbenzene-derived radical essential for the kinetic competition experiment (**1.14** in Scheme 1.11). In their preliminary report, they showed that compound **1.17** decomposes under aerobic conditions either thermally (37°C) or photolytically (300 nm) to generate non-conjugated peroxy radical **1.14**, permitting clock experiments using as little as 10 mM of compound **1.17**.



Scheme 1.12. A Peroxyester as a precursor to a peroxy radical clock.

Furthermore, the rate constant of β -fragmentation (k_β) of **1.14** was measured in a variety of organic solvents, which subsequently allowed for the measurement of kinetic solvent effects on the rates of H-atom transfer from phenolic antioxidants.

1.4 Phenolic Antioxidants

Phenolic antioxidants are the most widespread antioxidants found in nature and are used most frequently to protect synthetic organic materials from oxidative degradation. As previously shown, the antioxidant activity of phenols in an autoxidation process depends on their ability to transfer a phenolic H-atom to peroxy radicals (Eq. 7).

There are many variables that can affect the antioxidant properties of phenols. These apparently simple reactions can occur by at least three different, nonexclusive mechanisms: hydrogen atom transfer (HAT), proton-coupled electron transfer (PCET) or sequential proton-loss electron transfer (SPLET).⁴⁰ The balance between these three mechanisms depends upon both the structure of the reactants (substituent effects) and on the environment (kinetic solvent effects). In a biological context, solubility and transport to specific tissues also have dramatic effects on antioxidant potency, as well as the fate of the resulting aryloxy radical (ArO•). Therefore, the three most important factors to consider when discussing the reactivity of a particular antioxidant are its BDE, steric hindrance and solvent interactions.

1.4.1 Bond Dissociation Enthalpies

A phenol's O–H BDE is one of the most important determinants of its antioxidant efficacy and substituent effects dictate this property. In 1970 it was shown that a phenol with an electron donating (ED) substituent (4-OMe) had an O–H BDE several kcal/mol weaker than a phenol with an electron withdrawing (EW) substituent (3-EtOC(O)).⁴¹ It was concluded that the substituents were inducing changes in the O–H BDEs,⁴² a conclusion that has been supported over the past four decades both experimentally and computationally.

The Hammett equation (and related linear free energy relationships) has been one of the most widely used tools for studying organic reactions and their mechanisms. Experimental and theoretical evidence agree that O–H Δ BDEs in 4-substituted phenols give excellent linear correlations with σ^+ (Y).^{42,43} It has been demonstrated that for each substituent in the *ortho*, *meta* and *para* positions, an additive contribution may be derived to estimate BDEs of polysubstituted

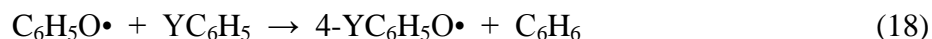
phenols for which experimental data is lacking.^{44,45} The bond dissociation enthalpies for phenolic antioxidants are most frequently measured using either photoacoustic calorimetry,⁴⁶ or by Radical Equilibrium EPR spectroscopy (REqEPR).⁴⁴ Photoacoustic calorimetry makes use of thermodynamic cycles by combining the heat of heterolysis of a given species and the redox potentials of the resulting ions. REqEPR spectroscopy determines the equilibrium constants between couples of phenols and the corresponding phenoxyl radicals, one of whose O–H BDE is known, allowing the derivation of the other.⁴⁷

Ionization potentials of *p*-substituted phenols are also linearly dependent on Hammett constants.⁴³ This linear dependence is expected because an electron-donating substituent on a phenol will usually lower both the BDE and the IP simultaneously by stabilizing the resulting radical and radical cation respectively, whereas an electron-withdrawing substituent will have a destabilizing effect on both. It has been confirmed computationally and experimentally that changes in BDE and IP induced by *para*-substitution are strongly correlated.^{48,49}

An important factor when considering substituent effects on bond dissociation enthalpies is the extent of molecule and radical stabilization/destabilization that is imparted by the substituent. The interaction of substituent (Y) on the parent OH group is referred to as the *molecule stabilization enthalpy* (MSE) and is determined using the isodesmic reaction:



The interaction enthalpies between Y and the O• group is referred to as the *radical stabilization enthalpy* (RSE), determined using the isodesmic reaction:



The *total stabilization energy* (TSE) is equal to ΔBDE and is calculated as the difference between the RSE and the MSE.

$$\text{TSE} = \Delta\text{BDE} = \text{RSE} - \text{MSE} \quad (19)$$

For 4-YC₆H₅OH molecules having substituents ranging from strong ED (e.g. Me₂N) to strong EW (e.g. NO₂), the RSEs and TSEs show excellent linear correlation with σ^+ (Y).⁴² For phenols, the MSEs do not correlate as well, but because the RSEs have a much larger contribution to the TSEs than do the MSEs, the TSEs are still well correlated by σ^+ (Y).

1.4.2 Sterics

In order for an antioxidant to be effective, the fate of the resulting aryloxy radical (ArO•) must be considered. Even though the rate of reaction between aryloxy radicals and lipids is very slow, it is possible that these chain-breaking antioxidants can regenerate LOO• radicals. This process has been observed for α -tocopherol within LDL particles and is known as tocopherol-mediated peroxidation (TMP).⁵⁰ A phenolic antioxidant is most effective when the resulting aryloxy radical is both *stable* and *persistent*. Stability is a thermodynamic property and improved delocalization of the unpaired electron enhances the stability of a radical. Persistent radicals are those whose longevity is due to steric crowding around the radical centre, making it physically difficult for them to react with another molecule. Examples of persistent phenolic antioxidants are butylated hydroxytoluene (BHT), butylated hydroxyanisole (BHA), and 2,4,6-trimethylphenol (TMP), which have been used extensively as food preservatives and in

lubricating oils. A consequence of steric crowding around the phenoxy radical is a decrease in the rate of termination, k_t . Shown below (Figure 1.2) are the self-reaction rate constants for some aryloxy radicals, and it can be seen that the addition of three *tert*-butyl groups to phenol causes the rate of termination to decrease by *nine orders* of magnitude.^{20,51,52}

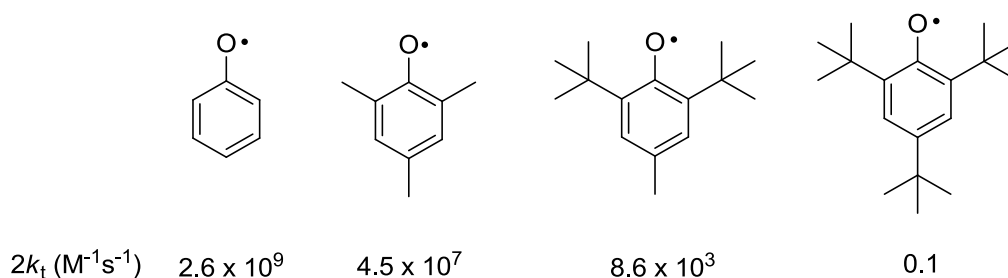
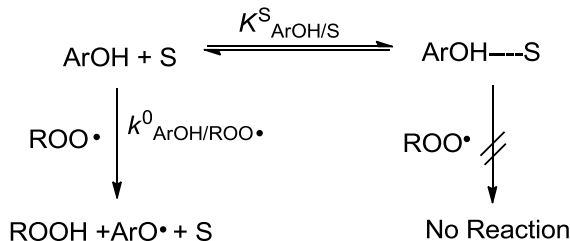


Figure 1.2. Termination rate constants ($2k_t$) for a series of para-substituted phenols.

1.4.3. Kinetic Solvent Effects and Reaction Mechanisms

Kinetic solvent effects (KSEs) have been studied since 1964 when values for k_3/k_7 (k_p/k_H) obtained from an inhibited autoxidation were originally reported for four different phenols in up to 12 solvents. It was observed that the ratio k_3/k_7 increased with increasing solvent polarity – changes that were eventually attributed to a reduction in k_7 induced by hydrogen bond (HB) formation between the phenolic hydroxyl group and HB-accepting solvents. The kinetic solvent effect for a hydrogen atom transfer mechanism is shown in Scheme 1.13 and the underlying assumption is that HAT cannot occur from the HB complex ($XH \cdots S$) for steric reasons and that the transfer only occurs from “free” XH .⁴⁰



Scheme 1.13. Hydrogen-atom transfer (HAT) and a Kinetic Solvent Effect.⁴⁰

According to Scheme 1.13, the experimental rate constant for HAT between X-H and Y• in a particular solvent, S, is given by:⁴⁰

$$k^S_{\text{XH/Y}\cdot} = k^0_{\text{XH/Y}\cdot} / (1 + K^S_{\text{XH/S}}) \quad (20)$$

This equation is important because it led to the prediction and experimental confirmation⁵³ that for any two solvents, S₁ and S₂, the ratio $k^{S_1}_{\text{XH/Y}\cdot} / k^{S_2}_{\text{XH/Y}\cdot}$ is independent of the reactivity of Y•. That is, the reduction in the rate of hydrogen atom abstraction should be *independent* of the reacting free radical and only dependent on the strength of the interaction between phenol and solvent, given as K^S in Scheme 1.13.³¹ Only very recently, Jha and Pratt have provided evidence that KSEs may not be totally independent of the nature of Y• as previously thought.³⁹

There also exists a linear free-energy relationship between the β_2^{H} values for relative HBA activities and the logarithm of the rate constant for the hydrogen atom transfer. The β_2^{H} constants represent a general thermodynamically related scale of solute HB basicities in CCl₄ and range from 0.00 for alkanes to 1.00 for hexamethylphosphortriamide (HMPA).⁵⁴ Plots of β_2^{H} vs. $\log k_{\text{H}} (\text{M}^{-1}\text{s}^{-1})$ for reaction 21 (where ArOH represents α -tocopherol and a variety of other phenols) all produced linear correlations,⁵⁵ the slopes of which were all proportional to Abraham

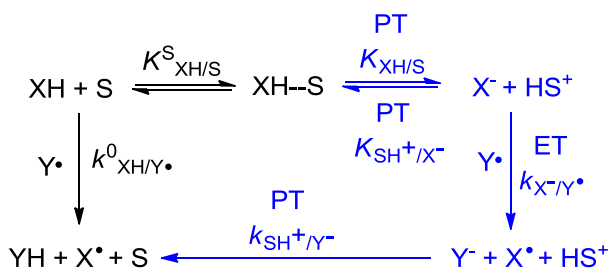
et al.'s α_2^H constants for XH.⁵⁴ The α_2^H constants represent a general thermodynamically related scale of substrate HB acidities in CCl₄, or a measure of HB donating ability.



These results allow the KSEs for HAT from phenols, hydroperoxides, anilines and hydrocarbons to be quantitatively described.⁵⁵

$$\log(k_{\text{XH/Y}\cdot}^S, \text{M}^{-1}\text{s}^{-1}) = \log(k_{\text{XH/Y}\cdot}^0, \text{M}^{-1}\text{s}^{-1}) - 8.38\alpha_2^H \quad (22)$$

Preliminary studies of HAT from α -TOH to cumylperoxyl and to alkyl radicals showed that in *tert*-butanol the peroxy reaction was much faster than predicted by equation 22, but the alkyl reaction occurred at the expected rate.⁵⁶ Further kinetic studies using 2,2-diphenyl-1-picrylhydrazyl (dpph \cdot) and a variety of phenolic antioxidants showed that in both alcoholic and non-alcoholic solvents the reactions followed bimolecular kinetics, but that the rate constants in alcoholic solvents were again much higher than predicted by equation 22. In fact, for some 2,6-di-*tert*-butyl-4-substituted phenols, the rate constants in methanol and ethanol were even larger than those in heptane. This led to the conclusion that ArOH/dpph \cdot reactions could occur by a combination of the classical HAT mechanism and sequential proton-loss electron transfer (SPLET),⁵⁷ a process involving the phenoxide anion as shown in Scheme 1.14.



Scheme 1.14. Sequential Proton-Loss Electron Transfer (SPLET).⁴⁰

It is clear that both the O–H BDEs and the ionization potentials (IPs) are important for determining which mechanism is more likely to occur. Both the H–atom transfer and the single electron transfer mechanisms may occur in parallel, but with different rates.⁴⁵

$$-d[Y\bullet]/dt = k^{\text{HAT}}[\text{XH}][Y\bullet] + k^{\text{ET}}[\text{X}^-][Y\bullet] \quad (23)$$

If the reaction occurs in a solvent with a high dielectric constant and the redox potential difference between $Y\bullet$ and ArOH , $\Delta E^\circ(Y\bullet-\text{ArOH})$, is >0 , a one-electron transfer mechanism is more likely involved,^{40,58} due to the stabilizing effect a polar solvent has on the ionic pair.

A third mechanism, proton-coupled electron transfer (PCET), was proposed by Mayer *et al.* after modeling identity reactions ($\text{XH} + \text{X}\bullet \rightarrow \text{X}\bullet + \text{XH}$) in an effort to determine why HAT between oxygen atoms occurs with higher rate constants and lower activation enthalpies than HAT between two carbon atoms. In this mechanism, complex formation between the peroxy and phenol via hydrogen bonding occurs between the OH and a lone pair on $\text{O}\bullet$ before the proton is transferred from its two bonding electrons to the radical's lone pair. The accompanying electron simultaneously moves from the π -HOMO of the phenol to the radical's SOMO (Figure 1.3).

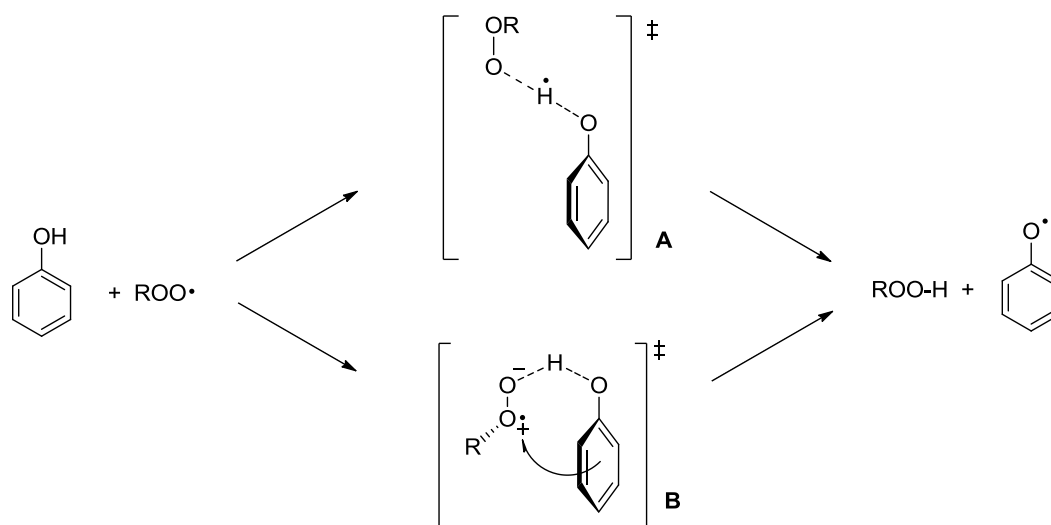


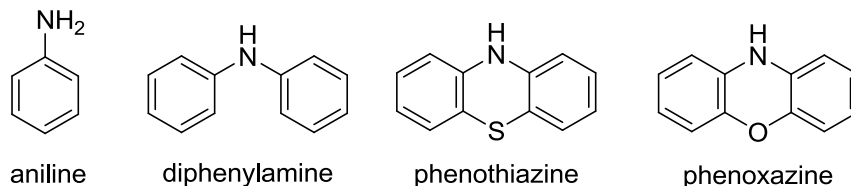
Figure 1.3. Reaction between a phenol and a peroxy radical proceeding via hydrogen-atom transfer (HAT, **A**) or proton-coupled electron transfer (PCET, **B**).⁴⁰

The PCET mechanism involves a proton and five electrons participating in the transition state, whereas a HAT reaction involves only a proton and three electrons. This mechanism has been proposed based on theoretical calculations only and it is unclear if PCET is relevant in solution or occurs simply in the gas phase, as distinguishing between the HAT and PCET mechanisms is expected to be difficult experimentally.

1.5 Aromatic Amine Antioxidants

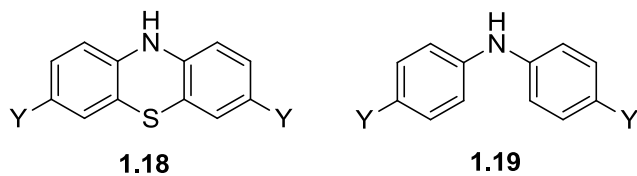
Aromatic amines have several industrial antioxidant applications, particularly in high temperature, low pressure applications such as jet fuel additives. They are also heavily used to inhibit oxidation of lubricating oils, rubbers and polymers. Phenothiazines and related derivatives have applications in medicinal chemistry due to their neuroleptic and antihistaminic properties.⁵⁹ Phenothiazine has been shown to inhibit the autoxidation of methyl linoleate and

phenoxazine to retard lipid peroxidation in rat brain tissue.⁶⁰ The major classes of diarylamine antioxidants are based on the structures below.



In comparison to their phenolic counterparts, aromatic amine antioxidants have received relatively little attention in the literature. This is partly due to the fact that the most biologically important antioxidant, α -tocopherol, is a phenolic antioxidant that also happens to be among the most effective antioxidants known. However, the major reason aromatic amines have not been investigated in as much detail remains the fact that they are generally far less stable in air than phenols, precluding detailed structure-activity studies. Nevertheless, the factors affecting N–H BDEs and their subsequent reactivity with alkyl, alkoxy and peroxy radicals have been investigated in a similar manner, only to a much less comprehensive extent. A major difference between phenolic and amine-based antioxidants is that aromatic amine antioxidants can exist as functionalized anilines or as more reactive diarylamines.

Pratt *et al.* found that the N–H BDEs series of 4-substituted anilines could not be analyzed using the radical-equilibrium EPR technique described previously for substituted phenols, because the spectra of 4- $\text{YC}_6\text{H}_5\text{NH}\cdot$ ($\text{Y} = \text{H}, \text{CH}_3, \text{OMe}$ and NH_2) were too weak to be useful.⁶¹ Instead, their calculated values for 4- $\text{YC}_6\text{H}_5\text{NH}\cdot$ were validated by comparing computational and experimental measurements of N–H ΔBDEs for 3,7-disubstituted phenothiazines (**1.18**) and 4,4'-disubstituted diphenylamines (**1.19**), which were in very good agreement.



The calculated Δ BDEs for 4-YC₆H₅NH• gave a linear correlation with σ_p^+ (Y), similar to results observed for substituted phenols. Bordwell *et al.*⁶² first reported that electron donating (ED) Y groups have a smaller effect on the 4-C₆H₅NH–H BDE than electron withdrawing (EW) Y groups and suggested that this was a consequence of the effect the substituents have on the stabilities of the parent anilines. The MSE, RSE and TSE values discussed previously for phenols (Eq. 17-19) can be determined for anilines using a similar set of isodesmic reactions. Pratt *et al.* found that for EW Y groups, the TSE values were very similar to those of phenol, but that the major contributor towards the TSE in anilines is the MSE, in contrast to the RSE being the major contributor for phenols.⁶¹ These larger MSE contributions can be attributed to the fact that the NH₂ group of aniline is a much stronger π -electron donor and a much weaker σ -electron acceptor than OH; hence the NH₂ group interacts more strongly with both π and σ accepting EW Y groups. In terms of destabilization of the parent molecule, there is not a significant change in the magnitude of the MSE when the already electron rich aromatic rings of anilines or phenols are substituted with Y = OMe, OH, NH₂ or (CH₃)₂N, despite the large change in ED abilities.

The RSE values for anilines correlate well with σ_p^+ (Y), similarly to phenols, but the values are lower for both ED and EW Y's. This is because the C–N bond in C₆H₅NH• is longer (1.34 Å) than the O–H bond in C₆H₅O• (1.25 Å) and as a result, there is a smaller 2p– π orbital overlap, causing the unpaired electron to be more localized on the heteroatom and less delocalized in the aromatic ring.⁶³ Consequently, the unpaired electron of an aminyl radical

interacts less strongly with π -acceptor and π -donor Y groups than the unpaired electron of a phenoxy radical.⁶¹

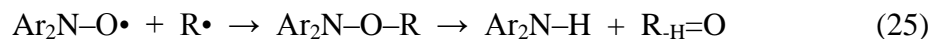
The reactivity of a series of substituted phenothiazines with alkyl, alkoxy and peroxy radicals has been studied by Lucarini *et al.*⁵⁹ These tricyclic compounds are excellent H-atom donors, having N–H BDEs comparable with the most active radical trapping phenols such as α -tocopherol, galvinoxol and 2,4,6-trimethoxyphenol. With alkyl radicals, phenothiazine derived compounds were characterized by k_H values in the range 10^4 - 10^5 $M^{-1}s^{-1}$, similar to the most effective phenols. These rate constants were obtained from competition kinetics using previously calibrated radical clocks.³⁷ To determine reactivity towards alkoxy radicals, competition kinetics were done using the hydrogen abstraction from $(TMS)_3SiH$, for which the rate constant for the reaction with *tert*-butoxy radicals is known ($k = 1 \times 10^8$ $M^{-1}s^{-1}$).⁶⁴ The obtained rate constants were similar to those measured for the most reactive phenols and approached the diffusion controlled limit. Similarly, for reactions with peroxy radicals it was found that phenothiazine reacts twice as fast as α -tocopherol and has a stoichiometric factor close to two.⁵⁹ Although phenothiazines and their derivatives serve as excellent H-atom donors, they encounter the same problems as the most reactive phenolic antioxidants in that the most electron-rich compounds are too reactive with oxygen to have reasonable applicability.

The kinetic solvent effects (KSEs) of HAT for amine antioxidants have not been studied as extensively as for phenolic antioxidants, but there have been studies for aniline and diphenylamine. As previously discussed, the strength of ArXH---S hydrogen bonds is dependent on the hydrogen bond accepting (HBA) ability of the solvent, S, and the hydrogen bond donating (HBD) ability of ArX-H. Smaller KSEs are expected with amines since aromatic amines are weaker acids than phenols. However, there is no monotonic relationship between the pK_a of

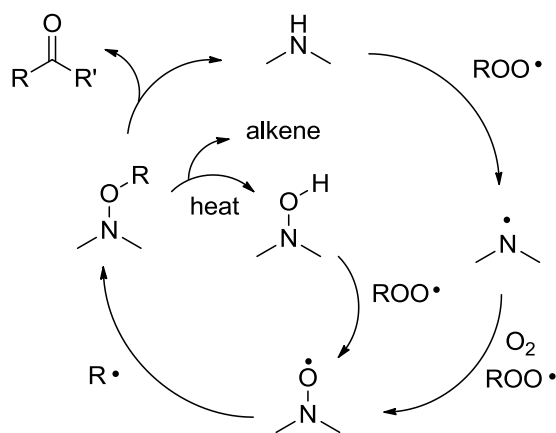
phenol (9.95 (water)), aniline (30.6) and diphenylamine (25.0) (both in 50% EtOH) and the magnitudes of their KSEs.⁶⁵ Although diphenylamine has a higher acidity than aniline, steric hindrance is more severe for diphenylamine than aniline and as a result, the KSE is smaller. Additionally, aniline is known to form both 1:1 and 1:2 complexes with HBA solvents, making it more difficult to correlate KSEs with acidities alone.⁶⁵ Due to the inherent air instability of most aromatic amines, the kinetic solvent effects have not been investigated for more reactive and industrially relevant amine antioxidants.

1.5.1 The Fate of Diarylaminy radicals – Potential Catalytic Inhibition

The fate of diarylaminy radicals can be very different from that of aryloxy radicals derived from phenolic antioxidants. Diphenylamines are chain-breaking antioxidants, donating an H-atom and forming a stable diarylaminy radical that can be destroyed either by reaction with another peroxy radical to give non-radical products (Eq. 11), or by combination with another diarylaminy radical (Eq. 10). However, diphenylamines differ from phenoxy radicals in that they are also capable of forming nitroxides. This is important because certain phenoxazines have stoichiometric factors (number of broken chains per molecule of antioxidant) as high as $n = 5$,⁵⁹ possibly a result of regeneration back to the amine via nitroxides.⁶⁶ In fact, the n values for diarylamines can reach quite substantial values – stoichiometric factors as high as $n = 40$ have been reported for diphenylamine in paraffin oil oxidizing at 130 °C.⁶⁷ It has been documented in the literature that under oxidative conditions, diarylaminy radicals can react with either molecular oxygen or ROO• to generate stable nitroxides. These nitroxides can then react with a chain-carrying carbon centred radical at near-diffusion controlled rates to form an *N*-alkoxy diarylamines that ultimately decompose to regenerate the diarylamine antioxidant.



Korcek *et al.* performed a series of inhibition reactions using synthetic nitroxide antioxidants and observed that as much as 70% of the $\text{Ar}_2\text{NO}\cdot$ was converted to Ar_2NH , depending on oxygen levels.⁶⁶ This established that a reaction path exists to rapidly convert $\text{Ar}_2\text{NO}\cdot$ or its reaction products to Ar_2NH .⁶⁶ This result stems from the fact that nitroxides are known to readily scavenge carbon-centred radicals at rates near diffusion,⁶⁸ while amines are most reactive toward peroxy radicals (as discussed previously). The work led Korcek *et al.* to propose the mechanism for catalytic inhibition by Ar_2NH and $\text{Ar}_2\text{NO}\cdot$ shown below.



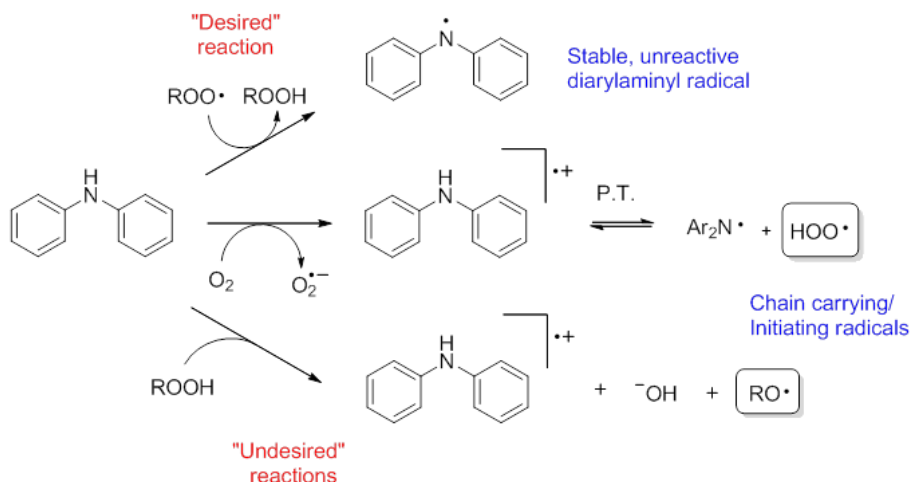
Scheme 1.16. Mechanism for catalytic inhibition by Ar_2NH and $\text{Ar}_2\text{NO}\cdot$ proposed by Korcek *et al.*⁶⁶

The thermal decomposition reaction that regenerates the starting amine is thought to occur via N-OR bond hemolysis of the alkoxyamine, followed by an in-cage disproportionation of the N- and O-centred radicals to give an amine and a carbonyl product. This reaction will

become more favorable as the viscosity of the polymeric material increases, due to very large ‘cage effects’ imposed on geminate radical pairs.⁶⁶ A second mechanism first proposed by Bolsman *et al.* suggests that the intermediate alkoxyamine undergoes thermal C–O homolysis to produce an olefin and a hydroxylamine – a reaction mechanism supported by deuterium kinetic isotope effects and by the need for β -H atoms on the trapped alkyl radical.⁶⁷

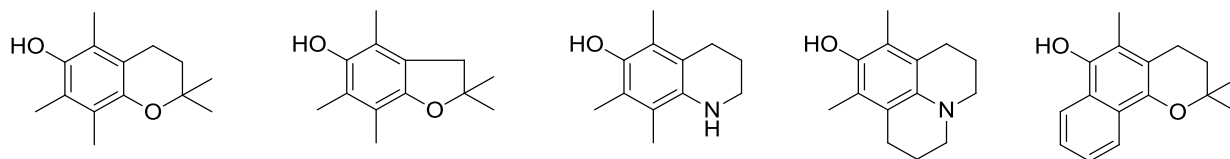
1.6 Improving Antioxidant Activity

Due to their widespread use throughout industry, there is a continued interest in designing antioxidants with higher reactivity towards both peroxy and alkyl radicals. The seemingly simple solution to this problem is to append electron-donating groups to the phenol or diphenylamine to weaken the O-H or N-H bond and increase the rate of H-atom transfer to a peroxy radical. However, as previously discussed, there is a correlation between the decrease in BDE and the decrease in ionization potential (IP). As a result, when BDE and IP are lowered to a threshold, the antioxidant is more likely to undergo a one-electron oxidation with molecular oxygen – generating superoxide and a radical cation. This negates any potential antioxidant activity and can result in the compound acting as a pro-oxidant.



Scheme 1.17. Reaction pathways for diphenylamine showing both the desired radical trapping pathway and the undesired one-electron oxidations with molecular oxygen or hydroperoxides yielding ROS that can initiate peroxidation.

The correlation between σ^+ of a substituent with both BDE and IP has been the largest obstacle to overcome in designing more efficacious antioxidants (phenols or diarylamines). Over the past few decades many modifications have been made to phenolic antioxidants to improve their reactivities, usually by some modification of α -tocopherol – the gold standard. Modifications include contraction of the 6-membered chroman nucleus of tocopherol to a 5-membered furan (to achieve better overlap of the oxygen lone pair), substituting more electron-donating amine groups for oxygen and extending the conjugation in the aromatic systems.



These changes all succeed in lowering the O-H BDEs of the phenols, but unfortunately their ionization potentials become so low that they are no longer air-stable.

A solution to this problem was found by Pratt *et al.* in 2001 when they discovered that inclusion of heteroatoms in the aromatic ring results in a dramatic increase in IPs relative to BDEs.⁴³ This result can be explained by considering the electronic effects that dictate BDEs and IPs – the BDE is affected by resonance π -interaction with *para*- and *ortho*-substituents while ionization potential is primarily affected by σ -induced electron density in the aromatic system. By incorporating nitrogen atom(s) into the aromatic system in the form of pyridine and pyrimidine rings, both BDEs and IPs were increased; however, the IPs increased much more due to the large destabilizing effect the electronegative nitrogen atom has on the charged radical cation formed by one-electron oxidation. To illustrate the dramatic effect nitrogen incorporation has on phenolic antioxidants, a series of calculations were done using models to predict X-H BDEs⁶⁹ and IPs⁷⁰ for phenol, pyridinols and pyrimidinols, summarized below.

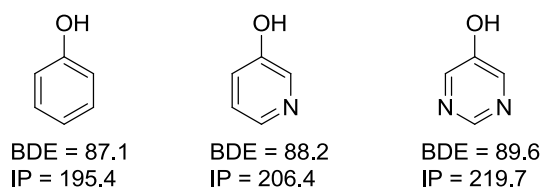


Figure 1.4. Calculated bond dissociation enthalpies (BDEs) and ionization potentials (IPs) in kcal/mol for a series of phenols with increasing nitrogen content.

Therefore, it would be expected that by incorporating two nitrogen atoms into the aromatic ring of phenol the O-H BDE will increase ~ 2.5 kcal/mol, whereas the IP will increase ~ 24.3 kcal/mol.⁴³ By extending this concept to *ortho/para*-substituted pyridinols and pyrimidinols, compounds were prepared that have very low O-H BDEs and maintained air stability.⁷¹ A few examples are shown below along with their BDEs, IPs and relative rate of peroxy trapping compared to α -tocopherol (k/k_{TOH}).

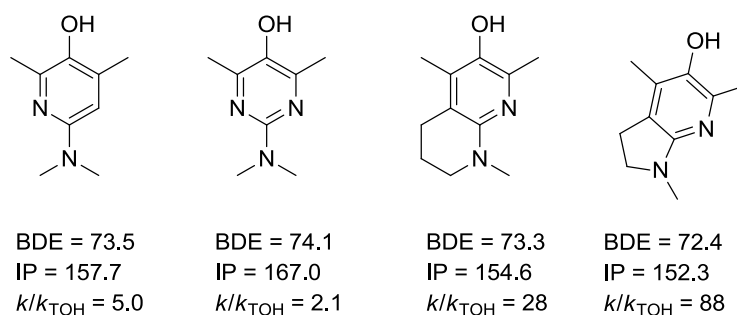


Figure 1.5. Calculated BDEs and IPs for a series of substituted pyri(mi)dinols in kcal/mol. k/k_{TOH} = ratio of rate constants for peroxy radical trapping relative to α -tocopherol ($k_{\text{H}} = 3.2 \times 10^6 \text{ M}^{-1}\text{s}^{-1}$).³⁸

1.7 Research Objectives

1.7.1. Air-Stable Diarylamine Antioxidants

Given the industrial importance of diarylamine antioxidants and the success of the pyridinol and pyrimidinol series of compounds, it seemed logical to extend the concept of heteroatom incorporation to diarylamines. We sought to apply the same approach to diarylamines to prepare very reactive, air-stable compounds that could be used commercially and that would allow us to better understand the structure-reactivity relationships for these compounds.

In contrast with pyridinols and pyrimidinols, nitrogen atoms can be incorporated in diarylamines in a multitude of substitution patterns. The compounds can be prepared symmetrically or unsymmetrically in terms of both heteroatom incorporation and *para*-substituents. Computational analyses of unsubstituted diarylamines suggested that incorporation of nitrogen at the 3 and 5 positions would afford the greatest increase in ionization potentials without compromising N-H BDEs. We envisioned synthesizing compounds bearing the

substitution patterns shown in Figure 1.6 to be able to comprehensively study the structure-activity relationships of pyridine and pyrimidine-based diarylamines.

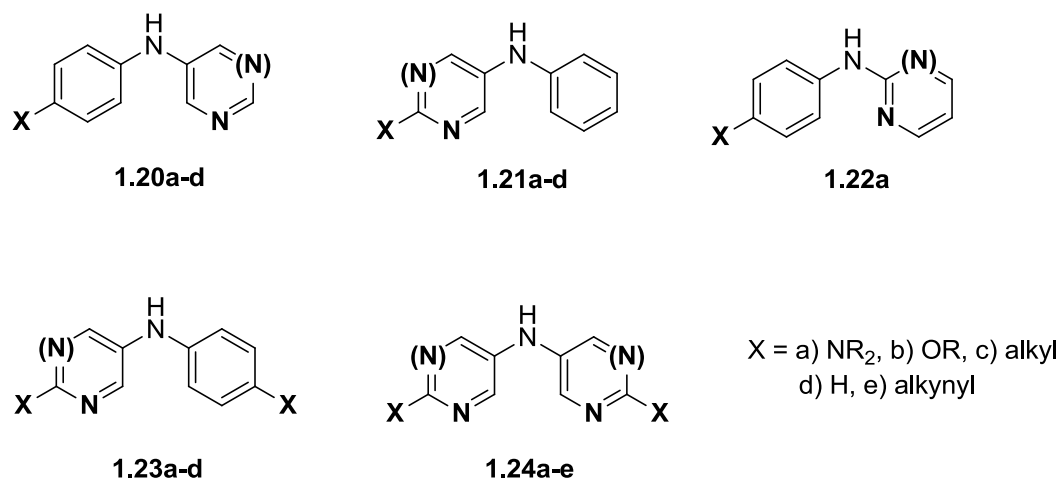


Figure 1.6. Target molecules showing different possible substitution patterns.

In recent years there has been an explosion in the literature regarding methods to prepare substituted diarylamines. The modern approach is to prepare these compounds by C-N bond forming reactions using transition-metal catalysis (i.e. Pd, Cu, Ni, Fe), but classically these molecules have been prepared by Smiles rearrangement of amides,⁷² Chapman rearrangement of imino ethers,⁷³ or by addition of phenylmagnesium halides to nitrobenzenes⁷⁴ or nitrosyl chloride.⁷⁵ However, there are very few examples of heterocycle-containing diarylamines such as those described in Figure 1.6. Of the structures represented in Figure 1.6, only compounds of sub-class' **1.20a-d**, **1.21c** and **1.22a** have been reported (**1.20a** (pyr, R = Me),⁷⁶ **1.20b** (pyr, R = OMe),⁷⁷ **1.20c** (pyr, R = Me),⁷⁸ **1.20d** (pyr, pym, R = H),^{79,80} **1.21c** (pyr, R = Me),⁸¹ and **1.22a** (pyr, R = Et, pym, R = Et),^{82,83}) in the literature. Our primary focus was to synthesize a diverse library of dialkylamino-substituted pyri(mi)dylamines, since these compounds should be the

most reactive/fundamentally interesting. However, to fully study structure-activity relationships we also wanted to prepare a number of alkoxy, alkynyl, alkyl and unsubstituted compounds. To synthesize these molecules we sought to develop a general, modular route that would allow for all substitution patterns to be prepared from common intermediates.

With the compounds in hand we can then explore their thermodynamic and kinetic properties by the following:

- 1) Characterization of their thermodynamic properties in the form of N-H BDEs by radical equilibrium EPR (collaboration with Dr. Luca Valgimigli, University of Bologna) and standard potentials (E°) using cyclic voltammetry (or anodic peak potentials with differential pulse voltammetry if the redox chemistry is irreversible).
- 2) Measurement of their reactivity with peroxy radicals, as well as kinetic solvent effects, deuterium kinetic isotope effects and Arrhenius parameters for these reactions using newly developed peroxy radical clocks.⁸⁴
- 3) Measurement of their reactivity with alkyl radicals in solution, using radical clock methods.⁸⁵

While we have focused this introduction on the antioxidant properties of phenols and diphenylamines, they are also used extensively as radical polymerization inhibitors, and we expect the same structure-reactivity relationships leading to more effective peroxy radical-

trapping antioxidants will also lead to more effective alkyl radical-trapping polymerization inhibitors.

1.7.2. Development of a New Peroxyester-based Peroxyl Radical Clock and Extending Peroxyl Radical Clock Methodology

In order to measure rate constants for reactions of peroxyl radicals and our diarylamines we turned to previously established peroxyl radical clock methodology,³⁹ but found that resolution of the product peaks by GC was often unsatisfactory. To improve the analytical aspect of the methodology, we sought to prepare a peroxyester clock based on a naphthyl-core with the idea that additional molecular weight would improve product resolution by pushing the products to longer retention times – away from solvent impurities and antioxidants or their derived products. A secondary goal of this project was to extend the peroxyl radical clock methodology to enable measurement of deuterium kinetic isotope effects and Arrhenius parameters for antioxidant reactions with peroxyl radicals.

1.7.3. Design and Application of a Fluorescent Dye for Rapid, High-Throughput Quantification of Hydroperoxides

One of the most established methods for measuring inhibition rate constants for reactions with peroxyl radicals is the inhibited autoxidation of styrene or other easily oxidizable substrates. This method relies on accurately determining hydroperoxide formation over time, usually by monitoring oxygen consumption or by HPLC analysis. Although very effective, oxygen uptake

measurements require specialized equipment (pressure transducer, etc.), user expertise and time-consuming calibration. HPLC analysis is also an effective analytical method, but requires lengthy analysis for each of the dozens of time points required to establish a good inhibited autoxidation profile.

Additionally, we would like to be able to measure our diarylamine antioxidants' ability to inhibit hexadecane oxidation at elevated temperatures (160 °C), conditions which simulate the operating environment experienced by lubricating oils in combustion engines and thus a possible industrial application for our diarylamines. These high temperature experiments will also provide a method to explore the catalytic reactivity of diarylamine antioxidants, by measuring accurate stoichiometric factors (n) and using authentic diarylnitroxide radicals as inhibitors. High temperature autoxidations using hexadecane have been reported by several groups, including Mahoney *et al.*⁸⁶ and Savage *et al.*,⁸⁷ and their analytical analyses were done by time consuming iodometric titrations and/or very complex GC or HPLC separations.

To improve the analytical aspect of inhibited autoxidation assays, we sought to prepare a redox-active fluorescent dye that can be used to quantify hydroperoxide concentrations in near real-time. The inspiration for this work came from phosphine dyes reported by Bertozzi *et al.*⁸⁸ and Onoda *et al.*⁸⁹ who showed that the oxidation state of phosphine can be used to mediate photoinduced electron transfer to a fluorophore – and that these compounds could be applied to detecting ROS. In the past decade there have been dozens of phosphine dyes reported in the literature for *detecting* specific ROS, but never an assay for rapid, *accurate quantification* of hydroperoxide concentrations.

The objectives of this project were to:

- 1) Synthesize a phosphine dye capable of reacting with hydroperoxides at a (relatively) rapid rate and that would have a sufficient quantum yield difference between reduced and oxidized phosphine states to allow effective detection of hydroperoxides.
- 2) Develop an assay for rapid, high-throughput, quantitative measurements of hydroperoxide concentrations and apply the assay to the measurement of inhibition rate constants.

1.7.4. Development of a New Precursor for Transient Absorption Kinetic Studies of Fast Peroxyl Radical Reactions

The most biologically important and studied antioxidant is α -tocopherol. As discussed previously, reactions between α -tocopherol and peroxyl radicals have been characterized very well in terms of rate constant, mechanism and solvent effects. What remains to be fully understood are the Arrhenius parameters – the activation energy for H-atom transfer reactions with peroxyl radicals. To the best of our knowledge, the best pre-exponential factor is estimated at $\log A = 8$, a value put forward by Benson⁹⁰ that would give a calculated activation energy of 1.6 kcal/mol (based on $k_H = 6.4 \times 10^6 \text{ M}^{-1}\text{s}^{-1}$ at 25 °C)⁸⁴ in chlorobenzene.

To accurately determine temperature dependence on fast peroxyl radical trapping reactions, a direct method such as laser flash photolysis must be used. One of the most common methods of generating peroxyl radicals and following reaction kinetics with phenols such as tocopherol is to photolyze di-*tert*-butylperoxide in the presence of a substrate with an

abstractable hydrogen atom in oxygenated solution and watch the growth of phenoxyl radical. However, this requires large amounts of peroxide and substrate, and generally precludes any determination of kinetic solvent effects on the reaction. Other methods have been developed for generating tertiary peroxy radicals (e.g. dicumylketone, azocumene) but these compounds do not circumvent the problem of photoionization of tocopherol at the wavelengths required for photolysis (266/308 nm or 355 nm respectively).

The objectives of this project were to develop a new precursor for transient absorption kinetic studies that allow the reaction kinetics to be monitored by watching the *decay* of the peroxy radical rather than the *growth* of tocopheroxyl. This would render the photoionization of tocopherol (or other antioxidants) insignificant and allow the temperature dependence on the rate of peroxy trapping to be accurately determined in a variety of organic media.

1.8 References

- (1) Weber, M.; Weber, M.; Kleine-Boymann, M.; Wiley-VCH: 2004; Vol. Phenol.
- (2) Wijtmans, M., Vanderbilt University, 2004.
- (3) Halliwell, B.; Gutteridge, J. M. C. *Free Radicals in Biology and Medicine*; 3rd ed.; Oxford University Press Inc: New York, 1999.
- (4) Czapski, G.; Goldstein, S.; Myerstein, D. *Free Radical Research Communications* **1988**, 4, 231.
- (5) Niki, E.; Noguchi, N. *Molecular and Cellular Biochemistry* **2002**, 234, 19.

- (6) Porter, N. A. *Accounts of Chemical Research* **1986**, *19*, 262.
- (7) Porter, N. A.; Caldwell, S. E.; Mills, K. A. *Lipids* **1995**, *30*, 277.
- (8) Pratt, D. A.; Porter, N. A.; Tallman, K. A. *Accounts of Chemical Research* **2011**, *44*, 458.
- (9) Kagan, V. E.; Quinn, P. J. *Antioxidants & Redox Signaling* **2004**, *6*, 199.
- (10) Voet, J. G.; Voet, D. *Biochemistry*; 3rd Edition ed., 2004.
- (11) Yau, T. M. *Mechanisms of Ageing and Development* **1979**, *11*, 137.
- (12) Tanel, A.; Averill-Bates, D. A. *Free Radical Biology and Medicine* **2007**, *42*, 798.
- (13) Harman, D. *Journal of Gerontology* **1956**, *11*, 298.
- (14) Niki, E. *Free Radical Research* **2000**, *33*, 693.
- (15) Wu, D.; Bayes, K. D. *International Journal of Chemical Kinetics* **1986**, *18*, 547.
- (16) Maillard, B.; Ingold, K. U.; Scaiano, J. C. *Journal of the American Chemical Society* **1983**, *105*, 5095.
- (17) Pratt, D. A.; Mills, J. H.; Porter, N. A. *Journal of the American Chemical Society* **2003**, *125*, 5801.
- (18) Howard, J. A.; Ingold, J. A. *Canadian Journal of Chemistry* **1967**, *45*, 793.
- (19) Russell, G. A. *Journal of the American Chemical Society* **1957**, *79*, 3871.
- (20) Pierini, M.; Punta, C. *Letters in Organic Chemistry* **2006**, *3*, 91.

- (21) Girotti, A. W. *Journal of Photochemistry and Photobiology B-Biology* **2001**, *63*, 103.
- (22) Greer, A. *Accounts of Chemical Research* **2006**, *39*, 797.
- (23) Karrer, S.; Baumler, W.; Abels, C.; Hohenleutner, U.; Landthaler, M.; Szeimies, R. M. *Lasers in Surgery and Medicine* **1999**, *25*, 51.
- (24) Porter, N. A.; Wujek, D. G. *Journal of the American Chemical Society* **1984**, *106*, 2626.
- (25) Tallman, K. A.; Pratt, D. A.; Porter, N. A. *Journal of the American Chemical Society* **2001**, *123*, 11827.
- (26) Burton, G. W.; Ingold, K. U. *Accounts of Chemical Research* **1986**, *19*, 194.
- (27) Yin, H.; Xu, L.; Porter, N. A. *Chemical Reviews* **2011**, *111*, 5944.
- (28) Foti, M. C. *Journal of Pharmacy and Pharmacology* **2007**, *59*, 1673.
- (29) Mahoney, L. R. *Angewandte Chemie-International Edition* **1969**, *8*, 547.
- (30) Denisov, E. T.; Khudyakov, I. V. *Chemical Reviews* **1987**, *87*, 1313.
- (31) Foti, M.; Ruberto, G. *Journal of Agricultural and Food Chemistry* **2001**, *49*, 342.
- (32) Valgimigli, L.; Amorati, R.; Petrucci, S.; Pedulli, G. F.; Hu, D.; Hanthorn, J. J.; Pratt, D. A. *Angewandte Chemie-International Edition* **2009**, *48*, 8348.
- (33) Lalevee, J.; Allonas, X.; Fouassier, J. P.; Ingold, K. U. *Journal of Organic Chemistry* **2008**, *73*, 6489.

- (34) Lalevee, J.; Allonas, X.; Fouassier, J. P. *Chemical Physics Letters* **2007**, *445*, 62.
- (35) Newcomb, M. *Tetrahedron* **1993**, *49*, 1151.
- (36) Brash, A. R. *Lipids* **2000**, *35*, 947.
- (37) Roschek, B.; Tallman, K. A.; Rector, C. L.; Gillmore, J. G.; Pratt, D. A.; Punta, C.; Porter, N. A. *Journal of Organic Chemistry* **2006**, *71*, 3527.
- (38) Wijtmans, M.; Pratt, D. A.; Valgimigli, L.; DiLabio, G. A.; Pedulli, G. F.; Porter, N. A. *Angewandte Chemie-International Edition* **2003**, *42*, 4370.
- (39) Jha, M.; Pratt, D. A. *Chemical Communications* **2008**, 1252.
- (40) Litwinienko, G.; Ingold, K. U. *Accounts of Chemical Research* **2007**, *40*, 222.
- (41) Mahoney, L. R.; DaRooge, M. A. *J. Am. Chem. Soc.* **1970**, *92*, 890.
- (42) Pratt, D. A.; Dilabio, G. A.; Mulder, P.; Ingold, K. U. *Accounts of Chemical Research* **2004**, *37*, 334.
- (43) Pratt, D. A.; DiLabio, G. A.; Brigati, G.; Pedulli, G. F.; Valgimigli, L. *Journal of the American Chemical Society* **2001**, *123*, 4625.
- (44) Brigati, G.; Lucarini, M.; Mugnaini, V.; Pedulli, G. F. *Journal of Organic Chemistry* **2002**, *67*, 4828.
- (45) Wright, J. S.; Johnson, E. R.; DiLabio, G. A. *Journal of the American Chemical Society* **2001**, *123*, 1173.

- (46) Laarhoven, L. J. J.; Mulder, P.; Wayner, D. D. M. *Accounts of Chemical Research* **1999**, *32*, 342.
- (47) Lucarini, M.; Pedrielli, P.; Pedulli, G. F.; Cabiddu, S.; Fattuoni, C. *Journal of Organic Chemistry* **1996**, *61*, 9259.
- (48) Miller, L. L.; Mayeda, E. A.; Nordblom, G. D. *Journal of Organic Chemistry* **1972**, *37*, 916.
- (49) Migliavacca, E.; Carrupt, P. A.; Testa, B. *Helvetica Chimica Acta* **1997**, *80*, 1613.
- (50) Bowry, V. W.; Ingold, K. U. *Accounts of Chemical Research* **1999**, *32*, 27.
- (51) Weiner, S. A.; Mahoney, L. R. *Journal of the American Chemical Society* **1972**, *94*, 5029.
- (52) Mahoney, L. R.; Weiner, S. A. *Journal of the American Chemical Society* **1972**, *94*, 585.
- (53) Valgimigli, L.; Banks, J. T.; Ingold, K. U.; Luszytk, J. *Journal of the American Chemical Society* **1995**, *117*, 9966.
- (54) Abraham, M. H.; Grellier, P. L.; Prior, D. V.; Duce, P. P.; Morris, J. J.; Taylor, P. *J. Journal of the Chemical Society-Perkin Transactions 2* **1989**, 699.
- (55) Snelgrove, D. W.; Luszytk, J.; Banks, J. T.; Mulder, P.; Ingold, K. U. *Journal of the American Chemical Society* **2001**, *123*, 469.
- (56) Franchi, P.; Lucarini, M.; Pedulli, G. F.; Valgimigli, L.; Lunelli, B. *Journal of the American Chemical Society* **1999**, *121*, 507.

- (57) Foti, M. C.; Daquino, C.; Geraci, C. *Journal of Organic Chemistry* **2004**, *69*, 2309.
- (58) Valgimigli, L.; Ingold, K. U.; Lusztyk, J. *Journal of the American Chemical Society* **1996**, *118*, 3545.
- (59) Lucarini, M.; Pedrielli, P.; Pedulli, G. F.; Valgimigli, L.; Gimes, D.; Tordo, P. *Journal of the American Chemical Society* **1999**, *121*, 11546.
- (60) Cini, M.; Fariello, R. G.; Bianchetti, A.; Moretti, A. *Neurochemical Research* **1994**, *19*, 283.
- (61) Pratt, D. A.; DiLabio, G. A.; Valgimigli, L.; Pedulli, G. F.; Ingold, K. U. *Journal of the American Chemical Society* **2002**, *124*, 11085.
- (62) Bordwell, F. G.; Zhang, X. M.; Cheng, J. P. *Journal of Organic Chemistry* **1993**, *58*, 6410.
- (63) Ingold, K. U.; Wright, J. S. *Journal of Chemical Education* **2000**, *77*, 1062.
- (64) Chatgialoglu, C.; Rossini, S. *Bulletin De La Societe Chimique De France* **1988**, 298.
- (65) MacFaul, P. A.; Ingold, K. U.; Lusztyk, J. *Journal of Organic Chemistry* **1996**, *61*, 1316.
- (66) Jensen, R. K.; Korcek, S.; Zinbo, M.; Gerlock, J. L. *Journal of Organic Chemistry* **1995**, *60*, 5396.

- (67) Bolsman, T.; Blok, A. P.; Frijns, J. H. G. *Recueil Des Travaux Chimiques Des Pays-Bas-Journal of the Royal Netherlands Chemical Society* **1978**, *97*, 310.
- (68) Beckwith, A. L. J.; Bowry, V. W.; Ingold, K. U. *Journal of the American Chemical Society* **1992**, *114*, 4983.
- (69) DiLabio, G. A.; Pratt, D. A.; LoFaro, A. D.; Wright, J. S. *Journal of Physical Chemistry A* **1999**, *103*, 1653.
- (70) DiLabio, G. A.; Pratt, D. A.; Wright, J. S. *Journal of Organic Chemistry* **2000**, *65*, 2195.
- (71) Valgimigli, L.; Brigati, G.; Pedulli, G. F.; DiLabio, G. A.; Mastragostino, M.; Arbizzani, C.; Pratt, D. A. *Chemistry-a European Journal* **2003**, *9*, 4997.
- (72) Truce, W.; Krieder, E.; Brand, W. *Organic Reactions* **1971**, *18*, 99.
- (73) Schulenburg, J. W.; Archer, S. *Organic Reactions* **1965**, *14*, 1.
- (74) Sapountzis, I.; Knochel, P. *Journal of the American Chemical Society* **2002**, *124*, 9390.
- (75) Waters, W. L.; Marsh, P. G. *Journal of Organic Chemistry* **1975**, *40*, 3349.
- (76) Maier-Bode, H. 1933.
- (77) Mazu, T. K.; Etukala, J. R.; Jacob, M. R.; Khan, S. I.; Walker, L. A.; Ablordeppey, S. Y. *European Journal of Medicinal Chemistry* **2011**, *46*, 2378.

- (78) Shen, Q. L.; Ogata, T.; Hartwig, J. F. *Journal of the American Chemical Society* **2008**, *130*, 8564.
- (79) Grasa, G. A.; Viciu, M. S.; Huang, J. K.; Nolan, S. P. *Journal of Organic Chemistry* **2001**, *66*, 7729.
- (80) Sato, M.; Katsushima, T.; Kinoshita, H. Japan, 1999.
- (81) Peterson, L. H.; Tolman, R. L. *Journal of Heterocyclic Chemistry* **1977**, *14*, 527.
- (82) Whitmore, F. C.; Mosher, H. S.; Goldsmith, D. P. J.; Rytina, A. W. *Journal of the American Chemical Society* **1945**, *67*, 393.
- (83) Adams, R. R.; Whitmore, F. C. *Journal of the American Chemical Society* **1945**, *67*, 735.
- (84) Hanthorn, J.; Pratt, D. A. *Journal of Organic Chemistry* **2012**, *77*, 276.
- (85) Burton, A.; Ingold, K. U.; Walton, J. C. *Journal of Organic Chemistry* **1996**, *61*, 3778.
- (86) Jensen, R. K.; Korcek, S.; Mahoney, L. R.; Zinbo, M. *Journal of the American Chemical Society* **1979**, *101*, 7574.
- (87) Blaine, S.; Savage, P. E. *Industrial & Engineering Chemistry Research* **1991**, *30*, 792.
- (88) Lemieux, G. A.; de Graffenried, C. L.; Bertozzi, C. R. *Journal of the American Chemical Society* **2003**, *125*, 4708.

- (89) Onoda, M.; Uchiyama, S.; Endo, A.; Tokuyama, H.; Santa, T.; Imal, K. *Organic Letters* **2003**, 5, 1459.
- (90) Benson, S. W. *Thermochemical Kinetics 2nd Edition*; John Wiley & Sons: New York, 1976.

CHAPTER 2: PREPARATION OF HIGHLY-REACTIVE PYRIDINE- AND PYRIMIDINE-CONTAINING DIARYLAMINE ANTIOXIDANTS

2.1 Preface

We recently reported a preliminary account of our efforts to develop novel diarylamine radical-trapping antioxidants (Hanthorn, J. J.; Valgimigli, L.; Pratt, D. A. *J. Am. Chem. Soc.* **2012**, DOI: 10/1021/ja300086z), wherein we suggested that the incorporation of ring nitrogens into diphenylamines affords compounds which display a compromise between H-atom transfer reactivity to radicals and stability to one-electron oxidation. Herein we provide the details of the synthetic efforts associated with that report, which have been substantially expanded to produce a library of substituted heterocyclic diarylamines that we have used to provide further insight into the structure-reactivity relationships of these compounds as antioxidants (see accompanying paper and Chapter 3). The diarylamines were prepared in short, modular sequences from 2-aminopyridine and 2-aminopyrimidine wherein aminations of intermediate pyri(mi)dyl bromides and then Pd-catalyzed cross-coupling reactions of the amines and precursor bromides were the key steps to yield the diarylamines. The cross-coupling reactions were found to proceed best with Pd(η^3 -1-PhC₃H₄)(η^5 -C₅H₅) as precatalyst, which gave higher yields than the conventional Pd source, Pd₂(dba)₃. This chapter is presented largely as it was when submitted to the *Journal of Organic Chemistry* as a back to back manuscript with the manuscript presented as Chapter 3;

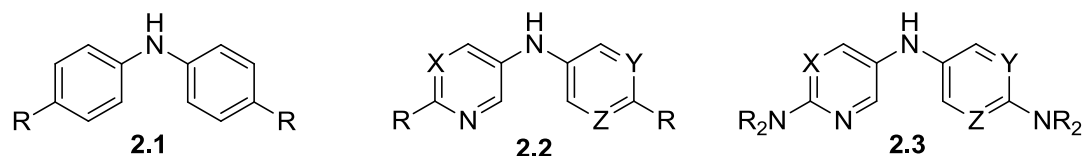
2.2 Introduction

Diarylamines (Ar_2NH) are among the most important additives to petroleum-derived products.¹ They are radical-trapping antioxidants which slow hydrocarbon autoxidation, the archetype free-radical chain reaction, through initial donation of their aminic H-atom to chain-carrying peroxy radicals (Eq. 1).² Subsequent reaction of the aminyl radical with another peroxy radical leads to non-radical products at ambient temperatures (Eq. 2) and nitroxide radicals at elevated temperatures ($>120^\circ\text{C}$, Eq. 3). The latter reaction is key to the catalytic antioxidant activity of alkylated diphenylamines (**2.1**), which has made them additives of choice to lubricating oils of combustion engines and in other high-temperature applications.³



In a recent communication,⁴ we described preliminary results of our attempts to improve the activity of diarylamine antioxidants. Our strategy involves the incorporation of nitrogen atoms into the aryl rings – enabling their substitution with strongly-electron donating groups to weaken their N-H bonds, thus accelerating their rates of formal H-atom transfer reactions (Eq. 1). Both modifications are believed to be required for optimizing reactivity, since ring substitution alone results in compounds that undergo one-electron oxidation by O_2 in the air or by product hydroperoxides, rendering them useless as antioxidants. In fact, we showed that analogs of **2.1** bearing either ring carbons or nitrogens at the positions indicated by X Y and Z in

2.2 were characterized by oxidation potentials that increased systematically with the number of N-atoms from less than 1 V to > 1.5 V (vs. NHE), while their reactivity towards peroxy radicals decreased only 6-fold at most (from $k_{\text{H}} = 1.8 \times 10^5 \text{ M}^{-1}\text{s}^{-1}$ for **2.1** to $k_{\text{H}} = 3.0 \times 10^4 \text{ M}^{-1}\text{s}^{-1}$ for **2.2** with X=Y=Z=N in chlorobenzene at 37°C). This permitted the design of diarylamines bearing strongly electron-donating *N,N*-dialkylamino groups (**2.3**) that were stable in air and reacted with peroxy radicals with temperature-independent rate constants up to 200-fold greater than those measured for **2.1** under the same conditions.



These exciting results prompted us to carry out a thorough study of the structure-reactivity relationships in these compounds. First, it was of interest to determine the optimal location of the ring nitrogen atoms. In our preliminary work, we studied only 3-pyridyl and 5-pyrimidyl amines, but clearly other arrangements are possible and should be investigated. Second, it was of interest to determine the relative reactivities of unsymmetrically substituted compounds as compared to the symmetric compounds studied to date. Third, it was necessary to expand the number of ring substituents that we have studied in order to establish well-defined structure-reactivity relationships that will provide meaningful insights into their chemistry and potential usefulness. Therefore, in addition to the alkyl- and *N,N*-dialkylamino-substituted compounds we studied in our preliminary report (i.e. **2.2** and **2.3**)⁴ we sought to prepare alkoxy-substituted compounds as well as the unsubstituted (parent) compounds. The compounds of interest are shown in Figure 2.1.

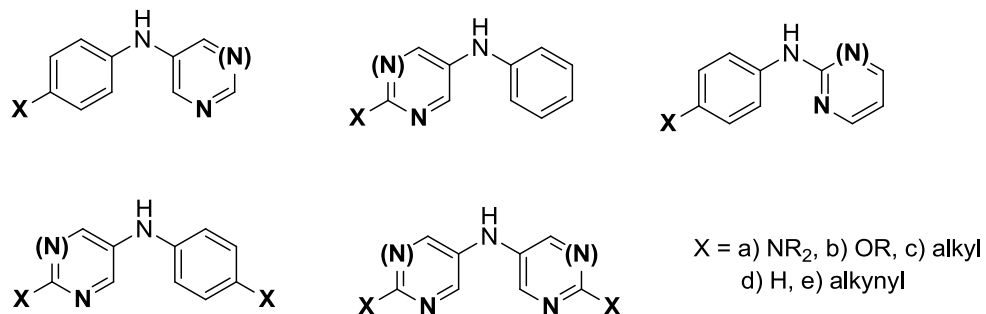
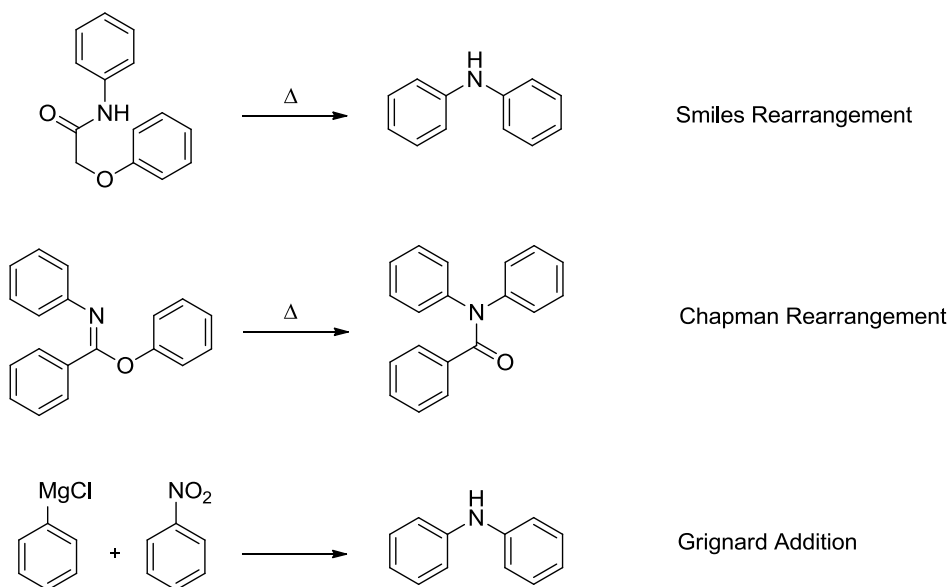


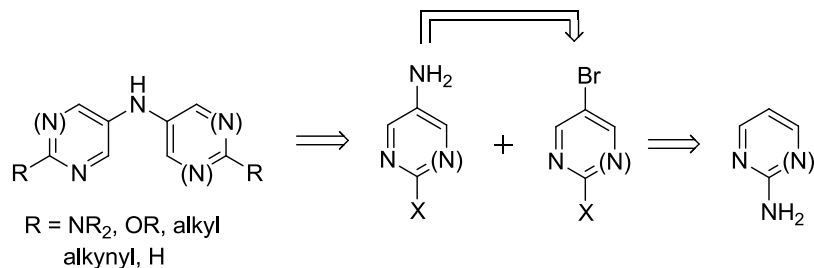
Figure 2.1. Target diarylamines.

It should be pointed out that few of these heterocyclic diarylamines have been described in the literature,⁵ and prior to our preliminary report,⁴ their radical chemistry had never been explored. The ‘modern’ method for preparing diarylamines is through the use of transition-metal catalysis; however, diarylamines can also be prepared by a number of ‘classical’ methods, including Smiles rearrangements of amides,⁶ Chapman rearrangement of imino ethers,⁷ or by addition of phenylmagnesium halides to nitrobenzenes⁸ or nitrosyl chlorides.⁹



Scheme 2.1. Non-transition metal catalyzed methods of preparing diarylamines.

We sought a modular synthetic strategy involving intermediates that could be used in multiple combinations to build up a small library that could be used to survey a broad a series of ring structures and substitutions (*cf.* figure 2.1). The development of transition-metal catalyzed (i.e. Pd, Cu, Ni, Fe) cross-coupling reactions of aryl halides and amines appeared to be the most convenient and versatile approach to accomplish this.¹⁰⁻¹² Herein we describe the application of this approach to the synthesis of a library of diarylamines that has enabled detailed studies of their radical-trapping antioxidant activities (see accompanying paper; Chapter 3).^{4,13}



Scheme 2.2. Library approach to heterocyclic diarylamines.

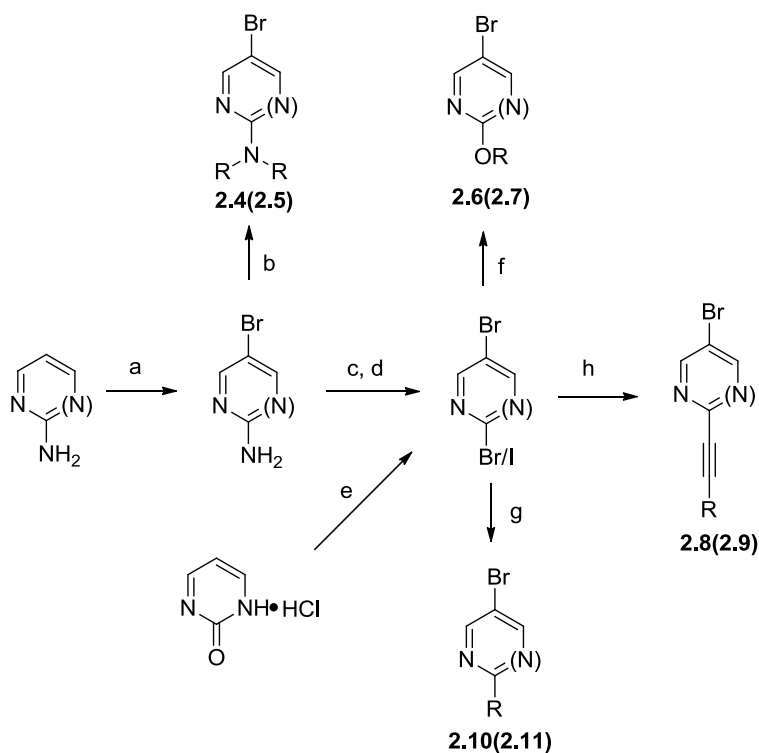
2.3 Results and Discussion

2.3.1 Preparation of 3-pyridyl and 5-pyrimidyl bromides

2-Aminopyridine and 2-aminopyrimidine were employed as common starting materials for each of the pyridyl and pyrimidyl halides due to their commercial availability at very low cost. Synthesis of the various pyridyl bromides began with bromination of the 5-position of 2-aminopyridine using NBS/NH₄OAc.¹⁴ This intermediate was either alkylated by reductive amination with appropriate aldehydes to prepare 5-bromo-2-*N,N*-dialkylaminopyridines (**2.4**) or subjected to aqueous¹⁵ or non-aqueous¹⁶ diazotization/halo-dediazotiation to afford 2,5-

dibromopyridine. This compound served as the precursor to all other substituted pyridines: 2-alkoxy-5-bromopyridines (**2.6**) were obtained by nucleophilic substitution with an appropriate sodium alkoxide,¹⁷ and 2-alkynyl-5-bromopyridine (**2.8**) and 2-alkyl-5-bromopyridines (**2.10**) were prepared via Sonogoshira¹⁸ and Negishi¹⁹ cross-coupling reactions, respectively.

The pyrimidyl bromides were prepared in a similar manner, beginning with bromination of 2-aminopyrimidine. *N*-Alkylation could not be achieved by reductive amination (presumably due to the decreased nucleophilicity of the amine) and was instead accomplished using NaH and an appropriate alkyl halide to give **2.5**. Non-aqueous diazotization/halo-dediazotiation was used to prepare 5-bromo-2-halopyrimidines, but in diminished yield relative to the analogous reaction with the 2-aminopyridine (again, presumably due to the decreased nucleophilicity of the amine group). Alternatively, 2-pyrimidinone could serve as a precursor to 5-bromo-2-halopyrimidines²⁰ or as a substrate for alkylation to generate 5-bromo-2-alkoxypyrimidines (**2.7**).²¹ Introduction of an alkyne substituent at the 2-position to give **2.9** proceeded satisfactorily under Sonogoshira conditions, but alkylation using Negishi conditions was unselective. Since reduction of the 2-alkynylpyrimidyl bromide **2.9** to the corresponding 2-alkyl pyrimidyl bromide **2.11** was complicated by competing removal of the bromine, we turned to 5-bromo-2-iodopyrimidine as a precursor for the cross coupling reactions and saw a dramatic improvement in selectivity and yields.



Scheme 2.3. Preparation of relevant pyri(mi)dyl halides **2.4-2.11**. Key: (a) NBS, NH_4OAc , MeCN, rt, 5 min, pyr: 85-90%; pym: quant; (b) pyr: RCHO, $\text{Na}(\text{CN})\text{BH}_3$, MeCN, reflux, 1-12h (82%, R = C_3H_{11}); pym: NaH, RI, THF, rt, overnight (85%, R = Me); (c) $\text{Me}_3(\text{Bn})\text{NBr}$, *t*-BuONO, CH_2Br_2 , rt, overnight, pyr: 77-83%; pym: 30-40%; (d) pym: HI, CH_2Cl_2 , 0 °C, 80-85%; (e) i. NaOH, Br_2 , H_2O , rt, 50-60%, ii. POCl_3 , PhNEt_2 , reflux, 4h, 75-85%, iii. HI, CH_2Cl_2 , 0°C, 80-85%; (f) ROH, Na, rt, 1-12 h, quant.; (g) RZnI , $\text{Cl}_2\text{Pd}(\text{PPh}_3)_2$, DMF/THF, rt, overnight, pyr (Br): 72% (R = C_6H_{13}), pym (I) 81%, (R = C_6H_{13}); (h) alkyne, CuI, $\text{Cl}_2\text{Pd}(\text{PPh}_3)_2$, Et_3N , MeCN, rt, 1-12 h, quant.

2.3.2 Preparation of 3-aminopyridines and 5-aminopyrimidines

With the substituted pyridyl and pyrimidyl bromides in hand, we attempted to install the amine functionality using a two-step procedure involving first a copper-catalyzed amination with benzylamine followed by reductive cleavage of the benzyl group.¹⁶ This method is attractive because the *N*-benzyl intermediate is stable to oxidative degradation, an attribute lacking in the more electron rich primary amines, which can undergo significant degradation upon prolonged storage. We found that CuI, L-proline and K_2CO_3 in DMSO at 80°C were general conditions that

afforded benzyl-protected amines in good yields from each of **2.4-2.11** as well as the unsubstituted 3-bromopyridine and 5-bromopyrimidine.

While removal of the benzyl group to afford the corresponding primary amines was easily achieved using Pd/C and ammonium formate in refluxing methanol for the more electron-rich compounds (R = NR₂, OR), these conditions were ineffective for the less electron-rich compounds (R = H, alkyl, alkynyl). Increasing catalyst loading, or changing to Pd(OH)₂ or Raney Nickel as catalyst did not improve the outcome up to several atmospheres of H₂.

To circumvent this problem, we attempted to install the desired primary amine directly. After screening reported conditions for the amination of aryl bromides with 'NH₂- equivalents' LiHMDS,²² ZnHMDS,²³ Li/NaNH₂¹² and *tert*-butylcarbamate²⁴ with either copper or palladium as catalysts with mixed results, we found that aqueous ammonia, in combination with CuI, L-proline and K₂CO₃ in DMSO at 90°C was most effective.²⁵ Coincidentally, this procedure was only successful for those pyridyl and pyrimidyl bromides for which the two-step benzylamination/hydrogenation sequence had failed at the latter step. The results are summarized in Table 2.1. Although the reactions generally proceeded with excellent conversions, the isolated yields reflect the difficulty associated with the purification of the more polar and/or oxidizable substrates and as such, the more electron rich amines were generally carried through without purification.

Table 2.1. Copper-catalyzed amination of 2-substituted 5-bromopyridines and 5-bromopyrimidines^a

Method A

Method B

Compound	R	Method	Yield ^b	Compound	R	Method	Yield ^b
	2.12 NMe ₂	A	74		2.19 NMe ₂	A	82
	2.13 N(C ₅ H ₁₁) ₂	A	87		2.20 NEt ₂	A	72
	2.14 OMe	A	62		2.21 OEtPh	A	51
	2.15 OBu	A	80		2.22 OCy	B	69
	2.16 C ₆ H ₉	B	95		2.23 C ₆ H ₉	B	84
	2.17 C ₆ H ₁₃	B	89		2.24 C ₆ H ₁₃	B	58
	2.18 H	B	93		2.25 H	B	66

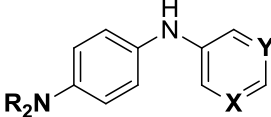
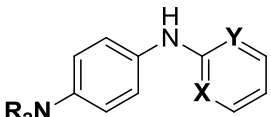
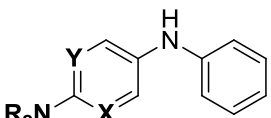
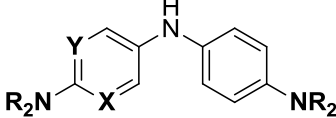
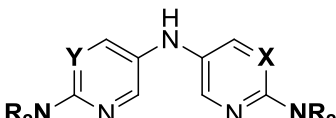
^aConditions A: 1.2 equiv BnNH₂, 1.5 equiv K₂CO₃, 0.1 equiv CuI, 0.2 equiv L-Proline, DMSO (1 mL/1.2 mmol ArBr) heated to 80 °C under argon. Conditions B: 1.5 equiv NH₄OH, 1.5 equiv K₂CO₃, 0.2 equiv CuI, 0.4 equiv L-Proline, DMSO (1 mL/1 mmol ArBr) heated to 90 °C in a sealed tube. ^bIsolated yields.

2.3.3 Preparation of Diarylamines

A great number of phosphine ligands have been developed for Pd-catalyzed C-N bond forming reactions, and indeed our original ligand screen showed a broad structural variety of phosphines were useful when coupling substituted bromo-pyri(mi)dines with aniline (e.g. BINAP, Josiphos, SPhos, DPPF). However, 2-dicyclohexylphosphino-2', 4', 6'-triisopropyl-biphenyl (XPhos)¹¹ gave consistently good results, showing the least sensitivity to the electronics of the aryl bromides and also has the added benefit of being air stable and therefore easily handled. Based on these results, we settled on a general catalytic system of 2 mol% Pd₂(dba)₃ as

a palladium source along with 4 mol% XPhos as a ligand. A series of dialkylamino-substituted pyridine and pyrimidine-based diarylamines was prepared, with alkyl groups varied to improve solubility in hydrocarbon solvents, as shown in Table 2.2. The conversions were very good for nearly all of the substrates shown, with the exception being 2-substituted pyrimidine **2.30**; however, the isolated yields in some cases do not reflect product conversion due to difficulty with purification and/or sensitivity to oxidation in solution. We surmise that the poor reactivity of 2-aminopyrimidine used to prepare **2.30** is due the relatively low pK_a (6.8) of this compound,²⁶ and corresponding poor nucleophilicity. Switching nucleophile and electrophile and using *N,N*-dimethylbenzene-1,4-diamine and 2-bromopyrimidine also resulted in poor yields due to competing reduction of the aryl bromide by the highly electron-rich aryl amine.

Table 2.2. *N,N*-Dialkylamino-substituted diarylamines prepared by palladium-catalyzed cross-couplings of aryl bromides and aryl amines.

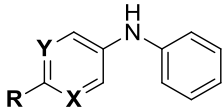
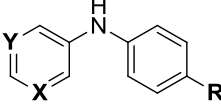
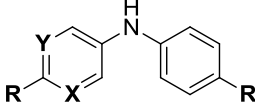
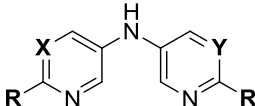
$\text{Ar-Br} + \text{Ar}'\text{-NH}_2 \xrightarrow[\text{toluene, 90 }^\circ\text{C}]{\text{Pd}_2\text{dba}_3, \text{XPhos, NaO}^t\text{Bu}}$				$\text{Ar-NH-Ar}'$	
Structure		X	Y	R	Yield ^a
	2.26	CH	CH	Me	93 b
	2.27	N	CH	Me	74 b
	2.28	N	N	Pr	77 b
	2.29	N	CH	Me	80 b
	2.30	N	N	Pr	45 b
	2.31	N	CH	Me	94
	2.32	N	N	Me	93
	2.33	CH	CH	Me	89
	2.34	N	CH	Me	62
	2.35	N	N	Pr	87 b
	2.36	CH	CH	Me	72
	2.37	N	CH	Et/Me	91
	2.38	N	N	Et	81 b

^aIsolated yields. Reaction conditions: ArBr (1.0 mmol), ArNH₂ (1.1 mmol), Pd (2 mol %), XPhos (4 mol%), NaO^tBu (1.4 mmol) in degassed toluene (2 mL) heated to 90 °C. ^bReactions done using Pd(η³-1-PhC₃H₄)(η⁵-C₅H₅) (**2.65**).

A similar set of compounds was prepared having alkyl substituents that will allow us to explore the effect of heteroatom incorporation on stability and reactivity using the industry standards (4,4'-dialkyldiphenylamines) as a baseline for comparison (Table 2.3). The isolated yields for these compounds are generally quite good. As noted previously, compounds such as those with unsubstituted pyrimidines (**2.45**) can be difficult to purify by chromatography.

Table 2.3. Alkyl-substituted diarylamines prepared by palladium-catalyzed cross-couplings of aryl bromides and aryl amines.

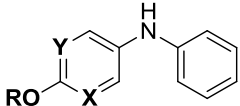
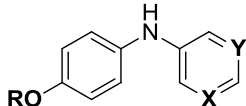
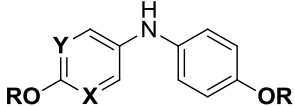
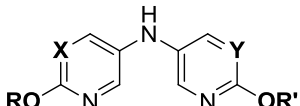
$$\text{Ar-Br} + \text{Ar}'\text{-NH}_2 \xrightarrow[\text{toluene, 90 } ^\circ\text{C}]{\text{Pd}_2\text{dba}_3, \text{XPhos, NaO}^t\text{Bu}} \text{Ar-NH-Ar}'$$

Compound	X	Y	R/R'	Yield ^a	
	2.39	CH	CH	C ₈ H ₁₇	86
	2.40	N	CH	C ₆ H ₁₃	88
	2.41	N	N	C ₇ H ₁₅	83
	2.42	N	CH	H	94 b
	2.43	N	N	H	82 b
	2.44	N	CH	Bu	73
	2.45	N	N	Bu	62
	2.46	CH	CH	C ₈ H ₁₇	86 b
	2.47	N	CH	C ₆ H ₁₃ /Bu	62
	2.48	N	N	C ₆ H ₁₃ /Bu	84
	2.49	CH	CH	C ₆ H ₁₃	85
	2.50	N	CH	C ₆ H ₁₃ /C ₇ H ₁₅	71
	2.51	N	N	C ₇ H ₁₅	81
	2.52	CH	CH	H	89 b
	2.53	N	N	H	77 b

^aIsolated yields. Reaction conditions: ArBr (1.0 mmol), ArNH₂ (1.1 mmol), Pd (2 mol %), XPhos (4 mol%), NaO^tBu (1.4 mmol) in degassed toluene (2 mL) heated to 90 °C. ^bReactions done using Pd(η³-1-PhC₃H₄)(η⁵-C₅H₅) (**2.65**).

To round out the series, a set of alkoxy-substituted compounds was prepared that should have reactivities/stabilities in between the dialkylamino- and alkyl-compounds (Table 2.4). In the case of alkoxy-substituted compounds the reaction becomes more complicated because the alkoxide represents a reasonable leaving group, and when in the electrophilic 2-position of a pyridine or pyrimidine ring and in the presence of a nucleophilic amine coupling partner a competing S_NAr reaction can occur. This is reflected in some of the isolated yields – although we found the use of bulkier alkyl groups helped to minimize the undesired substitution reaction.

Table 2.4. Alkoxy-substituted diarylamines prepared by palladium-catalyzed cross-couplings of aryl bromides and aryl amines.

Ar-Br + Ar'-NH ₂		Pd ₂ dba ₃ , XPhos, NaO ^t Bu toluene, 90 °C		Ar-NH-Ar'	
Compound	X	Y	R/R'	Yield ^a	
	2.54	CH	CH	Me	90
	2.55	N	CH	Me	93
	2.56	N	N	Cy	57
	2.57	N	CH	Me	98 b
	2.58	N	N	Me	87 b
	2.59	CH	CH	Me	96 b
	2.60	N	CH	Me	58 b
	2.61	N	N	EtPh	84 b
	2.62	CH	CH	Me	98
	2.63	N	CH	EtPh/Bu	43
	2.64	N	N	N/A	N/A

^aIsolated yields. Reaction conditions: ArBr (1.0 mmol), ArNH₂ (1.1 mmol), Pd (2 mol %), XPhos (4 mol%), NaO^tBu (1.4 mmol) in degassed toluene (2 mL) heated to 90 °C. ^bReactions done using Pd(η³-1-PhC₃H₄)(η⁵-C₅H₅) (**2.65**).

Unfortunately, the symmetrical 2-alkoxypyrimidine compound (**2.64**) could not be prepared by the C-N coupling approach as the amines always underwent nucleophilic substitution at the 2-position prior to the desired coupling. Because products were obtained for **2.56**, **2.61** and **2.63** – compounds which also feature 2-alkoxypyrimidine rings – we suspect the desired coupling reaction is sluggish due to the arylamine coupling partner not readily participating in the catalytic cycle. We attempted to decrease the rate of nucleophilic substitution relative to that of amine ligation to palladium by using relatively bulky alkyl substituents (-OCy, -OMeCy, -OBn, -OEtPh, etc.), keeping in mind that the substituent must be small enough to allow conjugation of the oxygen p-orbital (lone pair) with the pyrimidine ring to be effective as an antioxidant. However, none of these compounds gave the desired result.

2.3.4 Determining the Optimal Palladium Pre-catalyst

Although the Pd₂(dba)₃/XPhos catalyst system was clearly effective for the preparation of the bulk of the diarylamines shown in Tables 2.2-2.4, we later found that the use of the little used Pd(η³-1-PhC₃H₄)(η⁵-C₅H₅) precatalyst (**2.65**) in place of Pd₂(dba)₃ afforded higher isolated yields in essentially all cases where a direct comparison was made. We suspect that the increased yields from the **2.65**/XPhos system can be attributed to the rapid and *irreversible* formation of the active PdL₂ catalyst²⁷ compared to when Pd₂(dba)₃ is used, which remains in *equilibrium* with PdL₂. Although a detailed quantitative comparison of the performance of these two Pd precatalysts in Buchwald-Hartwig amination chemistry is well beyond the objectives of our work, we did monitor the reaction progress of three representative reactions under otherwise identical conditions to provide some insight into their differing performance. The first two reactions (Figure 2.2A and 2.2B) were randomly chosen from the many examples given above,

and the third was selected because it was a particularly problematic literature reaction (Figure 2.2C); the diarylamine product could be obtained in a modest 56% yield, but required high precatalyst loading ($\text{Pd}(\text{OAc})_2$, 15 mol%), large amounts of ligand (XantPhos, 30 mol%), long reaction time (48 h) and utilized 3-iodo-2-chloropyridine as a more reactive coupling partner than the corresponding 3-bromo-2-chloropyridine (which we used below).²⁸ In each case, we monitored reaction progress under typical preparative conditions at regular time intervals by gas chromatography using hexadecane as an internal standard. The results are shown in Figure 2.2.

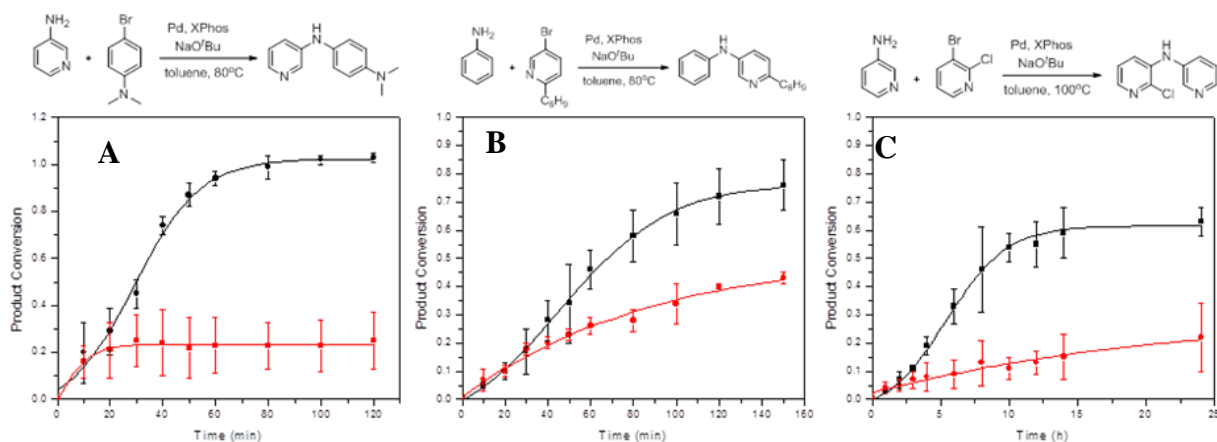


Figure 2.2. Comparative reaction profiles for a series of cross-coupling reactions where either **2.65** (●) or $\text{Pd}_2(\text{dba})_3$ (■) was used a pre-catalyst. Reactions A and B: Pd (1 mol %), XPhos (2 mol %), ArBr (1 mmol), ArNH₂ (1.1 mmol), NaO^tBu (1.4 mmol) in toluene (2 mL) at 80 °C. Reaction C: Pd (3 mol %), XPhos (6 mol %), ArBr (1 mmol), ArNH₂ (1.3 mmol), NaO^tBu (1.4 mmol) in toluene (3 mL) at 100 °C. All reactions were done with 0.1 mmol hexadecane as an internal standard. Data were fit to sigmoidal functions; no attempt was made to analyze the kinetics of these reactions.

The reaction progress data clearly show higher rates of catalyst turnover when **2.65** is used in place of $\text{Pd}_2(\text{dba})_3$ as the precatalyst. Since the actual catalyst in both cases is the same [$\text{Pd}(\text{XPhos})_2$], the different rates must arise from different concentrations of the catalyst available

to turnover. This is consistent with the observed rapid, *irreversible* formation of PdL₂ from **2.65** and phosphine ligands. It is interesting to note that the initial rates of the reactions utilizing **2.65** are slowed due to the presence of an induction period. We ascribe this induction period to the undesired formation of coordination complexes between the Lewis basic pyridines and **2.65** in competition with reductive elimination to form the active PdL₂ species (Scheme 2.4).²⁷ As the PdL₂ catalyst forms, it is less electrophilic than the precatalyst and less likely to form unreactive coordination complexes, leading to a steady increase in concentration of active catalyst and therefore an increased rate of product formation. A recent report comparing **2.65** with other Pd precatalysts for the Suzuki-Miyaura coupling of bromoanisole and phenylboronic acid do not display induction periods, presumably because of the lack of competitively coordinating substrates.²⁹



Scheme 2.4. Proposed origin of the induction periods observed in reactions shown in Figure 2.1: competition between reversible formation of the Lewis-base (B) coordination complex of **2.65** and irreversible reductive elimination of the Cp and Cinn ligands of **2.65** in the presence of XPhos to form the catalytically active Pd(XPhos)₂.

Unlike with **2.65**, the formation of inactive coordination complexes with Pd₂(dba)₃ remains in continuous equilibrium with formation of PdL₂ – each intermediate (e.g. (dba)PdL₂)³⁰ can form new complexes with Lewis bases. This equilibrium may explain why the product yields are much lower than reactions using **2.65** for A, B and C in Figure 2.2 – the concentration of active catalyst never reaches a sustained level suitable for catalysis to occur. The relative Lewis-basicities of the substrates support this explanation, as the Pd₂(dba)₃ product yields are lower for

the reactions with 3-aminopyridine as a substrate (A and C in Figure 2.2) than for 2-hexynylpyridine (Figure 2.2B).

3.4 Conclusions

Using our methodology, a small library of *para*-substituted symmetrical and unsymmetrical diarylamine antioxidants were synthesized, and upon their preparation we could readily see that with nitrogen incorporated into the aromatic rings the diarylamines were much more stable to oxidation. For example, on comparing the series of symmetrically-substituted diarylamines in Table 2.1, compounds **2.27** and **2.30** became intensely colored (due to formation of a radical cation, *vide supra*) almost immediately upon exposure to air in solution, while compounds **2.29**, **2.31** and **2.32** containing heteroatoms appear to be bench stable. Quantitative measurements (voltammetry) to determine each diarylamines' stability to one-electron oxidation as well as kinetic measurements to determine their reactivity with alkyl, alkoxy and peroxy radicals are detailed in a separate manuscript (Chapter 3).

In conclusion, we have presented a simple, modular approach to synthesizing a variety of *para*-substituted pyridine and pyrimidine-based diarylamine antioxidants. General conditions for Cu-catalyzed amination of pyridyl and pyrimidyl-bromides have been described, by choosing an appropriate nitrogen nucleophile to match the electronics of the aryl-bromide. We have also described general conditions for synthesizing heterocycle-based diarylamines under Buchwald-type amination conditions that are effective for electronically-diverse coupling partners.

2.5 Experimental Section

2.5.1 General

Reagents were purchased from commercial suppliers and used without further purification, unless otherwise indicated. $\text{Pd}(\eta^3\text{-1-PhC}_3\text{H}_4)(\eta^5\text{-C}_5\text{H}_5)$ (**2.65**) was synthesized from $[\text{Pd}(\eta^3\text{-1-PhC}_3\text{H}_4)\text{Cl}]_2$ and NaCp as described by Baird *et al.*²⁹ Column chromatography was carried out using flash silica gel (60 Å, 40-63 μ, 500 m²/g). ¹H and ¹³C NMR were recorded at 25 °C on a Bruker AVANCE spectrometer at 400 MHz and 100 MHz respectively, unless otherwise indicated. High resolution mass spectra were obtained by electron impact ionization on a Kratos Concept Tandem mass spectrometer. Melting points were obtained using a Gallenkamp melting point apparatus.

2.5.2 Cu-Catalyzed Benzylamination of Pyri(mi)dyl Bromides

To a schlenk flask was added ArBr (1.0 mmol), CuI (0.2 mmol), L-Proline (0.4 mmol) and K₂CO₃ (1.5 mmol). The flask was evacuated and backfilled with argon before degassed DMSO (1.5 mL) was added. After a few minutes of stirring, BnNH₂ (1.2 mmol) was added and the reaction heated to 80 °C until completion, as determined by TLC. The reaction was cooled, quenched with water and extracted with Et₂O. The combined organics were washed twice with water, washed with brine and dried over MgSO₄. Column chromatography (EtOAc/hexanes eluent) afforded pure products.

***N*⁵-benzyl-*N*²,*N*²-dimethylpyridine-2,5-diamine** (2.12)

Yield: 74% yellow solid. ¹H NMR (CDCl₃, 400 MHz) δ ppm 7.74 (d, *J* = 2.9 Hz, 1H), 7.38-7.31

(m, 4H), 7.28-7.25 (m, 1H), 6.95 (dd, $J = 8.9, 2.9$ Hz, 1H), 6.48 (dd, $J = 8.9, 0.6$ Hz, 1H), 4.27 (s, 2H), 3.56 (brs, 1H), 2.99 (s, 6H). ^{13}C NMR (CDCl_3 , 100 MHz) δ ppm 154.215, 139.465, 135.578, 133.392, 128.579, 127.537, 127.198, 124.804, 106.957, 49.613, 38.926. m.p. 69-70 °C. HRMS (EI) m/z calculated 224.1422, found 227.1419.

***N*⁵-benzyl-*N*²,*N*²-dipentylpyridine-2,5-diamine (2.13)**

Yield: 87% yellow needles. ^1H NMR (CDCl_3 , 400 MHz) δ ppm 7.71 (d, $J = 2.8$ Hz, 1H), 7.38-7.28 (m, 5H), 6.92 (dd, $J = 9.0, 2.8$ Hz, 1H), 6.36 (d, $J = 9.0$ Hz, 1H), 4.25 (s, 2H), 3.45 (brs, 1H), 3.34 (t, $J = 7.6$ Hz, 4H), 1.55 (qt, $J = 7.6$ Hz, 4H), 1.37-1.24 (m, 9H), 0.89 (t, $J = 7.0$ Hz, 6H). ^{13}C NMR (CDCl_3 , 100 MHz) δ ppm 152.456, 139.633, 134.657, 133.521, 128.341, 127.366, 126.909, 124.799, 106.084, 49.615, 48.829, 29.249, 27.378, 22.514, 13.973. m.p. 32-33 °C (Hexanes). HRMS (EI) m/z calculated 337.2518, found 337.2519.

***N*-benzyl-6-methoxypyridin-3-amine (2.14)**

Yield: 62% white solid. ^1H NMR (CDCl_3 , 400 MHz) δ ppm 7.59 (d, $J = 2.8$ Hz, 1H), 7.38-7.32 (m, 4H), 7.30-7.28 (m, 1H), 6.99 (dd, $J = 8.8, 2.8$ Hz, 1H), 6.61 (dd, $J = 8.8, 0.6$ Hz, 1H), 4.29 (s, 2H), 3.86 (s, 3H). ^{13}C NMR (CDCl_3 , 100 MHz) δ ppm 157.442, 138.982, 138.965, 130.422, 128.671, 127.494, 127.371, 125.811, 110.756, 53.299, 49.128. m.p. 62-64 °C. HRMS (EI) m/z calculated 214.1106, found 214.1104.

***N*-benzyl-6-butoxypyridin-3-amine (2.15)**

Yield: 80%. ^1H NMR (CDCl_3 , 400 MHz) δ ppm 7.60 (d, $J = 2.8$ Hz, 1H), 7.38-7.28 (m, 5H),

6.99 (dd, $J = 8.8, 2.8$ Hz, 1H), 6.63 (d, $J = 8.8$ Hz, 1H), 4.29 (s, 2H), 4.17 (t, $J = 6.8$ Hz, 2H), 3.79 (brs, 1H), 1.78 (qt, $J = 7.2$ Hz, 2H), 1.03 (t, $J = 7.2$ Hz, 3H). ^{13}C NMR (CDCl_3 , 100 MHz) δ ppm 157.319, 139.016, 138.831, 130.495, 128.585, 127.418, 127.262, 125.597, 110.799, 67.383, 49.038, 22.439, 10.489. m.p. 51-52 °C. HRMS (EI) m/z calculated 242.1419, found 242.1381.

***N*⁵-benzyl-*N*²,*N*²-dimethylpyrimidine-2,5-diamine (2.19)**

Yield: 82 % yellow solid. 7.93 (s, 2H), 7.36-7.24 (m, 5H), 4.25 (s, 2H), 3.11 (s, 6H). ^{13}C NMR (CDCl_3 , 100 MHz) δ ppm 144.541, 144.508, 138.485, 132.523, 128.715, 127.595, 127.507, 49.679, 37.644. m.p. 89-90 °C. HRMS (EI) m/z calculated 228.1375, found 228.1373.

***N*⁵-benzyl-*N*²,*N*²-diethylpyrimidine-2,5-diamine (2.20)**

Yield: 72% yellow solid. ^1H NMR (CDCl_3 , 400 MHz) δ ppm 7.93 (s, 2H), 7.37-7.27 (m, 5H), 4.24 (s, 2H), 3.55 (q, $J = 7.0$ Hz, 4H), 3.41 (brs, 1H), 1.15 (t, $J = 7.0$ Hz, 6H). ^{13}C NMR (CDCl_3 , 100 MHz) δ ppm 156.598, 145.035, 139.023, 132.458, 128.652, 127.538, 127.362, 49.867, 41.883, 13.202. m.p. 89-90 °C. HRMS (EI) m/z calculated 256.1688, found 256.1668.

***N*-benzyl-2-phenethoxypyrimidin-5-amine (2.21)**

Yield: 51% white solid. ^1H NMR ($(\text{CD}_3)_2\text{CO}$, 400 MHz) δ ppm 8.03 (s, 2H), 7.34-7.27 (m, 4H), 7.22-7.18 (m, 1H), 4.54 (brs, 1H), 4.40 (t, $J = 7.1$ Hz, 2H), 3.04 (t, $J = 7.1$ Hz, 2H). ^{13}C NMR ($(\text{CD}_3)_2\text{CO}$, 100 MHz) δ ppm 146.772, 140.748, 130.852, 130.147, 128.037, 69.079, 37.111. m.p. 78-79 °C. HRMS (EI) m/z calculated 215.1059, 215.1060.

2.5.3 Direct Amination of Pyri(mi)dyl Bromides

To a tube equipped with a threaded Teflon screw-cap was added ArBr (1.0 mmol), CuI (0.2 mmol), L-Proline (0.4 mmol) and K₂CO₃ (1.5 mmol). The vessel was evacuated and backfilled with argon before DMSO (1 mL). After stirring a few minutes, NH₄OH (28%, 1.5 mmol) was added, the tube was sealed and the reaction heated to 90 °C for 12 h. After cooling, the reaction was quenched with water and extracted with Et₂O. The organics were washed with brine and dried over MgSO₄. Column chromatography (EtOAc/hexanes/Et₃N eluent) afforded pure products.

6-(hex-1-ynyl)pyridin-3-amine **(2.16)**

Yield: 95% yellow solid. ¹H NMR (CDCl₃, 300 MHz) δ ppm 8.02 (s, 1H), 7.16 (d, *J* = 8.3 Hz, 1H), 6.88 (dd, *J* = 2.1, 8.3 Hz, 1H), 3.80 (s, 2H), 2.41 (t, *J* = 6.6 Hz, 2H), 1.44-1.64 (m, 4H), 0.93 (t, *J* = 7.1 Hz, 3H). ¹³C NMR (CDCl₃, 100 MHz) δ ppm 141.436, 137.152, 133.619, 127.103, 121.326, 88.497, 30.601, 22.025, 18.987, 13.614. HRMS (EI) *m/z* calculated 174.1157, found 174.1150.

6-hexylpyridin-3-amine **(2.17)**

Yield: 89% yellow oil. ¹H NMR (CDCl₃, 400 MHz) δ ppm 7.95 (t, *J* = 1.6 Hz, 1H), 6.86-6.85 (m, 2H), 3.56 (bs, 2H), 2.60 (t, *J* = 8.0 Hz, 2H), 1.63-1.55 (m, 2H), 1.28-1.19 (m, 6H), 0.82 (t, *J* = 6.8 Hz, 3H). ¹³C NMR (CDCl₃, 100 MHz) δ ppm 152.304, 140.050, 136.522, 122.416, 122.388, 37.182, 31.577, 30.014, 28.861, 22.436, 13.920. HRMS (EI) *m/z* calculated 178.147, found 178.1475.

3-aminopyridine (2.18)

Yield: 93% peach-coloured solid. Spectral data are consistent with those of commercially obtained material.

2-(cyclohexyloxy)pyrimidin-5-amine (2.22)

Yield: % white solid. ¹H NMR (CDCl₃, 400 MHz) δ ppm 8.02 (s, 2H), 4.87-4.80 (m, 1H), 3.35 (brs, 2H), 2.01-1.97 (m, 2H), 1.81-1.76 (m, 2H), 1.58-1.49 (m, 3H), 1.43-1.22 (m, 3H). ¹³C NMR (CDCl₃, 100 MHz) δ ppm 159.202, 146.271, 134.679, 74.688, 31.667, 25.557, 23.844. m.p. 94-96 °C. HRMS (EI) *m/z* calculated 193.1215, found 193.1206.

2-(hex-1-ynyl)pyrimidin-5-amine (2.23)

Yield: 84% yellow solid. ¹H NMR (CDCl₃, 400 MHz) δ ppm 8.12 (s, 2H), 3.94 (brs, 2H), 2.39 (t, *J* = 7.0 Hz, 2H), 1.58 (qt, *J* = 7.0 Hz, 2H), 1.45 (qt, *J* = 7.2 Hz, 2H), 0.89 (t, *J* = 7.2 Hz). ¹³C NMR (CDCl₃, 100 MHz) δ ppm 143.577, 142.691, 138.986, 87.352, 30.216, 21.987, 18.797, 13.539. HRMS (EI) *m/z* calculated 175.1109, found 179.1108.

6-hexylpyrimidin-5-amine (2.24)

Yield: 58% off white solid. ¹H NMR (CDCl₃, 400 MHz) δ ppm 8.13 (s, 2H), 6.34 (brs, 2H), 2.81 (t, *J* = 7.7 Hz, 2H), 1.73 (qt, *J* = 7.7 Hz, 2H), 1.33-1.27 (m, 6H), 0.84 (t, *J* = 7.0 Hz, 3H). ¹³C NMR (CDCl₃, 100 MHz) δ ppm 161.924, 143.401, 137.726, 38.409, 31.621, 28.997, 28.941, 22.508, 14.006. m.p. 107-108 °C HRMS (EI) *m/z* calculated 179.1423, found 179.1407.

5-aminopyrimidine

(2.25)

Yield: 66% pale-yellow solid. Spectral data are consistent with those of commercially obtained material.

2.5.4 Deprotection of N-benzylamines

To a solution of benzyl-protected amine (1.0 mmol) in EtOH (5 mL) degassed with argon was added 10% Pd/C (10 wt. %) and ammonium formate (5.0 mmol). The solution was heated to reflux until completion, as determined by TLC. When complete, the solution was cooled, diluted with EtOAc and filtered through a pad of silica. No further purification was attempted due to oxidative instability and difficulty associated with chromatographing these compounds.

2.5.5 General procedure for synthesis of diarylamines

To a schlenk flask was added **2.65** (or Pd₂dba₃, 0.005-0.02 mmol) and XPhos (Pd:L = 1:2). The flask was evacuated and backfilled with argon before degassed toluene (2 mL) was added and the solution heated to 60 °C. After 10 min, ArBr (1.0 mmol), ArNH₂ (1.1 mmol) and NaO^tBu (1.4 mmol) were added and the reaction was heated to the desired temperature. Once complete, the mixture was cooled and quenched by filtering through celite. Column chromatography (EtOAc/Hexanes eluent with 1-5% Et₃N added depending on substrate) afforded pure products.

*N*¹,*N*¹-dimethyl-*N*⁴-phenylbenzene-1,4-diamine

(2.26)

Yield: 93 % off-white needles. ¹H NMR ((CD₃)₂CO, 400 MHz) δ ppm 7.13-7.09 (m, 2H), 7.01 (dt, *J* = 8.5, 3.5 Hz, 2H), 6.88-6.86 (m, 2H), 6.80 (brs, 1H), 6.70-6.65 (m, 3H), 3.24 (d, *J* = 7.5

Hz, 4H), 1.59 (sextet, $J = 7.5$ Hz, 4H), 0.92 (t, $J = 7.5$ Hz, 6H). m.p. 129-130 °C. HRMS (EI) m/z calculated 212.1313, found 212.1304. Spectral data are consistent with those in the literature.³¹

***N*¹,*N*¹-dimethyl-*N*⁴-(pyridin-3-yl)benzene-1,4-diamine** (2.27)

Yield: 74 % yellow needles. ¹H NMR ((CD₃)₂CO, 400 MHz) δ ppm 8.23 (d, $J = 2.6$ Hz, 1H), 7.91 (dd, $J = 4.5, 1.2$ Hz, 1H), 7.20 (ddd, $J = 8.3, 2.6, 1.2$ Hz, 1H), 7.13 (brs, 1H), 7.10-7.06 (m, 3H), 6.79-6.75 (m, 2H), 2.89 (s, 6H). ¹³C NMR ((CD₃)₂CO, 100 MHz) δ ppm 149.303, 144.865, 140.867, 139.425, 133.391, 125.254, 124.568, 124.493, 121.149, 115.595, 42.117. m.p. 145-147 °C. HRMS (EI) m/z calculated 213.1266, found 213.1257.

***N*¹,*N*¹-dipropyl-*N*⁴-(pyrimidin-5-yl)benzene-1,4-diamine** (2.28)

Yield: 93 % greenish solid. ¹H NMR (*d*₆-DMSO, 400 MHz) δ ppm 8.45 (s, 1H), 8.27 (s, 2H), 8.00 (brs, 1H), 7.02-6.98 (m, 2H), 6.66-6.61 (m, 2H), 3.19 (t, $J = 7.4$ Hz, 4H), 1.51 (sextet, $J = 7.5$ Hz, 4H), 0.88 (t, $J = 7.4$ Hz, 6H). ¹³C NMR (*d*₆-DMSO, 100 MHz) δ ppm 148.825, 145.968, 141.979, 141.026, 127.259, 124.656, 112.543, 52.982, 20.312, 11.373. m.p. 79-80 °C. HRMS (EI) m/z calculated 270.1845, found 270.1837.

***N*¹,*N*¹-dimethyl-*N*⁴-(pyridin-2-yl)benzene-1,4-diamine** (2.29)

Yield: 80% green solid. ¹H NMR (CDCl₃, 400 MHz) δ ppm 8.13 (ddd, $J = 5.0, 1.9, 0.9$ Hz, 1H), 7.39 (ddd, $J = 8.7, 7.2, 1.9$ Hz, 1H), 7.18 (d, $J = 8.7$ Hz, 1H), 6.75 (d, $J = 8.6$ Hz, 1H), 6.65-6.55 (m, 3H), 2.94 (s, 6H). ¹³C NMR (CDCl₃, 100 MHz) δ ppm 158.037, 148.322, 148.050,

137.490, 129.614, 124.903, 113.707, 113.555, 106.683, 40.977. m.p. 129-130 °C. HRMS (EI) m/z calculated 213.1266, found 213.1260.

***N*¹,*N*¹-dipropyl-*N*⁴-(pyrimidin-2-yl)benzene-1,4-diamine** (2.30)

Yield: 45 % dark green solid. ¹H NMR (CDCl₃, 400 MHz) δ ppm 8.33 (d, *J* = 4.8 Hz, 2H), 7.34-7.30 (m, 2H), 6.97 (brs, 1H), 6.62-6.22 (m, 2H), 6.59 (t, *J* = 4.8 Hz, 1H), 3.21 (t, *J* = 7.6 Hz, 4H), 1.65-1.55 (m, 4H), 0.92 (t, *J* = 7.4 Hz, 6H). ¹³C NMR (CDCl₃, 100 MHz) δ ppm 161.172, 158.069, 145.353, 127.228, 123.401, 112.314, 111.394, 53.182, 20.430, 11.461. m.p. 84-86 °C. HRMS (EI) m/z calculated 270.1844, found 270.1864.

***N*²,*N*²-dimethyl-*N*⁵-phenylpyridine-2,5-diamine** (2.31)

Yield: 94 % yellow solid. ¹H NMR (CDCl₃, 400 MHz) δ ppm 8.07 (d, *J* = 2.6 Hz, 1H), 7.36 (dd, *J* = 8.9, 2.7 Hz, 1H), 7.20-7.16 (m, 2H), 6.80-6.76 (m, 3H), 6.54 (d, *J* = 9.3 Hz, 1H), 5.35 (brs, 1H), 3.09 (s, 3H). ¹³C NMR (CDCl₃, 100 MHz) δ ppm 156.731, 146.475, 143.649, 133.943, 129.272, 127.533, 118.801, 114.256, 106.092, 38.450. m.p. 134-136 °C. HRMS (EI) m/z calculated 213.1266, found 213.1185.

***N*²,*N*²-dimethyl-*N*⁵-phenylpyrimidine-2,5-diamine** (2.32)

Yield: 93% yellow solid. ¹H NMR (CDCl₃, 400 MHz) δ ppm 8.26 (s, 2H), 7.21-7.16 (m, 2H), 6.80 (tt, *J* = 7.3, 1.0 Hz, 1H), 6.73-6.70 (m, 2H), 5.23 (brs, 1H), 3.20 (s, 6H). ¹³C NMR (CDCl₃,

100 MHz) δ ppm 159.913, 154.978, 146.353, 129.380, 125.268, 119.080, 113.893, 37.379. m.p. 111-112 °C. HRMS (EI) m/z calculated 214.1218, found 214.1197.

***N*¹-(4-(dimethylamino)phenyl)-*N*⁴,*N*⁴-dimethylbenzene-1,4-diamine (2.33)**

Yield: 89% beige solid. ¹H NMR ((CD₃)₂CO, 400 MHz) δ ppm 6.90 (d, J = 8.3 Hz, 4H), 6.70 (dt, J = 8.4, 3.4 Hz, 4H), 6.41 (brs, 1H), 2.82 (s, 12H). ¹³C NMR ((CD₃)₂CO, 100 MHz) Spectral data are consistent with that reported in the literature.³²

***N*⁵-(4-(dimethylamino)phenyl)-*N*²,*N*²-dimethylpyridine-2,5-diamine (2.34)**

Yield: 62% dark green solid. ¹H NMR (CDCl₃, 400 MHz) δ ppm 7.94 (d, J = 2.8 Hz, 1H), 7.28 (dd, J = 8.9, 2.8 Hz, 1H), 6.86-6.82 (m, 2H), 6.72-6.68 (m, 2H), 6.57 (dd, J = 8.9, 0.5 Hz, 1H), 6.39 (brs, 1H), 2.99 (s, 6H), 2.82 (s, 6H). ¹³C NMR (CDCl₃, 100 MHz) δ ppm 157.212, 147.357, 141.179, 138.789, 133.454, 131.217, 119.668, 116.501, 107.804, 42.732, 39.629. m.p. 111-112 °C. HRMS (EI) m/z calculated 256.1688, found 256.1674.

***N*⁵-(4-(dimethylamino)phenyl)-*N*²,*N*²-dimethylpyrimidine-2,5-diamine (2.35)**

Yield: 87% yellow needles. ¹H NMR (*d*-6 DMSO, 400 MHz) δ ppm 8.15 (s, 2H), 7.15 (brs, 1H), 6.74 (dd, J = 2.4, 6.8 Hz, 2H), 6.65 (dd, J = 2.4, 6.8 Hz, 2H), 3.07 (s, 3H), 2.77 (s, 3H). ¹³C NMR (*d*-6 DMSO, 100 MHz) δ ppm 157.971, 149.638, 144.656, 136.186, 128.849, 116.514, 114.485, 41.106, 36.959. m.p. 116-117 °C. HRMS (EI) m/z calculated 257.1640, found 257.1632.

***N*⁵-(6-(dimethylamino)pyridin-3-yl)-*N*²,*N*²-dimethylpyridine-2,5-diamine** (2.36)

Yield: 72% pale-green plates. ¹H NMR (CDCl₃, 400 MHz) δ ppm 7.91 (d, *J* = 2.4 Hz, 2H), 7.15 (dd, *J* = 2.8, 8.8 Hz, 2H), 6.46 (d, *J* = 8.8 Hz, 2H), 4.96 (brs, 1H), 3.02 (s, 12H). ¹³C NMR (CDCl₃, 100 MHz) δ ppm 155.707, 139.145, 131.279, 121.439, 106.440, 38.677. m.p. 113-114 °C. HRMS (EI) *m/z* calculated 257.1640, found 257.1646.

***N*⁵-(6-(dimethylamino)pyridin-3-yl)-*N*²,*N*²-diethylpyrimidine-2,5-diamine** (2.37)

Yield: 91% metallic green solid. ¹H NMR (CDCl₃, 400 MHz) δ ppm 8.11 (s, 2H), 7.87 (d, *J* = 2.8 Hz, 1H), 7.10 (dd, *J* = 2.8, 8.8 Hz, 1H), 6.46 (d, *J* = 8.8 Hz, 1H), 4.74 (brs, 1H), 3.58 (q, *J* = 7.0 Hz, 4H), 3.03 (s, 3H), 1.18 (t, *J* = 7.0 Hz, 6H). ¹³C NMR (*d*₆-acetone, 100 MHz) δ ppm 159.481, 157.140, 152.018, 139.499, 134.195, 131.236, 129.480, 108.020, 43.473, 39.636, 14.533. m.p. 102-103 °C. HRMS (EI) *m/z* calculated 286.1906, found 286.1907.

***N*⁵-(2-(diethylamino)pyrimidin-5-yl)-*N*²,*N*²-diethylpyrimidine-2,5-diamine** (2.38)

Yield: 78% yellow needles. ¹H NMR ((CD₃)₂CO, 400 MHz) δ ppm 8.11 (s, 4H), 6.24 (brs, 1H), 3.62 (q, 7.0 Hz, 8H), 1.14 (t, 7.0 Hz, 12H). ¹³C NMR ((CD₃)₂CO, 100 MHz) δ ppm 159.471, 151.307, 131.521, 43.488, 14.524. m.p. 72-73 °C. HRMS (EI) *m/z* calculated 315.2171, found 315.2150.

4-butyl-*N*-phenylaniline (2.39)

Yield: 95% yellow oil. ¹H NMR (CDCl₃, 400 MHz) δ ppm 7.27-7.23 (m, 2H), 7.10 (d, *J* = 6.0

Hz, 2H), 7.04-7.02 (m, 4H), 6.89 (t, $J = 7.2$ Hz, 1H), 5.68 (brs, 1H), 2.57 (t, $J = 6.7$ Hz, 2H), 1.63-1.57 (m, 2H), 1.37 (sextet, $J = 7.4$ Hz, 2H), 0.94 (t, $J = 7.4$ Hz, 3H). ^{13}C NMR (CDCl_3 , 100 MHz) δ ppm 143.810, 140.412, 136.029, 129.256, 129.168, 120.282, 118.662, 116.915, 34.911, 33.814, 22.334, 13.976. HRMS (EI) m/z calculated 225.1517, found 225.1495.

6-hexyl-*N*-phenylpyridin-3-amine (2.40)

Yield: 88% off-white semi-solid. ^1H NMR (CDCl_3 , 400 MHz) δ ppm 8.31 (d, $J = 2.4$ Hz, 1H), 7.37 (dd, $J = 8.4, 2.5$ Hz, 1H), 7.28-7.23 (m, 2H), 7.04-7.00 (m, 3H), 6.93 (tt, $J = 7.4, 1.0$ Hz, 1H), 5.92 (brs, 1H), 2.73 (t, $J = 7.8$ Hz, 2H), 1.70 (qt, $J = 7.4$ Hz, 2H), 1.37-1.26 (m, 6H), 0.88 (t, $J = 6.9$ Hz, 3H). ^{13}C NMR (CDCl_3 , 100 MHz) δ ppm 154.970, 142.860, 140.103, 137.057, 129.373, 125.389, 122.537, 121.038, 117.103, 37.478, 31.653, 30.002, 28.997, 22.526, 14.029. HRMS (EI) m/z calculated 254.1783, found 254.1796.

2-heptyl-*N*-phenylpyrimidin-5-amine (2.41)

Yield: 83% off-white solid. ^1H NMR (CDCl_3 , 400 MHz) δ ppm 8.49 (s, 2H), 7.30 (t, $J = 7.5$ Hz, 2H), 7.04 (d, $J = 7.5$ Hz, 2H), 7.01 (t, $J = 7.4$ Hz, 1H), 5.61 (brs, 1H), 2.90 (t, $J = 7.7$ Hz, 2H), 1.80 (qt, $J = 7.6$ Hz, 2H), 1.41-1.27 (m, 8H), 0.87 (t, $J = 6.8$ Hz, 3H). ^{13}C NMR (CDCl_3 , 100 MHz) δ ppm 163.995, 146.390, 141.558, 135.272, 129.699, 122.319, 117.759, 38.633, 31.759, 29.356, 29.137, 28.915, 22.637, 14.078. m.p. 71-72 °C. HRMS (EI) m/z calculated 269.1892, found 269.1873.

***N*-phenylpyridin-5-amine** (2.42)

Yield: 94% peachy solid. ¹H NMR (CDCl₃, 400 MHz) δ ppm 8.38 (d, *J* = 2.8 Hz, 1H), 8.16 (dd, *J* = 4.6, 1.2 Hz, 1H), 7.41 (ddd, *J* = 8.3, 2.8, 1.2 Hz, 1H), 7.33-7.28 (m, 2H), 7.16 (ddd, *J* = 8.3, 4.6, 0.4 Hz, 1H), 7.10-7.07 (m, 2H), 6.99 (tt, *J* = 7.4, 1.1 Hz, 1H), 5.88 (brs, 1H). ¹³C NMR (CDCl₃, 100 MHz) δ ppm 141.902, 141.813, 140.055, 139.806, 129.512, 123.667, 123.370, 121.999, 118.272. m.p. 139-140 °C. HRMS (EI) *m/z* calculated 170.0844, found 170.0820.

***N*-phenylpyrimidin-5-amine** (2.43)

Yield: 82% white solid. ¹H NMR ((CD₃)₂CO, 400 MHz) δ ppm 8.61 (s, 1H), 8.55 (d, *J* = 1.6 Hz, 2H), 7.72 (brs, 1H), 7.35-7.30 (m, 2H), 7.20-7.18 (m, 2H), 6.99 (tt, *J* = 7.4, 1.0 Hz, 1H). ¹³C NMR ((CD₃)₂CO, 100 MHz) δ ppm 152.006, 146.068, 143.581, 140.837, 131.367, 123.873, 120.146. m.p. 214-215 °C. HRMS (EI) *m/z* calculated 171.0796, found 171.0789.

***N*-(4-butylphenyl)pyridin-3-amine** (2.44)

Yield: 73%. ¹H NMR (CDCl₃, 400 MHz) δ ppm 8.33 (d, *J* = 2.8 Hz, 1H), 8.11 (dd, *J* = 4.6, 1.2 Hz, 1H), 7.35 (ddd, *J* = 8.2, 2.8, 1.2 Hz, 1H), 7.16-7.11 (m, 3H), 7.02 (dt, *J* = 8.4, 2.2 Hz, 2H), 5.67 (brs, 1H), 2.58 (t, *J* = 7.8 Hz, 2H), 1.63-1.55 (m, 2H), 1.36 (sextet, *J* = 7.4 Hz, 2H), 0.93 (t, *J* = 7.4 Hz, 3H). ¹³C NMR (CDCl₃, 100 MHz) δ ppm 140.931, 140.609, 139.094, 137.304, 129.422, 123.732, 122.606, 119.290, 99.971, 34.944, 33.754, 22.321, 13.962. m.p. 78-79 °C. HRMS (EI) *m/z* calculated 226.1470, found 226.1469.

***N*-(4-butylphenyl)pyrimidin-3-amine** (2.45)

Yield: 62% . ¹H NMR (CDCl₃, 400 MHz) δ ppm 8.72 (s, 1H), 8.49 (s, 2H), 7.17 (d, *J* = 8.4 Hz, 2H), 7.05 (d, *J* = 8.4 Hz, 2H), 5.76 (brs, 1H), 2.60 (t, *J* = 7.7 Hz, 2H), 1.64-1.56 (m, 2H), 1.36 (sextet, *J* = 7.5 Hz, 2H), 0.94 (t, *J* = 7.3 Hz, 3H). ¹³C NMR (CDCl₃, 100 MHz) δ ppm 149.610, 143.779, 139.197, 138.737, 137.487, 129.703, 120.132, 34.989, 33.663, 22.307, 13.937. m.p. 161-162 °C. HRMS (EI) *m/z* calculated 277.1422, found 227.1387.

Bis(4-octylphenyl)amine (2.46)

Yield: 86% beige solid. ¹H NMR (CDCl₃, 400 MHz) δ ppm 7.06 (d, *J* = 8.2 Hz, 4H), 6.97 (d, *J* = 8.2 Hz, 4H), 5.53 (brs, 1H), 2.54 (t, *J* = 7.6 Hz, 4H), 1.59 (quintet, *J* = 7.6 Hz, 4H), 1.37-1.27 (m, 20 H), 0.89 (t, *J* = 6.8 Hz, 6H). ¹³C NMR (CDCl₃, 100 MHz) δ ppm 141.219, 135.379, 129.121, 117.763, 35.221, 31.900, 31.717, 29.507, 29.337, 29.286, 22.678, 14.115. m.p. 35-36 °C.

***N*-(4-butylphenyl)-6-hexylpyridin-3-amine** (2.47)

Yield: 62% pale yellow solid. ¹H NMR (CDCl₃, 400 MHz) δ ppm 8.28 (d, *J* = 2.6 Hz, 1H), 7.32 (dd, *J* = 8.4, 2.8 Hz, 1H), 7.08 (d, *J* = 8.4 Hz, 2H), 7.02 (d, *J* = 8.4 Hz, 1H), 6.96 (dd, *J* = 8.4, 2.8 Hz, 2H), 5.60 (brs, 1H), 2.72 (t, *J* = 7.8 Hz, 2H), 2.56 (d, *J* = 7.6 Hz, 2H), 1.73-1.68 (m, 2H), 1.62-1.54 (m, 2H), 1.40-1.29 (m, 8H), 0.93 (d, *J* = 7.3 Hz, 3H), 0.88 (d, *J* = 7.0 Hz, 3H). ¹³C NMR (CDCl₃, 100 MHz) δ ppm 154.396, 140.187, 139.333, 137.813, 136.335, 129.330, 124.632, 122.575, 118.118, 37.440, 34.896, 33.783, 31.728, 30.060, 29.058, 22.591, 22.321, 14.075, 13.953. m.p. 39-40 °C. HRMS (EI) *m/z* calculated 310.2409, found 310.2406.

***N*-(4-butylphenyl)-2-hexylpyrimidin-5-amine** (2.48)

Yield: 84% off white solid. ^1H NMR (CDCl_3 , 400 MHz) δ ppm 8.44 (s, 2H), 7.12 (d, $J = 8.4$ Hz, 2H), 6.98 (d, $J = 8.4$ Hz, 2H), 5.54 (brs, 1H), 2.88 (t, $J = 7.8$ Hz, 2H), 2.57 (t, $J = 7.7$ Hz, 2H), 1.79 (qt, $J = 7.7$ Hz, 2H), 1.62-1.55 (m, 2H), 1.40-1.30 (m, 8H), 0.93 (d, $J = 7.3$ Hz, 3H), 0.88 (d, $J = 7.0$ Hz, 3H). ^{13}C NMR (CDCl_3 , 100 MHz) δ ppm 154.343, 140.205, 139.395, 137.760, 136.157, 129.260, 124.457, 122.489, 117.981, 37.458, 34.850, 33.748, 31.684, 30.044, 29.020, 22.549, 22.280, 14.039, 13.917. m.p. 73-74 °C. HRMS (EI) m/z calculated 311.2362, found 311.2360.

Bis(6-hexylpyridin-3-yl)amine (2.49)

Yield: 85% light red solid. ^1H NMR (CDCl_3 , 400 MHz) δ ppm 8.27 (d, $J = 2.8$ Hz, 2H), 7.29 (dd, $J = 8.4, 2.8$ Hz, 2H), 7.02 (d, $J = 8.4$ Hz, 2H), 5.96 (brs, 1H), 2.71 (t, $J = 7.8$ Hz, 4H), 1.68 (qt, $J = 7.8$ Hz, 4H), 1.35-1.28 (m, 12H), 0.86 (t, $J = 6.8$ Hz, 6H). ^{13}C NMR (CDCl_3 , 100 MHz) δ ppm 155.371, 139.724, 136.890, 124.839, 122.660, 37.513, 31.669, 29.977, 29.003, 22.542, 14.033. m.p. 44-45°C HRMS (EI) m/z calculated 339.2674, found 339.2685.

2-heptyl-*N*-(6-hexylpyridin-3-yl)pyrimidin-5-amine (2.50)

Yield: 71% white solid. ^1H NMR (CDCl_3 , 400 MHz) δ ppm 8.44 (s, 2H), 8.33 (d, $J = 2.8$ Hz, 1H), 7.35 (d, $J = 8.4, 2.8$ Hz, 1H), 7.09 (d, $J = 8.4$ Hz, 1H), 5.69 (brs, 1H), 2.90 (t, $J = 7.8$ Hz, 2H), 2.75 (d, $J = 7.8$ Hz, 2H), 1.83-1.67 (m, 4H), 1.39-1.27 (m, 14H), 0.89-0.85 (m, 6H). ^{13}C NMR (CDCl_3 , 100 MHz) δ ppm 164.473, 156.471, 146.049, 140.084, 135.760, 135.040, 125.542, 122.962, 38.664, 37.475, 31.752, 31.676, 29.916, 29.337, 29.125, 29.005, 28.887,

22.631, 22.566, 14.071, 14.058. m.p. 64-65 °C. HRMS (EI) m/z calculated 354.2784, found 354.2773.

Bis(2-heptylpyrimidin-5-yl)amine (2.51)

Yield: 81% white solid. ^1H NMR (CDCl_3 , 400 MHz) δ ppm 8.48 (s, 4H), 5.58 (brs, 1H), 2.92 (t, $J = 7.6$ Hz, 4H), 1.84-1.76 (m, 4H), 1.36-1.28 (m, 16H), 0.87 (t, $J = 6.4$ Hz, 6H). ^{13}C NMR (CDCl_3 , 100 MHz) δ ppm 165.473, 146.585, 134.057, 38.664, 31.743, 29.316, 29.108, 28.809, 22.627, 14.071. m.p. 103-104 °C. HRMS (EI) m/z calculated 369.2893, found 369.2892.

Dipyridin-3-ylamine (2.52)

Yield: 89% off-white solid. ^1H NMR ($(\text{CD}_3)_2\text{SO}$, 400 MHz) δ ppm 8.56 (brs, 1H), 8.37 (d, $J = 2.4$ Hz, 2H), 8.08 (dd, $J = 4.6, 1.2$ Hz, 2H), 7.50 (ddd, $J = 8.3, 2.4, 1.2$ Hz, 2H), 7.26 (dd, $J = 8.3, 4.6$ Hz, 2H). ^{13}C NMR ($(\text{CD}_3)_2\text{SO}$, 100 MHz) δ ppm 141.221, 139.387, 139.105, 123.830, 122.672. m.p. 129-131 °C. HRMS (EI) m/z calculated 171.0797, found 171.0787.

Dipyrimidin-5-ylamine (2.53)

Yield: 77% off-white solid. ^1H NMR ($(\text{CD}_3)_2\text{SO}$, 400 MHz) δ ppm 8.88 (brs, 1H), 8.75 (s, 2H), 8.66 (s, 4H). ^{13}C NMR ($(\text{CD}_3)_2\text{SO}$, 100 MHz) δ ppm 150.867, 145.043, 136.959. m.p. 226-228 °C. HRMS (EI) m/z calculated 173.0702, found 173.0692.

4-methoxy-*N*-phenylaniline (2.54)

Yield: 90 % white solid. m.p. 102-104 °C. Spectral data are consistent with those reported in the literature.³³

6-methoxy-*N*-phenylpyridin-3-amine (2.55)

Yield: 93% yellow oil. ¹H NMR (CDCl₃, 400 MHz) δ ppm 8.00 (dd, *J* = 2.8, 0.4 Hz, 1H), 7.45 (dd, *J* = 8.8, 2.8 Hz, 1H), 7.25-7.20 (m, 2H), 6.88-6.84 (m, 3H), 6.72 (dd, *J* = 8.8, 0.4 Hz, 1H), 5.44 (brs, 1H), 3.93 (s, 3H). ¹³C NMR (CDCl₃, 100 MHz) δ ppm 160.246, 144.819, 139.714, 133.208, 132.779, 129.414, 119.996, 115.396, 111.006, 53.521. HRMS (EI) *m/z* calculated 200.0950, found 200.0934.

2-(cyclohexyloxy)-*N*-phenylpyrimidin-5-amine (2.56)

Yield: 57% white needles. ¹H NMR (CDCl₃, 400 MHz) δ ppm 8.38 (s, 2H), 7.26-7.22 (m, 2H), 6.92-6.86 (m, 3H), 5.39 (brs, 1H), 4.98-4.91 (m, 1H), 2.07-2.03 (m, 2H), 1.86-1.80 (m, 2H), 1.65-1.57 (m, 5H), 1.47-1.26 (m, 3H). ¹³C NMR (CDCl₃, 100 MHz) δ ppm 161.003, 152.719, 143.986, 131.338, 129.590, 120.715, 115.527, 75.412, 31.642, 25.530, 23.860. m.p. 164-165 °C. HRMS (EI) *m/z* calculated 269.1528, found 269.1520.

***N*-(4-methoxyphenyl)pyridin-3-amine** (2.57)

Yield: 98% . ¹H NMR (CDCl₃, 400 MHz) δ ppm 8.25 (d, *J* = 2.4 Hz, 1H), 8.06 (dd, *J* = 4.7, 1.3 Hz, 1H), 7.20 (ddd, *J* = 8.3, 2.4, 1.3 Hz, 1H), 7.10 (d, *J* = 4.7 Hz, 1H), 7.09-7.06 (m, 2H), 6.90-

6.86 (m, 2H), 5.58 (brs, 1H), 3.81 (s, 3H). ¹³C NMR (CDCl₃, 100 MHz) δ ppm 155.910, 141.654, (140.660, 140.637), 138.372, 134.342, 123.635, 122.710, 121.127, 114.826, 55.550. m.p. 123-125 °C. HRMS (EI) *m/z* calculated 200.0950, found 200.0932.

***N*-(4-methoxyphenyl)pyrimidin-5-amine** (2.58)

Yield: 87% purple needles. ¹H NMR (CDCl₃, 400 MHz) δ ppm 8.69 (s, 1H), 8.35 (s, 2H), 7.13-7.09 (m, 2H), 6.93-6.89 (m, 2H), 5.47 (brs, 1H), 3.82 (s, 3H). ¹³C NMR (CDCl₃, 100 MHz) δ ppm 156.707, 149.992, 142.989, 139.917, 132.659, 123.445, 115.052, 55.562. m.p. 211-212 °C. HRMS (EI) *m/z* calculated 201.0902, found 201.0904.

Bis(4-methoxyphenyl)amine (2.59)

Yield: 96% white needles. m.p. 98-99 °C. Spectra are consistent with those reported in the literature.³⁴

6-methoxy-*N*-(4-methoxyphenyl)pyridin-3-amine (2.60)

Yield: 58% reddish oil. ¹H NMR (CDCl₃, 400 MHz) δ ppm 7.89 (d, *J* = 2.8 Hz, 1H), 7.31 (dd, *J* = 8.8, 2.8 Hz, 1H), 6.90-6.87 (m, 2H), 6.83-6.80 (m, 2H), 6.67 (d, *J* = 8.8 Hz, 1H), 5.32 (brs, 1H), 3.90 (s, 3H), 3.77 (s, 3H). ¹³C NMR (CDCl₃, 100 MHz) δ ppm 159.122, 154.392, 137.384, 136.604, 134.935, 130.669, 119.172, 114.751, 110.810, 55.559, 53.468. HRMS (EI) *m/z* calculated 230.1055, found 230.1042.

2-phenethoxy-N-(4-phenethoxyphenyl)pyrimidin-5-amine (2.61)

Yield: 84% white solid. ^1H NMR (CDCl_3 , 400 MHz) δ ppm 8.29 (d, $J = 1.2$ Hz, 2H), 7.35-7.29 (m, 8H), 7.23-7.20 (m, 2H), 7.02-6.98 (m, 2H), 6.90-6.86 (m, 2H), 4.47 (t, $J = 7.0$ Hz, 2H), 4.17 (t, $J = 6.9$ Hz, 2H), 3.09-3.04 (m, 4H). ^{13}C NMR (CDCl_3 , 100 MHz) δ ppm 155.692, 150.192, 141.216, 136.575, 130.872, 130.179, 128.068, 121.029, 117.417, 70.727, 69.452, 37.435, 37.031. m.p. 143-144 °C. HRMS (EI) m/z calculated 411.1947, found 411.1931.

Bis(6-methoxypyridin-3-yl)amine (2.62)

Yield: 98 % pale yellow oil. ^1H NMR ($(\text{CD}_3)_2\text{CO}$, 400 MHz) δ ppm 7.89 (d, $J = 2.8$ Hz, 2H), 7.41 (dd, $J = 8.8, 2.8$ Hz, 2H), 6.96 (brs, 1H), 6.69 (d, $J = 8.8$ Hz, 2H), 3.83 (s, 6H). ^{13}C NMR ($(\text{CD}_3)_2\text{CO}$, 100 MHz) δ ppm 160.756, 137.739, 137.158, 131.560, 112.461, 54.383. HRMS (EI) m/z calculated 231.1008, found 231.0996.

N-(6-butoxypyridin-3-yl)-2-phenethoxypyrimidin-5-amine (2.63)

Yield: 43 %. ^1H NMR ($(\text{CD}_3)_2\text{CO}$, 400 MHz) δ ppm 8.30 (d, $J = 1.2$ Hz, 2H), 7.92 (d, $J = 2.9$ Hz, 1H), 7.48 (dd, $J = 8.8, 2.9$ Hz, 1H), 7.35-7.29 (m, 4H), 7.23-7.19 (m, 1H), 7.05 (brs, 1H), 6.71 (d, $J = 8.5$ Hz, 1H), 4.48 (t, $J = 7.0$ Hz, 2H), 4.24 (d, $J = 6.6$ Hz, 2H), 3.08 (t, $J = 7.0$ Hz, 2H), 1.75-1.68 (m, 2H), 1.47 (st, $J = 7.5$ Hz, 2H), 0.96 (t, $J = 7.4$ Hz, 3H). ^{13}C NMR ($(\text{CD}_3)_2\text{CO}$, 100 MHz) δ ppm 162.034, 161.236, 150.207, 140.581, 138.667, 138.622, 136.396, 136.323, 135.591, 135.884, 132.160, 132.126, 130.878, 130.187, 128.115, 112.836, 69.514, 67.070, 37.016, 32.978, 20.955, 15.141. HRMS (EI) m/z calculated 364.1899, found 364.1895.

2.6 References

- (1) Klemchuk, P. P. In *Ullmann's Encyclopedia of Industrial Chemistry*; Wiley-VCH Verlag GmbH & Co. KGaA: **2000**.
- (2) Ingold, K. U. *Chemical Reviews* **1961**, *61*, 563.
- (3) Jensen, R. K.; Korcek, S.; Zinbo, M.; Gerlock, J. L. *Journal of Organic Chemistry* **1995**, *60*, 5396.
- (4) Hanthorn, J. J.; Valgimigli, L.; Pratt, D. A. *Journal of the American Chemical Society* **2012**, *Articles ASAP*. DOI: 10.1021/ja300086z
- (5) a) Mazu, T. K.; Etukala, J. R.; Jacob, M. R.; Khan, S. I.; Walker, L. A.; Ablordeppey, S. Y. *European Journal of Medicinal Chemistry* **2011**, *46*, 2378. b) Shen, Q. L.; Ogata, T.; Hartwig, J. F. *Journal of the American Chemical Society* **2008**, *130*, 8564. c) Grasa, G. A.; Viciu, M. S.; Huang, J. K.; Nolan, S. P. *Journal of Organic Chemistry* **2001**, *66*, 7729. d) Sato, M.; Katsushima, T.; Kinoshita, H. Japan, 1999. e) Peterson, L. H.; Tolman, R. L. *Journal of Heterocyclic Chemistry* **1977**, *14*, 527. f) Whitmore, F. C.; Mosher, H. S.; Goldsmith, D. P. J.; Rytina, A. W. *Journal of the American Chemical Society* **1945**, *67*, 393. g) Adams, R. R.; Whitmore, F. C. *Journal of the American Chemical Society* **1945**, *67*, 735.
- (6) Truce, W.; Krieder, E.; Brand, W. *Organic Reactions* **1971**, *18*, 99.
- (7) Schulenburg, J. W.; Archer, S. *Organic Reactions* **1965**, *14*, 1.
- (8) Sapountzis, I.; Knochel, P. *Journal of the American Chemical Society* **2002**, *124*, 9390.
- (9) Waters, W. L.; Marsh, P. G. *Journal of Organic Chemistry* **1975**, *40*, 3349.

- (10) Wolfe, J. P.; Wagaw, S.; Marcoux, J. F.; Buchwald, S. L. *Accounts of Chemical Research* **1998**, *31*, 805.
- (11) Anderson, K. W.; Tundel, R. E.; Ikawa, T.; Altman, R. A.; Buchwald, S. L. *Angewandte Chemie-International Edition* **2006**, *45*, 6523.
- (12) Schlummer, B.; Scholz, U. *Advanced Synthesis & Catalysis* **2004**, *346*, 1599.
- (13) Hanthorn, J. J.; Amorati, R.; Valgimigli, L.; Pratt, D. A. Accompanying Manuscript (Chapter 3).
- (14) Das, B.; Venkateswarlu, K.; Majhi, A.; Siddaiah, V.; Reddy, K. R. *Journal of Molecular Catalysis a-Chemical* **2007**, *267*, 30.
- (15) Bhasin, K. K.; Kumar, R.; Mehta, S. K.; Raghavaiah, P.; Jacob, C.; Klapotke, T. *M. Inorganica Chimica Acta* **2009**, *362*, 2386.
- (16) Nara, S. J.; Jha, M.; Brinkhorst, J.; Zemanek, T. J.; Pratt, D. A. *Journal of Organic Chemistry* **2008**, *73*, 9326.
- (17) Comins, D. L.; Killpack, M. O. *Journal of Organic Chemistry* **1990**, *55*, 69.
- (18) Tilley, J. W.; Zawoiski, S. *Journal of Organic Chemistry* **1988**, *53*, 386.
- (19) Getmanenko, Y. A.; Twieg, R. J. *Journal of Organic Chemistry* **2008**, *73*, 830.
- (20) Lutz, F.; Kawasaki, T.; Soai, K. *Tetrahedron-Asymmetry* **2006**, *17*, 486.
- (21) Kokatla, H. P.; Lakshman, M. K. *Organic Letters* **2010**, *12*, 4478.
- (22) Lee, S.; Jorgensen, M.; Hartwig, J. F. *Organic Letters* **2001**, *3*, 2729.
- (23) Lee, D. Y.; Hartwig, J. F. *Organic Letters* **2005**, *7*, 1169.
- (24) Qin, L. J.; Cui, H. M.; Zou, D. P.; Li, J. Y.; Wu, Y. J.; Zhu, Z. W.; Wu, Y. S. *Tetrahedron Letters* **2010**, *51*, 4445.
- (25) Kim, J.; Chang, S. *Chemical Communications* **2008**, 3052.

- (26) McGowan, M. A.; Henderson, J. L.; Buchwald, S. L. *Organic Letters* **2012**, *14*, 1432.
- (27) Norton, D. M.; Mitchell, E. A.; Botros, N. R.; Jessop, P. G.; Baird, M. C. *Journal of Organic Chemistry* **2009**, *74*, 6674.
- (28) Patriciu, O. I.; Finaru, A. L.; Massip, S.; Leger, J. M.; Jarry, C.; Guillaumet, G. *European Journal of Organic Chemistry* **2009**, 3753.
- (29) Fraser, A. W.; Besaw, J. E.; Hull, L. E.; Baird, M. C. *Organometallics* **2012**, *Articles ASAP*. DOI: 10.1021/om300154m
- (30) Amatore, C.; Jutand, A. *Coordination Chemistry Reviews* **1998**, *178*, 511.
- (31) Hill, L. L.; Smith, J. A.; Brown, W. S.; Moore, L. R.; Guevera, P.; Pair, E. S.; Porter, J.; Chou, J.; Wolterman, C. J.; Craciun, R.; Dixon, D. A.; Shaughnessy, K. H. *Tetrahedron* **2008**, *64*, 6920.
- (32) Pratt, D. A.; DiLabio, G. A.; Valgimigli, L.; Pedulli, G. F.; Ingold, K. U. *Journal of the American Chemical Society* **2002**, *124*, 11085.
- (33) Carroll, M. A.; Wood, R. A. *tetrahedron* **2007**, *63*, 11349.
- (34) McNulty, J.; Cheekoori, S.; Bender, T. P.; Coggan, J. A. *European Journal of Organic Chemistry* **2007**, 1423.

CHAPTER 3: THE REACTIVITY OF AIR-STABLE PYRIDINE- AND PYRIMIDINE-CONTAINING DIARYLAMINE ANTIOXIDANTS

3.1 Preface

We recently reported a preliminary account of our efforts to develop novel diarylamine radical-trapping antioxidants (Hanthorn et al. *J. Am. Chem. Soc.* **2012**, DOI: 10/1021/ja300086z), wherein we suggested that the incorporation of ring nitrogens into diphenylamines affords compounds which display a compromise between H-atom transfer reactivity to radicals and stability to one-electron oxidation. Herein we report the results of thermochemical and kinetic experiments on an expanded set of diarylamines which provides a complete picture of the structure-reactivity relationships of these compounds as antioxidants. Expanded substrate scope includes dialkoxy-substituted, mono-alkoxy-substituted and mono-*N,N*-dialkylamino-substituted diphenylamines that incorporate ring nitrogens and again show increased stability to one-electron oxidation without compromising antioxidant efficacy. These compounds provide evidence for additive substituent effects (Hammett correlations) with respect to rates of peroxy radical trapping. With expanded sets of N-H BDE data, rate constants for reactions with peroxy and primary alkyl radicals, Arrhenius parameters for reactions with peroxy radicals, kinetic solvent effect measurements and transition state calculations, we have compiled strong evidence that electron-rich diarylamines react with peroxy radicals via a proton-coupled electron transfer (PCET) mechanism. This chapter is largely as it was submitted to the *Journal of Organic Chemistry* as a back-to-back manuscript with the manuscript presented as Chapter 2.

3.2 Introduction

Diarylamines and phenols are widely used radical-trapping antioxidant additives that slow the oxidative degradation of oils, lubricants, polymers, plastics and fine chemicals.¹ Phenolic antioxidants are generally regarded as the more important of the two types, due to their prominence *in vivo* and the relative ease with which their reactivity can be manipulated by substitution of the aromatic ring. The introduction of electron-donating substituents (e.g. alkyl, alkoxy) weakens the phenolic O-H bond by stabilizing the inherently electron-poor phenoxyl radical that results from H-atom transfer to autoxidation chain-carrying peroxy radicals (Eq. 1):



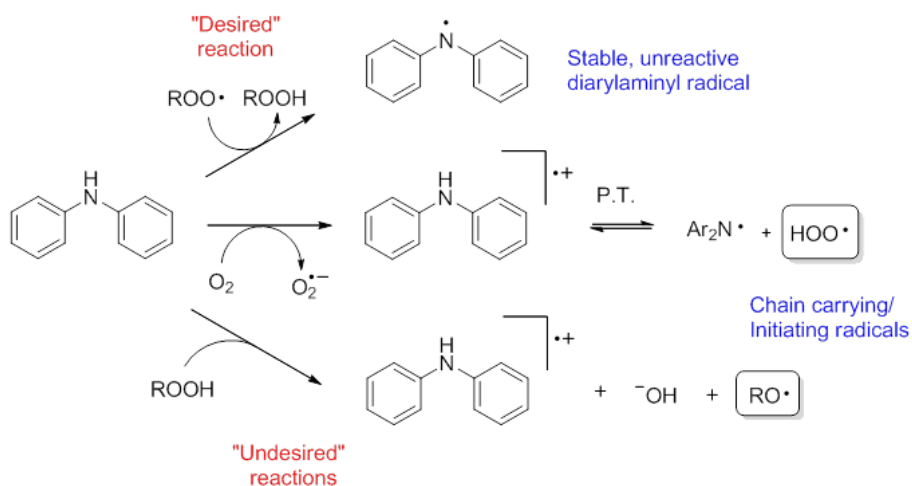
A well-established Evans-Polanyi relationship relates the O-H bond strength of the phenol to the rate constant for the reaction in Eq. 1, established largely by the drive to understand why α -tocopherol (**3.1**), the most potent form of vitamin E, is such an effective peroxy radical-trapping antioxidant; its substitution pattern weakens the O-H bond by 10 kcal/mol relative to phenol itself (77.2 vs. 87.2 kcal/mol), enabling it to react much more quickly with peroxy radicals ($k_1 = 3.2 \times 10^6$ vs. $2.9 \times 10^3 \text{ M}^{-1}\text{s}^{-1}$ in benzene and styrene, respectively).²

In contrast, optimization of the reactivity of diarylamine antioxidants to peroxy radicals (Eq. 2):



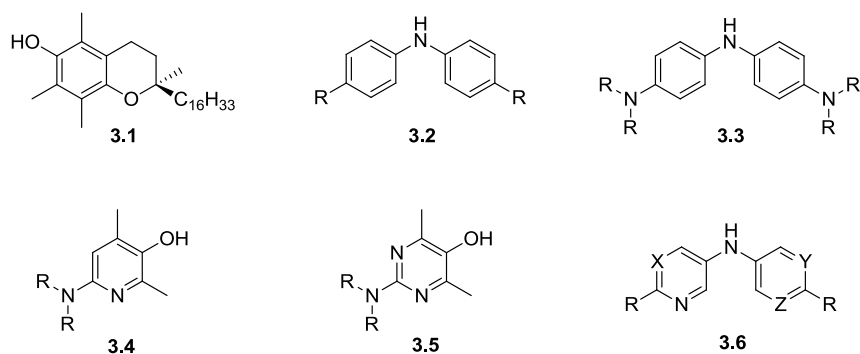
has lagged behind their phenolic counterparts. The industry standards are 4,4'-dialkyldiphenylamines (**3.2**, N-H BDEs of ~82 kcal/mol and $k_2 \sim 2 \times 10^5 \text{ M}^{-1}\text{s}^{-1}$), which have rate constants only marginally higher than unsubstituted diphenylamine (N-H BDE of 84.7 kcal/mol and $k_2 \sim 4.4 \times 10^4 \text{ M}^{-1}\text{s}^{-1}$). Similarly to phenols, it is known that addition of electron-donating

groups at the *para*-positions relative to the aminic N-H weaken the bond (e.g. 4,4'-(*N,N*-dimethylamino)-diphenylamine (**3.3**) has an N-H BDE of 78.4 kcal/mol),³ but these compounds are generally not employed as antioxidants since they are sufficiently electron rich to undergo direct reactions with O₂ and product hydroperoxides, rendering them pro-oxidants as opposed to antioxidants (Scheme 3.1)



Scheme 3.1. Competing antioxidant and proantioxidant reactions of electron-rich diphenylamines antioxidants.

Over the past decade, we have described the development of phenolic-like antioxidants, 3-pyridinols and 5-pyrimidinols, that have rate constants for reactions with peroxy radicals that are up to 88-fold higher than that of α -tocopherol – making them the most effective peroxy radical trapping antioxidants described to date. The design strategy centered on the incorporation of nitrogen atoms in the phenolic ring, which raises the oxidation potentials of the phenols and allows them to be substituted with stronger electron-donating groups (i.e. *N,N*-dialkylamino) as in **3.4** and **3.5**, further weakening the O-H bond compared to compounds such as **3.1**, but not at the expense of their one-electron oxidation by O₂.⁴⁻⁶



In a recent communication,⁷ we described preliminary results of our attempts to improve the activity of diphenylamine antioxidants using the same strategy. We showed that analogs of diphenylamine **3.2** bearing either ring carbons or nitrogens at the positions indicated by X Y and Z in **3.6** were characterized by oxidation potentials that increased systematically with the number of N-atoms from less than 1 V to > 1.5 V (vs. NHE), while their reactivity to peroxy radicals decreased only 6-fold at most (from $k_H = 1.8 \times 10^5 \text{ M}^{-1} \text{ s}^{-1}$ for **3.2** to $k_H = 3.0 \times 10^4 \text{ M}^{-1} \text{ s}^{-1}$ for **3.6** with X=Y=Z=N in chlorobenzene at 37°C). This permitted the design of pyridyl and pyrimidyl analogs of the very electron-rich diphenylamine **3.3** that were stable in air and reacted with peroxy radicals with temperature-independent rate constants up to 200-fold greater than those measured for α -tocopherol (**3.1**) under the same conditions. These exciting results prompted us to carry out a thorough study of the structure-reactivity relationships in these compounds, which we describe here.

3.3 Results

3.31 Theoretical Calculations

Quantum chemical calculations using the complete basis set approach at the CBS-QB3 level⁸ were carried out in order to predict the effects that heteroatom incorporation would have on the N-H BDE and IP of diphenylamine. We first considered all of the possible positions of attachment of either a pyridine or pyrimidine ring to the diphenylamine nitrogen in place of one of the phenyl rings (Table 3.1). The incorporation of each of the 2-, 3- and 4-pyridyl substituents resulted in increases in both the calculated N-H BDE and the IP, with the 2-pyridyl substituent giving rise to the largest increase in BDE (+3.7 kcal/mol), but the smallest increase in IP (+2.7 kcal/mol). The largest increase in IP was predicted for the 4-pyridyl substituent (+10 kcal/mol), which was accompanied by an increase in the BDE of 2.5 kcal/mol. The best compromise between a negligible effect on BDE (0.4 kcal/mol), but significant increase in IP (6.4 kcal/mol) was predicted for the 3-pyridyl substituent. The same trends were predicted when each of 2-, 4- and 5-pyrimidyl substituents were incorporated in place of one of the phenyl rings.

The foregoing results make it clear that incorporation of nitrogen atoms at the 3- and 5-positions strikes the best compromise between maximally increasing the IP while minimally increasing the N-H BDE. Since both phenyl rings in diphenylamine could be replaced with pyridyl and/or pyrimidyl rings, we expanded our calculations to include the corresponding dipyridylamines and dipyrimidylamines as well as the unsymmetric pyridyl pyrimidyl amines (Table 3.2). The results suggest that the N-H BDEs in diarylamines are almost invariant with nitrogen incorporation at the 3 and/or 5 positions relative to the amine nitrogen (predicted to be within 0.6 kcal/mol of each other), and that ionization potentials increase systematically by roughly 6 kcal/mol per nitrogen atom.

Table 3.1. CBS-QB3 Calculated gas phase N-H bond dissociation enthalpies (BDEs) and ionization potentials (IPs) for a series of heteroatom-containing diphenylamines in kcal/mol.

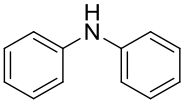
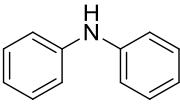
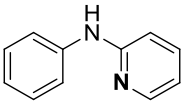
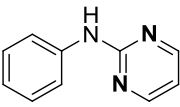
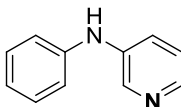
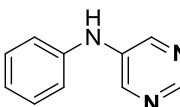
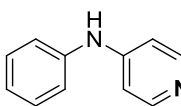
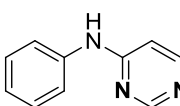
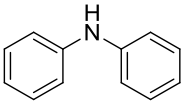
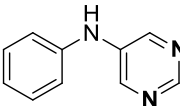
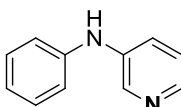
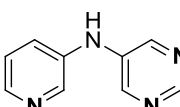
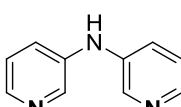
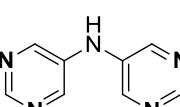
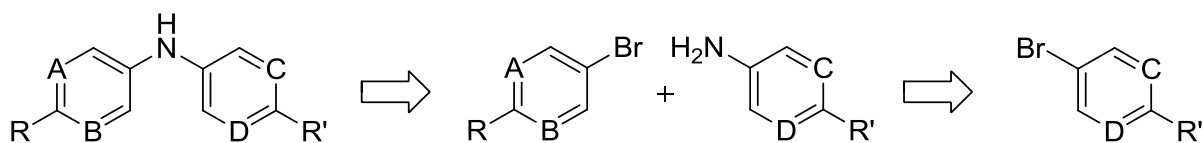
Structure	BDE	IP	Structure	BDE	IP
	86.4	168.3		86.4	168.3
	90.1	171.0		96.0	175.4
	86.8	174.7		86.4	179.3
	88.9	178.3		92.8	181.0

Table 3.2. Calculated N-H bond dissociation enthalpies (BDEs) and ionization potentials (IPs) for a series of diphenylamines incorporating heteroatoms at the 3- and 5-positions. Values are in kcal/mol.

Structure	BDE	IP	Structure	BDE	IP
	86.4	168.3		86.4	179.3
	86.8	174.7		86.6	186.0
	87.0	180.2		86.5	193.0

3.3.2 Synthesis

A small library of diarylamines with the core structures shown in Table 3.2 was prepared as described in detail in the accompanying manuscript (Chapter 2).⁹ Briefly, the syntheses were accomplished by a modular approach which utilized Buchwald-Hartwig Pd-catalyzed amination chemistry as the ultimate step. The approach was modular in that the aryl bromides used in the construction of the diarylamines (which were easily prepared from the common starting materials 2-aminopyridine and 2-aminopyrimidine), also served as precursors to their arylamine coupling partners (Scheme 3.2).



Scheme 3.2. Synthetic approach to substituted diarylamines (A-D = CH or N; R = H, alkyl, alkoxy or *N,N*-dialkylamino).

Through our modular approach we were able to prepare a series of substituted diarylamines varying in heteroatom distribution and substitution. Symmetric and unsymmetric compounds were prepared, both with respect to heteroatom incorporation and/or substituents and in the case of unsymmetrical compounds the substituent was appended to either a phenyl or heterocyclic ring (See chapter 2 for further details).

3.3.3 Electrochemistry

To quantitatively determine the propensity of the diarylamines to undergo one-electron oxidation we utilized electrochemical techniques. For compounds having reversible or quasi-reversible redox chemistry we turned to cyclic voltammetry to measure standard potentials (E°), while differential pulse voltammetry was used to measure anodic peak potentials (E_{pa}) for series of compounds with irreversible redox chemistry. A representative set of cyclic voltammograms are shown in Figure 3.1A (vs. Ag/AgNO₃) and a representative set of differential pulse voltammograms are shown in Figure 3.1B (vs. Ag/AgNO₃) and the measured potentials of all compounds are summarized in Tables 3.3-3.6 (vs. NHE).

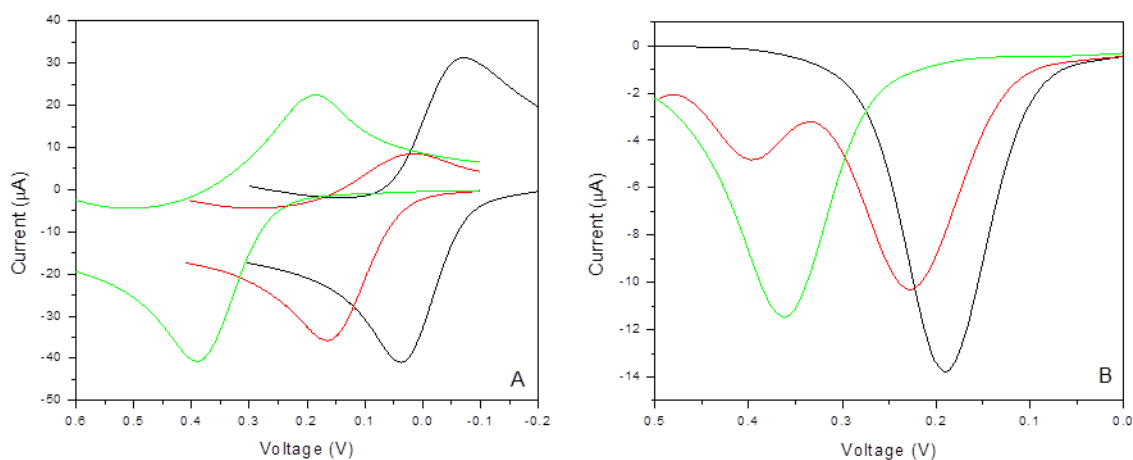
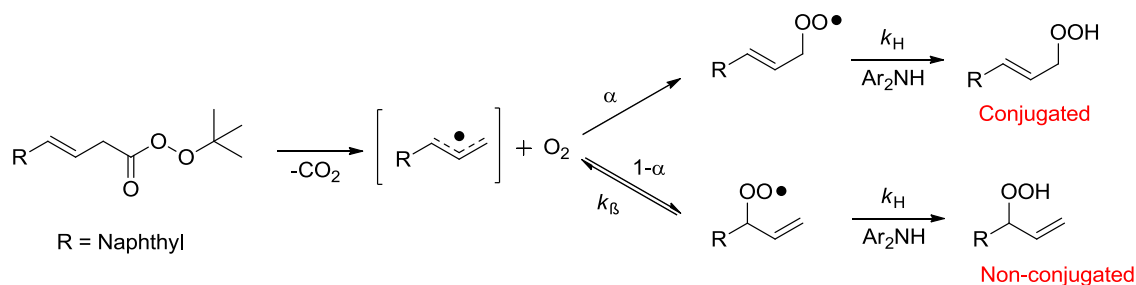


Figure 3.1. (A) Cyclic voltammogram obtained for **3.20-3.22** in MeCN at 25 °C vs. Ag/AgNO₃. (B) Differential pulse voltammograms obtained for **3.15-3.17** in MeCN at 25 °C vs. Ag/AgNO₃. For both (A) and (B) only the first oxidations are shown for clarity.

The redox chemistry was reversible or quasi-reversible for all of the *N,N*-dialkylamino-substituted compounds (be they symmetrical **3.9-3.14** or unsymmetrical **3.20-3.24**) and irreversible for nearly all of the alkyl- and alkoxy-substituted compounds up to a scan rate of 5 V/s.

3.3.4 Peroxyl Radical Kinetics

To determine the kinetics of H-atom abstraction from the diarylamines by peroxy radicals we turned to a peroxy-radical clock approach.^{10,11} The method used here¹² relies on the competition between the β -fragmentation of the non-conjugated 2-naphthyl allylperoxy radical ($k_{\beta} = 3.0 \times 10^5 \text{ s}^{-1}$ in benzene at 37 °C) and the bimolecular H-atom transfer reaction of interest, having an unknown rate constant (k_{H}) as shown in Scheme 3.3 (also, see chapter 4).



Scheme 3.3. Reaction scheme illustrating the application of the peroxy radical clock methodology, where R = naphthyl and α represents the oxygen partition coefficient (see chapters 1 and 4).

By measuring the ratio of conjugated/non-conjugated products we can determine the rate constant for H-atom transfer (k_{H}) using Equation 3:

$$\frac{[\text{Conjugated}]}{[\text{Non-Conjugated}]} = \frac{k_{\beta}}{k_{\text{H}}[\text{Ar}_2\text{NH}]} \left(\frac{1-\alpha}{\alpha} \right) + \frac{1-\alpha}{\alpha} \quad (3)$$

Using this technique, inhibition rate constants (k_{H}) were measured for five sets of diarylamine antioxidants – those substituted with alkyl, alkoxy and *N,N*-dialkylamino groups symmetrically (i.e. the same *para*-substituents on both aromatic rings) and those substituted with alkoxy and *N,N*-dialkylamino groups unsymmetrically (i.e. *para*-substituents on only one aromatic ring). A representative data set used to determine k_{H} for **3.16** and **3.28** is shown in Figure 3.2 and the inhibition rate constants obtained at 37 °C are summarized in Tables 3.3-3.6.

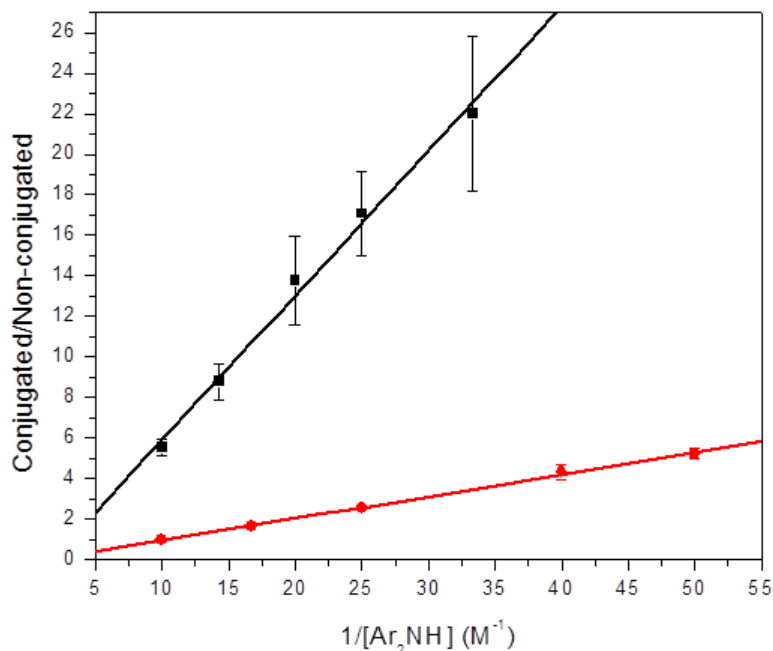


Figure 3.2. Double reciprocal plot of clock product ratios (scheme 3.3) vs. $1/[3.28]$ (■) and $1/[3.16]$ (●) in chlorobenzene at 37 °C used to obtain $k_{\text{H}} = 2.1(\pm 0.4) \times 10^5 \text{ M}^{-1}\text{s}^{-1}$ and $k_{\text{H}} = 1.4(\pm 1.0) \times 10^6 \text{ M}^{-1}\text{s}^{-1}$ respectively. The error associated with k_{H} represents the standard deviation from a minimum of 3 experimentally determined k_{H} values.

Table 3.3 Reactivity of disubstituted alkylated diarylamines **3.7-3.12** towards peroxy radicals and their corresponding oxidation potentials

Ar_2NH					$\text{R, R}'^{\text{a}}$	$k_{\text{H}} (\times 10^5)^{\text{b}}$	E^{oc}
	A	B	C	D			
3.7	CH	CH	CH	CH	C_8, C_8	1.8 ± 1.1	1.02
3.8	N	CH	CH	CH	C_6, C_4	1.5 ± 1.1	0.95
3.9	N	N	CH	CH	C_7, C_4	1.3 ± 0.1	1.13
3.10	N	CH	N	CH	C_6, C_6	0.9 ± 0.3	1.12
3.11	N	N	N	CH	C_7, C_6	0.8 ± 0.1	1.50
3.12	N	N	N	N	C_7, C_7	0.3 ± 0.1	1.55

^aLinear alkyl chain of indicated lengths. ^bValues in $\text{M}^{-1}\text{s}^{-1}$ determined at 37 °C in PhCl using the peroxy radical clock methodology. ^cAnodic peak potentials in V vs. NHE determined at 25 °C by differential pulse voltammetry in CH_3CN (0.1 M $\text{Bu}_4\text{N}^+\text{PF}_6^-$ electrolyte).

Table 3.4. Reactivity of disubstituted *N,N*-dialkylaminated diarylamines **3.13-3.18** towards peroxy radicals and their corresponding oxidation potentials.

Ar₂NH	A	B	C	D	R, R'	<i>k_H</i> (× 10⁷)^a	<i>E</i>^o^b
3.13	CH	CH	CH	CH	Me, Me	-- ^c	0.34
3.14	N	CH	CH	CH	Me, Me	-- ^c	0.37
3.15	N	N	CH	CH	Me, Me	3.7±1.0	0.44
3.16	N	CH	N	CH	Me, Me	3.4±1.1	0.44
3.17	N	N	N	CH	Me, Et	3.1±1.2	0.50
3.18	N	N	N	N	Et, Et	1.8±1.9	0.65

^aValues in M⁻¹s⁻¹ determined at 37 °C in PhCl using the peroxy radical clock methodology. ^bValues in V vs. NHE determined at 25 °C by cyclic voltammetry in acetonitrile (0.1 M Bu₄N⁺PF₆⁻ electrolyte). ^cCompounds were unstable under reaction conditions.

Table 3.5. Reactivity of disubstituted alkoxyated diarylamines **3.19-3.23** towards peroxy radicals and their corresponding oxidation potentials.

Ar₂NH	A	B	C	D	R, R' ^a	<i>k_H</i> (× 10⁶)^b	<i>E_{pa}</i>^c
3.19	CH	CH	CH	CH	Me, Me	3.7±0.4	0.70
3.20	N	CH	CH	CH	Me, Me	1.4±1.0	0.74
3.21	N	N	CH	CH	PhEt, Bu	nd	0.88
3.22	N	CH	N	CH	Me, Me	0.9±0.2	0.95
3.23	N	N	N	CH	PhEt, Bu	0.6±0.1	1.03

^aLinear alkyl chain of indicated lengths. ^bValues in M⁻¹s⁻¹ determined at 37 °C in PhCl using the peroxy radical clock methodology. ^cAnodic peak potentials in V vs. NHE determined at 25 °C by differential pulse voltammetry in CH₃CN (0.1 M Bu₄N⁺PF₆⁻ electrolyte).

Table 3.6. Reactivity of mono-substituted diarylamines **3.24-3.33** towards peroxy radicals and their associated one-electron oxidation potentials.

Ar₂NH	A	B	C	D	R^a	k_H (× 10⁷)^b	E^oc
3.24	CH	CH	CH	CH	Me	1.3±1.6	0.51
3.25	N	CH	CH	CH	Me	1.1±0.8	0.60
3.26	N	N	CH	CH	Me	0.3±0.1	0.81
3.27	CH	CH	N	CH	Me	0.8±0.2	0.53
3.28	CH	CH	N	N	Bu	0.8±0.1	0.56

Ar₂NH	A	B	C	D	R^a	k_H (× 10⁵)^b	E_{pa}^d
3.29	CH	CH	CH	CH	Me	3.0±0.5	0.94
3.30	N	CH	CH	CH	Me	2.9±0.6	1.02
3.31	N	N	CH	CH	C ₇	0.6±0.1	1.17
3.32	CH	CH	N	CH	Bu	2.1±0.4	0.90
3.33	CH	CH	N	N	C ₁₂	nd	1.34

^aLinear alkyl chain of indicated lengths. ^bValues in M⁻¹s⁻¹ determined at 37 °C in PhCl using the peroxy radical clock methodology. ^cValues in V vs NHE determined at 25°C by cyclic voltammetry in acetonitrile. ^dAnodic peak potentials in V vs. NHE determined at 25 °C by differential pulse voltammetry in CH₃CN.

The same trends are observed for each subset of compounds – oxidation potentials increase upon nitrogen atom incorporation (as little as 0.3 V and as much as 0.53 V for max number of N-atoms) and the inhibition rate constants decrease ca. 2-6 fold upon incorporation of N-atoms, depending on the *para*-substituents.

3.3.5 N-H Bond Dissociation Enthalpies

To understand the effect of nitrogen incorporation on the thermodynamics of H-atom transfer reactions of the diarylamines, the N-H BDEs of a representative set of compounds were measured using the radical-equilibrium electron paramagnetic resonance (EPR) technique.¹³⁻¹⁵ The diarylaminy radical was generated *in situ* by photolysis of solutions of the diarylamine in benzene containing di-*tert*-butylperoxide and allowed to reach equilibrium with a hindered phenol of similar O-H bond strength compared to the diarylamine of interest (Eq. 4-6). Representative EPR spectra of equilibrated mixtures are shown in Figure 3.3 (more are given as Supporting Information) and the N-H BDEs we obtained are provided in Table 3.7.



The incorporation of nitrogen into the aromatic rings of the substituted diphenylamines leads to a small increase in the N-H bond strength. While the difference seems rather dramatic in the case of comparing diphenylamine with bis(3-pyridyl)amine (2.7 kcal/mol), the differences appear to get smaller on substitution of the rings (0.9 kcal/mol for the alkyl- and alkoxy-substituted derivatives and 0.4 kcal/mol for the dialkylamino-substituted derivatives).

The persistence of the diarylaminy radical with dimethylamino substitution suggested they would serve as the best candidates to examine the effect of nitrogen incorporation in each of the four positions. Indeed, five of the six possibilities were characterized by N-H BDEs that hardly varied upon incorporation of nitrogen atoms in the aryl rings at the 3 and/or 5-positions (< 0.8 kcal/mol).

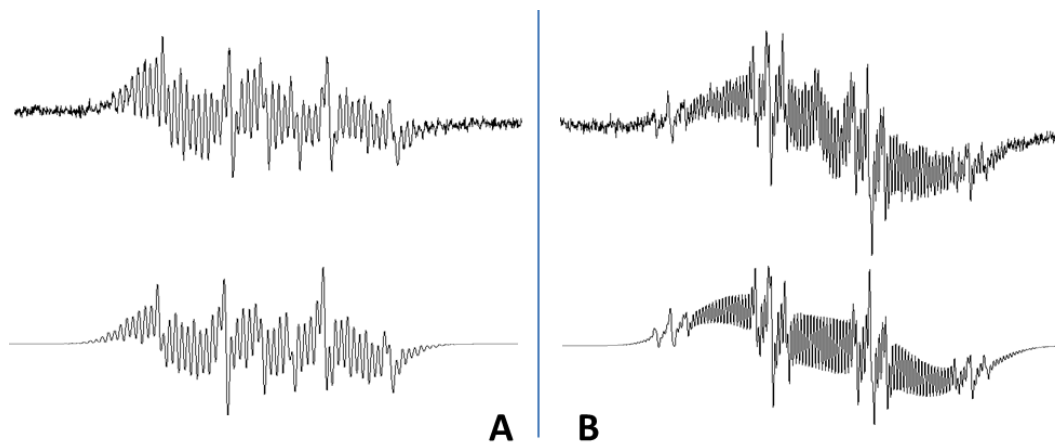


Figure 3.3. (A) (top) EPR spectrum of an equilibrated mixture of the di-arylaminy radical derived from **31** and 3,5-di-*tert*-butylphenoxyl radical in benzene at 298 K and. (bottom) the associated simulated spectrum for a 100:6.3 ratio of the two equilibrating radicals. (B) (top) EPR spectrum of an equilibrated mixture of the di-arylaminy radical derived from **12** and 3,5-di-*tert*-butylphenoxyl radical in benzene at 298 K and. (bottom) the associated simulated spectrum for a 100:1 ratio of the two equilibrating radicals.

Table 3.7. N-H Bond dissociation enthalpies of representative diarylamines measured by the radical equilibration EPR technique in benzene at 298 K. Values in kcal/mol. ^aTaken from reference 3.

Y	A	B	C	D	BDE
H	CH	CH	CH	CH	84.7±0.7 ^a
H	N	CH	N	CH	87.4±0.4
CH ₃	CH	CH	CH	CH	82.2±0.6 ^a
CH ₃	N	CH	N	CH	83.1±0.4
C ₈ H ₁₇	N	N	N	N	84.1±0.5
OCH ₃	CH	CH	CH	CH	80.7±0.3 ^a
OCH ₃	N	CH	N	CH	81.6±0.5
N(CH ₃) ₂	CH	CH	CH	CH	78.4±0.5 ^a
N(CH ₃) ₂	N	CH	CH	CH	78.8±0.3
N(CH ₃) ₂	N	CH	N	CH	78.8±0.8
N(CH ₃) ₂	N	N	CH	CH	79.0±0.5
N(CH ₃) ₂	N	N	N	N	79.2±0.5

3.3.6 Mechanistic Studies

The peroxy radical clock methodology easily affords the ability to measure solvent effects on the reaction of the diarylamines with peroxy radicals,^{10,12} which provides insight on the mechanism of the reaction.¹⁷ We measured the rate constants for diarylamines **3.16** and **3.18** in five different solvents (chlorobenzene, benzene, anisole, acetonitrile and ethyl acetate) and found an excellent correlation with the hydrogen bond accepting (HBA) ability of the solvent when plotted versus Abraham's solvent HBA scale β_2^H (Figure 3.4).¹⁸

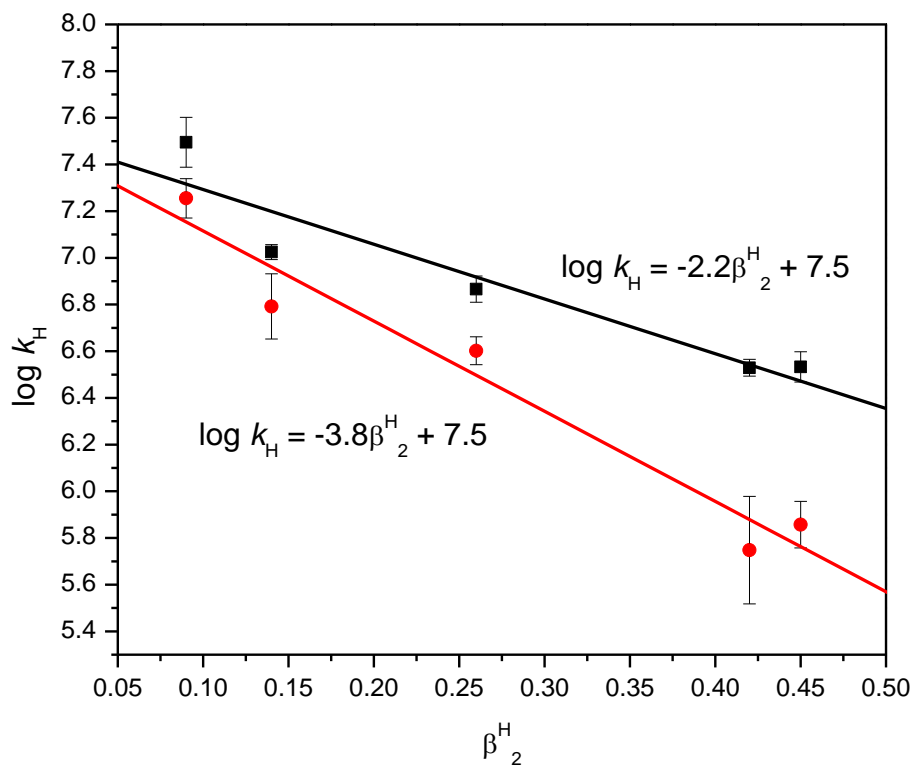


Figure 3.4. Rate constants for the reaction of diarylamines **3.16** (■) and **3.18** (●) with peroxy radicals as a function the H-bond accepting ability (β_2^H) of the solvent. Solvents used in the correlation (and their corresponding β_2^H parameter) are chlorobenzene (0.09), benzene (0.14), anisole (0.26), MeCN (0.42) and EtOAc (0.45).

The temperature dependence on the rate of hydrogen-atom abstraction by peroxy radicals from representative diarylamines was also studied for a representative set of diarylamines using the peroxy radical clock methodology, where the β -fragmentation of the secondary (non-conjugated) peroxy radical has been calibrated ($\log A = 12.8$ and $E_a = 9.6$ kcal/mol) in the temperature range of 37-95 °C.¹² The data are in Figure 3.5 and the Arrhenius parameters determined from them are given in Table 3.8.

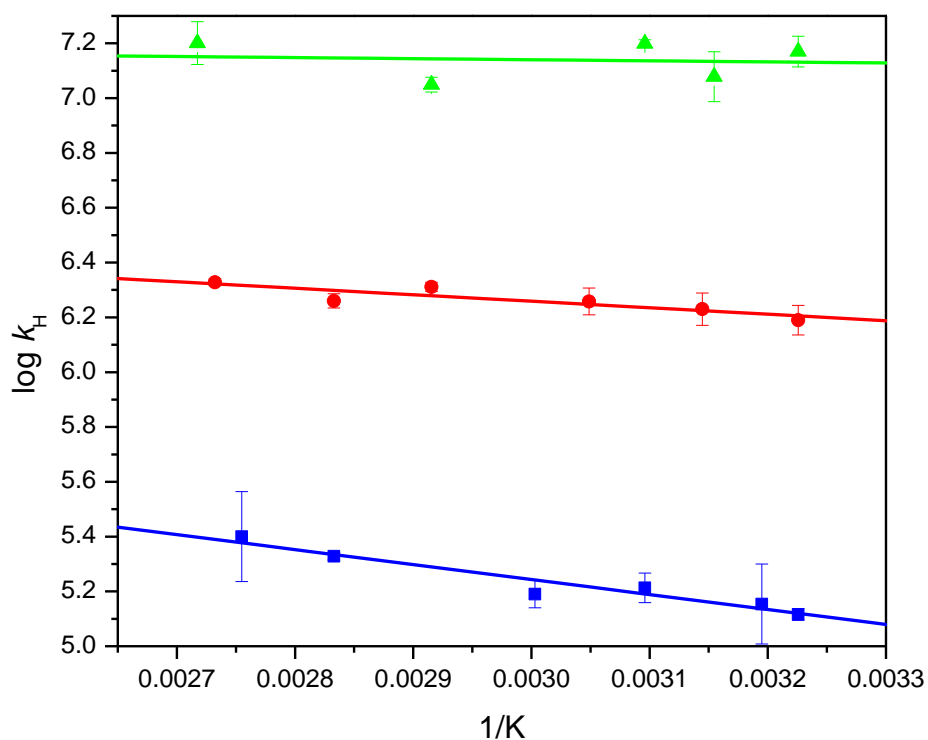


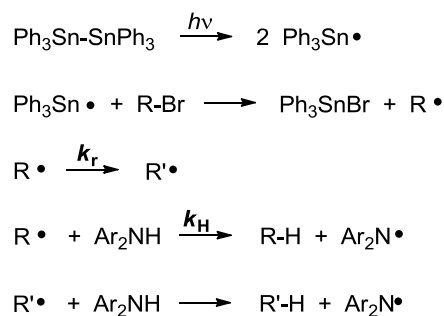
Figure 3.5. Temperature dependence of the rate constants for reactions of diarylamines 3.7 (■), 3.22 (●) and 3.28 (▲) with peroxy radicals in chlorobenzene in the range of 37-95 °C.

Table 3.8. Arrhenius parameters for the reactions of selected diarylamines with secondary peroxy radicals derived from rate constants measured from 37 to 95°C in chlorobenzene.

Ar ₂ NH	logA	E _a (kcal/mol)
3.7	6.9±0.2	2.5±0.4
3.22	7.0±0.1	1.1±0.3
3.28	7.1±0.1	0

3.3.7 Alkyl Radical Kinetics

The kinetics of the reactions of alkyl radicals with a representative series of diarylamines (i.e. those for which we measured N-H BDEs) were determined using the radical clock technique. Similar to the peroxy radical clock methodology described above, the alkyl radical clock approach involves the kinetic competition between a unimolecular process with a known rate constant (k_r) and the bimolecular reaction under investigation (k_H) (Chapter 1.3.4). We utilized the 1,2-aryl migration of 2-methyl-2-(2-naphthyl)-1-propyl (MNP) radical, having $k_r = 1.4 \times 10^4 \text{ s}^{-1}$ at 298 K¹⁹ as the calibrated unimolecular process, and generated the radicals by photolysis of a deoxygenated solution of MNP-Br in the presence of hexaphenyldistannane according to the reactions given in Scheme 3.4.



Scheme 3.4. Reaction scheme illustrating the application of the alkyl radical clock methodology.

The alkyl radicals react with the diarylamine under investigation, which is present in varying concentrations, with concentration ranges chosen to maintain pseudo first-order kinetics. Under these conditions, the product ratios (determined by GC) can be used to determine the rate of H-atom transfer (k_H) to the primary alkyl radical, calculated according to equation 7. The results are shown in Table 3.9.

$$k_H [\text{Ar}_2\text{NH}] = k_r \frac{[\text{RH}]}{[\text{R}'\text{H}]} \quad (7)$$

Table 3.9. Second-order rate constants for the reactions of selected diarylamines with primary alkyl radicals in chlorobenzene at 25 °C.

Ar_2NH	$k_H \text{ (M}^{-1}\text{s}^{-1}\text{)}$
3.13	$(2.3 \pm 0.9) \times 10^5$
3.16	$(1.5 \pm 0.2) \times 10^5$
3.18	$(1.4 \pm 0.1) \times 10^5$
3.19	$(2.5 \pm 0.1) \times 10^4$
2.22	$(1.9 \pm 0.2) \times 10^4$
3.7	$(1.3 \pm 2.9) \times 10^3$
3.10	$(9.7 \pm 2.3) \times 10^2$

3.4 Discussion

The design of synthetic radical-trapping antioxidants and the identification and characterization of natural products with antioxidant properties have long been objectives of academic and industrial researchers around the globe. Compounds with increased reactivity are desirable not only because they ensure that chain-carrying or chain-transfer reactions in the

radical-mediated autoxidation of hydrocarbons are less competitive, but by increasing the reactivity, the amounts of antioxidant required to achieve a desired performance level can be decreased. This has the potential benefits of lower cost and minimizing the undesirable properties of the antioxidant (e.g. interactions with other constituents) or oxidation products derived therefrom (e.g. undesired colouring).

Over the past decade, we established that the incorporation of nitrogen atoms into the aromatic ring of phenolic antioxidants leads to compounds that are much more stable to electron transfer reactions (to O₂ and/or hydroperoxides) due to higher inherent IPs, but which remain highly reactive to H-atom transfer reactions (to peroxy and alkyl radicals) since they still possess relatively low O-H BDEs.⁴⁻⁶ The success of this approach to stabilize the one-electron reactivity of highly electron-rich phenols, such as those substituted with dialkylamino groups, led to the development of the most effective peroxy radical-trapping antioxidants ever described (see Chapter 1). This prompted us to extend the approach to diarylamines.

Our work with phenols revealed that the maximum benefits of heteroatom incorporation (minimal increase in O-H BDE and maximum increase in IP) are achieved when the nitrogen atoms are incorporated in the 3- and 5-positions relative to the reactive phenolic O-H moiety. Incorporation of nitrogen atoms at the 2 and/or 6 positions results in isomerization of the aryl alcohols to the corresponding pyridinone and/or pyrimidinone tautomers, which predominate at equilibrium and decrease the antioxidant activity since the N-H bonds are stronger.

In contrast to phenolic antioxidants, a greater number of possibilities exist for the incorporation of nitrogen atoms into diarylamines – not just because there are two aromatic rings that can be modified, but also because tautomers of heteroarylamines are not likely to be relevant as they are higher energy species compared to their heteroaryl alcohol counterparts. To pare

down the number of compounds to be studied in detail, we carried out CBS-QB3 calculations on a series of unsubstituted diarylamines incorporating N-atoms in all of the possible positions. The results of these calculations suggested that the 3 and 5 positions were optimal for maximizing the ionization potentials of the compounds while maintaining a minimal perturbation on the N-H BDE (*cf.* Table 3.1). When considering the patterns that incorporate N-atoms in the 3 and/or 5 positions (*cf.* Table 3.2), calculations suggested that N-H BDEs should be almost invariant with N-atom incorporation and that IPs were predicted to increase systematically by ca. 6 kcal/mol per nitrogen atom.

On the basis of these calculations, a series of symmetrical (with respect to the reactive amine N-H) alkyl- and *N,N*-dialkylamino-substituted diarylamines that incorporated nitrogen atoms in the 3 and/or 5 positions were prepared. The alkylated compounds are representative of the scaffold of the current industry standard (**3.2**) and the *N,N*-dialkylamino-substituted compounds (**3.3**) represent a very electron-rich scaffold that is difficult to prepare, isolate, store and use in an air atmosphere. We were pleased to see that while both series of compounds had increased one-electron oxidation potentials which correlated systematically with N-atom content (between 1.02 and 1.55 V for the alkyl-substituted series and 0.34 and 0.65 V for the *N,N*-dialkylamino-substituted series), they maintained their reactivities towards peroxy radicals (*cf.* Tables 3.3 and 3.4). In fact, the *N,N*-dialkylamino substituted compounds were excellent peroxy radical trapping antioxidants, having rate constants ca. 200-fold higher than that of the industry standard **3.2**. Delighted with these results, we sought to expand the structure/reactivity understanding of symmetrically substituted heterocyclic diarylamines by preparing and characterizing the corresponding alkoxy-substituted compounds, which were predicted to have reactivity between the *N,N*-dialkylamino and alkyl-substituted compounds. Additionally, we

sought to determine the effects of N-atom incorporation into unsymmetrical diarylamines, i.e. those having only one substituent (in the *para*-position relative to the amine N-atom).

Indeed, we found that the oxidation potentials for the series of symmetrically-substituted alkoxyated diarylamines systematically increased with N-atom incorporation and spanned the gap in between the symmetrical alkyl- and N,N-dialkylamino-substituted compounds (0.7 – 1.03 V), as did the peroxy-trapping rate constants ($k_H \sim 10^6 \text{ M}^{-1}\text{s}^{-1}$).

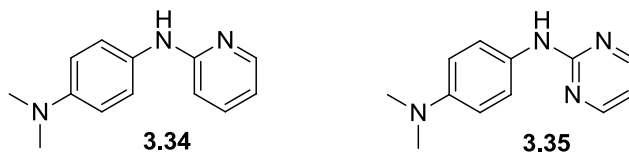
To determine whether or not the diarylamines displayed additive substituent effects with respect to rates of peroxy radical trapping, we prepared a series of mono-substituted compounds having either alkoxy or *N,N*-dialkylamino substituents on either an aryl or heteroaryl ring (Table 6). Interestingly, the substituent effects on the one-electron oxidation potential and rate constants for peroxy trapping appear to be greater when the substituent group was placed on the heteroaryl ring. At first glance, it is unclear as to why this may be the case. Combining these data with the data for the symmetrically substituted compounds, we correlated the reactivity of each diarylamine towards peroxy radicals on the basis of N-atom incorporation atom by plotting $\log k_H$ vs. $\Sigma\sigma_p^+$ for the *para*-substituents.^{3,20} Each subset afforded an excellent linear correlation with ρ^+ , with the reaction constants and correlation coefficients as shown in Table 3.10.

Table 3.10. Reaction constants (ρ^+) from plots of $\log k_H$ vs. $\Sigma\sigma_p^+$ for the reactions of substituted diarylamines containing either phenyl, 3-pyridyl or 5-pyrimidyl rings.

Ar-NH-Ar'	Compounds	ρ^+ (r^2)
Ph-NH-Ph	3.7, 3.13, 3.19, 3.24, 3.29	1.59±0.17 (0.98)
Pyr-NH-Ph	3.8, 3.14, 3.20, 3.25, 3.30, 3.27, 3.32	1.51±0.27 (0.98)
Pym-NH-Ph	3.9, 3.15, 3.21, 3.26, 3.31, 3.28	1.00±0.17 (0.93)
Pyr-NH-Pyr	3.10, 3.16, 3.24	0.94±0.05 (0.99)
Pym-NH-Pyr	3.11, 3.17, 3.23	0.91±0.07 (0.99)

The negative reaction constants in Table 3.10 imply that the reaction centre becomes more electrophilic in the transition state compared to the starting material. This follows the established trend that the N-H bond dissociation enthalpies of diphenylamines correlate with σ_p^+ because EDGs stabilize the electron-poor diarylaminy radical (and destabilize the electron-rich diarylamine). Interestingly, the magnitudes of the ρ^+ -values *decrease* with increasing heteroatom incorporation into the aryl rings. This can be attributed to the electronegative nitrogen atoms inductively counteracting the effects of the EDGs thereby reducing their effect on the reactivity of the diarylamines.

To verify that the substitution patterns predicted by the calculations are indeed optimal for reactivity/oxidative stability we prepared the mono-substituted 2-pyridyl and 2-pyrimidyl derivatives **3.34** and **3.35** and compared their reactivities to the 3-pyridyl and 5-pyrimidyl compounds **3.27** and **3.28**.



We found $k_H = (6.4 \pm 0.8) \times 10^6 \text{ M}^{-1} \text{ s}^{-1}$ and $E^\circ = 0.57 \text{ V}$ for **3.34**, and $k_H = (1.5 \pm 0.4) \times 10^5 \text{ M}^{-1} \text{ s}^{-1}$ and $E^\circ = 0.64 \text{ V}$ for **3.35**. Although these compounds have only slightly higher one-electron oxidation potentials than their counterparts having nitrogen atoms in the 3 and 5 positions (**3.27**, $E^\circ = 0.53 \text{ V}$ and **3.28**, $E^\circ = 0.56 \text{ V}$), their inhibition rate constants are depressed 1.3-fold and 53-fold respectively for reactions with peroxy radicals. Although it is indeed the case that the 2-pyridyl and 2-pyrimidyl analogs are less effective as radical-trapping antioxidants than their 3-pyridyl and 5-pyrimidyl counterparts, the difference is less obvious than was expected from the results of our calculations on the unsubstituted compounds (*cf.* Table 3.1) when comparing the pyridyl derivatives. Nevertheless, based on these results, the scaffolds containing N-atoms in the 2 and/or 6 positions were not further pursued.

To provide a thermodynamic rationale for the trends in the kinetics of the radical-trapping reactions of the diarylamines, the N-H BDEs of selected examples were measured using the radical-equilibrium EPR spectroscopy approach (Table 3.7). We found that the changes in the N-H BDEs are much smaller than the differences in the E° (or E_{pa}) values – consistent with the expectation that N-atom incorporation into the aryl rings destabilizes the radical cations formed by one-electron oxidation of the diarylamines more than it destabilizes the corresponding diarylaminy radical formed by H-atom abstraction. It was also interesting to note that the magnitudes of the changes in N-H BDEs and k_H values upon N-atom incorporation are much smaller than those observed for phenolic compounds (ca. 1.2-1.5 kcal/mol per N-atom).^{4,6} We

attribute this difference to the fact that the diphenylaminy radical is inherently less electron-poor than the phenoxy radical and therefore is less destabilized by the incorporation of the electronegative nitrogen atoms into the aryl rings.

The rate constants determined for reactions of the diarylamines with peroxy radicals afforded a good correlation with their corresponding N-H BDEs (Figure 3.6). Interestingly, when the data relating the kinetics of the reactions of phenols with peroxy radicals to their corresponding O-H BDEs was included in the same plot, it became obvious that the reactions of diarylamines were faster when the thermodynamics of the reactions were comparable (i.e. for reactions of diphenylamines and phenols whose N-H and O-H BDEs, respectively, were similar).

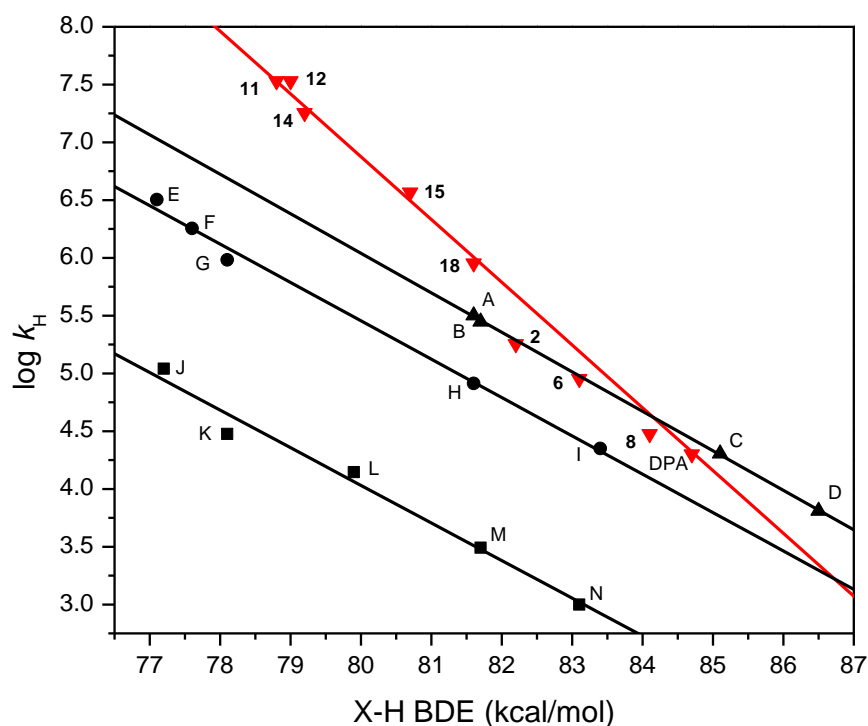


Figure 3.6. Plots of $\log k_H$ vs. N-H BDEs of diarylamines (■) and O-H BDEs of some 4-substituted phenols (▲), 2,6-dimethyl-4-substituted phenols (●) and 2,6-di-*tert*-butyl-4-substituted phenols.^{5,6} Legend: A = 4-(methylselanyl)phenol; B = 4-methoxyphenol; C = 4-methylphenol; D = phenol; E = α -TOH; F = 2,6-dimethyl-4-(methylselanyl)phenol; G = 2,6-dimethyl-4-methoxyphenol; H = 2,4,6-trimethylphenol; I = 2,6-dimethylphenol; J =

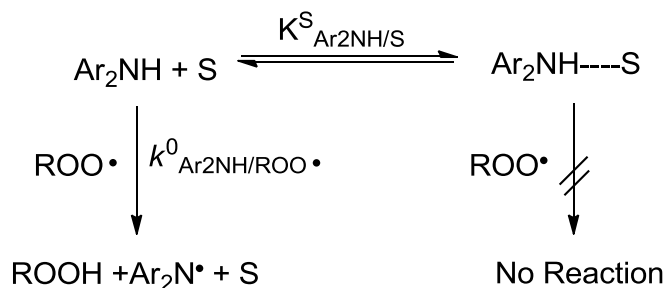
2,6-di-*tert*-butyl-4-methoxyphenol; K = 2,6-di-*tert*-butyl-4-thiomethylphenol; L = 2,6-di-*tert*-butyl-4-methylphenol; M = 2,6-di-*tert*-butylphenol; N = 2,6-di-*tert*-butyl-4-cyanophenol; DPA = diphenylamine.

The difference was most striking for the most electron-rich compounds; the rate constants for the *N,N*-dialkylamino-substituted compounds **3.15**, **3.16** and **3.18** were 2-5 fold faster than the rate constant for α -TOH established under the same conditions ($k_{\text{H}} = 7.1 \times 10^6 \text{ M}^{-1}\text{s}^{-1}$) despite the fact that the N-H BDEs of these diarylamines were measured to be 1.3-1.9 kcal/mol greater than the O-H BDE of α -TOH (77.3 kcal/mol). We can be confident in the relative accuracy of these measurements since the peroxy radical clock used to obtain the inhibition rate constants (k_{H}) for the diarylamines was calibrated (k_{β}) using α -TOH, and the X-H BDEs were measured by the same laboratory using the same technique (radical equilibrium EPR, *vide infra*) under the same conditions. At first glance, these results imply that the entropic demand for the reaction of phenols with peroxy radicals must be greater. However, the only reported pre-exponential factor for a diarylamine reacting with peroxy radicals was reported as $\log A = 5.1 \pm 0.5$ by Benson²¹ (*N*- α -naphthyl-*N*-phenylamine with *tert*-butylperoxy radical) versus values of $\log A \sim 8$ commonly ascribed to the reactions of phenols with peroxy radicals.

This prompted us to measure the temperature dependence of k_{H} for representative diarylamines **3.7**, **3.22** and **3.28** (Figure 3.5, Table 3.8) using the peroxy radical clock method (which was calibrated using an $\log A = 8$ for α -TOH),^{12,21} and from this data obtained pre-exponential factors of $\log A = 7.0 \pm 0.1$ for each reaction and E_a values that correlated with the strength of the N-H bonds (**3.7** > **3.22** > **3.28**). In fact, the rate constants for the reactions of **3.28** with peroxy radicals were invariant with temperature, implying $E_a \approx 0$. Thus, from this data we can conclude that the high reactivity of diarylamines **3.15-3.18** compared to α -TOH (and other

similarly reactive phenols) does not originate from decreased entropic demand ($\log A \approx 8$ for α -TOH and $\log A \approx 7$ for diarylamines), but rather from inherently lower activation energies.

To confirm that the reactions of the most electron-rich diarylamines were not simply electron-transfer reactions – which would mean that their kinetics would not be directly comparable with the reactions of phenols – we measured solvent effects on the inhibition rate constants for compounds **3.16** and **3.18**. While there were no obvious correlations of the kinetics with the polarity of the medium – which would be expected if an electron transfer mechanism was operative – there were excellent (negative) correlations with the H-bond accepting strength of the medium (Figure 3.4). This solvent effect follows the trends observed for phenols, and can be explained by a simple pre-dissociation model (Scheme 3.5) wherein only the non-H-bonded diarylamine is reactive to peroxy radicals – fully consistent with a formal H-atom transfer, as for phenols.



Scheme 3.5. Kinetic solvent effect on the reaction of diarylamines with peroxy radicals.

Ingold and co-workers have shown that the rate constants for reactions of phenols with alkoxy and hydrazyl radicals in a given solvent (k^{S}) are a function of the hydrogen bond-accepting ability of the solvent (β_2^{H}) and hydrogen bond-donating ability of the substrate (α_2^{H}).^{22,23}

$$\log k^S = \log k^0 - 8.3\alpha_2^H\beta_2^H \quad (8)$$

and we subsequently showed that this extends to the reactions of phenols with peroxy radicals.¹⁰ The results above point to the same relationship holding for diarylamines. Furthermore, they clearly show how the incorporation of nitrogen into the aromatic rings results in much stronger H-bonding interactions, since the slope of the line of best fit for the bis-pyrimidine **3.18** is almost twice as large (-3.8) as that for the bis-pyridine **3.16** (-2.2), which is similar to diphenylamine (-2.5)¹⁰ for which $\alpha_2^H = 0.324$.¹⁸ Thus, the replacement of two phenyl rings with two pyridyl rings is mostly offset by the presence of the two *N,N*-dimethylamino groups on comparing the H-bond donating ability of **3.16** with diphenylamine, but the introduction of two more nitrogen atoms as in the bis-pyrimidyl **3.18** leads to a much better H-bond donor (larger α_2^H value) and it displays a much larger kinetic solvent effect.

Confident that the reactions between peroxy radicals and diarylamines are indeed formal H-atom transfer reactions analogous to the reactions between peroxy radicals and phenols, we looked to the calculated transition state structures for these reactions for insight as to why diarylamines are inherently more reactive. As for the reaction of phenol with peroxy radicals,^{24,25} the calculated transition-state structure for the reaction of diphenylamine with peroxy radicals⁷ is best described as a proton-coupled electron transfer (PCET) reaction,⁷ wherein the proton moves between the diphenylamine and peroxy radical via two nominal lone pairs on the N atom and terminal oxygen atom, respectively, while an electron moves from the π -HOMO of the amine to the π -SOMO of the peroxy radical (drawn schematically as its charge-separated resonance structure in Figure 3.7). Based on these structures, it follows that reactants with higher HOMO energies should have lower activation energies since they will provide better orbital overlap with the π -SOMO of the peroxy radical and facilitate proton-coupled electron

transfer. Indeed, diphenylamines have much higher HOMO energies when compared to phenols that possess similar X-H BDEs; for example, while α -TOH has $E^\circ = 0.97$ V (vs. NHE),²⁶ the values we show for **3.15-3.18** are comparatively lower (Table 3.4).

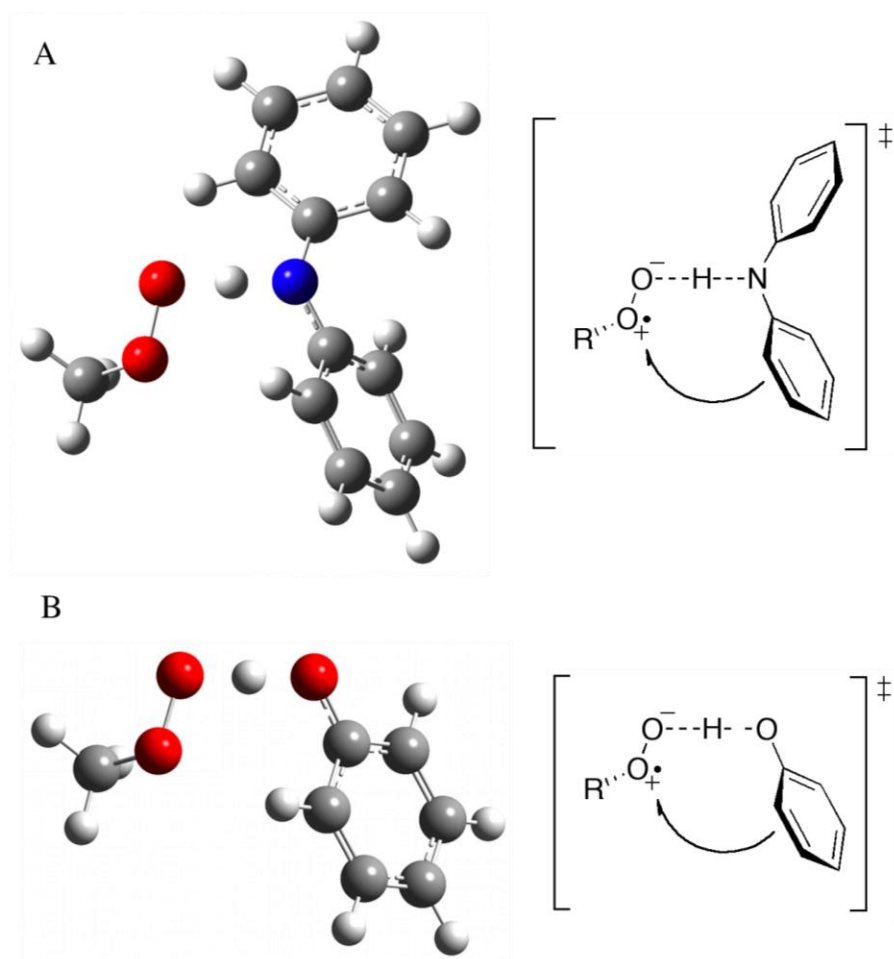


Figure 3.7. Calculated transition state structures for the formal H-atom transfer from diphenylamine (A) and phenol (B) to the methylperoxyl radical.

The transition state structures in Figure 3.7 may also provide some insight into the trends we observed in the mono-substituted diarylamines in Table 3.6. Consider the *N,N*-dialkylamino substituted diarylamines which differ in whether nitrogen(s) are incorporated into the substituted

ring or the unsubstituted ring. When two nitrogens are incorporated in the aryl ring bearing the substituent (**3.26**), the rate constant for reaction with peroxy radicals drops 4.3-fold, whereas when they are incorporated in the aryl ring that does not contain the substituent (**3.28**), the rate constant drops only 1.6-fold. This is consistent with the preferred interaction of the peroxy radical with the more electron-rich aryl ring of the two (in a transition state structure analogous to that in Figure 3.7A), which would be the same for **3.24**, **3.27** and **3.28** (and the di-substituted diarylamine **3.15**, which may have slightly higher reactivity simply due to the two-fold symmetry of the molecule, which would result in a slightly higher $\log A$ value). This observation merits further investigation.

The kinetics of the reactions of these new diarylamines with alkyl radicals were also examined. This reactivity is relevant since diarylamines can act as antioxidants via their reactions with chain-carrying alkyl radicals in autoxidations which take place at low partial pressures of oxygen, and also in the application of diarylamines as polymerization inhibitors (monomer stabilizers). Indeed, we found that the diarylamines reacted very rapidly with primary alkyl radicals (*cf.* Table 3.9) and that the rate constants correlated nicely with the strength of the N-H bond, as one might expect (Figure 3.8). Interestingly, when this relationship was plotted alongside literature data for the reactions of phenolic antioxidants with primary alkyl radicals²⁷ (also obtained by competition kinetics using the radical clock methodology), the trend opposed that which we observed with peroxy radicals; that is, diarylamines with a given N-H BDE reacted slower than phenols with comparable O-H BDEs (with the exception of the 2,6-di-*tert*-butylated phenols which react more slowly due to steric hindrance). This result implies that the two reactions have different mechanisms.

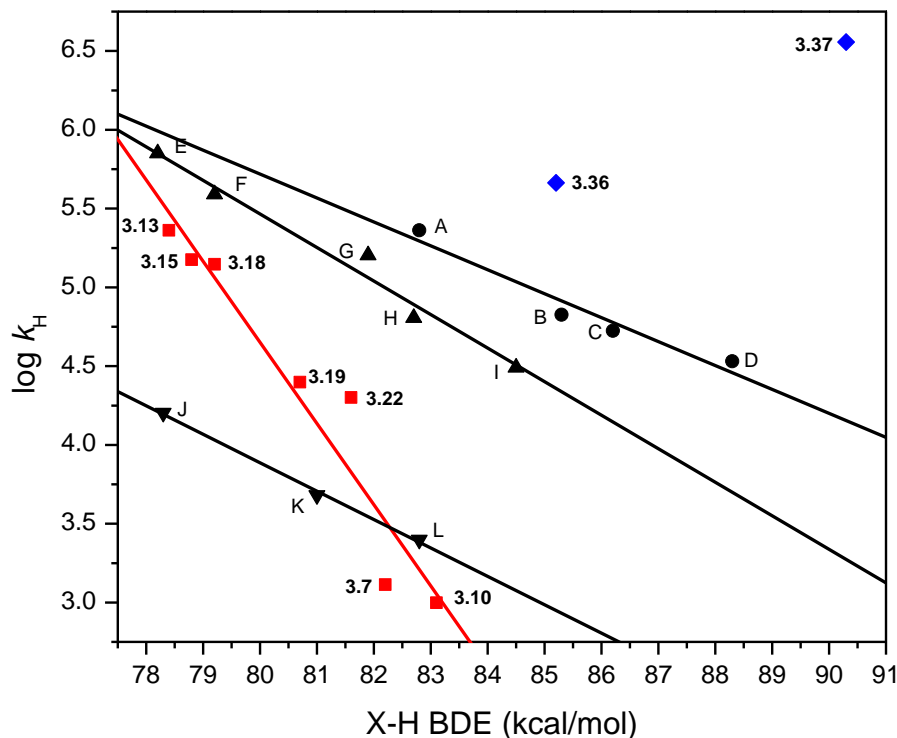
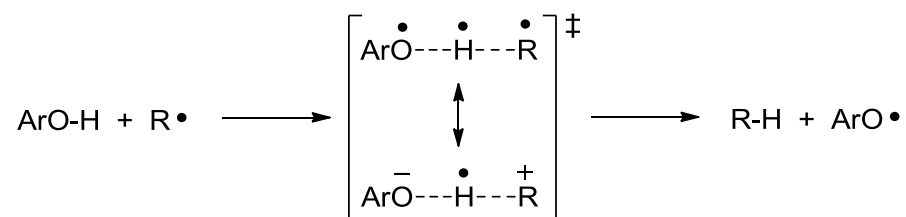


Figure 3.8. Correlations of the second-order rate constants ($\log k_{\text{H}}$) vs. N-H BDEs for diarylamines (■) and O-H BDEs of phenols (●), *ortho*-methylated phenols (▲), *ortho-tert*-butylated phenols (▼) and pyrimidinols (◆). Legend: A = 4-methoxyphenol; B = 4- *tert*-butylphenol; C = 4-methylphenol; D = phenol; E = 2,2,5,7,8-pentamethyl-6-chromanol ; F = 4-methoxy-2,3,6-trimethylphenol; G = 4-methoxy-2,3,5,6-tetramethylphenol; H = 2,4,6-trimethylphenol; I = 2,6-dimethylphenol; J = 2,6-di-*tert*-butyl-4-methoxyphenol; K = 2,6-di-*tert*-butyl-4-methylphenol; L = 2,6-di-*tert*-butylphenol.

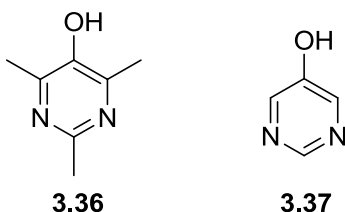
Since alkyl radicals cannot H-bond the diarylamines/phenols and do not possess an adjacent lone pair, their reactions necessarily take place by a H-atom transfer mechanism (HAT) as opposed to the PCET mechanism described above for their reactions with peroxy radicals. As such, the inherently higher reactivity of diarylamines that we see in reactions with peroxy radicals is not observed here. The high reactivities of phenols towards alkyl radicals has been explained on the basis of a polar effect in the transition state of the HAT reaction. This can be

conceptualized by the contribution of the charge-separated resonance form shown below (scheme 3.6), which lowers the energy of the transition state, accelerating the rate of reaction.



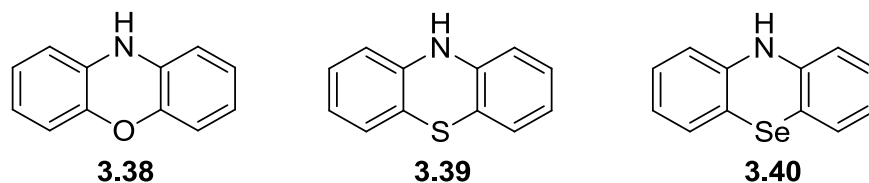
Scheme 3.6. The polar effect in the reaction of phenols with alkyl radicals.

As such, the contribution of the polar effect in HAT reactions with alkyl radicals is most obvious for compounds which can best accommodate a partial negative charge on the atoms from which the H-atom is being abstracted – i.e. those with lower pK_{a} s. Perhaps the best examples are in reactions of pyrimidinols which are not substituted with strong electron donating groups, such as **3.37** and **3.36**, which have O-H BDEs of 90.3 kcal/mol and 85.2 kcal/mol but rate constants for reactions with alkyl radicals of $3.6 \times 10^6 \text{ M}^{-1}\text{s}^{-1}$ and $4.6 \times 10^5 \text{ M}^{-1}\text{s}^{-1}$, respectively (which deviate significantly from the correlations in Figure 3.8). The polar effect makes reactions of phenols having higher O-H BDEs (they are not substituted with strong EDGs and therefore have lower pK_{a} s) much faster than those of diarylamines with comparable N-H BDEs.



The only other extensive structure-reactivity study on the reactions of aromatic amines with alkyl and peroxy radicals was carried out some time ago on diphenylamine, as well as the analogs

which featured a second connection between the two aryl rings: phenoxazines (**3.38**), phenothiazines (**3.39**) and phenoselenazines (**3.40**).²⁸



When the data for **3.38-3.40** and a series of substituted phenothiazines were plotted alongside the current data for the reactions of the diarylamines with both alkyl and peroxy radicals (*cf.* Figure 3.9), two excellent correlations were obtained – one relating the rate constants for the reactions of both sets of amines with alkyl radicals and the other relating the rate constants of both sets of amines with peroxy radicals. The correlations are almost perfectly parallel, but are separated in the vertical dimension by 2 orders of magnitude. Therefore, while the reactions of diarylamines with primary alkyl radicals are ca. 12 kcal/mol *more exothermic* than their reactions with peroxy radicals (the RCH₂-H BDE is 100 kcal/mol, while the ROO-H BDE is 88 kcal/mol), the reactions are *two orders of magnitude slower*. This has been explained²⁸ on the basis of lesser triplet repulsion in the transition state for H-atom transfer between a nitrogen atom and an oxygen, compared to a nitrogen atom and a carbon; a concept first advanced by Zavitsas.²⁹

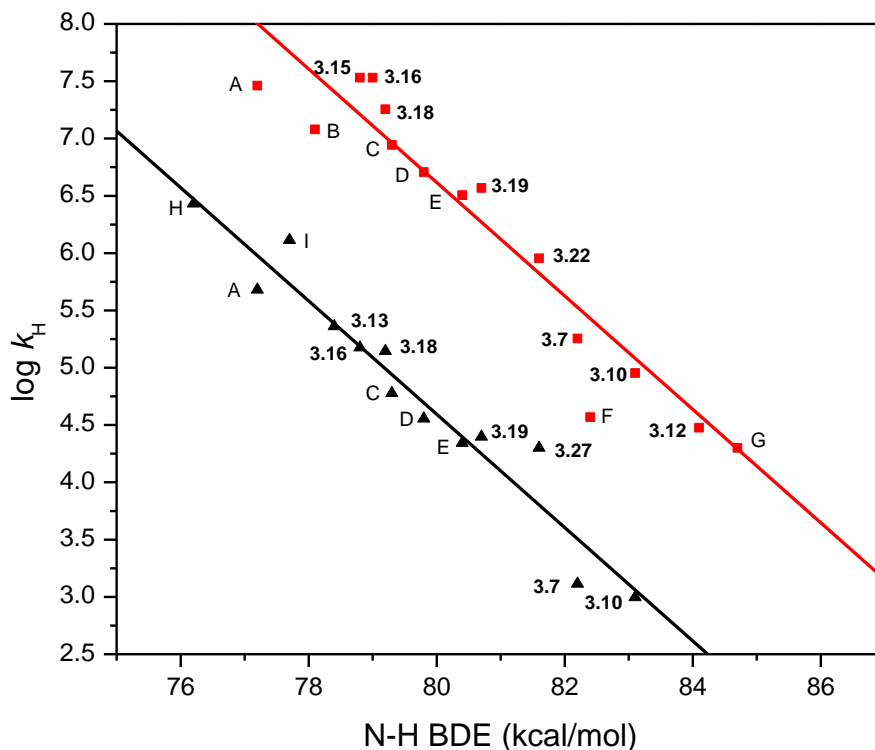


Figure 3.9. Correlation between N-H BDEs and $\log k_{\text{H}}$ for reaction of diarylamines, phenothiazines and phenoxazines for reaction with primary alkyl radicals (▲) and peroxy radicals (■).^{28,30} Data for diarylamines was obtained at 298 K while phenothiazines/phenoxazines were measured at 323 K. Legend: A = phenoxazine; B = 1,9-di-*tert*-butylphenothiazine; C = phenothiazine; D = 3,7-dichlorophenothiazine; E = phenoselenazine; F = 5*H*-dibenz[*b,f*]azepine; G = diphenylamine; H = 3,7-dimethoxyphenothiazine; I = 1,9-dimethylphenothiazine. Correlations are $\log k_{\text{H}} = -0.495x + 46.2$ ($r^2 = 0.92$) and $\log k_{\text{H}} = -0.495x + 44.2$ ($r^2 = 0.94$) respectively. Note that phenothiazine and phenoxazine N-H BDEs were revised downward by 1.1 kcal/mol as suggested by Mulder *et al.*³⁰

However, in light of the different reactivities of phenols and diarylamines towards peroxy radicals (*vide supra*),³¹ it would appear that the trends in Figure 3.9 would be better explained by the simple fact that the reactions of diarylamines with alkyl radicals and peroxy radicals proceed by two different mechanisms: H-atom transfer for the former and proton-coupled electron transfer for the latter.

3.5 Conclusions

We have prepared a series of heterocycle-containing diarylamine antioxidants and demonstrated that incorporation of nitrogen atoms affords compounds with increased one-electron oxidation potentials without compromising their H-atom transfer reactivity – quantified kinetically via rates of their peroxy radical-trapping reactions and thermodynamically via determination of their N-H bond dissociation enthalpies. Rate constants for the most reactive compounds (mono- or di-*N,N*-dialkylamino-substituted) trapping peroxy radicals were shown to be 100- to 200-fold greater than the industry standard dialkylated diphenylamine and shown to proceed with pre-exponential values of $\log A \sim 7$ and negligible activation energies. Additionally, we have shown the substituent effects on diarylamine radical trapping to be additive, but that for *N,N*-dialkylamino-substituted compounds the difference between mono- and di-substituted compounds is very small; meaning that mono-substituted diarylamines, which are less synthetically demanding (and cheaper) to prepare can be easily substituted. Reactions with primary alkyl radicals were shown to be strongly correlated to N-H BDEs and the correlation was found to be larger than for phenols with similar entropic demands due to the absence of polar effects in the hydrogen atom transfer transition states.

3.6 Experimental Section

3.6.1 General

Diarylamines were prepared according to the procedures in the accompanying manuscript.³² Solvents for kinetic studies were purified according to the procedures given in ‘purification of laboratory chemicals’.³³ All other commercially available reagents were used without further purification, unless otherwise specified.

3.6.2 Electrochemistry

Standard potentials (CV) and anodic peak potentials (DPV) were measured using a BASi potentiostat with a glassy-carbon working electrode, a platinum counter electrode and an Ag/AgNO₃ (0.005 M) reference electrode. Samples were measured in dry acetonitrile using Bu₄N•PF₆ (0.1 M) as an electrolyte at 25 °C. For compounds displaying reversible redox chemistry, cyclic voltammograms were obtained using a scan rate of 100 mV/s. For compounds displaying irreversible redox chemistry, differential pulse voltammograms were obtained using a scan rate of 20 mV/s.

3.6.3 Peroxyl Radical Kinetics

Peroxyl radical clock experiments to determine inhibition rate constants, kinetic solvent effects, Arrhenius parameters and deuterium kinetic isotope effects were performed according to the procedures given in our previous reports.^{7,12}

3.6.4 Alkyl Radical Kinetics

Rate constants for trapping alkyl radicals were obtained by alkyl radical clock techniques. A 100 μL sample containing diarylamine (0.02-0.25 M, depending on k_H), bis(triphenylstannane) (0.01 M) and 2-(2-bromo-1,1-dimethylethyl)-naphthalene¹⁹ (0.01 M) in chlorobenzene was degassed by sparging with argon for 2 minutes. The sample was then irradiated for 20 minutes in a Luzchem photoreactor equipped with UVC germicidal lamps (strong line at 254 nm). The samples were transferred to GC vials and diluted with acetonitrile (300 μL) for analysis. GC analysis was carried out using an Agilent DB-5 column (30 m x 0.32 μm x 0.25 μm) with the following temperature profile: 70 °C hold 0.5 min, 1 °C/min to 82 °C, 20 °C/min to 280 °C, hold

5 min. Preparation of GC standards: 2-*tert*-butylnaphthalene and 2-*iso*-butyl-naphthalene were prepared by treating 2-(2-bromo-1,1-dimethylethyl)-naphthalene with AgClO_4 and LiAlH_4 (obtained as a 16:1 mixture by ^1H NMR).³⁴ 2-(2-methyl-1-propen-1-yl)-naphthalene was prepared via Wittig reaction.³⁵

3.6.5 Electrochemical Data

Cyclic voltammograms (or differential pulse voltammograms) for compounds **3.7-3.35**

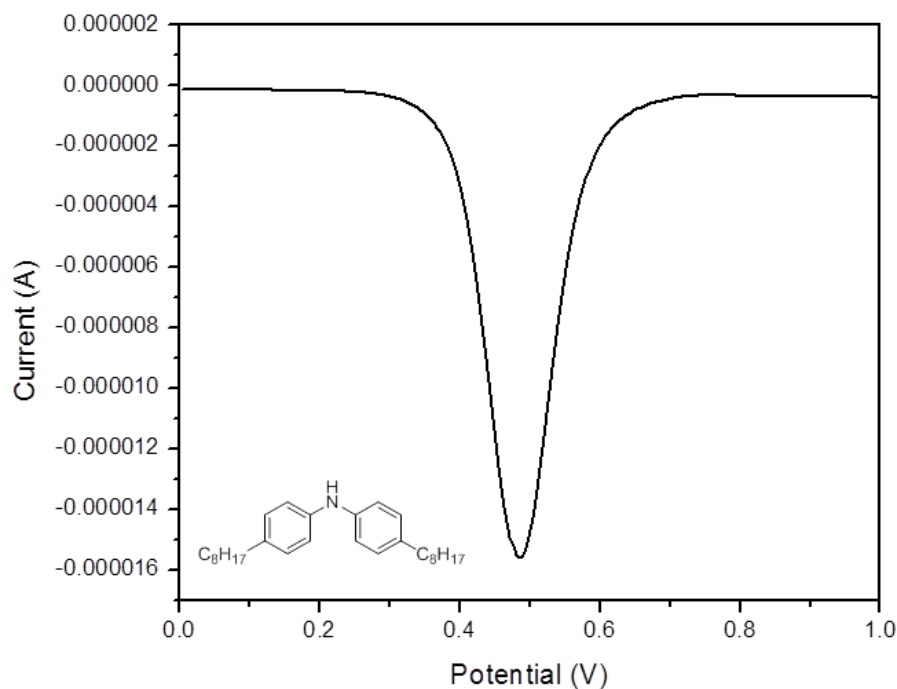


Figure 3.6.1. Differential pulse voltammogram of **3.7** vs. Ag/Ag^+ . $E_{\text{pa}} = 1.02$ V vs. NHE.

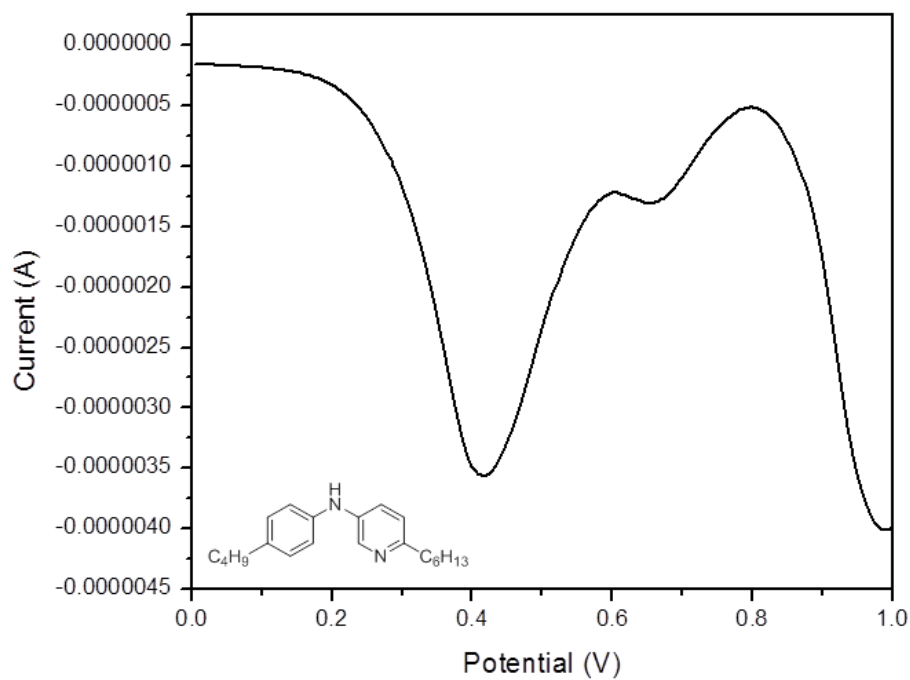


Figure 3.6.2. Differential pulse voltammogram of **3.8** vs. Ag/Ag^+ . $E_{\text{pa}} = 0.95$ V vs. NHE.

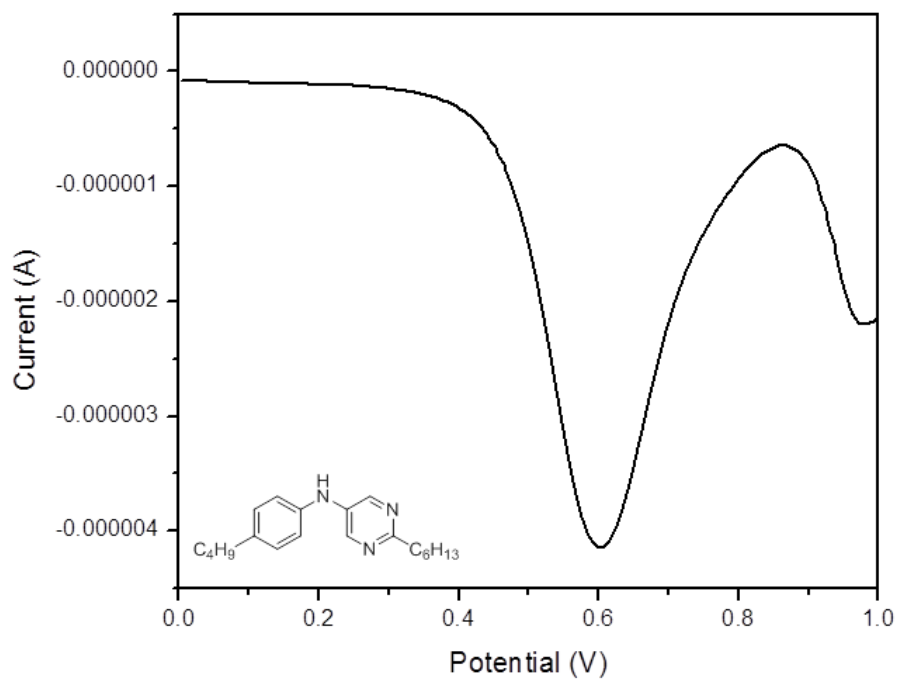


Figure 3.6.3. Differential pulse voltammogram of **3.9** vs. Ag/Ag^+ . $E_{\text{pa}} = 0.95$ V vs. NHE.

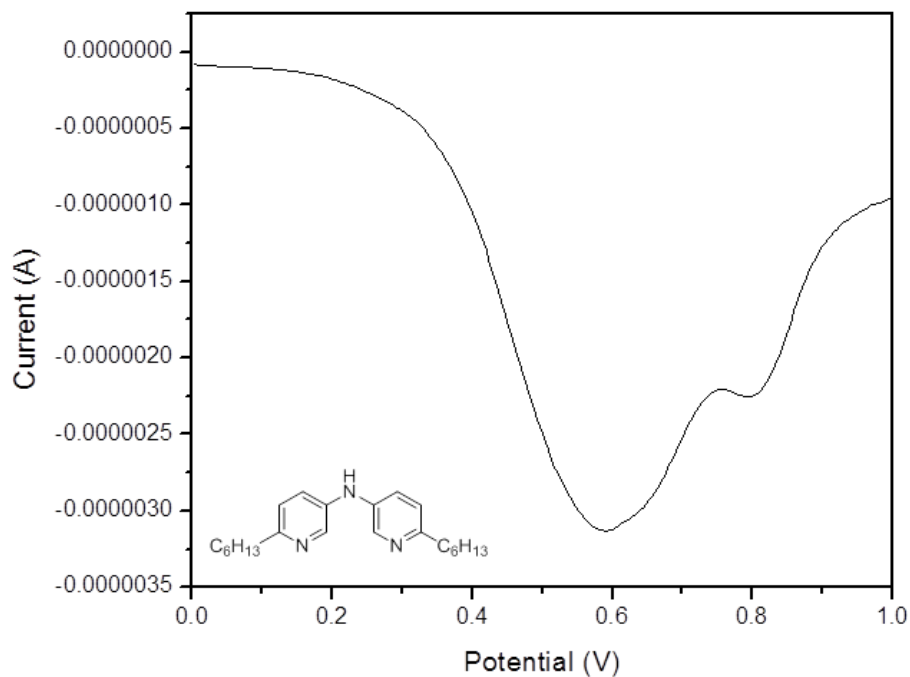


Figure 3.6.4. Differential pulse voltammogram of **3.10** vs. Ag/Ag^+ . $E_{\text{pa}} = 1.12$ V vs. NHE.

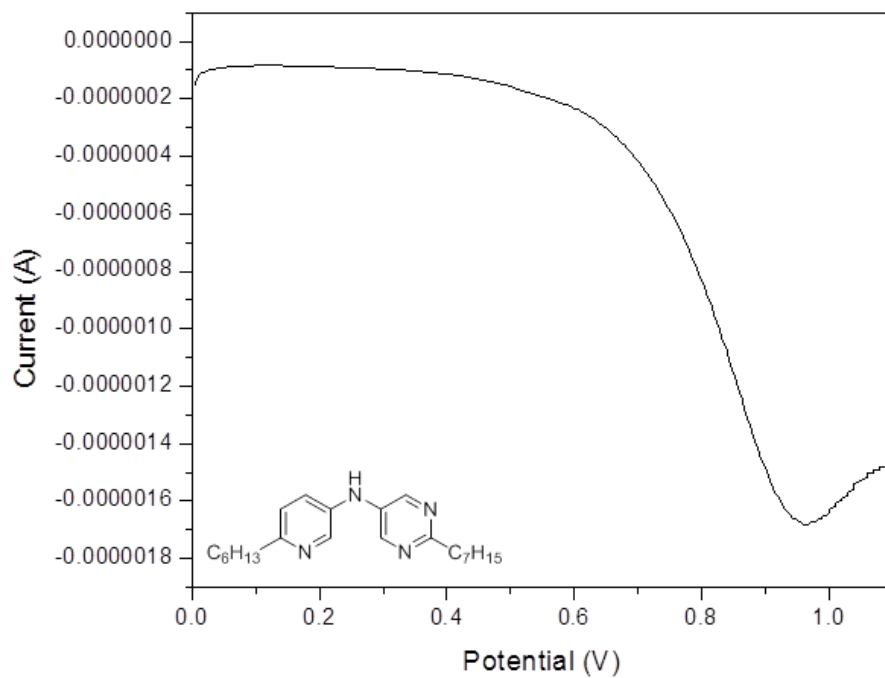


Figure 3.6.5. Differential pulse voltammogram of **3.11** vs. Ag/Ag^+ . $E_{\text{pa}} = 1.50$ V vs. NHE.

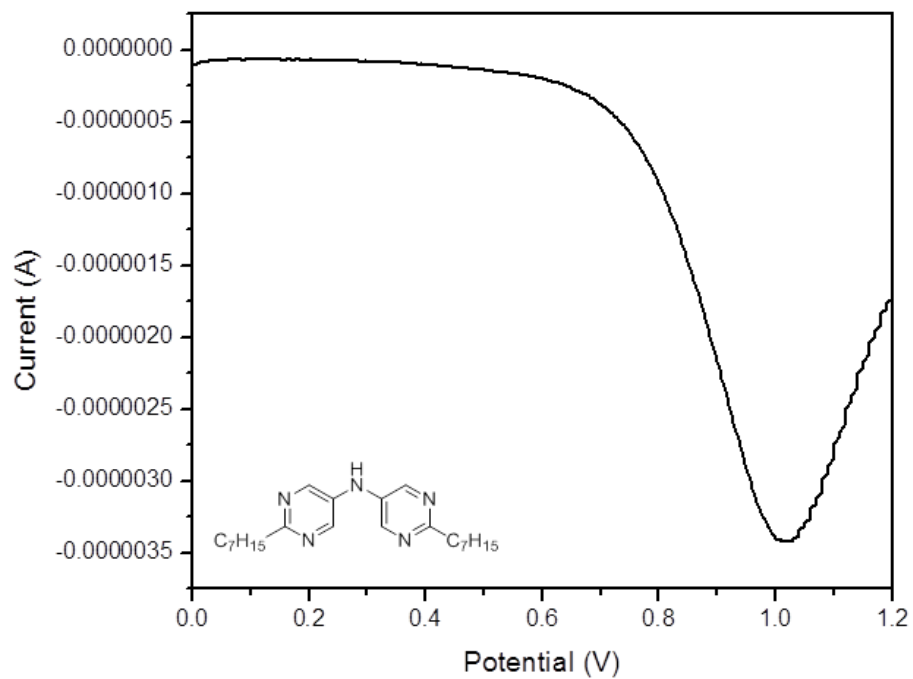


Figure 3.6.6. Differential pulse voltammogram of **3.12** vs. Ag/Ag⁺. E_{pa} = 1.55 V vs. NHE.

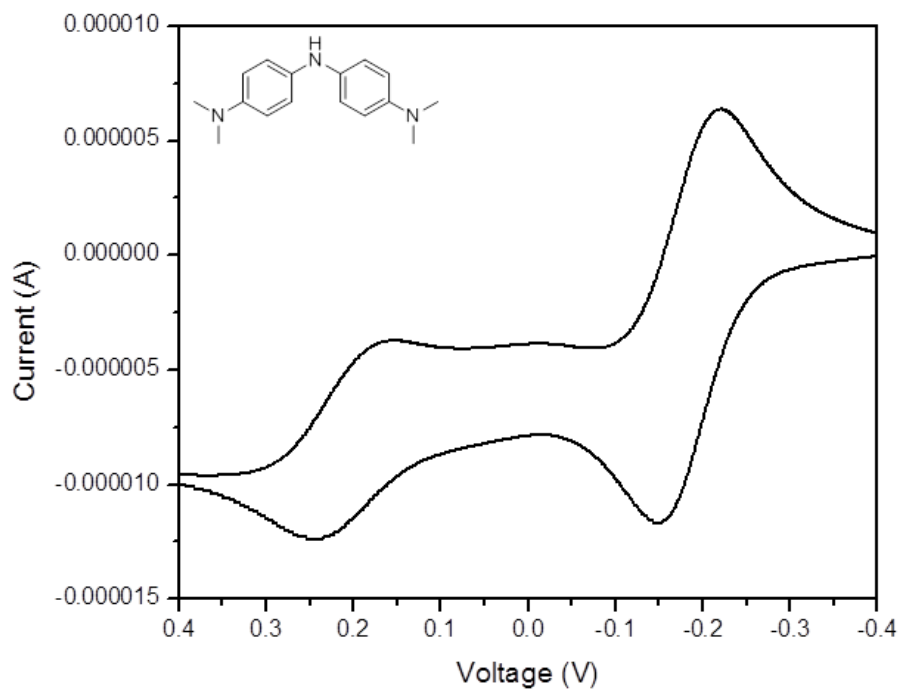


Figure 3.6.7. Cyclic voltammogram of **3.13** vs. Ag/Ag⁺. E° = 0.34 V vs. NHE.

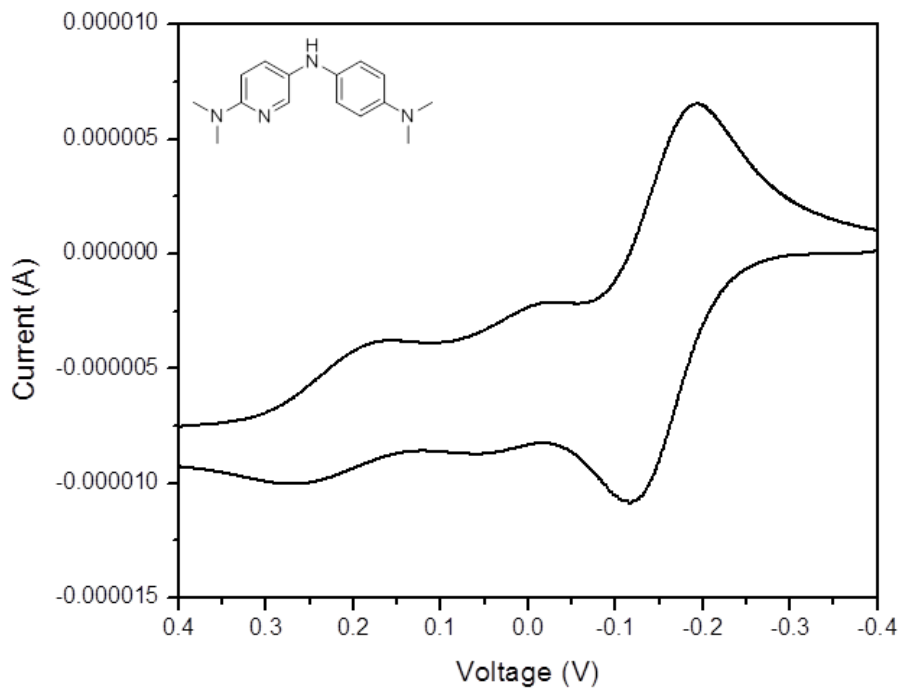


Figure 3.6.8. Cyclic voltammogram of **3.14** vs. Ag/Ag^+ . $E^\circ = 0.37$ V vs. NHE.

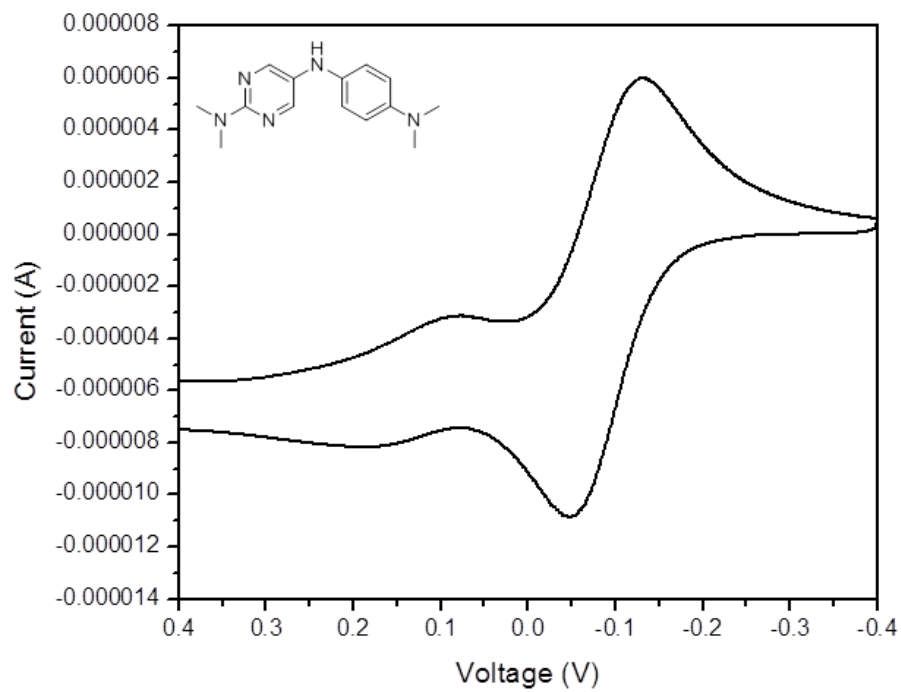


Figure 3.6.9. Cyclic voltammogram of **3.15** vs. Ag/Ag^+ . $E^\circ = 0.44$ V vs. NHE.

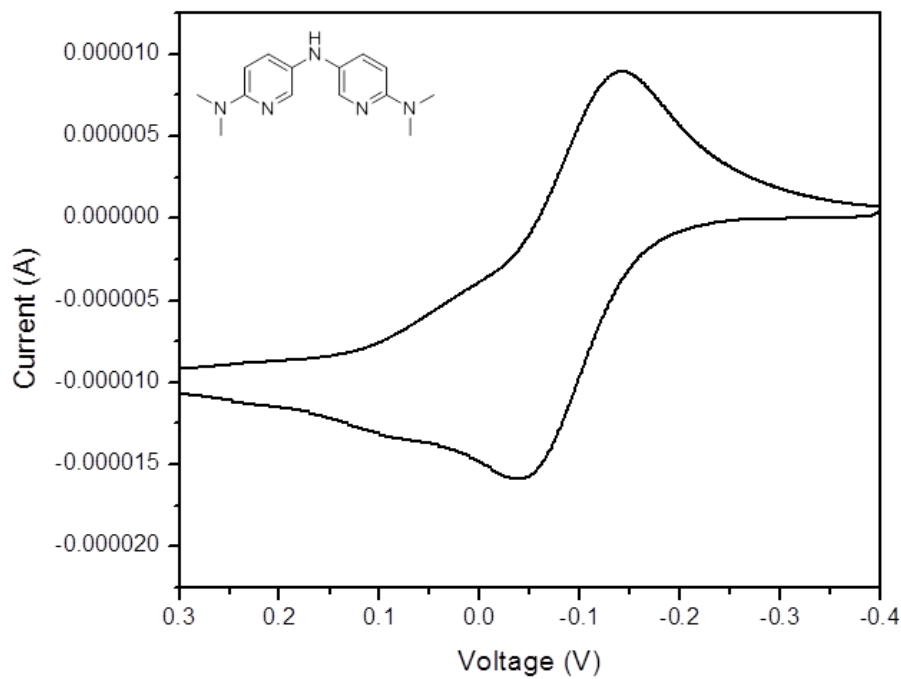


Figure 3.6.10. Cyclic voltammogram of **3.16** vs. Ag/Ag^+ . $E^\circ = 0.44$ V vs. NHE.

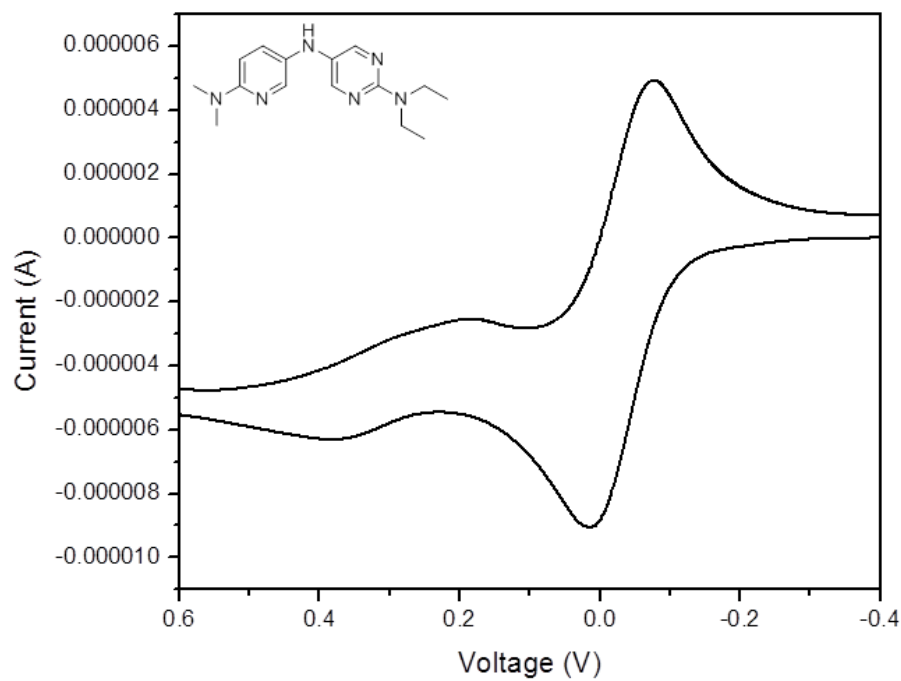


Figure 3.6.11. Cyclic voltammogram of **3.18** vs. Ag/Ag^+ . $E^\circ = 0.50$ V vs. NHE.

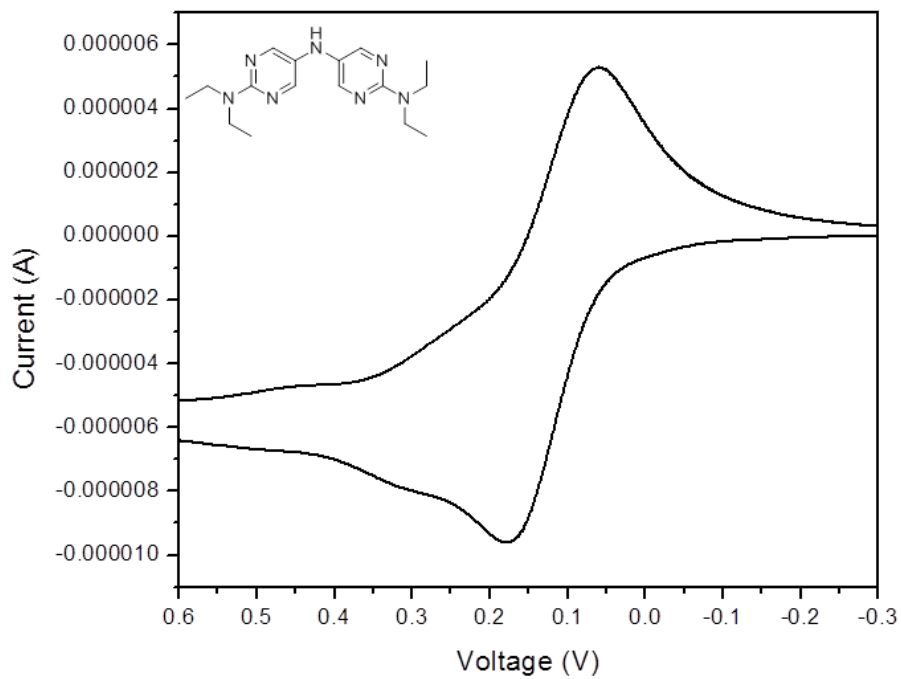


Figure 3.6.12. Cyclic voltammogram of **3.18** vs. Ag/Ag^+ . $E^\circ = 0.65$ V vs. NHE.

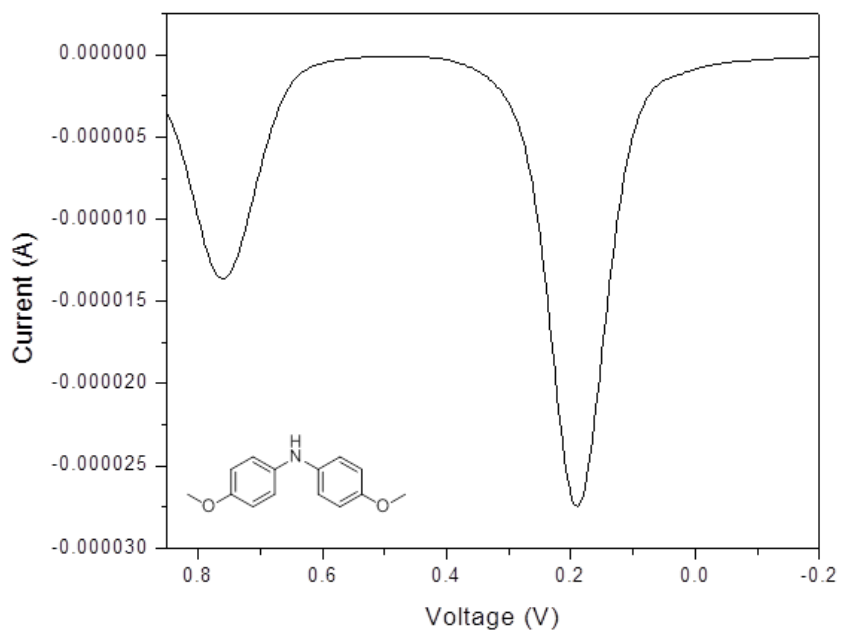


Figure 3.6.13. Cyclic voltammogram of **3.19** vs. Ag/Ag^+ . $E_{\text{pa}} = 0.70$ V vs. NHE.

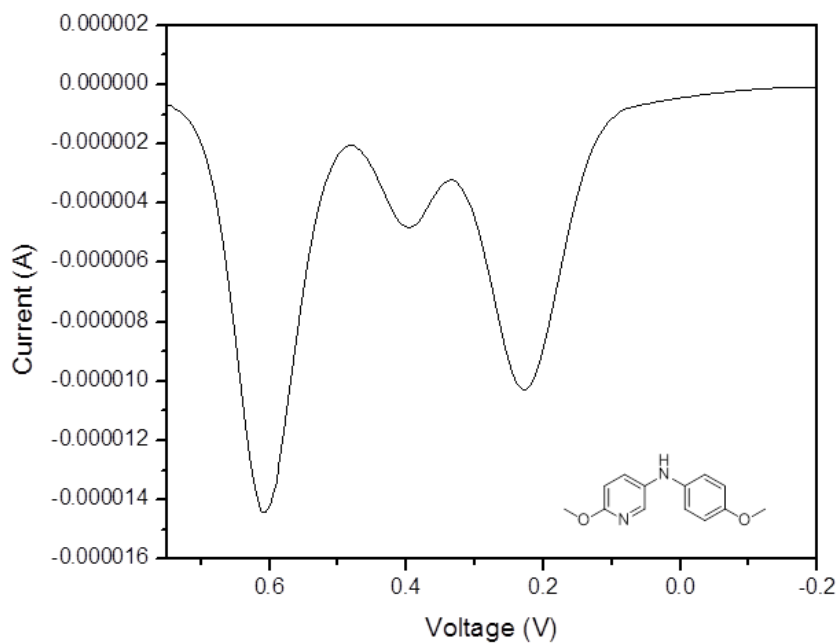


Figure 3.6.14. Cyclic voltammogram of **3.20** vs. Ag/Ag^+ . $E_{\text{pa}} = 0.74$ V vs. NHE.

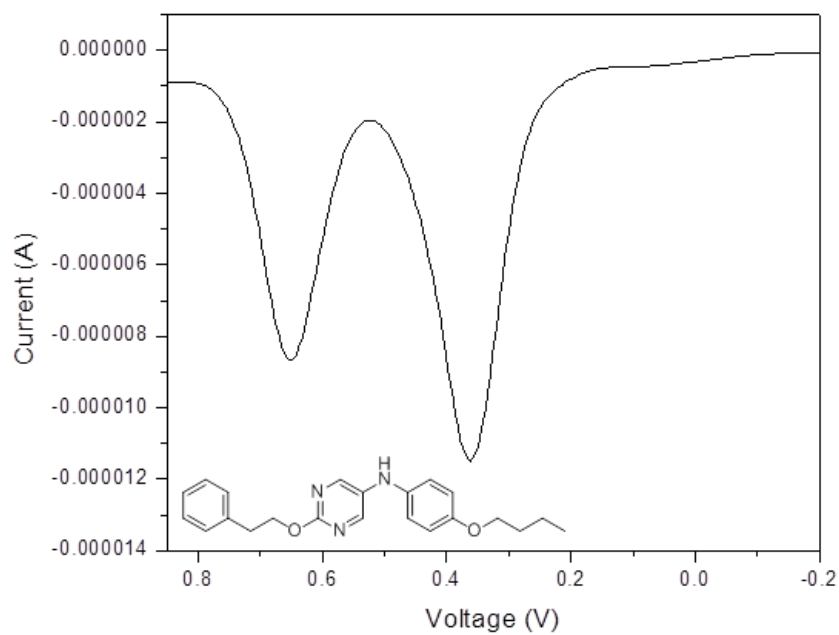


Figure 3.6.15. Cyclic voltammogram of **3.21** vs. Ag/Ag^+ . $E_{\text{pa}} = 0.88$ V vs. NHE.

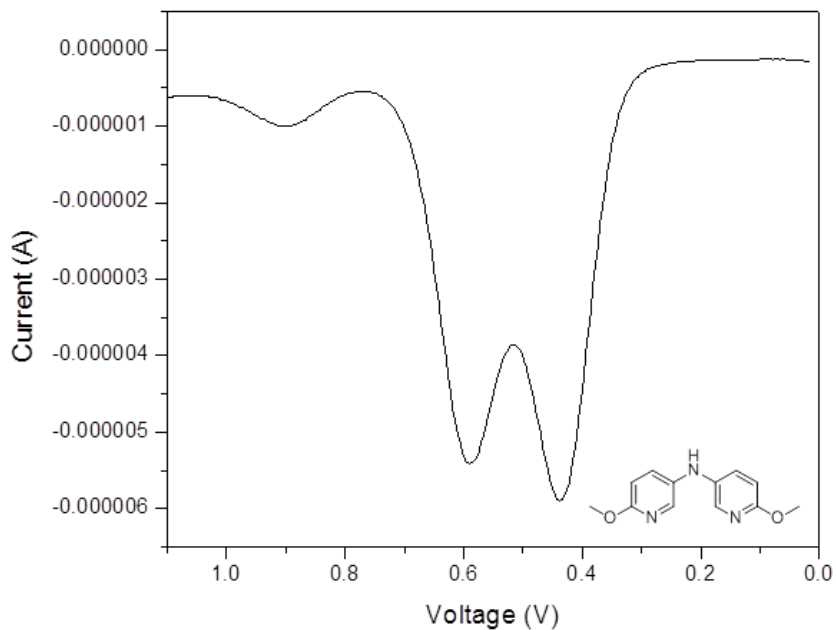


Figure 3.6.16. Cyclic voltammogram of **3.22** vs. Ag/Ag^+ . $E_{\text{pa}} = 0.95$ V vs. NHE.

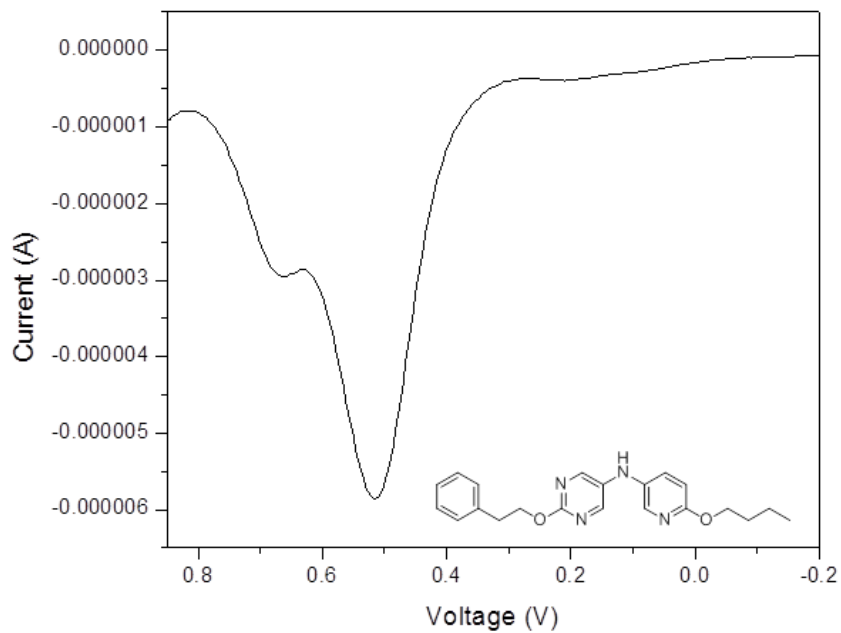


Figure 3.6.17. Cyclic voltammogram of **3.23** vs. Ag/Ag^+ . $E_{\text{pa}} = 1.03$ V vs. NHE.

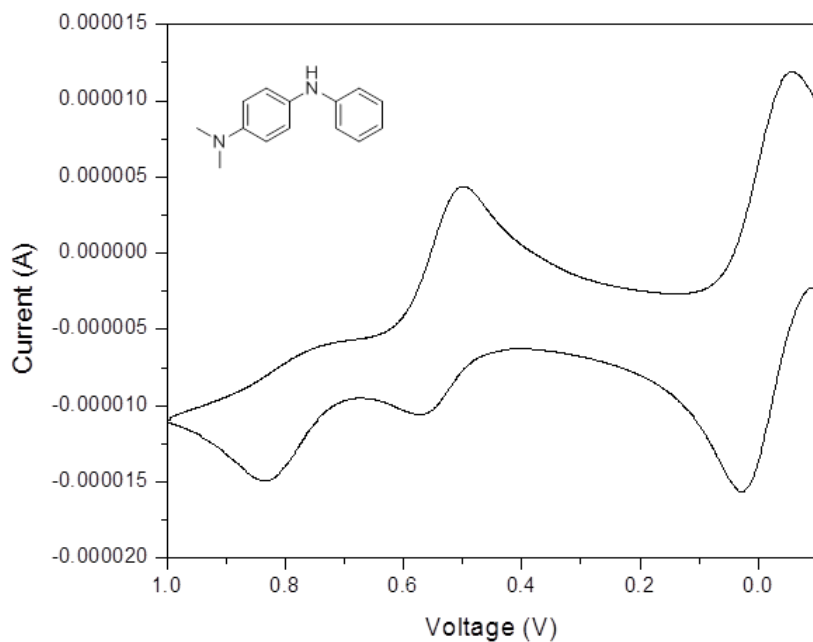


Figure 3.6.18. Cyclic voltammogram of **3.24** vs. Ag/Ag^+ . $E^\circ = 0.51$ V vs. NHE.

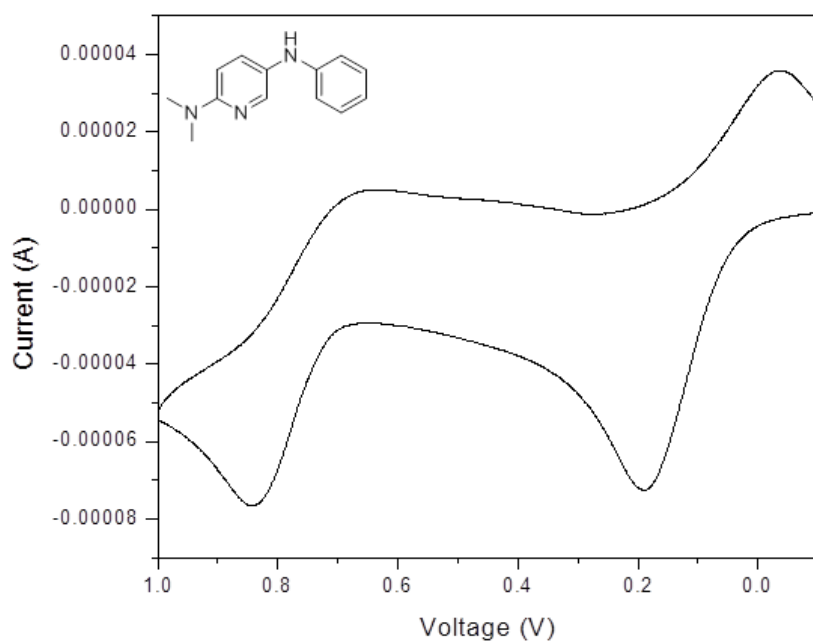


Figure 3.6.19. Cyclic voltammogram of **3.25** vs. Ag/Ag^+ . $E^\circ = 0.60$ V vs. NHE.

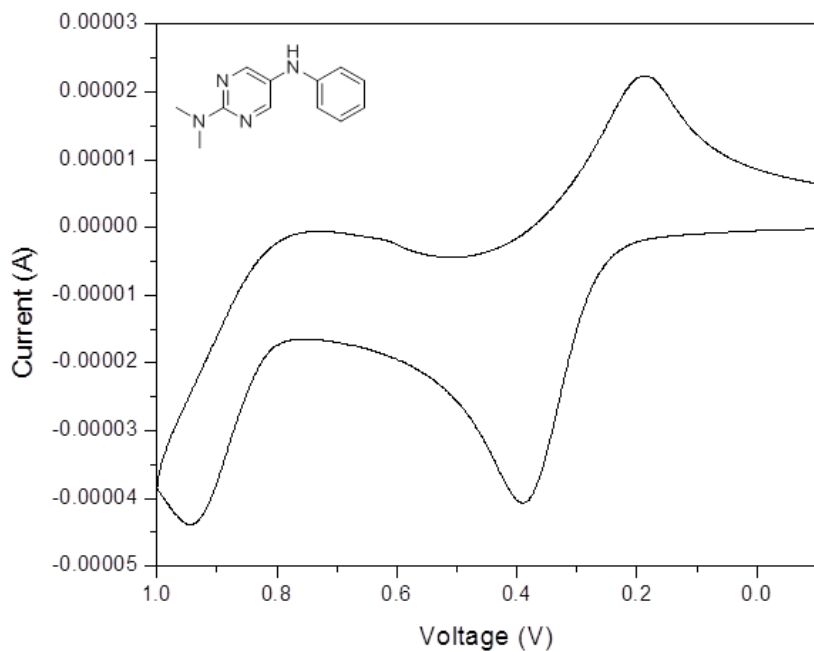


Figure 3.6.20. Cyclic voltammogram of **3.26** vs. Ag/Ag^+ . $E^\circ = 0.81$ V vs. NHE.

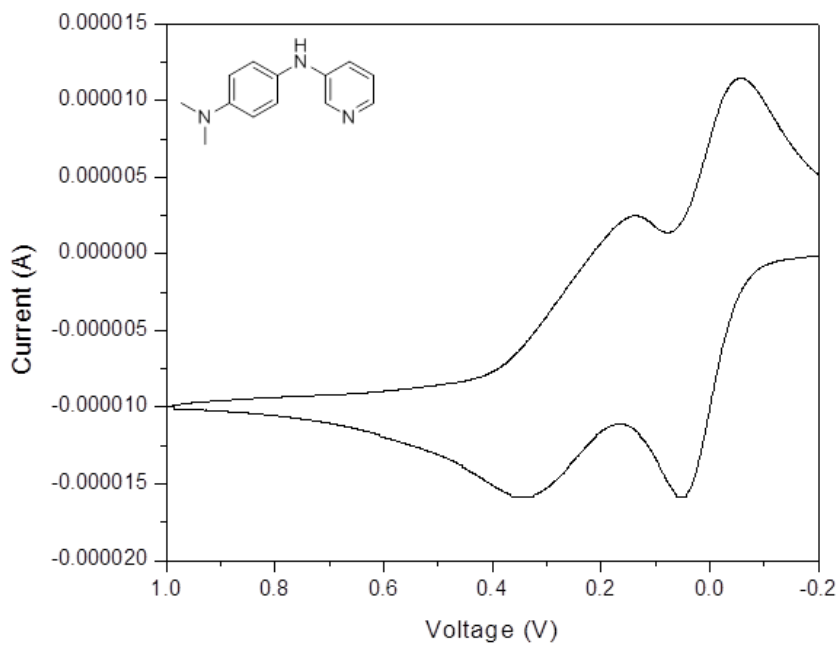


Figure 3.6.21. Cyclic voltammogram of **3.27** vs. Ag/Ag^+ . $E^\circ = 0.53$ V vs. NHE.

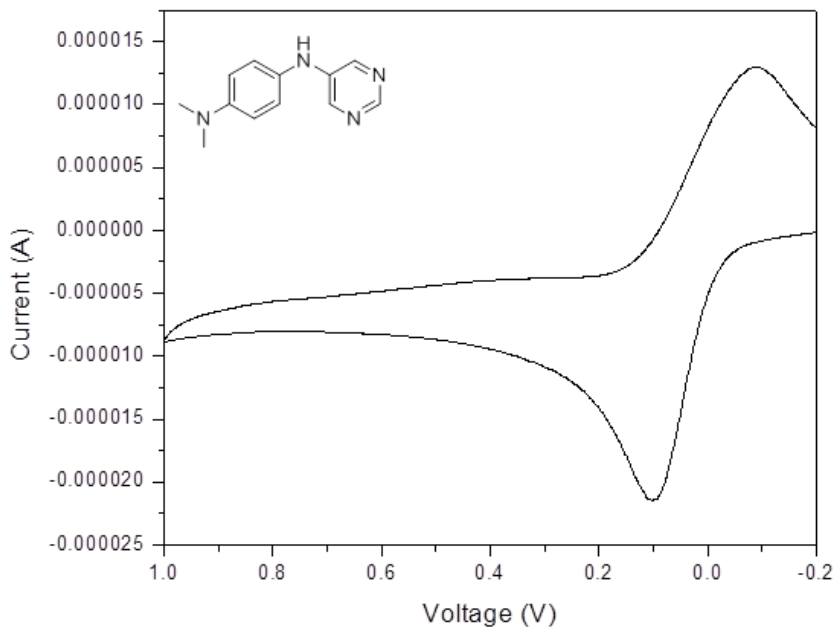


Figure 3.6.22. Cyclic voltammogram of **3.28** vs. Ag/Ag^+ . $E^\circ = 0.56$ V vs. NHE.

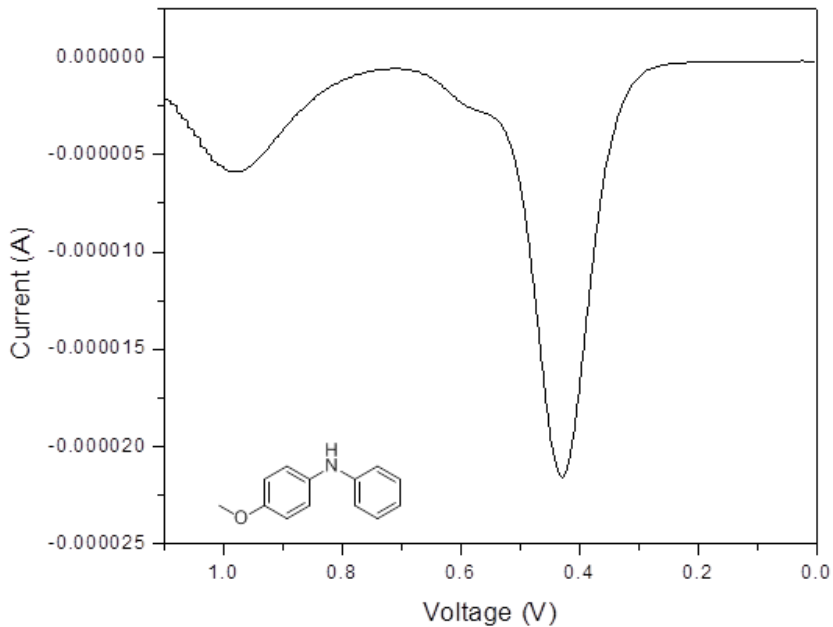


Figure 3.6.23. Cyclic voltammogram of **3.29** vs. Ag/Ag^+ . $E_{\text{pa}} = 0.94$ V vs. NHE.

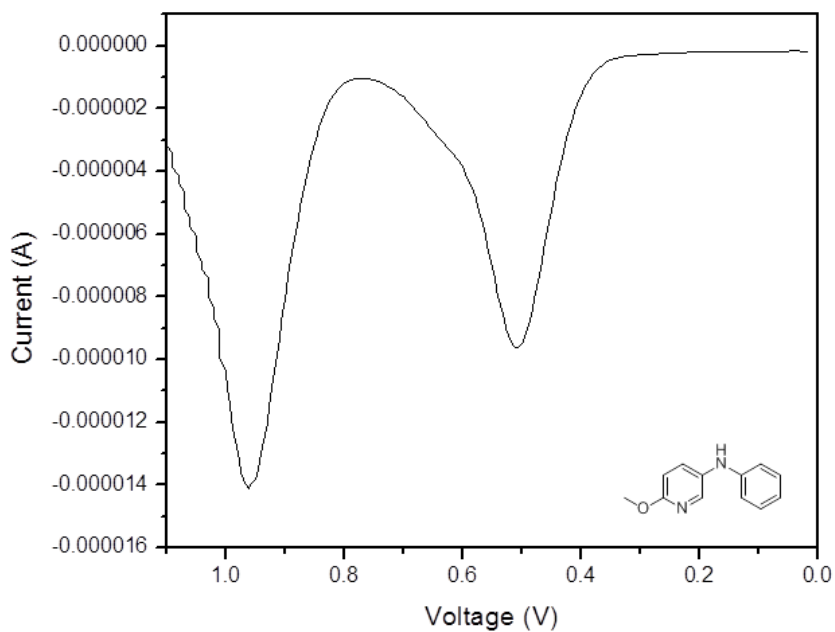


Figure 3.6.24. Cyclic voltammogram of **3.30** vs. Ag/Ag^+ . $E_{\text{pa}} = 1.02$ V vs. NHE.

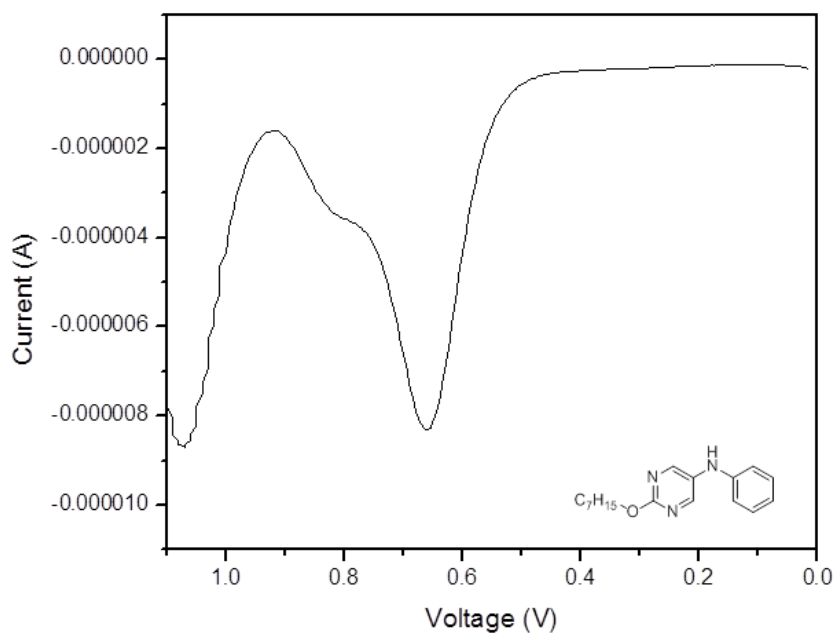


Figure 3.6.25. Cyclic voltammogram of **3.31** vs. Ag/Ag^+ . $E_{\text{pa}} = 1.17$ V vs. NHE.

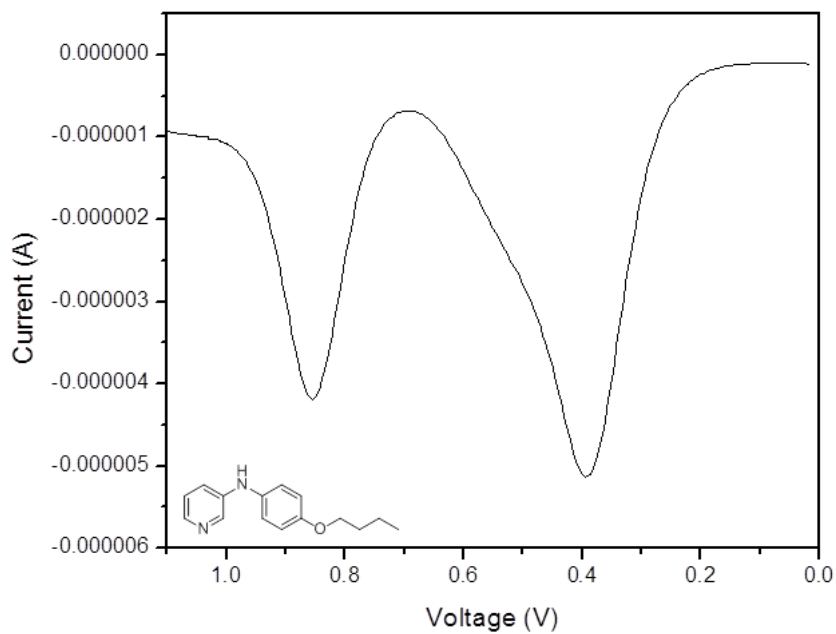


Figure 3.6.26. Cyclic voltammogram of **3.32** vs. Ag/Ag^+ . $E_{\text{pa}} = 0.90$ V vs. NHE.

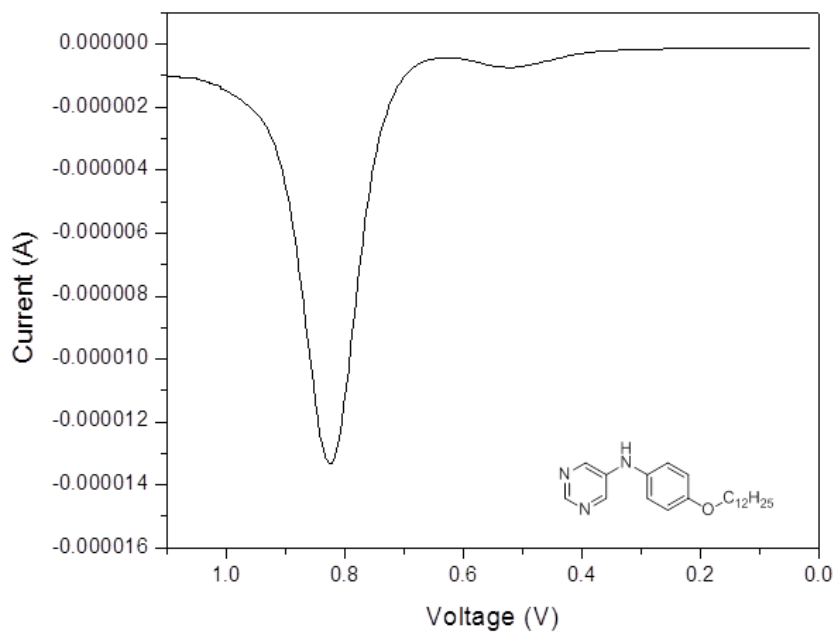


Figure 3.6.27. Cyclic voltammogram of **3.33** vs. Ag/Ag^+ . $E_{\text{pa}} = 1.34$ V vs. NHE.

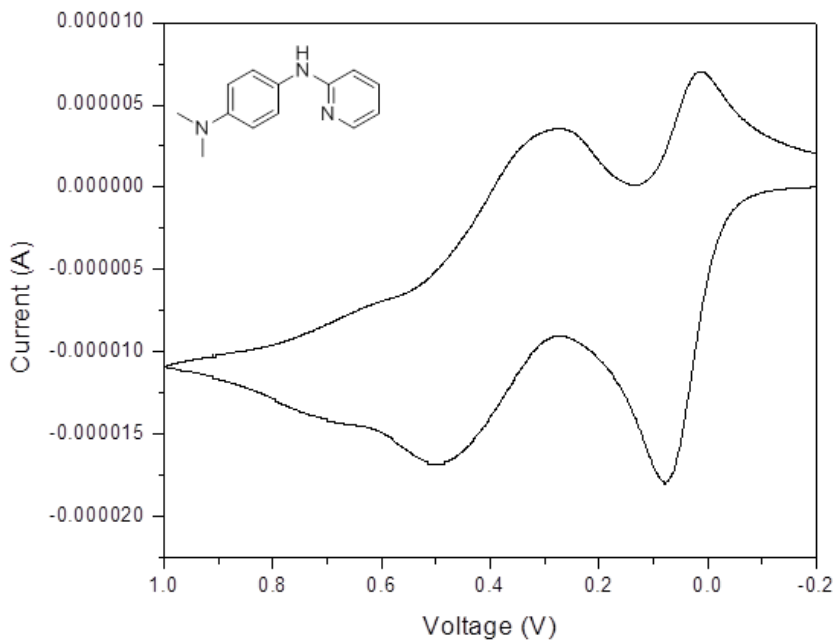


Figure 3.6.28. Cyclic voltammogram of **3.34** vs. Ag/Ag^+ . $E_{\text{pa}} = 0.57$ V vs. NHE.

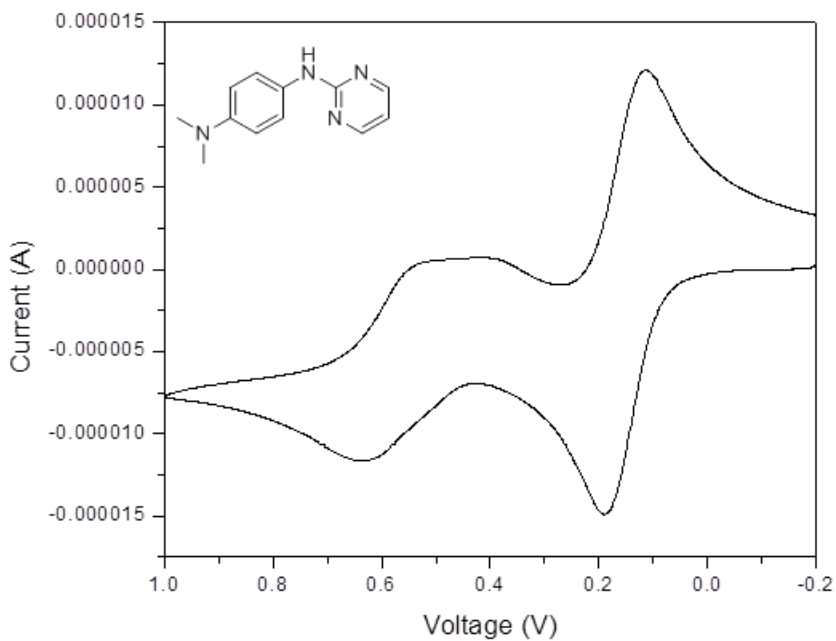


Figure 3.6.29. Cyclic voltammogram of **3.35** vs. Ag/Ag^+ . $E_{\text{pa}} = 0.64$ V vs. NHE.

3.6.6 Peroxyl Kinetics Data

Plotted data from peroxy radical clock experiments used to determine k_H for **3.7-3.35**.

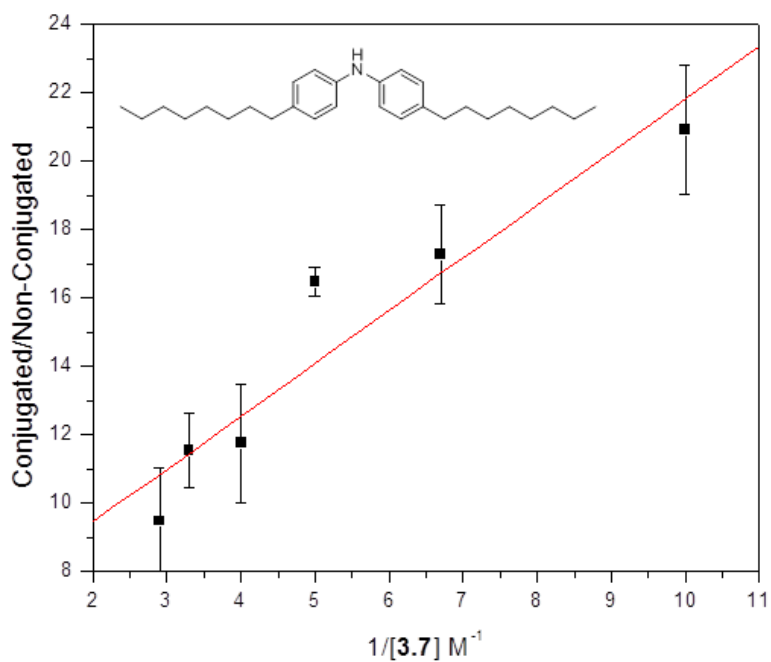


Figure 3.6.30. Double reciprocal plot used to obtain $k_1 = 1.8 \times 10^5 \text{ M}^{-1}\text{s}^{-1}$ for compound **3.7**.

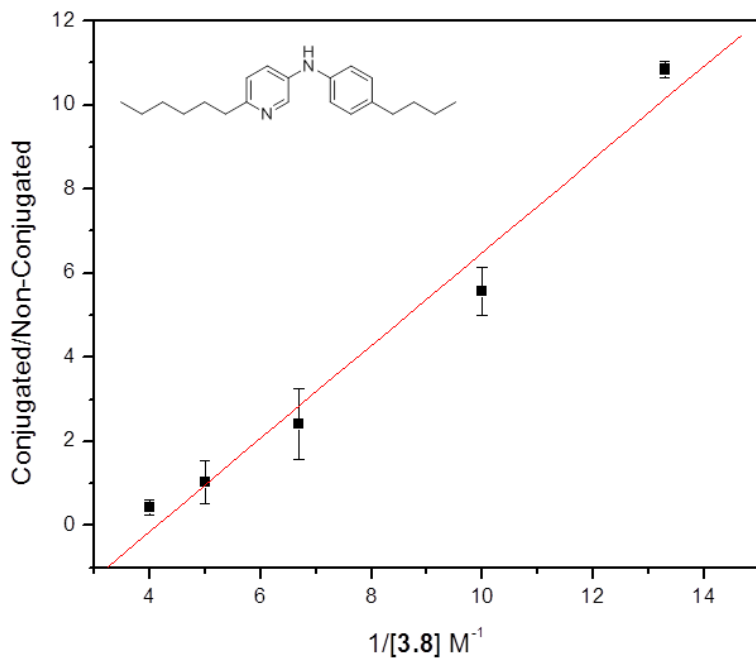


Figure 3.6.31. Double reciprocal plot used to obtain $k_1 = 1.5 \times 10^5 \text{ M}^{-1}\text{s}^{-1}$ for compound **3.8**.

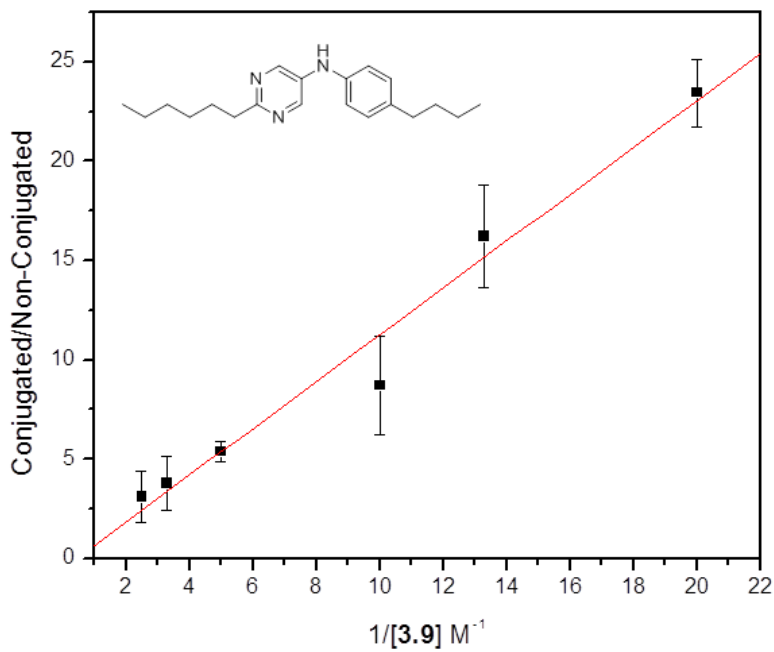


Figure 3.6.32. Double reciprocal plot used to obtain $k_1 = 1.5 \times 10^5 \text{ M}^{-1}\text{s}^{-1}$ for compound **3.9**.

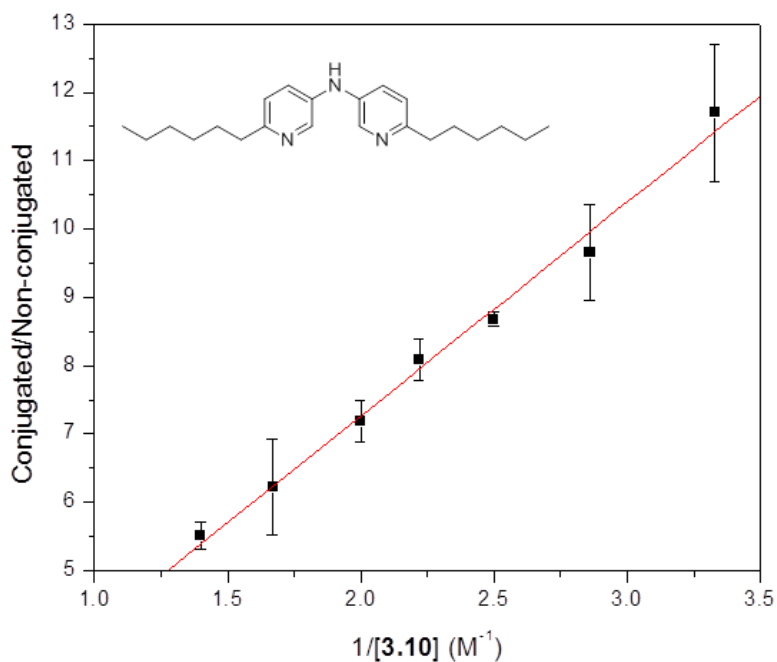


Figure 3.6.32. Double reciprocal plot used to obtain $k_1 = 9.4 \times 10^4 \text{ M}^{-1}\text{s}^{-1}$ for compound **3.10**. Measurement was made using a phenyl-based peroxyester to improve resolution of a co-eluting peak observed when using the naphthyl-peroxyester described above.²

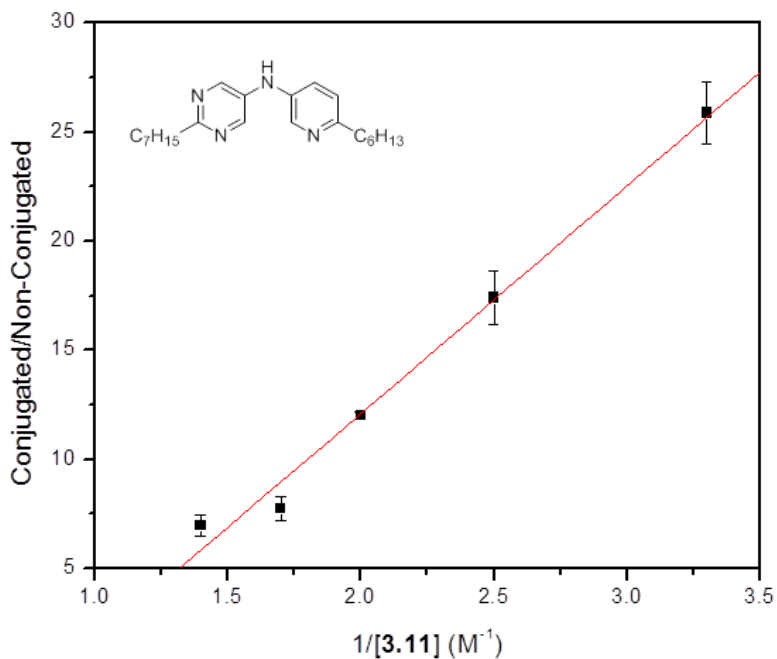


Figure 3.6.33. Double reciprocal plot used to obtain $k_1 = 7.7 \times 10^4 \text{ M}^{-1}\text{s}^{-1}$ for compound **3.11**.

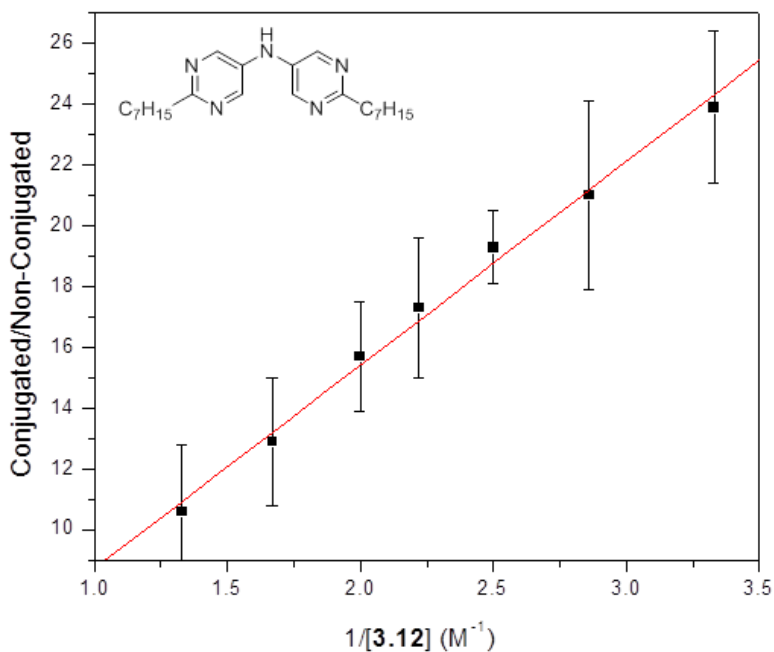


Figure 3.6.34. Double reciprocal plot used to obtain $k_1 = 2.4 \times 10^4 M^{-1}s^{-1}$ for compound 3.12.

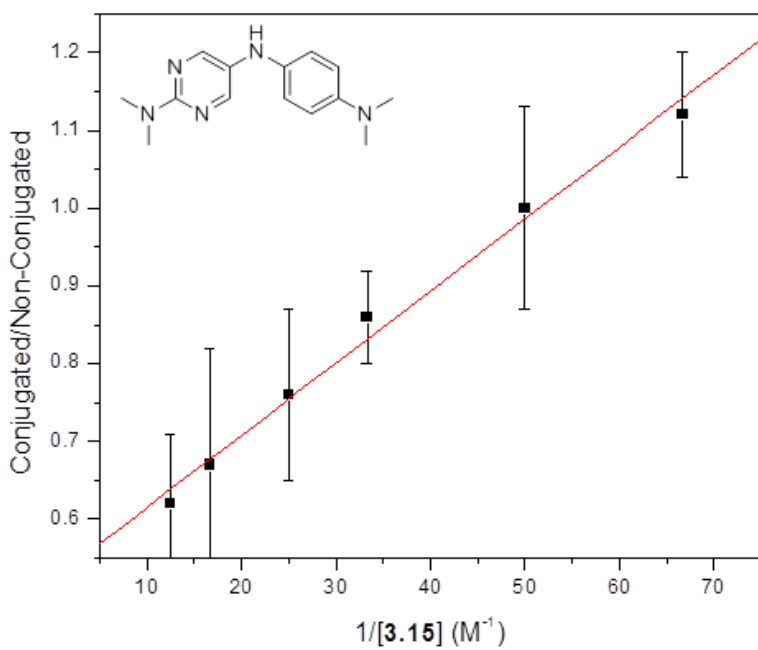


Figure 3.6.35. Double reciprocal plot used to obtain $k_1 = 3.7 \times 10^7 M^{-1}s^{-1}$ for compound 3.15.

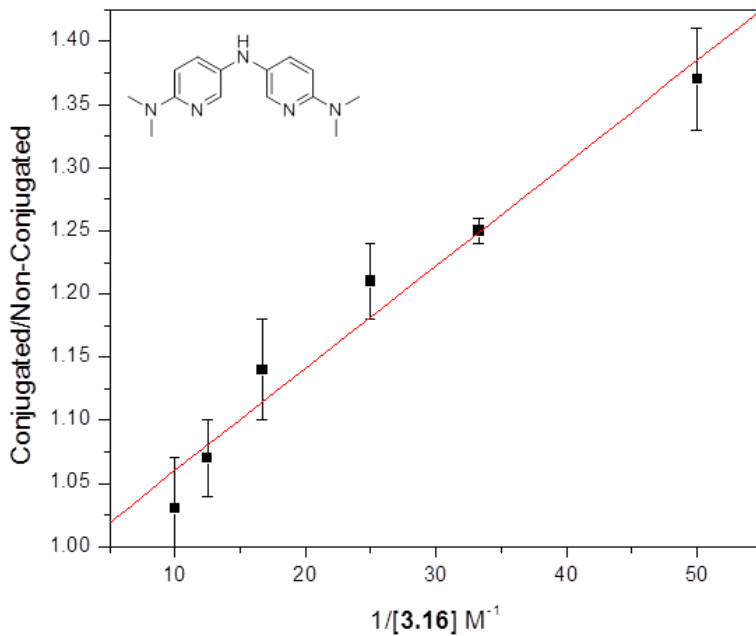


Figure 3.6.36. Double reciprocal plot used to obtain $k_1 = 3.4 \times 10^7 \text{ M}^{-1}\text{s}^{-1}$ for compound **3.16**.

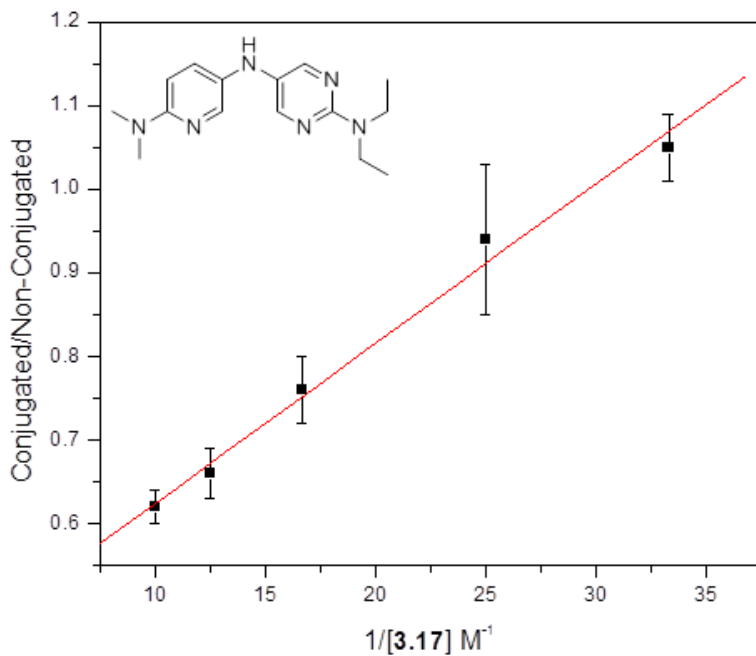


Figure 3.6.37. Double reciprocal plot used to obtain $k_1 = 3.1 \times 10^7 \text{ M}^{-1}\text{s}^{-1}$ for compound **3.17**.

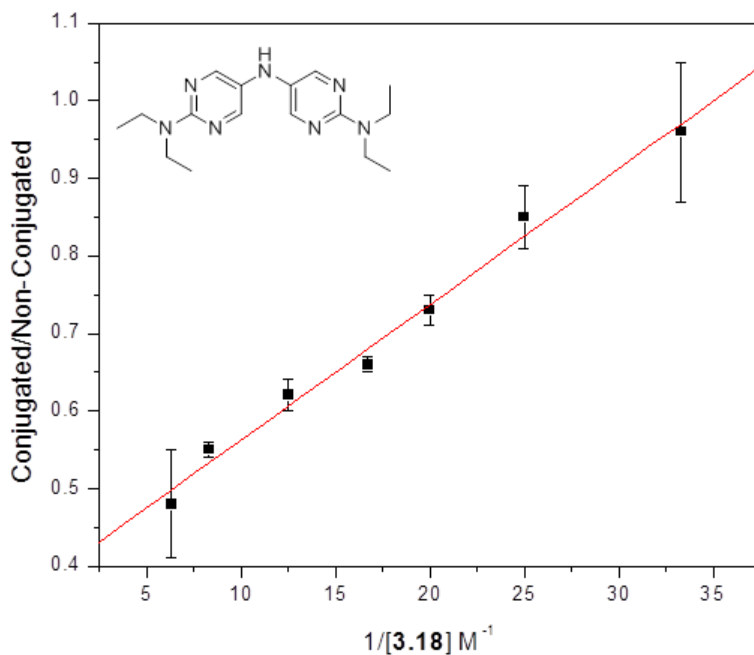


Figure 3.6.38. Double reciprocal plot used to obtain $k_1 = 1.8 \times 10^7 \text{ M}^{-1}\text{s}^{-1}$ for compound **3.18**.

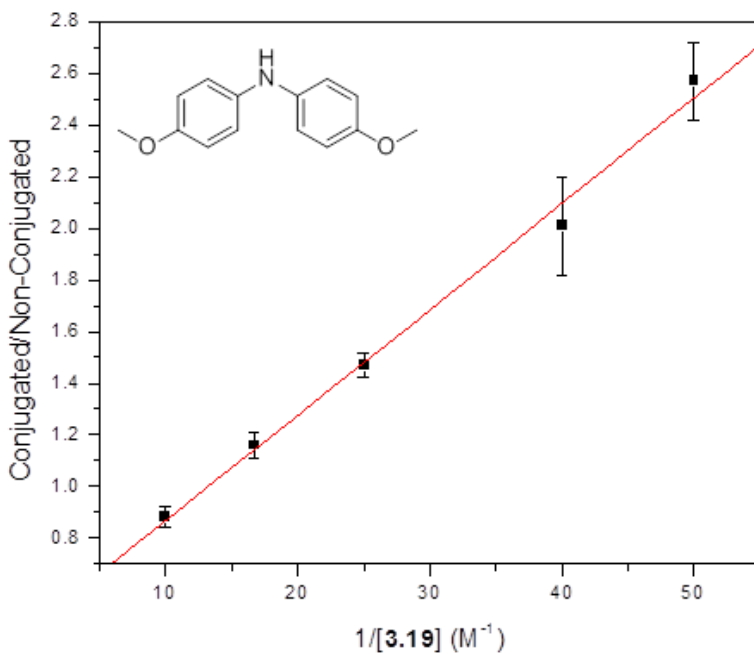


Figure 3.6.39. Double reciprocal plot used to obtain $k_1 = 3.7 \times 10^6 \text{ M}^{-1}\text{s}^{-1}$ for compound **3.19**.

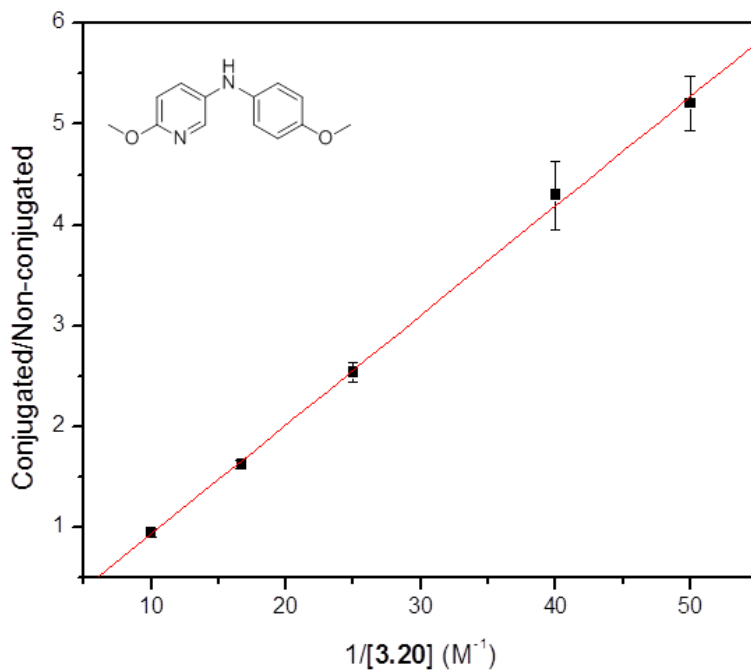


Figure 3.6.40. Double reciprocal plot used to obtain $k_1 = 1.4 \times 10^6 M^{-1}s^{-1}$ for compound 3.20.

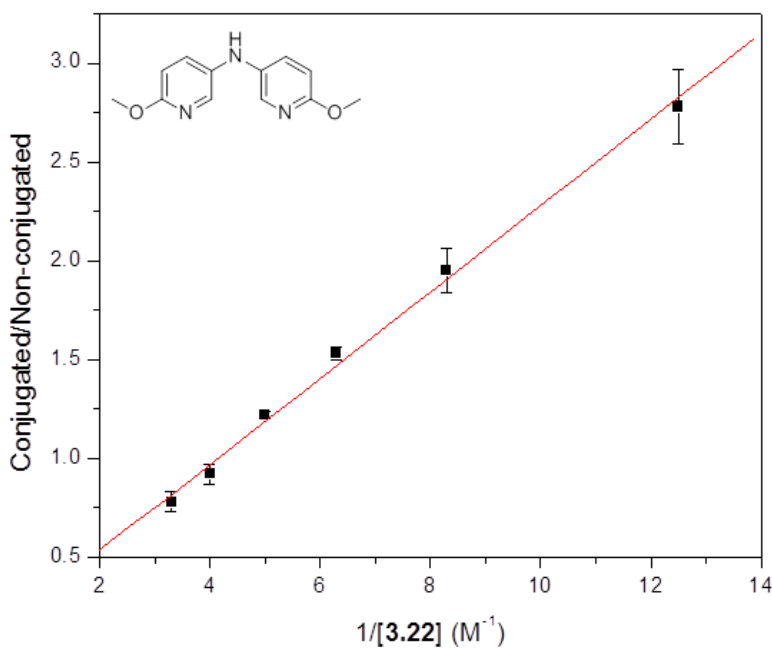


Figure 3.6.41. Double reciprocal plot used to obtain $k_1 = 9.0 \times 10^5 M^{-1}s^{-1}$ for compound 3.22.

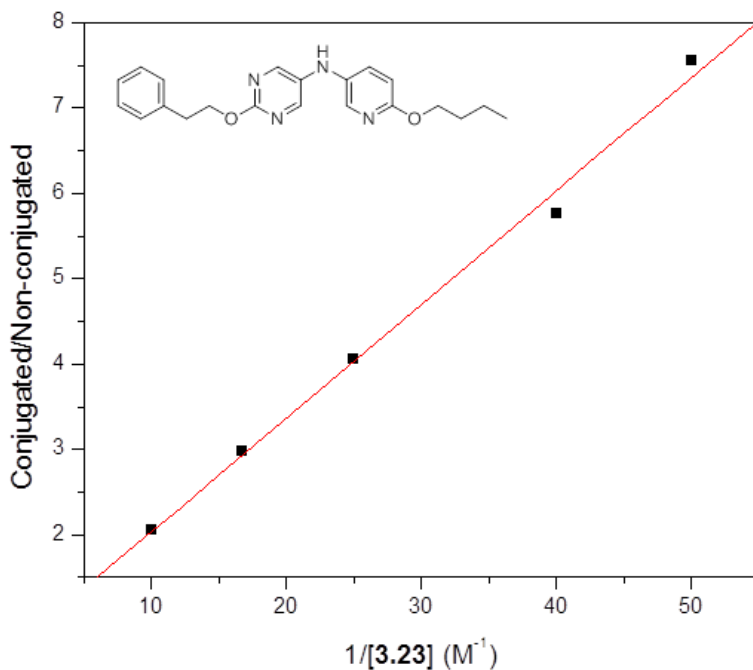


Figure 3.6.42. Double reciprocal plot used to obtain $k_1 = 6.0 \times 10^5 \text{ M}^{-1}\text{s}^{-1}$ for compound **3.23**.

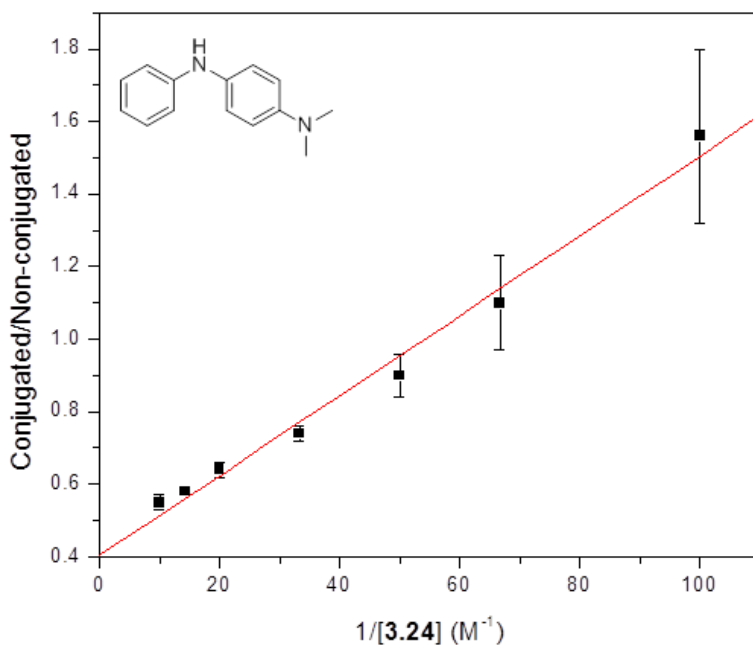


Figure 3.6.43. Double reciprocal plot used to obtain $k_1 = 1.3 \times 10^7 \text{ M}^{-1}\text{s}^{-1}$ for compound **3.24**.

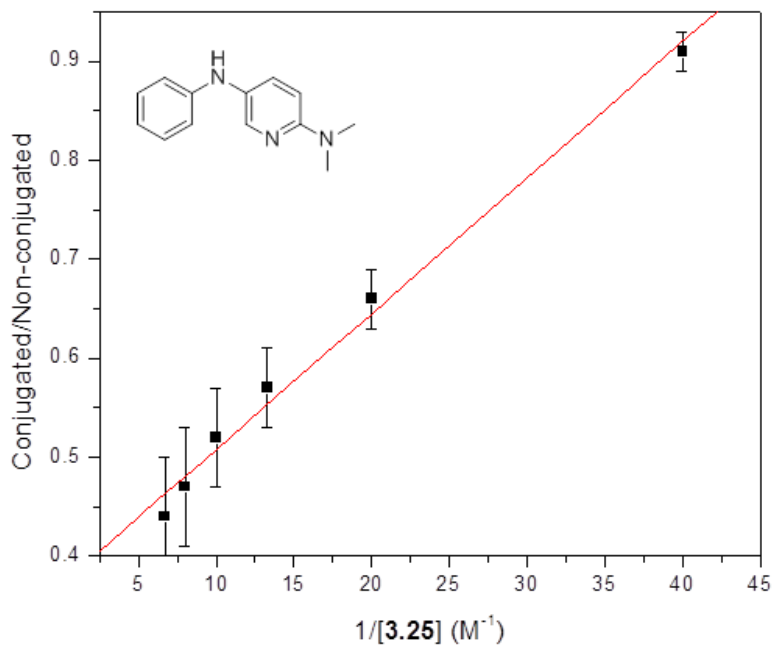


Figure 3.6.44. Double reciprocal plot used to obtain $k_1 = 1.1 \times 10^7 M^{-1}s^{-1}$ for compound **3.25**.

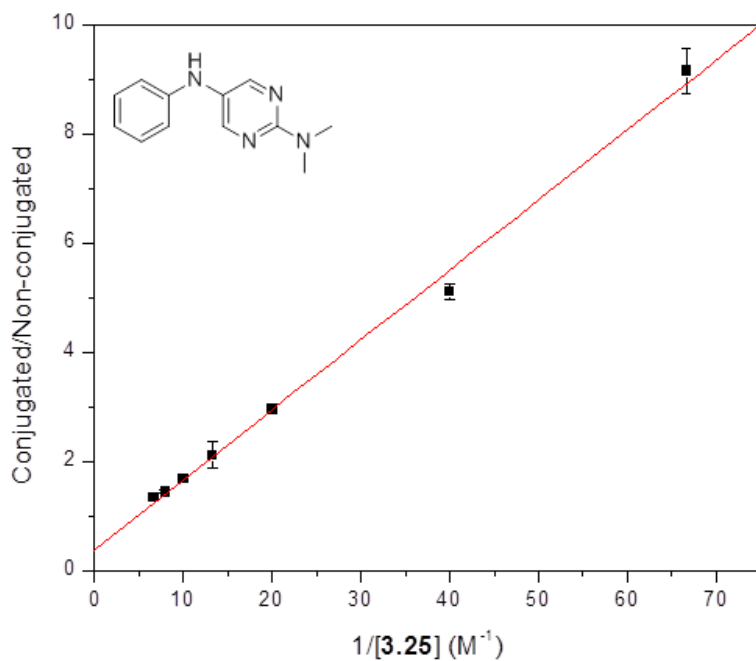


Figure 3.6.45. Double reciprocal plot used to obtain $k_1 = 3.0 \times 10^6 M^{-1}s^{-1}$ for compound **3.26**.

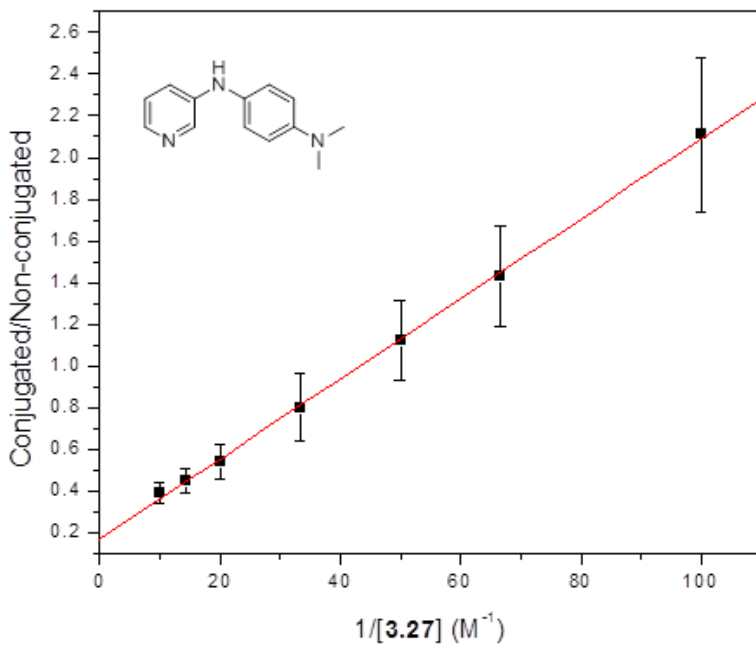


Figure 3.6.46. Double reciprocal plot used to obtain $k_1 = 8.0 \times 10^6 \text{ M}^{-1}\text{s}^{-1}$ for compound **3.27**.

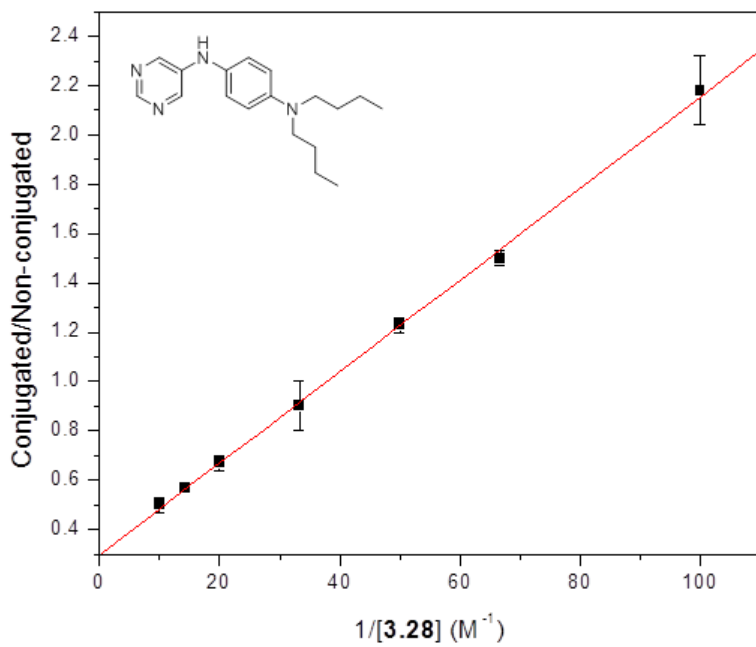


Figure 3.6.47. Double reciprocal plot used to obtain $k_1 = 8.0 \times 10^6 \text{ M}^{-1}\text{s}^{-1}$ for compound **3.28**.

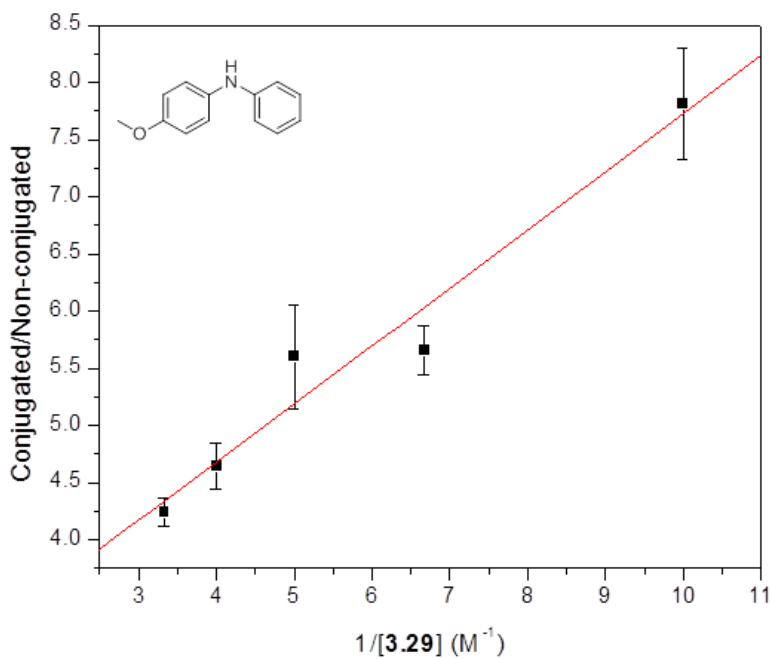


Figure 3.6.48. Double reciprocal plot used to obtain $k_1 = 3.2 \times 10^5 M^{-1}s^{-1}$ for compound **3.29**.

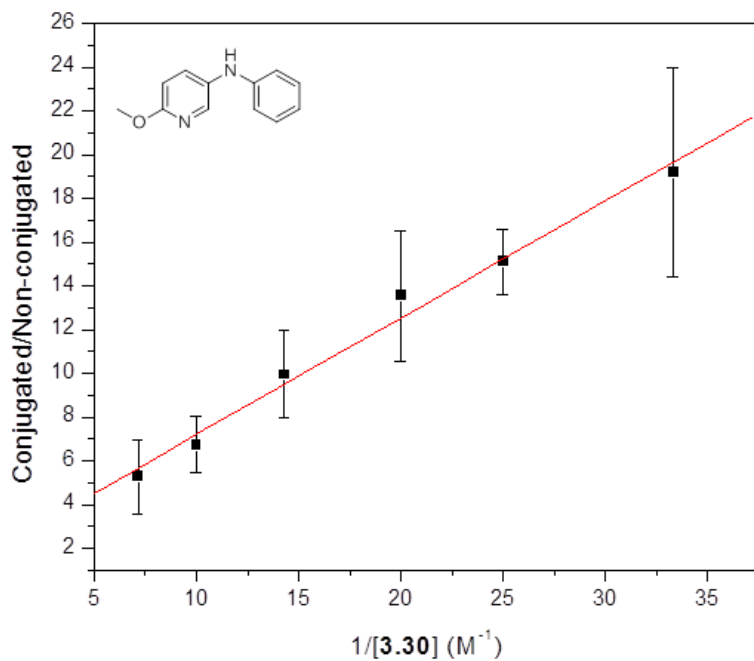


Figure 3.6.49. Double reciprocal plot used to obtain $k_1 = 2.9 \times 10^5 M^{-1}s^{-1}$ for compound **3.30**.

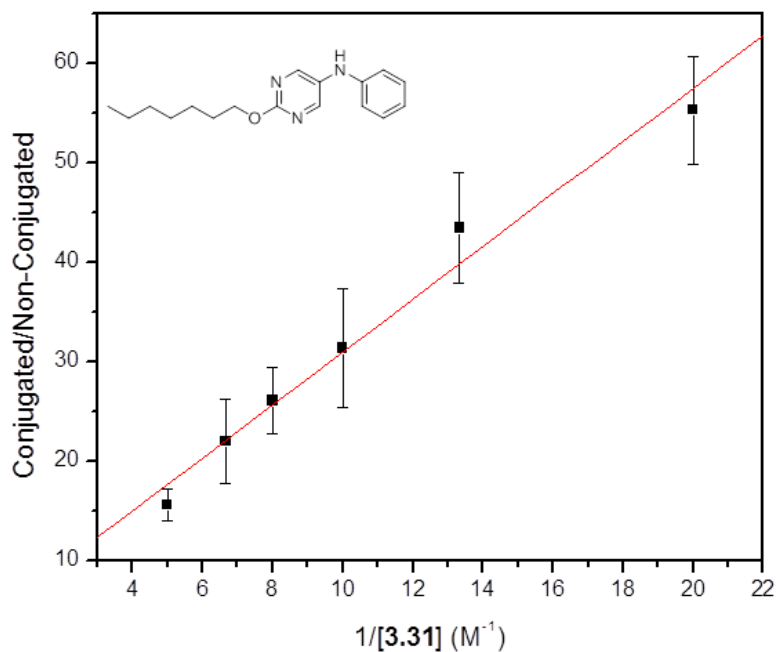


Figure 3.6.50. Double reciprocal plot used to obtain $k_1 = 6.0 \times 10^4 M^{-1}s^{-1}$ for compound 3.31.

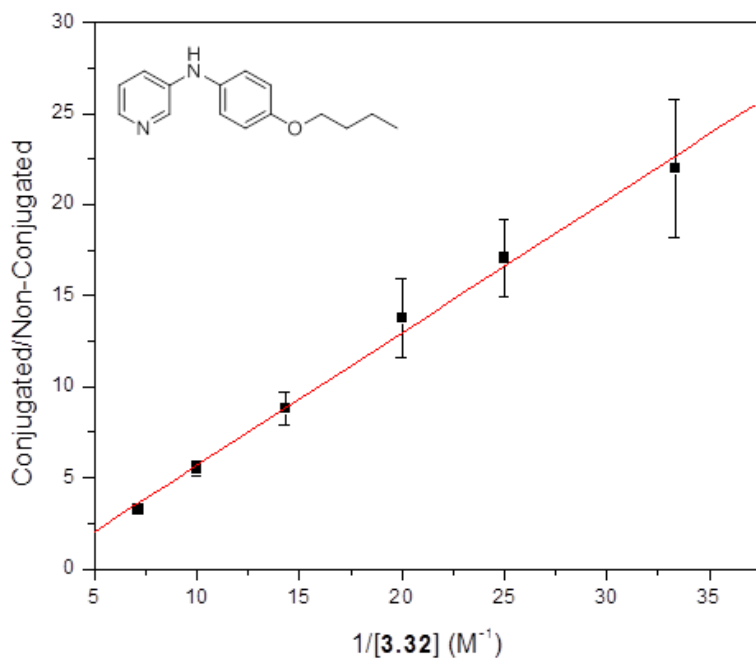


Figure 3.6.51. Double reciprocal plot used to obtain $k_1 = 2.1 \times 10^5 M^{-1}s^{-1}$ for compound 3.32.

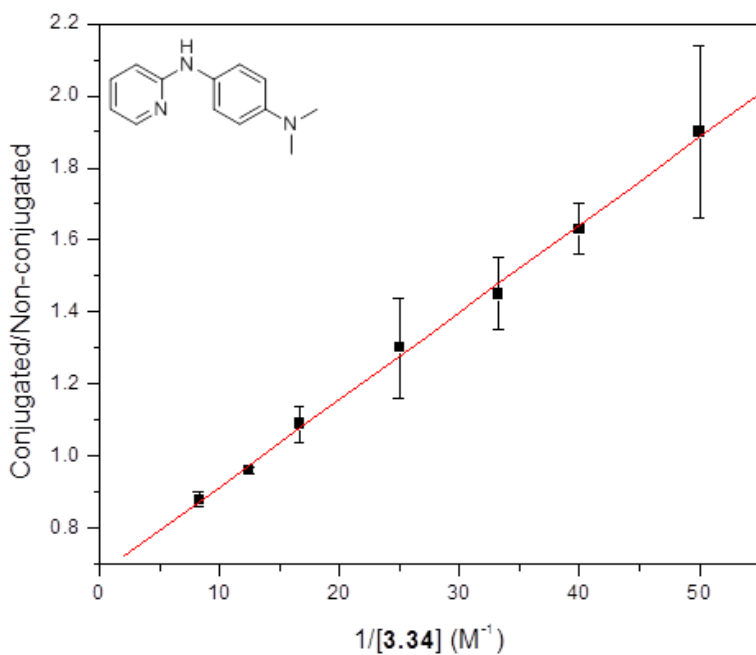


Figure 3.6.52. Double reciprocal plot used to obtain $k_1 = 6.4 \times 10^6 \text{ M}^{-1}\text{s}^{-1}$ for compound **3.34**.

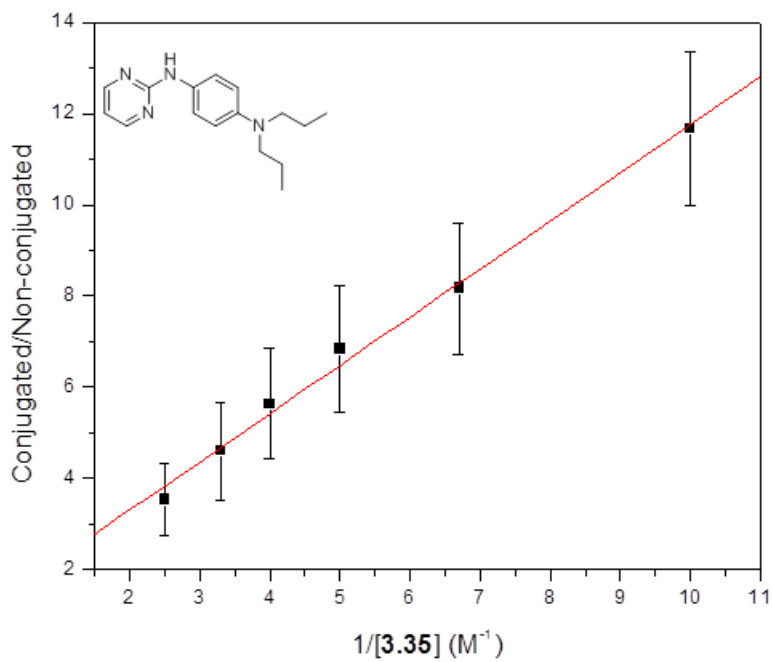


Figure 3.6.53. Double reciprocal plot used to obtain $k_1 = 1.5 \times 10^5 \text{ M}^{-1}\text{s}^{-1}$ for compound **3.35**.

3.6.7 Alkyl Radical Kinetic Data

Data used to obtain rate constants for reactions between diarylamines and primary alkyl radicals.

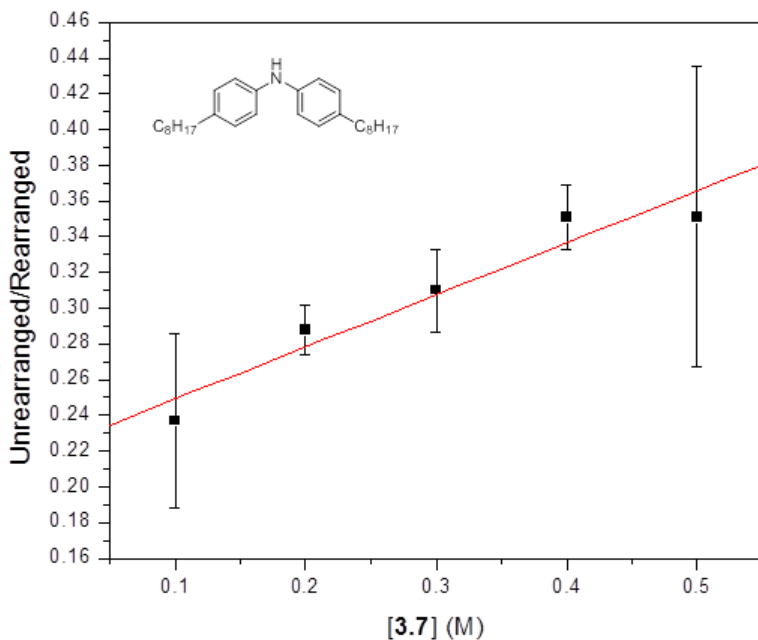


Figure 3.6.54 plot used to obtain $k_H = 1.3(\pm 2.9) \times 10^3 \text{ M}^{-1}\text{s}^{-1}$ for compound 3.7.

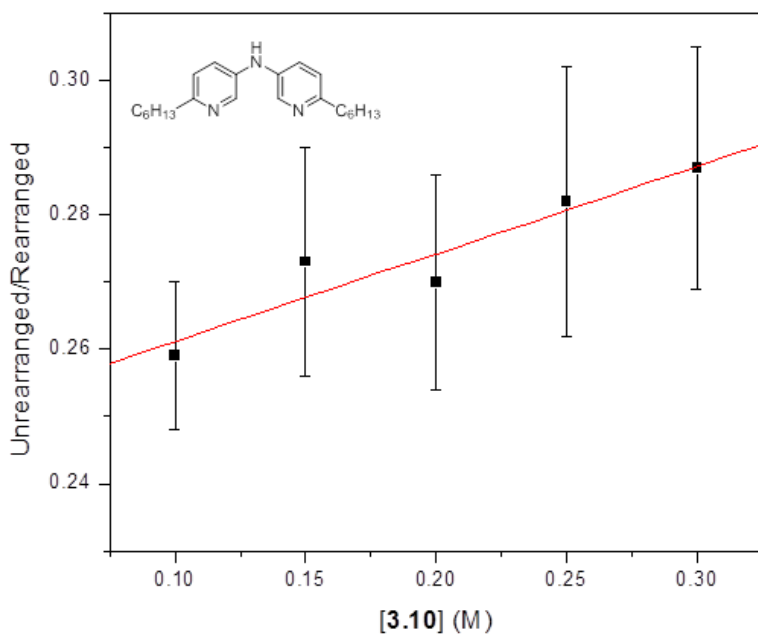


Figure 3.6.55 plot used to obtain $k_H = 9.7(\pm 2.3) \times 10^2 \text{ M}^{-1}\text{s}^{-1}$ for compound 3.10.

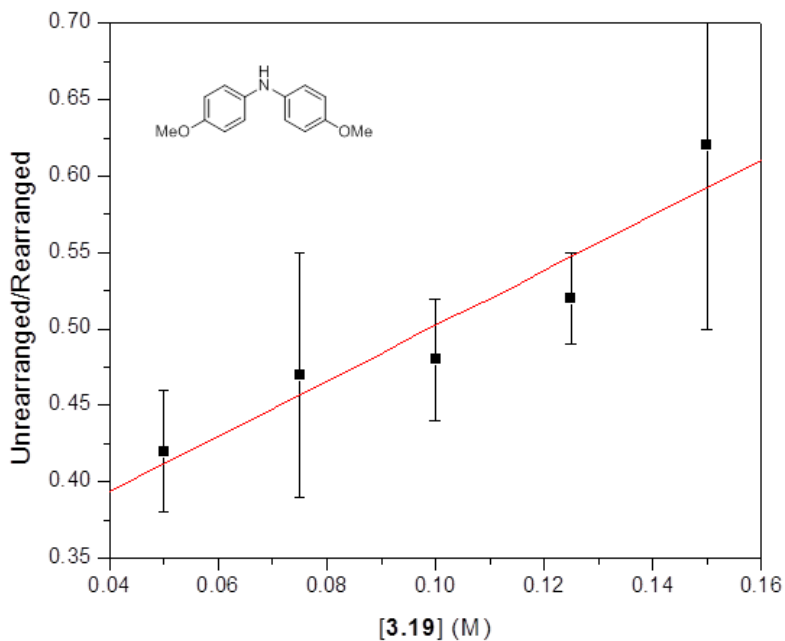


Figure 3.6.56 plot used to obtain $k_H = 2.5(\pm 0.6) \times 10^4 \text{ M}^{-1}\text{s}^{-1}$ for compound **3.19**.

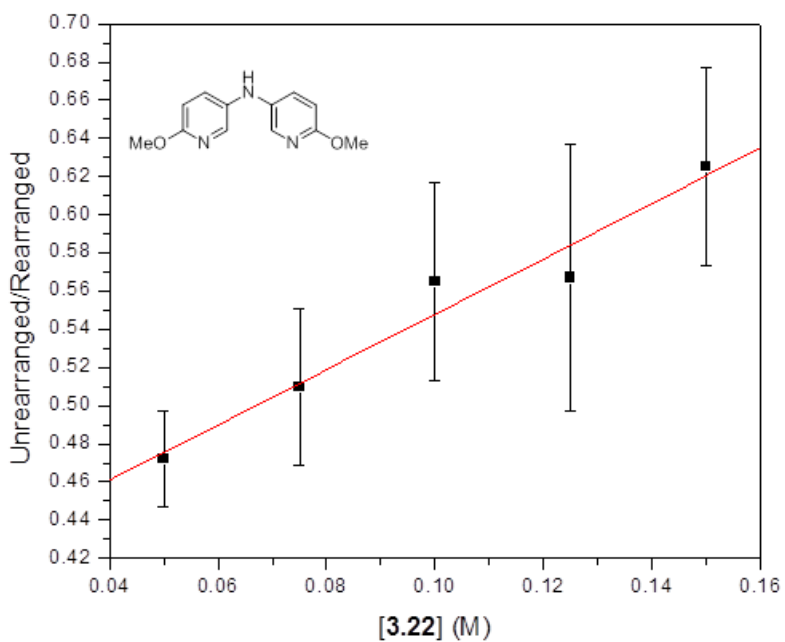


Figure 3.6.57 plot used to obtain $k_H = 1.9(\pm 0.2) \times 10^4 \text{ M}^{-1}\text{s}^{-1}$ for compound **3.22**.

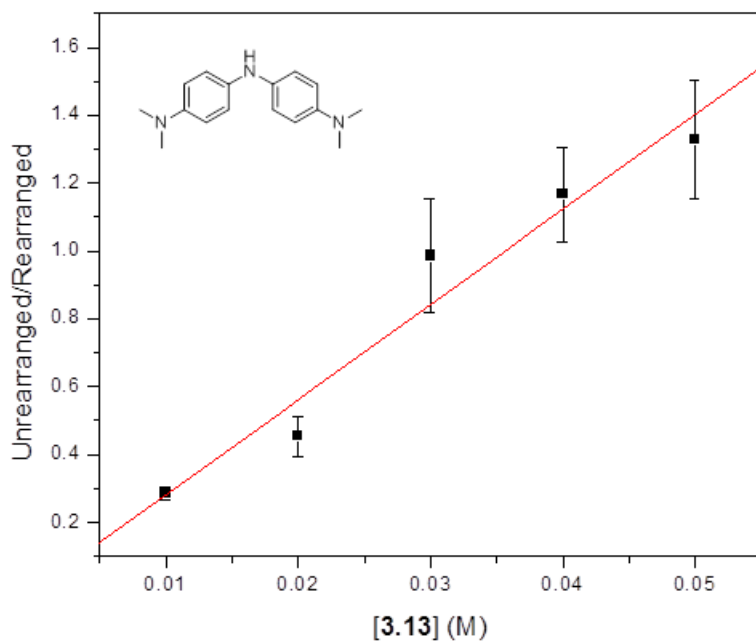


Figure 3.6.58 plot used to obtain $k_H = 2.3(\pm 0.9) \times 10^5 \text{ M}^{-1}\text{s}^{-1}$ for compound **3.13**.

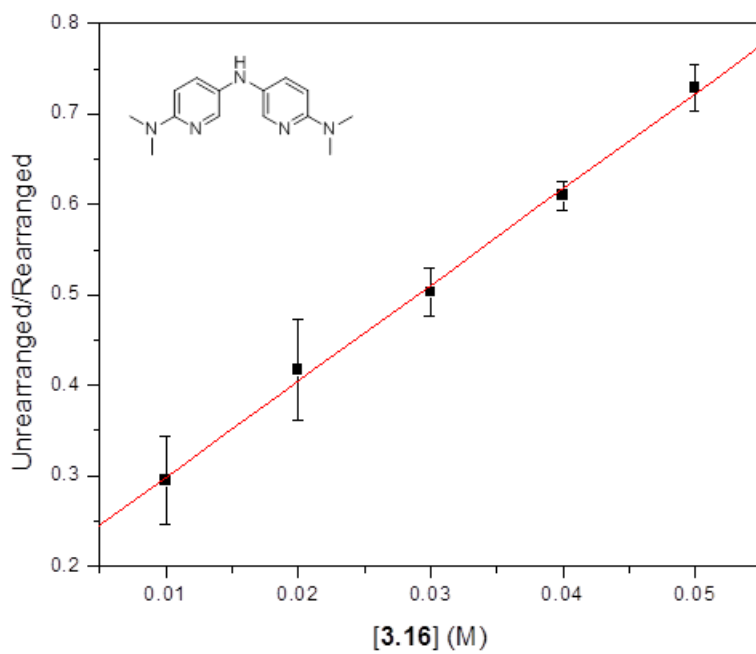


Figure 3.6.59 plot used to obtain $k_H = 1.5(\pm 0.2) \times 10^5 \text{ M}^{-1}\text{s}^{-1}$ for compound **3.16**.

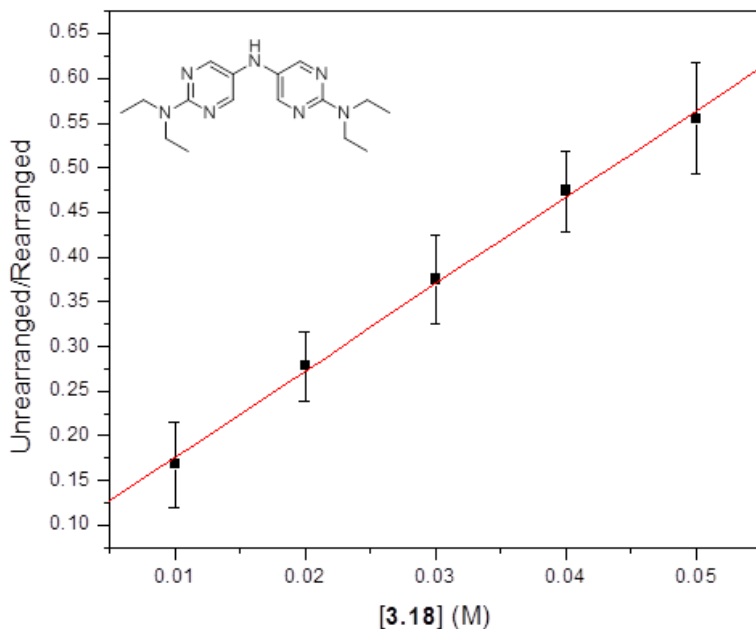


Figure 3.6.60 plot used to obtain $k_H = 1.4(\pm 0.1) \times 10^5 \text{ M}^{-1}\text{s}^{-1}$ for compound **3.18**.

3.7 References

- (1) Klemchuk, P. P. In *Ullmann's Encyclopedia of Industrial Chemistry*; Wiley-VCH Verlag GmbH & Co. KGaA: 2000.
- (2) Valgimigli, L.; Banks, J. T.; Luszyk, J.; Ingold, K. U. *Journal of Organic Chemistry* **1999**, *64*, 3381.
- (3) Pratt, D. A.; DiLabio, G. A.; Valgimigli, L.; Pedulli, G. F.; Ingold, K. U. *Journal of the American Chemical Society* **2002**, *124*, 11085.
- (4) Pratt, D. A.; DiLabio, G. A.; Brigati, G.; Pedulli, G. F.; Valgimigli, L. *Journal of the American Chemical Society* **2001**, *123*, 4625.

- (5) Valgimigli, L.; Brigati, G.; Pedulli, G. F.; DiLabio, G. A.; Mastragostino, M.; Arbizzani, C.; Pratt, D. A. *Chemistry-a European Journal* **2003**, *9*, 4997.
- (6) Wijtmans, M.; Pratt, D. A.; Valgimigli, L.; DiLabio, G. A.; Pedulli, G. F.; Porter, N. A. *Angewandte Chemie-International Edition* **2003**, *42*, 4370.
- (7) Hanthorn, J. J.; Valgimigli, L.; Pratt, D. A. *Journal of the American Chemical Society* **2012**, *Articles ASAP*.
- (8) Montgomery, J. A.; Frisch, M. J.; Ochterski, J. W.; Petersson, G. A. *Journal of Chemical Physics* **1999**, *110*, 2822.
- (9) Hanthorn, J. J.; Valgimigli, L.; Pratt, D. A. (Accompanying manuscript, Chapter 2)
- (10) Jha, M.; Pratt, D. A. *Chemical Communications* **2008**, 1252.
- (11) Yin, H.; Xu, L.; Porter, N. A. *Chemical Reviews* **2011**, *111*, 5944.
- (12) Hanthorn, J.; Pratt, D. A. *Journal of Organic Chemistry* **2012**, *77*, 276.
- (13) Brigati, G.; Lucarini, M.; Mugnaini, V.; Pedulli, G. F. *Journal of Organic Chemistry* **2002**, *67*, 4828.
- (14) Lucarini, M.; Pedrielli, P.; Pedulli, G. F.; Cabiddu, S.; Fattuoni, C. *Journal of Organic Chemistry* **1996**, *61*, 9259.
- (15) Bordwell, F. G.; Zhang, X. M.; Cheng, J. P. *Journal of Organic Chemistry* **1993**, *58*, 6410.
- (16) Howard, J. A.; Ingold, K. U. *Canadian Journal of Chemistry-Revue Canadienne De Chimie* **1963**, *41*, 1744.
- (17) Litwinienko, G.; Ingold, K. U. *Accounts of Chemical Research* **2007**, *40*, 222.

- (18) Abraham, M. H.; Grellier, P. L.; Prior, D. V.; Duce, P. P.; Morris, J. J.; Taylor, P. *J. Journal of the Chemical Society-Perkin Transactions 2* **1989**, 699.
- (19) Leardini, R.; Lucarini, P.; Pedulli, G. F.; Valgimigli, L. *Journal of Organic Chemistry* **1999**, 64, 3726.
- (20) Brown, H. C.; Okamoto, Y. *Journal of the American Chemical Society* **1958**, 80, 4979.
- (21) Benson, S. W. *Thermochemical Kinetics 2nd Edition*; John Wiley & Sons: New York, 1976.
- (22) Snelgrove, D. W.; Lusztyk, J.; Banks, J. T.; Mulder, P.; Ingold, K. U. *Journal of the American Chemical Society* **2001**, 123, 469.
- (23) Valgimigli, L.; Banks, J. T.; Ingold, K. U.; Lusztyk, J. *Journal of the American Chemical Society* **1995**, 117, 9966.
- (24) Valgimigli, L.; Amorati, R.; Petrucci, S.; Pedulli, G. F.; Hu, D.; Hanthorn, J. J.; Pratt, D. A. *Angewandte Chemie-International Edition* **2009**, 48, 8348.
- (25) DiLabio, G. A.; Johnson, E. R. *Journal of the American Chemical Society* **2007**, 129, 6199.
- (26) Webster, R. D. *Electrochemistry Communications* **1999**, 1, 581.
- (27) Franchi, P.; Lucarini, M.; Pedulli, G. F.; Valgimigli, L.; Lunelli, B. *Journal of the American Chemical Society* **1999**, 121, 507.
- (28) Lucarini, M.; Pedrielli, P.; Pedulli, G. F.; Valgimigli, L.; Gimes, D.; Tordo, P. *Journal of the American Chemical Society* **1999**, 121, 11546.
- (29) Zavitsas, A. A. *Journal of the American Chemical Society* **1972**, 94, 2779.

- (30) Mulder, P.; Korth, H. G.; Pratt, D. A.; DiLabio, G. A.; Valgimigli, L.; Pedulli, G. F.; Ingold, K. U. *Journal of Physical Chemistry A* **2005**, *109*, 2647.
- (31) It should be pointed out that triplet repulsion cannot account for the increased reactivities of diarylamines compared to phenols. Based on this concept, it's expected that less triplet repulsion would contribute to the TS for HAT between two oxygen atoms compared to the TS for HAT between an oxygen atom and a nitrogen atom since the N-O bond will be stronger than an O-O bond.
- (32) Hanthorn, J. J.; Valgimigli, L.; Pratt, D. A. Accompanying manuscript.
- (33) Perrin, D. D.; Amarego, W. L. F.; Perrin, D. R. *Purification of Laboratory Chemicals*; fifth edition ed.; Pergamon Press: University of Michigan, 2007.
- (34) Shimizu, N.; Watanabe, K.; Tsuno, Y. *Chemistry Letters* **1983**, 1877.
- (35) Kraus, G. A.; Choudhury, P. K. *Synlett* **2004**, 97.

CHAPTER 4: SECOND GENERATION PEROXYL RADICAL CLOCKS

4.1 Preface

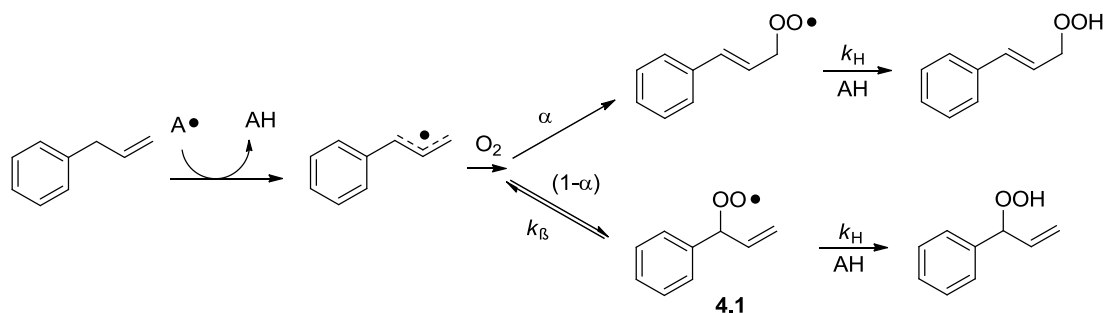
The reactions of peroxy radicals are at the centre of the oxidative degradation of essentially all petroleum-derived hydrocarbons and biological lipids, and consequently, the inhibition of these processes by radical-trapping antioxidants is extremely important. Recently described peroxy radical clocks offer a simple, convenient and inexpensive method of determining rate constants for H-atom transfer reactions to peroxy radicals, greatly enabling the kinetic and mechanistic characterization of compounds with antioxidant properties. We follow-up a preliminary communication (Jha, M; Pratt, D. A.; *Chem. Commun.*, **2008**, 1252) on the development of a methodology utilizing *tert*-butyl styrylperacetate as a precursor to a versatile peroxy radical clock with the present paper, wherein we describe a novel naphthyl analog which provides for much improved product resolution for analysis and provide the complete details associated with its development and application. Using this new precursor, and with consideration of the expanded set of reaction products, inhibition rate constants were measured for a variety of representative phenolic and diarylamine radical-trapping antioxidants. We also provide details for the use of this methodology for the determination of mechanistic information, such as kinetic solvent effects, Arrhenius parameters and kinetic isotope effects. This chapter is largely as it was published in the *Journal of Organic Chemistry* (Hanthorn, J. J; Pratt, D. A; *J. Org. Chem.*, **2012**, 77(1), 276).

4.2 Introduction

Peroxyl radicals are the key intermediates in the radical-mediated oxidative degradation (autoxidation) of all organic materials, including primary petroleum products, polymers, foodstuffs and biological molecules.¹⁻³ To slow the rate of autoxidation, radical-trapping antioxidants (including phenols, non-tertiary amines and organosulfur compounds) are employed industrially (e.g. BHT and 4,4'-dialkyldiphenylamines) and in Nature (e.g. α -tocopherol, the most potent form of vitamin E) to 'trap' peroxyl radicals as hydroperoxides to prevent radical-chain propagation.⁴⁻⁶ These compounds donate a hydrogen atom to a chain-carrying peroxyl radical, forming a hydroperoxide and a more stable/persistent (i.e. less reactive) antioxidant-derived radical at a rate dependent on antioxidant structure and reaction medium.⁷ Understanding the kinetics of H-atom transfer from antioxidants to peroxyl radicals provides important mechanistic information about structure-activity relationships relevant to radical-trapping antioxidants. Several methods have been developed for measuring inhibition rate constants, including inhibited autoxidation, laser flash photolysis and pulse radiolysis. However, these methods all suffer the drawback of requiring specialized equipment and expertise to obtain reliable kinetic data, and they are often limited in the time domain and solvents in which they can be carried out.

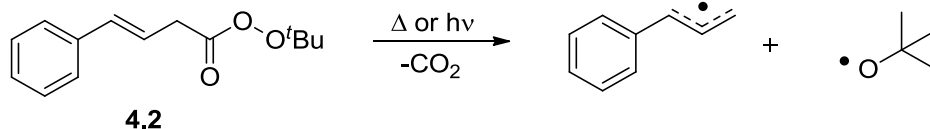
Recently, Porter and co-workers⁸ introduced a peroxyl radical clock approach based on the kinetic competition between the unimolecular β -fragmentation of non-conjugated peroxyl radical (e.g. **4.1** derived from allylbenzene as in Scheme 4.1) and its trapping in a bimolecular reaction with an antioxidant A-H. This methodology requires no specialized equipment other than a GC or HPLC for product analysis. Although the approach is effective for measuring rates of H-atom transfer from many phenols to peroxyl radicals in benzene, a major limitation of this

method is that it requires the antioxidant-derived radical ($A\bullet$) to abstract a hydrogen atom from allylbenzene to propagate the chain reaction. This becomes problematic if the antioxidant gives rise to either persistent (e.g. BHT) or highly stabilized (e.g. 6-amino-3-pyridinols)⁹ radicals that cannot efficiently propagate the chain. To offset low propagation rate constants – even for the most ideal A-H – a high concentration of oxidizable substrate (e.g. 2.6 M allylbenzene) must be used to ensure enough oxidation products are formed for reproducible analysis. A consequence of using such high concentrations of oxidizable substrate is that it precludes accurate kinetic or mechanistic studies in any solvent other than benzene.



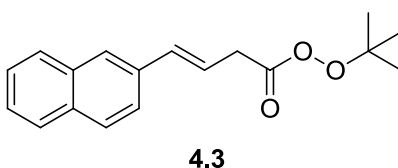
Scheme 4.1. Kinetic scheme describing the allylbenzene-based peroxy radical clock.

To address the limitations associated with this approach, we recently described the synthesis and utility of the homoconjugated peroxyester **4.2**,¹⁰ which serves as a precursor to the same delocalized allylbenzene-derived radical essential for the kinetic competition experiment. In our preliminary report, we showed that compound **4.2** decomposes under aerobic conditions either thermally (37°C) or photolytically (300 nm) to generate non-conjugated peroxy radical **4.1**, permitting clock experiments using as little as 10 mM of compound **4.2**. Furthermore, the rate constant of β -fragmentation (k_β) of **4.1** was measured in a variety of organic solvents, which subsequently allowed for the measurement of kinetic solvent effects on the rates of H-atom transfer from phenolic antioxidants.



Scheme 4.2. Decomposition of a peroxyester under thermal or photolytic conditions.

Although the peroxyester approach was successful in obtaining both inhibition rate constants (k_H in Scheme 4.1) and the effect of solvent upon them for several phenolic antioxidants, one of the aspects we sought to improve was the resolution of the product alcohols (the hydroperoxides are reduced with PPh_3 for analysis by gas chromatography with flame ionization detection), which often had poorly resolved peaks and/or peaks with similar retention times to common phenolic antioxidants and their derivatives. Herein we describe a second generation peroxy radical clock, derived from the naphthyl-based perester **4.3**, which yields greatly improved chromatographic resolution *and revealed previously unidentified products* in the region of the conjugated and non-conjugated alcohols. The origin of these products and their contribution to the accurate measurement of inhibition rate constants using this approach was explored, as well as the role played by the antioxidants in their formation. To demonstrate the utility of the peroxyester approach beyond simple phenolic compounds, we use compound **4.3** to measure inhibition rate constants for some highly reactive pyrimidinols, pyridinols and diarylamines.



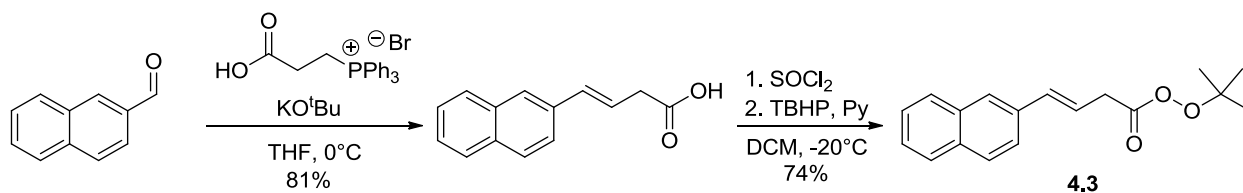
Furthermore, we use **4.3** to measure deuterium kinetic isotope effects (DKIEs) for a variety of phenolic antioxidants, and are able to provide Arrhenius parameters for the β -

fragmentation of the non-conjugated peroxy radical derived from **4.3**, such that it may be applied in the future to study the temperature dependence of inhibition reactions.

4.3 Results

4.3.1. Synthesis of Peroxyester **4.3** and its Derived Products

Synthesis of the acid precursor to (*E*)-*tert*-butyl 4-(naphthalen-2-yl)but-3-eneperoxoate **4.3** was achieved via a Wittig reaction between commercially available 2-naphthaldehyde and the phosphonium salt derived from 3-bromopropionic acid. Subsequent formation of the acid chloride and substitution with *tert*-butyl hydroperoxide afforded the product in 60% yield over the 3 steps.

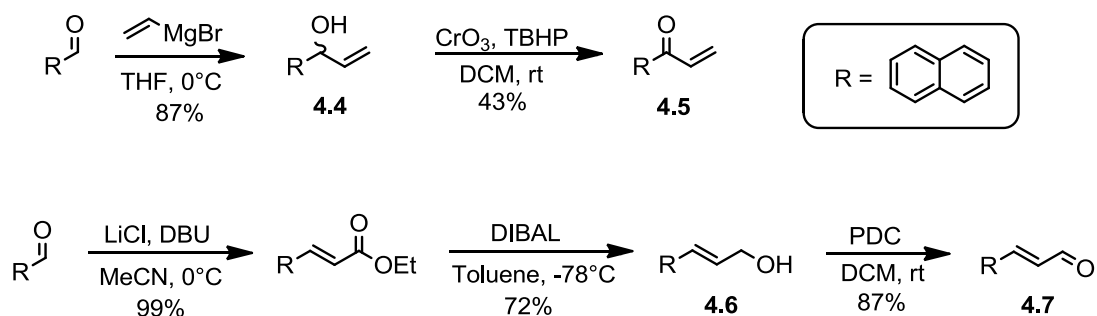


Scheme 4.3. Synthesis of (*E*)-*tert*-butyl 4-(naphthalen-2-yl)but-3-eneperoxoate.

A clear advantage of using perester **4.3** over the analogous phenyl compound **4.2** is its higher crystallinity and ease of recrystallization – resulting in a longer shelf-life at ambient temperatures.

The corresponding non-conjugated (**4.4**) and conjugated (**4.6**) alcohol products used as GC standards for kinetic analysis were also synthesized from 2-naphthaldehyde. Compound **4.4**

was prepared via a Grignard reaction with vinylmagnesium bromide and compound **4.6** via a Horner-Wadsworth-Emmons reaction followed by DIBAL reduction of the resulting ester.



Scheme 4.4. Synthesis of conjugated and non-conjugated products used as GC standards.

Although these two products (the phenyl analogs of **4.4** and **4.6**) are the only products reported for decomposition of peroxyester **4.2**, in our calibration experiments with peroxyester **4.3** with α -tocopherol (*vide infra*), we observed additional peaks in the same region as **4.4** and **4.6**. GC/MS studies indicated they were the corresponding higher oxidized products – ketone **4.5** seemingly derived from the non-conjugated hydroperoxide, and aldehyde **4.7** seemingly derived from the conjugated hydroperoxide. Therefore, we prepared authentic standards of these compounds as well. The non-conjugated ketone **4.5** was prepared by CrO_3 /*tert*-butyl hydroperoxide oxidation of alcohol **4.4** and the conjugated aldehyde **4.7** via PDC oxidation of alcohol **4.6**.

If the peroxyester is instead photolyzed to yield the naphthyl analog of radical **4.1**, epoxide products may also be expected.¹⁰ This is thought to occur by photolysis of the O-O bond of the conjugated hydroperoxide to generate a primary alkoxy radical that can rapidly undergo a

3-*exo* cyclization with the adjacent alkene, forming an epoxide and a benzylic radical. This carbon-centred radical then reacts with O₂ to form a peroxy radical that is trapped as the hydroperoxide, leading to an epoxy-alcohol upon PPh₃ reduction. It should be noted that to simplify product analysis, the experiments described throughout the manuscript were performed via thermal decomposition.

4.3.2. Calibration of Peroxyl Radical Clock Derived From 4.3

In order to ‘calibrate’ the radical clock derived from **4.3** (determination of k_{β}), we decomposed **4.3** in the presence of various concentrations of α -tocopherol (α -TOH, **4.8**) at 37°C (or by photolysis at 300 nm, not shown). The resulting hydroperoxides were reduced to their corresponding alcohols with PPh₃ and the products analyzed by GC-FID. Examples of gas chromatograms obtained at high and low concentrations of α -TOH are shown in Figure 4.1. The resulting ratios of non-conjugated/conjugated products vs. [α -TOH] were plotted and fit according to the equation shown in Figure 4.2 to determine the rate constant for β -fragmentation of the non-conjugated peroxy radical in a given solvent. Values for k_H used to determine k_{β} were obtained by laser flash photolysis for the reaction of α -TOH with cumylperoxy radicals in several different solvents.¹¹

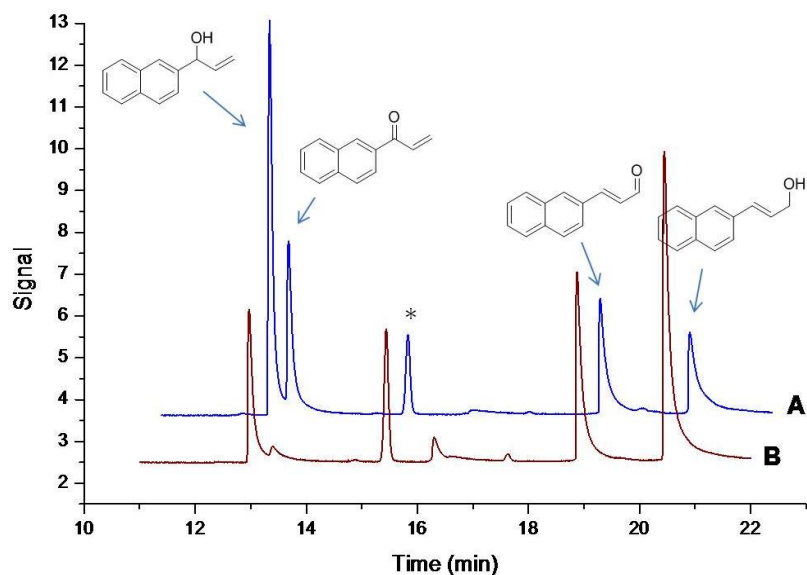


Figure 4.1. Representative gas chromatograms (GC-FID) in the retention time range of product elution following the incubation of peroxyester **4.3** with 1.0 M α -TOH (A) and 0.03 M α -TOH (B) for 4 hours at 37°C in chlorobenzene. The peak labelled * is observed in most chromatograms and could not be identified; however the peak area does not change as a function of antioxidant concentration and therefore appears not to be relevant in our kinetic analysis.

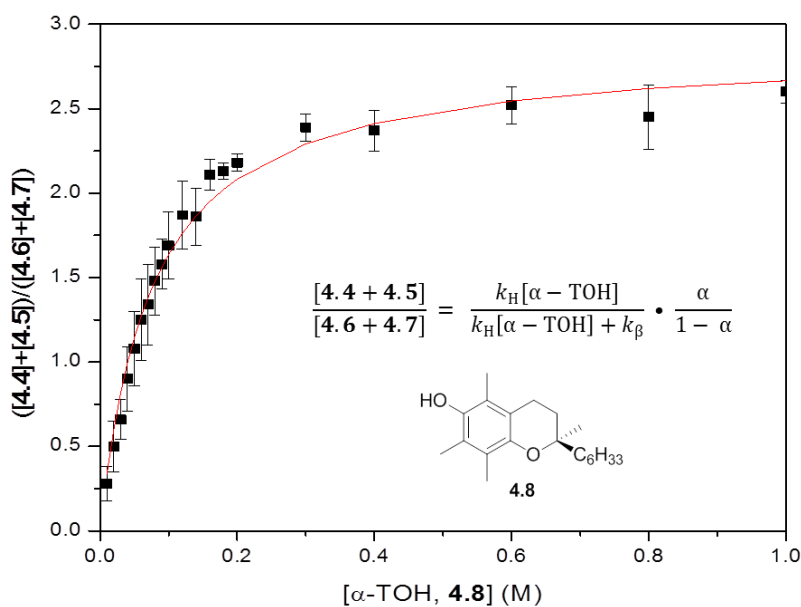


Figure 4.2. Ratio of non-conjugated ([4.4] + [4.5]) to conjugated ([4.6] + [4.7]) oxidation products formed in the decomposition of **4.3** as a function of [α -TOH, **4.8**] following incubation for 12 hours at 37°C in benzene.

Table 4.1. β -Fragmentation rate constants and oxygen partition coefficients of the non-conjugated peroxy radical derived from **4.3** as a function of solvent. Inhibition rate constants used in the determination of k_{β} and α are given for reference.

Solvent	k_{β} (s ⁻¹) ^a	α ^b	k_{inh} (M ⁻¹ s ⁻¹)
Hexanes	1.6(±0.2) x 10 ⁶	0.65	2.1 x 10 ⁷
Chlorobenzene	5.7(±0.3) x 10 ⁵	0.79	7.1 x 10 ⁶ ^d
Benzene	3.0(±0.9) x 10 ⁵	0.74	3.9 x 10 ⁶
Anisole	1.9(±0.5) x 10 ⁵	0.69	1.8 x 10 ⁶
Benzonitrile	1.4(±0.1) x 10 ⁵	0.78	4.7 x 10 ⁵ ^e
Ethyl Acetate	9.5(±0.3) x 10 ⁴	0.76	2.9 x 10 ⁵
Acetic acid	5.1(±0.2) x 10 ⁴	0.57	1.0 x 10 ⁶
Propionitrile	2.8(±0.1) x 10 ⁴	0.65	4.7 x 10 ⁵ ^e

^aFrom decomposition of **4.3** at 37°C. ^bValues are dimensionless and have errors of ±0.01. ^cDetermined directly by laser flash photolysis in the given solvent at 25°C¹¹ and corrected to 37°C using logA = 8 and $E_a = 1.6$ kcal/mol, see text. ^dSee footnote ¹². ^eValue determined in acetonitrile, which has the same β_2^H value (0.45).¹³

4.3.3. Representative Clocking Experiments Using Perester **4.3**

To confirm the accuracy of the peroxy radical clock methodology utilizing **4.3**, k_H values were determined in chlorobenzene for a representative set of antioxidants having varied structure and reactivity: 2,4,6-trimethylphenol (**4.9**), 2,6-di-*tert*-butyl-4-methoxyphenol (**4.10**), diphenylamine (**4.11**), phenothiazine (**4.12**), a pyrimidinol (**4.13**) and a pyridinol (**4.14**). The values were obtained simply by decomposing **4.3** in the presence of varying amounts of the

antioxidant, and plotting the ratio of non-conjugated to conjugated products as a function of antioxidant concentration as in Figure 4.3. The inhibition rate constants determined in this way are shown in Table 4.2, and are in good-to-excellent agreement (generally within a factor of 2-3) with literature values obtained by the inhibited autoxidation of styrene.

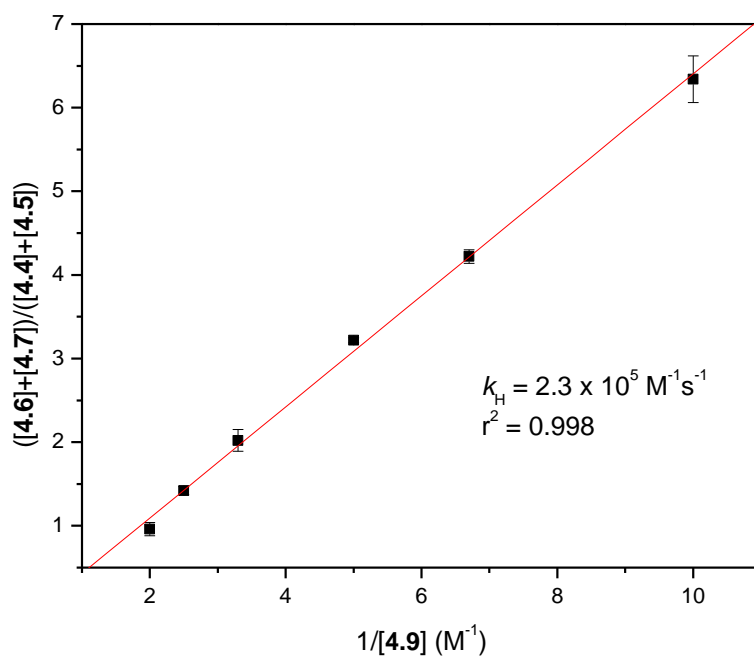
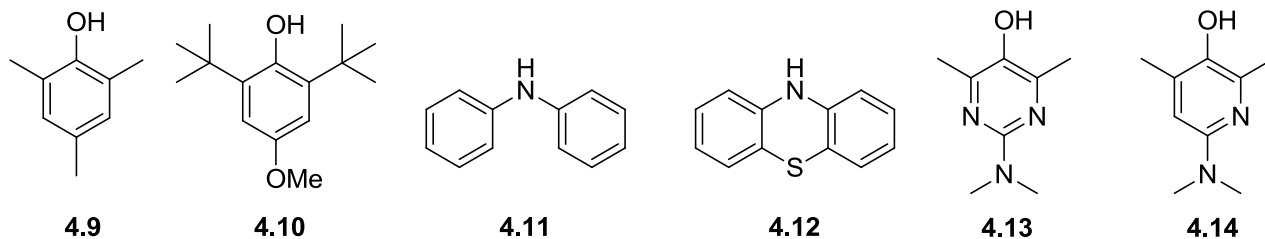


Figure 4.3. Representative double-reciprocal plot used to obtain inhibition rate constants. Shown are data obtained for 2,4,6-trimethylphenol (**4.9**) in chlorobenzene at 37°C.

Table 4.2. Rate constants for reactions of **4.9-4.14** with peroxy radicals generated from perester **4.3** at 37°C in chlorobenzene. Literature values obtained by inhibited autoxidation of styrene at the given temperatures are shown for comparison.



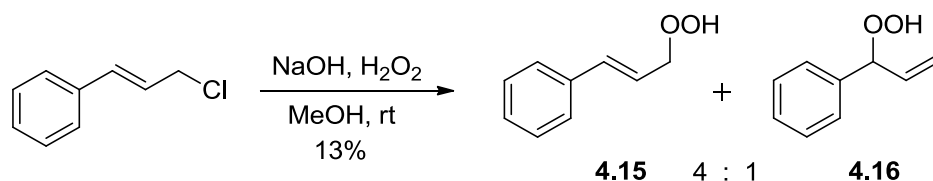
Compound	Clock k_H ($M^{-1}s^{-1}$)	Lit k_H ($M^{-1}s^{-1}$)	T , Ref.
4.9	$2.3(\pm 0.1) \times 10^5$	8.5×10^4	30 °C, ¹⁴
4.10	$5.6(\pm 1.7) \times 10^5$	1.1×10^5	30 °C, ¹⁴
4.11	$4.6(\pm 0.5) \times 10^4$	4.4×10^4	65 °C, ¹⁵
4.12	$8.5(\pm 0.6) \times 10^6$	8.8×10^6	50 °C, ¹⁶
4.13	$1.7(\pm 2.5) \times 10^7$	8.6×10^6 ^a	50 °C, ¹⁷
4.14	$3.2(\pm 1.1) \times 10^7$	1.6×10^7	30 °C, ⁹

^aIn benzene.

4.3.4. Origin of Carbonyl-Containing Products

Authentic conjugated and non-conjugated hydroperoxides were prepared in order to probe the conditions under which they could serve as a source for the carbonyl products observed when phenothiazine **4.12**, pyrimidinol **4.13** or pyridinol **4.14** were clocked, or when the clock was calibrated with α -TOH in polar media. Bloodworth *et al.* have reported that cinnamyl-

derived hydroperoxides can be prepared from the corresponding cinnamyl chloride by reaction with excess hydrogen peroxide and NaOH, albeit in low yield (11%) as an inseparable mixture of isomers (conjugated/non-conjugated).¹⁸ When the analogous (*E*)-2-(3-chloroprop-1-enyl)naphthalene was subjected to the same conditions in a number of different solvents the desired hydroperoxides were not isolated – likely due to the solubility of the starting material under these conditions. Therefore, we decided to study the reactivity of the cinnamyl-derived products given that their reactivity should be essentially the same as their naphthyl analogs. Following the literature procedure, we were able to isolate the cinnamyl-derived hydroperoxides as a 4:1 mixture of conjugated (**4.15**) and non-conjugated (**4.16**) hydroperoxides.



Scheme 4.5. Synthesis of conjugated and non-conjugated cinnamyl-derived hydroperoxides.

To test the stability of the hydroperoxides under the conditions of the clocking experiment, the mixture of isomers **4.15** and **4.16** were incubated at 37°C for 14 hours in chlorobenzene or acetonitrile. The mixture was then reduced with PPh₃ and analyzed by GC. The product analysis showed only alcohols **4.4** and **4.6** in the same 4:1 ratio observed when the hydroperoxide mixture was reduced with PPh₃ and analyzed immediately. Next, the hydroperoxides were incubated at 37°C for 14 hours in chlorobenzene or acetonitrile containing either **4.10**, **4.11**, 2,2,5,7,8-pentamethyl-6-chromanol (PMC, a truncated version of α-tocopherol,

4.17) or N^1,N^1 -dimethyl- N^4 -phenylbenzene-1,4-diamine (**4.18**) over 14 hours at different concentrations. Representative chromatograms are shown in Figure 4.4.

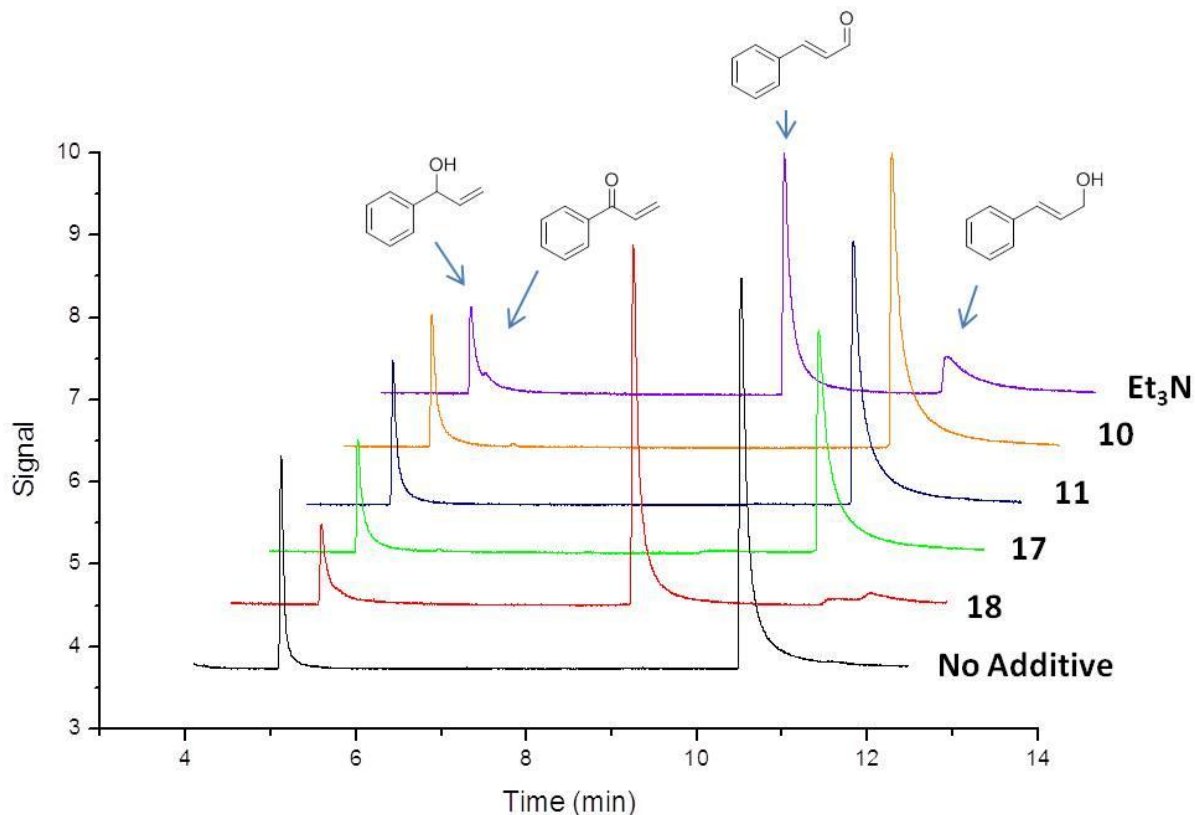


Figure 4.4. Stacked plot of gas chromatograms (GC-FID) showing product distribution (phenyl analogs of **4.4**, **4.5**, **4.6** and **4.7**) arising from hydroperoxide decomposition (5 mM) in the presence of various additives (50 mM) incubated at 37°C in chlorobenzene. Initial ratio of conjugated/non-conjugated products (**4.15/4.16**) was 4:1.

Importantly, while there was a difference in the product composition (alcohols and carbonyls) as a function of antioxidant structure and solvent, there was no significant change in the 4:1 ratio of conjugated:non-conjugated alcohol+carbonyl products. Whilst it would appear that the hydroperoxide products persist in the presence of the phenols **4.10** and **4.17** and the diarylamine **4.11**, they appear to dehydrate to carbonyls in the presence of amine **4.18**.¹⁹ Furthermore, the yield of carbonyl products increases upon changing the solvent from

chlorobenzene to acetonitrile (see the Supporting Information, Table S1). In fact, in acetonitrile, carbonyl products are now also observed for phenol **4.17**.

4.3.5. Temperature Dependence of Beta-Fragmentation

To estimate Arrhenius parameters for the β -fragmentation of the non-conjugated peroxy radical, **4.3** was decomposed in the presence of varying concentrations (0.02-1.0 M) of α -tocopherol (α -TOH, **4.8**) at 6 additional temperatures (45, 50, 60, 70, 80 and 95°C) in chlorobenzene. Values for k_{inh} used to determine k_{β} at these temperatures were estimated based on $k_{\text{inh}} = 6.4 \times 10^6 \text{ M}^{-1}\text{s}^{-1}$ in chlorobenzene at 25°C and $\log A = 8$ (an estimated value, *vide infra*). The resulting Arrhenius plot is shown in Figure 4.5, whose slope and intercept yield $E_a = 9.6(\pm 0.9)$ kcal/mol and $\log A = 12.8(\pm 0.6)$.

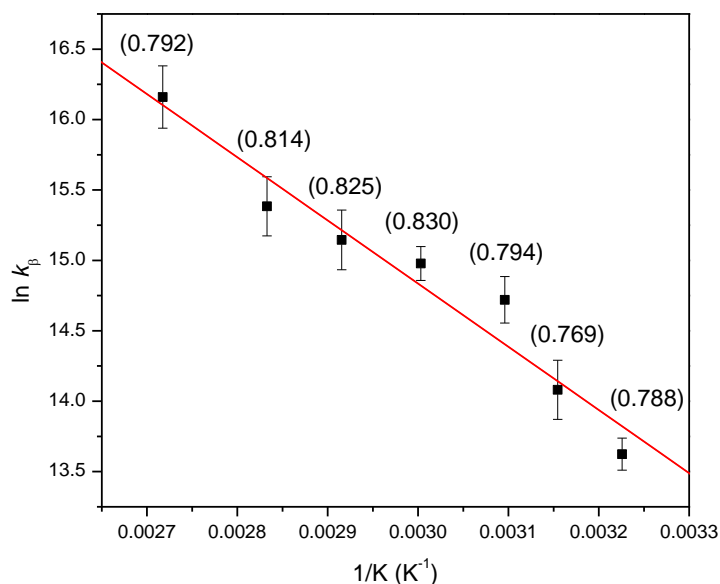


Figure 4.5. Temperature dependence of the β -fragmentation of the non-conjugated peroxy radical derived from **4.3**, which yields $E_a = 9.6(\pm 0.9)$ kcal/mol and $\log A = 12.8(\pm 0.6)$. Corresponding oxygen partition coefficients (α) for each temperature are given in brackets next to each data point.

4.3.6. Kinetic Isotope Effect Measurements

Deuterium kinetic isotope effects were measured for a representative set of phenolic antioxidants using the peroxy radical clock methodology. Prior to each experiment, the antioxidant was stirred with an excess (typically 1-5%) of D₂O (and an equivalent amount of H₂O in a parallel experiment as a control).²⁰ Furthermore, the experiment was carried out in the presence of 1% D₂O to ensure adventitious water in the solvent did not shift the equilibrium. A representative plot is shown in Figure 4.6 for 2,2,5,7,8-pentamethyl-6-chromanol (**4.17**), and the KIEs for it and the other 4 phenols we examined are summarized in Table 4.3. For comparison, DKIE values were also measured using the “first generation” methyl linoleate clock of Porter and co-workers, and are reported alongside.

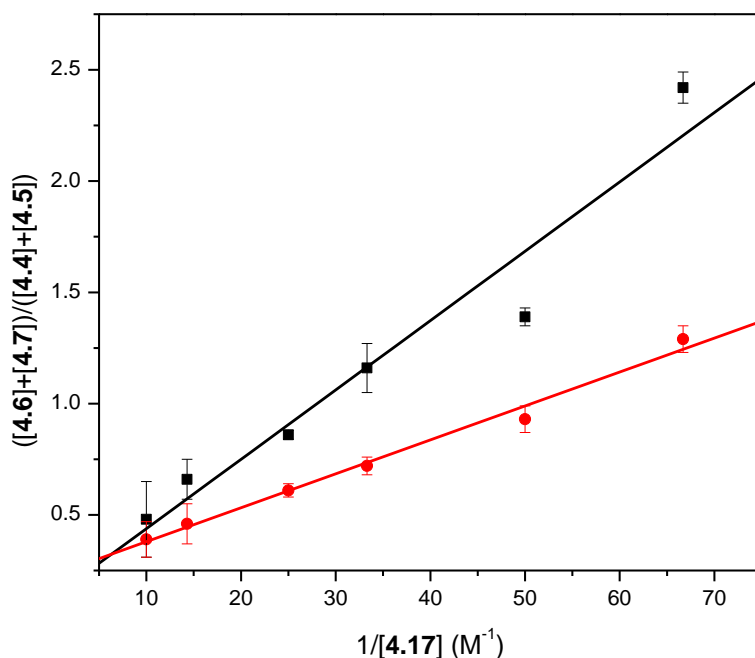
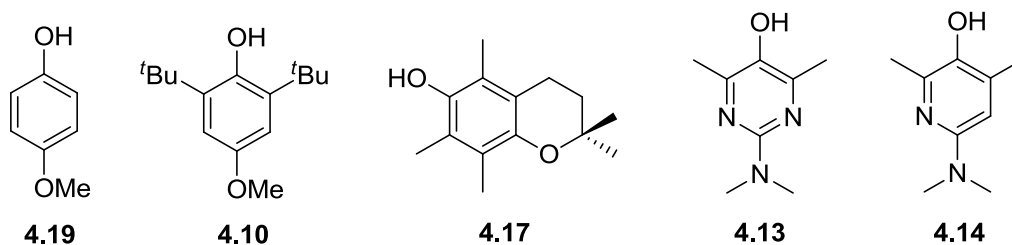


Figure 4.6. Kinetic isotope effect on the product distribution arising from the decomposition of **4.3** in the presence of 2,2,5,7,8-pentamethyl-6-chromanol (**4.17**) and either 1% D₂O (■) or 1% H₂O (●), which yield $k_{\text{H}} = 5.0 \times 10^6 \text{ M}^{-1}\text{s}^{-1}$ and $k_{\text{D}} = 2.4 \times 10^6 \text{ M}^{-1}\text{s}^{-1}$ for $k_{\text{H}}/k_{\text{D}} = 2.1$.

Table 4.3. Deuterium kinetic isotope effects (k_H/k_D) on the reactions of a representative group of phenols with peroxy radicals determined by the peroxy radical clock methodology with peroxyester **4.3** at 37°C. Values obtained by inhibited autoxidation of styrene and the methyl linoleate-based peroxy radical clock are presented alongside for comparison.



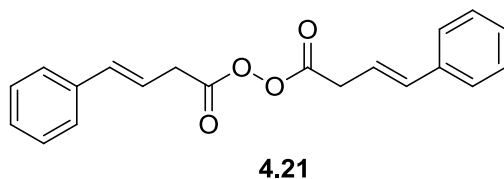
Compound	k_H/k_D by methodology		
	Peroxyester clock (4.3)	Methyl Linoleate clock	Inhibited Autoxidation (ref.)
4.19 ^a	2.5	2.5	n/a
4.10 ^a	2.2	2.3	n/a
4.17 ^a	2.1	2.4	5.1 (21)
4.13 ^b	2.1	1.5	3.1 (17)
4.14 ^b	1.6	1.5	n/a

^aObtained in chlorobenzene containing 1% D₂O (or 1% H₂O) as described below. ^bObtained in benzene containing 1% D₂O (or 1% H₂O) as described in ref. ²².

4.4 Discussion

Radical clocks based on the carbon-skeleton rearrangements of alkyl radicals have become an indispensable tool in kinetic and mechanistic investigations of reactions where alkyl radicals have been proposed as potential intermediates. Despite the ease with which these types of experiments can be carried out, heteroatom-centered radical clock approaches are few. Among the limited examples are the particularly useful radical clocks based upon competition between the β -fragmentation of a non-conjugated peroxy radical and its reduction to the corresponding hydroperoxide by an H-atom donor, which greatly enables the determination of rate constants for peroxy-molecule reactions.

The first generation of peroxy radical clocks relied on the chain transfer reaction of the antioxidant-derived radical A^\bullet with the oxidizable substrate R-H in order to set up the clock (Scheme 4.1). Since this chain-transfer reaction is quite slow (e.g. $0.1 \text{ M}^{-1}\text{s}^{-1}$ for $A^\bullet = \alpha$ -tocopheroxyl and R-H = methyl linoleate, for which $\Delta H \sim 2 \text{ kcal/mol}$), and will be slowed as A^\bullet becomes more stable/persistent and R-H less oxidizable (e.g. allylbenzene, *vide supra*), this approach is limited. This prompted us to consider other precursors to delocalized radicals that could set up the clock reaction. We first considered diacylperoxides, such as **4.21**, but quickly found that they were simply too labile to be practical.



We next turned to peroxyester **4.2**, which worked nicely as reported in our preliminary communication,⁹ but whose oxidation products often appear in the same part of the (gas)

chromatogram as the antioxidant or antioxidant-derived products. We surmised that by replacing the phenyl ring in **4.2** with a naphthyl ring as in **4.3**, we could push the retention times of the products much later in the chromatogram, improving the resolution and reliability of the analysis. This worked well, with the retention times shifting from ca. 5-8 minutes on our optimized column/temperature conditions to ca. 12-22 min under the same conditions, and importantly, resolving the expected alcohols and unexpected corresponding carbonyl compounds that were not apparent when **4.2** was used as precursor to set up the clock (*vide infra*).

The rate constant for β -fragmentation (k_{β}) of the non-conjugated peroxy radical derived from **4.3** was determined in the same way as we did for **4.2**, and was expectedly similar: $k_{\beta} = 3.0(\pm 0.9) \times 10^5 \text{ s}^{-1}$ for the naphthyl analog compared to $k_{\beta} = 1.7(\pm 0.1) \times 10^5 \text{ s}^{-1}$ for the phenyl analog⁹ at 37°C using $k_{\text{H}} = 3.9 \times 10^6 \text{ M}^{-1}\text{s}^{-1}$ at 37°C for the standard reaction of α -tocopherol with peroxy radicals in benzene.²³ The slight increase in rate constant may reflect the greater delocalization of the allylic radical by the naphthyl π -system as opposed to the phenyl π -system. Likewise, the oxygen partition coefficient (α) is highly similar: 0.74 ± 0.01 for the naphthyl analog versus 0.76 ± 0.01 for the phenyl analog.⁹ This suggested that the clocks could be used essentially interchangeably.

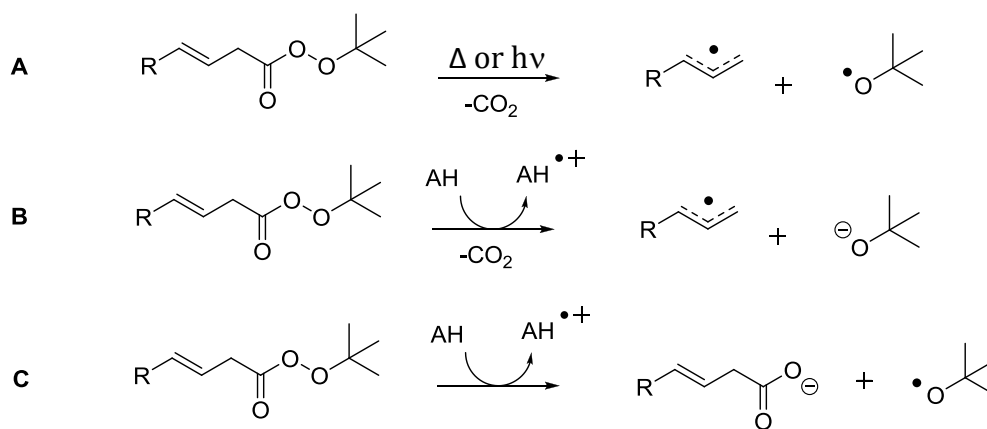
The solvent effects on the β -fragmentation rate constants observed for the non-conjugated peroxy radical derived from **4.3** reflect the same trends as those observed for that derived from **4.2**,⁹ although the absolute values vary slightly from solvent to solvent. The overall trend is generally one wherein solvents with greater polarity generally slow the rate of β -fragmentation – consistent with the idea that the peroxy radical is better solvated than the transition state for C-OO• bond dissociation as the polarity of the medium increases.⁹ The

oxygen partition coefficients (α) show much higher variance between the two clocks, presumably due to slightly differing orbital interactions of the dioxygen SOMO with the SOMOs of the naphthyl- or phenyl-substituted allyl radicals.^{3,24} Since oxygen partitioning across delocalized carbon-centered radicals is influenced by both sterics *and* electronics rationalization of solvent effects on these trends beyond this is difficult.

Nevertheless, with k_{β} and α defined for a given solvent, the clock can be applied with confidence. We were able to accurately clock reactions of phenols, diarylamines, pyridinols and pyrimidinols with inhibition rate constants ranging over roughly three orders of magnitude ($10^4 - 10^7 \text{ M}^{-1}\text{s}^{-1}$) – the range of greatest interest for the assessment of natural products with perceived radical-trapping antioxidant activity and the development of novel synthetic compounds. The rate constants were generally within a factor of 2 or better than literature values obtained using the conventional inhibited autoxidation of styrene methodology.

In carrying out these experiments, we noticed that the amount of products observed in the chromatograms varied with antioxidant. This suggested that the antioxidant may play a role in the decomposition of the peroxyester. The decomposition of peroxyesters under both photolytic and thermal conditions is well documented (reaction **A** in Scheme 4.6). Homolytic cleavage of the weak O–O bond in conjunction with (what is believed to be concerted)²⁵ rupture of the C–C bond results in extrusion of CO_2 and formation of a stabilized allylic radical and a *tert*-butoxyl radical (in the case of **4.2** or **4.3**). Additionally, peroxyester decomposition can be induced by electron-rich compounds (e.g. *N,N*-dimethylaniline) through donation of an electron into the σ^* orbital of the O–O bond, affording decomposition to either an acyloxyl radical and an alkoxide (**B**) or a carboxylate anion and an alkoxy radical (**C**) as shown in Scheme 4.6.²⁶ Indeed, when the total area of the product peaks obtained from clocking experiments at the same concentration

of antioxidant ($[ArOH] = 0.06 \text{ M}$) were plotted as a function of the standard potential of the phenolic antioxidant under study (E° ranging from 0.12-0.9 V²⁷) a linear correlation was obtained (see supporting information), supporting induced decomposition of the peroxyester by the antioxidant. Since the experiments is carried out under pseudo first order conditions where the antioxidant is in large excess, this reaction does not confound our kinetic analysis and serves to improve the yield of products for more reactive (i.e. electron rich) compounds.



Scheme 4.6. Decomposition pathways for peroxyester **4.3**.

In the clocking experiments for compounds **4.9-4.14** shown in Table 4.2, carbonyl products were observed in chromatograms from reactions containing **4.12-4.14**, but not in those containing **4.9-4.11**. Since **4.12-4.14** each contain basic nitrogen atoms, we surmised that a base-catalyzed dehydration mechanism may be responsible for the formation of these carbonyls.²⁸ Indeed, when mixtures of the conjugated and non-conjugated hydroperoxides **4.15** and **4.16** were incubated with varying concentrations of different antioxidants under the same experimental conditions as used in the clocking experiments, the corresponding carbonyl-containing products were observed for those antioxidants containing basic nitrogen atoms. Furthermore, when the

solvent medium was changed from chlorobenzene to acetonitrile, the carbonyl-containing compounds were observed in solutions containing the same additive, but in greater yield. And, when the antioxidant was replaced with triethylamine, the same carbonyl compounds were formed, and in quantities that correlated with triethylamine concentration. The analogous carbonyl products derived from **4.2** were not identified in our preliminary report,¹⁰ presumably because no compounds having sufficient basicity were examined. In fact, when **4.2** is used to clock these ‘basic’ antioxidants (i.e. **4.12-4.14** or **4.18**), cinnamaldehyde (conjugated aldehyde) and 1-phenylprop-2-en-1-one (non-conjugated ketone) are indeed observed as major products, and in approximately the same ratios as **4.5** and **4.7** when peroxyester **4.3** was used as the clock.

Expectedly, decomposition of **4.3** at higher temperatures gave way to higher yields of products. The product ratios were again dependent on α -TOH concentration and could be fit to the kinetics in Scheme 4.1. The solution of this expression for k_{β} and α at the higher temperatures required k_{H} for α -tocopherol at these temperatures. To the best of our knowledge, Arrhenius parameters for the reaction of α -TOH with peroxy radicals are not available, but given the typical $\log A \sim 8$ for H-atom transfer reactions as suggested by Benson,²⁹ and the inhibition rate constant for α -TOH in chlorobenzene of $6.4 \times 10^6 \text{ M}^{-1}\text{s}^{-1}$ at 25°C ,¹¹ we calculated $E_{\text{a}} = 1.6 \text{ kcal/mol}$ and were able to estimate the k_{H} at the required temperatures (37, 45, 50, 60, 70, 80 and 95°C). The resulting Arrhenius plot for the β -fragmentation of the non-conjugated peroxy radical yields $E_{\text{a}} = 9.6 \pm 0.9 \text{ kcal/mol}$ and $\log A = 12.8 \pm 0.6$ ³⁰ While these are only estimates, they seem reasonable. For example, the calculated bond dissociation enthalpy (BDE) of the C-OO• bond in the non-conjugated peroxy radical calculated by ROB3P86/6-311G**//UB3P86/6-311G** is 9.8 kcal/mol .³¹ This method has been shown to give C-OO• BDEs in excellent agreement with experimental values; e.g. for benzylperoxyl the calculated C-

OO• BDE value was 22.2 kcal/mol and it was determined to be 21.8 ± 0.9 kcal/mol experimentally.³²

We anticipate that the use of **4.3** to measure inhibition rate constants at higher temperatures will be useful in estimating Arrhenius parameters for various phenolic and aromatic amine antioxidants. There are little of these data in the literature owing to how difficult it has been to carry out the measurements, and the trends in the limited data available are difficult to understand. For example, while phenol and aniline were found to have $\log A = 7.2(\pm 0.5)$, $E_a = 5.2(\pm 0.5)$ kcal/mol³³ and $\log A = 6.6(\pm 0.5)$, $E_a = 5.0(\pm 0.5)$ kcal/mol,³³ respectively, butylated hydroxytoluene (BHT) and *N*-phenyl- α -naphthylamine were found to have $\log A = 4.2(\pm 0.3)$, $E_a = 1.4(\pm 0.3)$ kcal/mol³⁴ and $\log A = 5.1(\pm 0.5)$, $E_a = 1.0(\pm 0.4)$ kcal/mol,³⁴ respectively. The latter result is particularly troublesome given that inhibition rate constants of up to 10^7 M⁻¹s⁻¹ have been measured for diarylamines.¹⁵

Deuterium kinetic isotope effects (DKIEs) have long provided direct mechanistic support for H-atom transfer (HAT) or proton-coupled electron transfer (PCET)³⁵ reactions between phenolic and aromatic amine antioxidants and peroxy radicals. Hammond and co-workers originally found very small KIEs for these reactions, leading them to suggest that the mechanism of their chain-breaking activity was due to rate-determining electron transfer followed by a rapid proton transfer.³⁶ Shortly thereafter, Ingold and Howard demonstrated that Hammond's experimental approach had been flawed (protium from product hydroperoxides in inhibited autoxidations could rapidly exchange with the deuterium in the deuterated phenol, precluding the observation of the DKIE), and demonstrated that there was indeed a sizeable DKIE in these reactions.²⁰ Since then, DKIEs for the reactions of several phenols with peroxy radicals have been measured by inhibited autoxidation of styrene in the presence of excess D₂O (usually 1%

by volume), and generally fall into a range of ~3-5 in chlorobenzene at ambient temperatures.^{17,21,37}

Utilizing peroxyester **4.3** (and excess D₂O/H₂O), we obtained highly reproducible primary DKIEs for a representative series of compounds (cf. Table 4.4), but whose magnitude were roughly half of what were obtained by inhibited autoxidation of styrene where comparison was possible. As an independent check, we measured DKIEs for the same compounds using the ‘first-generation’ peroxy radical clock methodology with methyl linoleate as the oxidizable substrate,⁸ and found essentially the same isotope effects as those obtained using the peroxyester approach. The reason for the discrepancy between our measured DKIEs and those obtained using the inhibited autoxidation of styrene method is unclear and under further investigation.⁴⁰

4.5 Conclusion

β,γ -Unsaturated peroxyesters are convenient and versatile precursors to delocalized radicals for use in peroxy radical clock experiments. In particular, peroxyester **4.3** yields products which are most conveniently separated by gas chromatography, and resolution of the corresponding alcohol and carbonyl products has allowed us to expand the application of the clock methodology to compounds containing even mildly basic moieties with confidence. Additionally, we have demonstrated the utility of peroxyester **4.3** in measuring deuterium kinetic isotope effects (DKIEs) for a variety of phenolic antioxidants, and also discussed its potential in the determination of Arrhenius parameters for peroxy radical-trapping reactions.

4.6 Experimental Details

Complete supporting information can be found with the original manuscript (Hanthorn, J.J and Pratt, D. A. *J. Org. Chem.*, **2012**, 77(1), 276).

4.6.1 Synthesis of Peroxyester 4.3

(E)-tert-butyl-4-(naphthalen-2-yl)but-3-eneperoxoate. To a suspension of *(E)*-4-(naphthalen-2-yl)but-3-enoic acid (3.00 g, 14.2 mmol) in dry benzene (45 mL) was added SOCl₂ (3.38 g, 28.4 mmol) in one portion. The reaction mixture was heated at 50°C until complete as indicated by TLC (ca. 2h). The solvent was evaporated *in vacuo* and the yellow solid obtained was dissolved in dry CH₂Cl₂ (75 mL) and cooled to 0°C. *Tert*-Butyl hydroperoxide (6.7 mL of 5.5 M solution in decane, 36.9 mmol) was then added drop-wise, followed by pyridine (freshly distilled over CaH₂, 4.04 g, 51.1 mmol) as a solution in 20 mL CH₂Cl₂ drop-wise. The reaction was stirred at 0°C until complete as indicated by TLC (ca. 40 min). The reaction mixture was poured into 50 mL of ice-water and extracted with CH₂Cl₂ (2 x 30 mL). The organics were washed with 10% HCl (2 x 20 mL), sat. NaHCO₃ (2 x 20 mL), brine (20 mL) and dried over MgSO₄. Column chromatography (1:9 Et₂O/Pet. Ether) afforded pure product as a white solid. Crystalline product was obtained by recrystallization from ether/hexanes at -20°C. Yield: 2.67 g (66%). ¹H NMR (CDCl₃, 400 MHz) δ ppm 7.81-7.77 (m, 3H), 7.72 (s, 1H), 7.58 (dd, *J* = 2.0, 4.8 Hz, 1H), 7.49-7.42 (m, 2H), 6.72 (d, *J* = 15.8 Hz, 1H), 6.39 (td, *J* = 7.1, 15.8 Hz, 1H), 3.33 (dd, *J* = 1.4, 7.1 Hz, 2H), 1.35 (s, 9H). ¹³C NMR (CDCl₃, 100 MHz) δ ppm 168.7, 134.3, 133.9, 133.4, 133.0, 128.2, 127.9, 127.6, 126.2, 126.2, 125.9, 123.3, 120.5, 83.6, 35.6, 26.0. HRMS (EI) *m/z* calculated 284.1412, found 284.1451. The starting acid,⁴¹ non-conjugated alcohol **4.4**,³⁸ non-conjugated

ketone **4.5**,³⁸ conjugated alcohol **4.6**,³⁹ conjugated aldehyde **4.7**,³⁹ epoxy alcohol⁴⁰ and epoxy ketone⁴⁰ were prepared according to literature procedures.

4.6.2. Calibration Experiments to Determine k_{β}

To a screw-capped GC vial was added peroxyester **4.3** (0.01 M final conc.), α -TOH (**4.8**) (0.02 – 1.0 M final conc.) and the desired solvent to a total volume of 100 μ L. The samples were incubated for 2-14 hours, quenched with 100 μ L of 1 M PPh₃ and diluted to 1 mL with acetonitrile for analysis. GC analysis was carried out using an Agilent DB-5 column (30 m x 0.32 μ m x 0.25 μ m) with the following temperature profile: 130°C hold 5 min, 2°C/min to 162°C, 30°C/min to 280°C, hold 5 min. Response factors for the non-conjugated alcohol **4.4**, non-conjugated ketone **4.5**, conjugated alcohol **4.6** and conjugated aldehyde **4.7** are 1.85, 1.25, 1.21 and 1.83 respectively relative to benzyl alcohol. The resulting plot of $([4.4]+[4.5])/([4.6]+[4.7])$ vs. $[\alpha\text{-TOH}]$ was fit using non-linear regression to obtain k_{β} and α .

4.6.3. Clocking Experiments

To a screw-capped GC vial was added peroxyester **4.3** (0.01 M final conc.), H-atom donor (0.02 – 1.0 M final conc. depending on k_{H}) and the desired solvent to a total volume of 100 μ L. The samples were incubated for 2-14 hours, quenched with 100 μ L of 1 M PPh₃ and diluted to 1 mL with acetonitrile for analysis. GC analysis was carried out using an Agilent DB-5 column (30 m x 0.32 μ m x 0.25 μ m) with the following temperature profile: 130°C hold 5 min, 2°C/min to 162°C, 30°C/min to 280°C, hold 5 min. A plot of $([4.6]+[4.7])/([4.4]+[4.5])$ vs. $1/[\text{H-}]$

atom donor] was fit linearly to obtain k_H . Deuterium kinetic isotope effects were obtained by carrying out measurements in the same manner as above, with the addition of 1% D₂O (or 1% H₂O as a control) to the solvent (after distillation over CaH₂).

4.7 References

- (1) Ingold, K. U. *Accounts of Chemical Research* **1969**, 2, 1.
- (2) Porter, N. A. *Accounts of Chemical Research* **1986**, 19, 262.
- (3) Pratt, D. A.; Porter, N. A.; Tallman, K. A. *Accounts of Chemical Research* **2011**, 44, 458.
- (4) Ingold, K. U. *Chemical Reviews* **1961**, 61, 563.
- (5) Mahoney, L. R. *Angewandte Chemie-International Edition* **1969**, 8, 547.
- (6) Burton, G. W.; Ingold, K. U. *Accounts of Chemical Research* **1986**, 19, 194.
- (7) Valgimigli, L.; Pratt, D. In *Encyclopedia of Radicals in Chemistry, Biology and Materials*; Chatgillialogu, C., Studer, A., Eds.; Wiley: 2011.
- (8) Roschek, B.; Tallman, K. A.; Rector, C. L.; Gillmore, J. G.; Pratt, D. A.; Punta, C.; Porter, N. A. *Journal of Organic Chemistry* **2006**, 71, 3527.
- (9) Wijtmans, M.; Pratt, D. A.; Valgimigli, L.; DiLabio, G. A.; Pedulli, G. F.; Porter, N. A. *Angewandte Chemie-International Edition* **2003**, 42, 4370.
- (10) Jha, M.; Pratt, D. A. *Chemical Communications* **2008**, 1252.
- (11) Valgimigli, L.; Banks, J. T.; Luszyk, J.; Ingold, K. U. *Journal of Organic Chemistry* **1999**, 64, 3381.

- (12) When the $\log k_{\text{inh}}$ values for α -TOH obtained by Valgimigli *et al.* using laser flash photolysis are plotted vs. solvent β_2^{H} an excellent linear correlation is obtained on which all points reside with the exception of chlorobenzene (see Figure S1). Since the rate constant obtained in chlorobenzene is almost certainly in error (it is lower than that obtained in benzene, which has a higher β_2^{H} value), we used the k_{inh} value derived from the $\log k_{\text{inh}}-\beta_2^{\text{H}}$ correlation, which is $6.4 \times 10^6 \text{ M}^{-1}\text{s}^{-1}$ at 25°C .
- (13) Abraham, M. H.; Grellier, P. L.; Prior, D. V.; Duce, P. P.; Morris, J. J.; Taylor, P. *J. Journal of the Chemical Society-Perkin Transactions 2* **1989**, 699.
- (14) Burton, G. W.; Doba, T.; Gabe, E. J.; Hughes, L.; Lee, F. L.; Prasad, L.; Ingold, K. U. *Journal of the American Chemical Society* **1985**, 107, 7053.
- (15) Brownlie, I. T.; Ingold, K. *Canadian Journal of Chemistry* **1966**, 44, 861.
- (16) Lucarini, M.; Pedrielli, P.; Pedulli, G. F.; Valgimigli, L.; Gimes, D.; Tordo, P. *Journal of the American Chemical Society* **1999**, 121, 11546.
- (17) Pratt, D. A.; DiLabio, G. A.; Brigati, G.; Pedulli, G. F.; Valgimigli, L. *Journal of the American Chemical Society* **2001**, 123, 4625.
- (18) Bloodworth, A. J.; Curtis, R. J.; Spencer, M. D.; Tallant, N. A. *Tetrahedron* **1993**, 49, 2729.
- (19) Kornblum, N.; DeLaMare, H. E. *Journal of the American Chemical Society* **1951**, 73, 880.
- (20) Ingold, K. U.; Howard, J. A. *Nature* **1962**, 195, 280.
- (21) Valgimigli, L.; Amorati, R.; Petrucci, S.; Pedulli, G. F.; Hu, D.; Hanthorn, J. J.; Pratt, D. A. *Angewandte Chemie-International Edition* **2009**, 48, 8348.
- (22) Russell, G. A. *Journal of the American Chemical Society* **1957**, 79, 3871.

- (23) To exclude any role of self-association of α -TOH on the determination of k_{β} at the higher concentrations required to accurately calibrate the clock, we also calibrated the clock using 2,6-di-*tert*-butyl-4-methoxyphenol as the H-atom donor ($k_{\text{inh}} = 1.1 \times 10^5 \text{ M}^{-1}\text{s}^{-1}$ at 30°C in chlorobenzene by the inhibited autoxidation of styrene compared to $k_{\text{inh}} = 3.2 \times 10^6 \text{ M}^{-1}\text{s}^{-1}$ for α -TOH determined by the same investigators under the same conditions)¹³ and found a difference of 3.1-fold on k_{β} . In this case, the double-reciprocal plots were compared for [antioxidant] = 0.02- 1.8 M, since fitting of the data obtained for 2,6-di-*tert*-butyl-4-methoxyphenol was not possible due to its slower reaction with peroxy radicals.
- (24) Hu, D.; Pratt, D. A. *Chemical Communications* **2010**, 46, 3711.
- (25) Bartlett, P. D.; Hiatt, R. R. *Journal of the American Chemical Society* **1958**, 80, 1398.
- (26) Antonello, S.; Formaggio, F.; Moretto, A.; Toniolo, C.; Maran, F. *Journal of the American Chemical Society* **2001**, 123, 9577.
- (27) Lien, E. J.; Ren, S. J.; Bui, H. Y. H.; Wang, R. B. *Free Radical Biology and Medicine* **1999**, 26, 285.
- (28) Ellam, R. M.; Padbury, J. M. *Journal of the Chemical Society-Chemical Communications* **1972**, 1086.
- (29) Benson, S. W. *Thermochemical Kinetics 2nd Edition*; John Wiley & Sons: New York, 1976.
- (30) If $\log A = 7.5$ is used for the reaction of α -TOH with peroxy radicals, $\log A$ and E_a for the β -fragmentation of the non-conjugated peroxy radical becomes 12.3 and 8.9 kcal/mol, respectively. Similarly, if $\log A = 8.5$ is used for the reaction of α -TOH

with peroxy radicals, $\log A$ and E_a for the β -fragmentation of the non-conjugated peroxy radical becomes 13.3 and 10.3 kcal/mol, respectively.

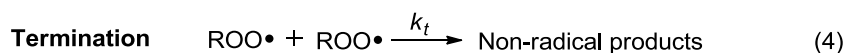
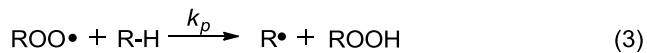
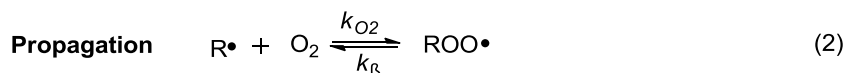
- (31) DiLabio, G. A.; Pratt, D. A. *Journal of Physical Chemistry A* **2000**, *104*, 1938.
- (32) Fenter, F. F.; Noziere, B.; Carlap, P.; Lesclaux, R. *International Journal of Chemical Kinetics* **1994**, *26*, 171.
- (33) Chenier, J. H. B.; Furimsky, E.; Howard, J. A. *Canadian Journal of Chemistry* **1974**, *52*, 3682.
- (34) Howard, J. A.; Furimsky, E. *Canadian Journal of Chemistry* **1973**, *51*, 3738.
- (35) Litwinienko, G.; Ingold, K. U. *Accounts of Chemical Research* **2007**, *40*, 222.
- (36) Hammond, G. S.; Boozer, C. E.; Hamilton, C. E.; Sen, J. N. *Journal of the American Chemical Society* **1955**, *77*, 3238.
- (37) Burton, G. W.; Ingold, K. U. *Journal of the American Chemical Society* **1981**, *103*, 6472.
- (38) Hospital, B. W.; E., A. S. C.; S., W. M.; Han Xun, W.; Office, E. P., Ed. 2009.
- (39) Caiazza, D.; Culbert, J. A.; Taylor, D. K.; Tiekink, E. R. T. *Journal of Organic Chemistry* **2005**, *70*, 8344.
- (40) Chang, C.-L.; Kumar, M. P.; Liu, R.-S. *Journal of Organic Chemistry* **2004**, *68*, 2793.

CHAPTER 5: DEVELOPMENT OF A FLUORESCENCE ASSAY FOR QUANTITATING HYDROPEROXIDES AND ITS APPLICATION TO KINETIC STUDIES OF INHIBITED AUTOXIDATIONS

5.1 Introduction

Peroxyl radicals are key intermediates in the oxidative degradation (autoxidation) of oils, lubricants, plastics and essentially all other petroleum-derived products. Peroxyl radicals also play a key role in certain pathological conditions, such as lipid peroxidation – a process which has been implicated as one of the causative factors for aging, cancer and atherosclerosis. The primary products of lipid peroxidation are lipid-hydroperoxides (LOOH) and therefore they can be used as markers for oxidative stress.¹

Hydroperoxides are formed in peroxidations of organic substrates as peroxyl radicals that have abstracted a hydrogen atom either from another molecule of oxidizable substrate (e.g. lipid) – a process known as uninhibited autoxidation – or from an antioxidant (e.g. α -tocopherol) – a process known as inhibited autoxidation. Both of these processes involve a common chain reaction with two propagation steps, reactions 2 and 3 shown below:

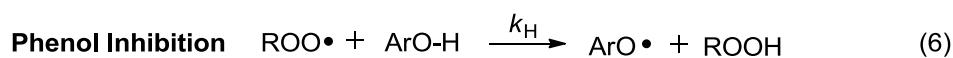


Following abstraction of a hydrogen atom from the substrate to form a carbon-centred radical, oxygen is added at or near the diffusion controlled rate² ($k_{O_2} \approx 10^9 \text{ M}^{-1}\text{s}^{-1}$) in a reaction

that can be reversible for many stabilized carbon-centred radicals^{3,4} ($k_{\beta} \lll k_{O_2}$). The overall rate of hydroperoxide formation in uninhibited peroxidation is described by Eq. 5.

$$\frac{d[\text{ROOH}]}{dt} = \frac{k_p[\text{RH}]R_i^{1/2}}{(2k_t)^{1/2}} \quad (5)$$

Autoxidations can be inhibited (or retarded) by addition of low concentrations of peroxy radical-trapping, chain-breaking antioxidants. Such antioxidant compounds are employed industrially (e.g. BHT and 4,4'-dialkyldiphenylamines) and in nature (e.g. α -tocopherol, the most potent form of vitamin E) to 'trap' peroxy radicals as hydroperoxides and prevent radical-chain propagation.⁵⁻⁷ The reactions that describe peroxy radical-trapping by a phenolic antioxidant are shown in equations 6 and 7, where a phenol first donates a hydrogen atom to a peroxy, forming an aryloxy radical ($\text{ArO}\cdot$) that is generally unreactive towards the substrate and is destroyed by very rapid reaction with another peroxy radical.



Thus, two oxidation chains can be terminated per molecule of phenol. The overall rate of hydroperoxide formation under inhibited autoxidation conditions is described by Eq. 8:

$$\frac{d[\text{ROOH}]}{dt} = \frac{k_p[\text{RH}]R_i}{2k_H[\text{ArOH}]} \quad (8)$$

Eq. 8 shows that the efficacy of the antioxidant is correlated with the magnitude of k_H – the inhibition rate constant – which is dependent on antioxidant structure and reaction medium.^{8,9} Understanding the kinetics of H-atom transfer from antioxidants to peroxy radicals provides important mechanistic information about structure-activity relationships relevant to radical-

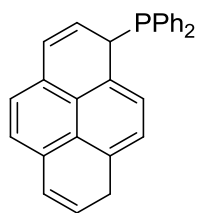
trapping antioxidants and allows for design and implementation of custom antioxidants to suit a variety of important industrial applications.

The kinetics of inhibited autoxidation can be determined either by monitoring the rate of disappearance of the reactants – most commonly O_2 – or by monitoring the rate of product formation – most commonly hydroperoxides. The rate of oxygen consumption (rate of oxygen consumption = rate of hydroperoxide formation) can be accurately determined using a number of methods, with the most established method being a closed system equipped with a differential pressure transducer.^{10,11} Alternatively, the rate of formation of oxidation products (i.e. hydroperoxides) in an inhibited autoxidation should mirror the rate of oxygen consumption and thus can be treated kinetically the same way. This approach is often used when conducting autoxidations of biological samples (e.g. LDLs) or models of biological samples (e.g. micelles and liposomes) and therefore has rarely been used to determine absolute inhibition rate constants (k_H).¹² The traditional method for quantifying hydroperoxides originating from autoxidation reactions is iodometric analysis, which is based on a sodium thiosulfate titration of the iodine (I_2) that is produced when a sample containing hydroperoxides is incubated with potassium iodide (I^-).^{13,14} Alternative methods for quantifying oxidation products include: enzymatic methods,¹⁵ GC/HPLC analysis (of the corresponding alcohols following PPh_3 reduction of hydroperoxides)^{16,17} or fluorescence-based assays.¹⁸⁻²¹

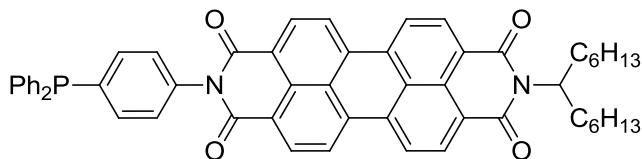
To develop a more efficient method for measuring inhibition rate constants (k_H), we sought to improve the analytical aspect of the inhibited autoxidation technique. Although monitoring oxygen consumption can give very precise quantification of hydroperoxides, the technique requires very delicate calibration and a specialized setup as well as user expertise. More user-friendly methods such as GC or HPLC separation of oxidation products generally

require lengthy analysis times for quantification of all hydroperoxide products at each of dozens of time intervals. Switching to a fluorescence-based assay would offer the potential for automation, where autoxidations could be run in parallel in the wells of a microplate and simply quenched/titrated with dye at various time intervals in order to determine the hydroperoxide concentration in real-time.

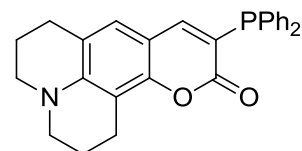
In recent years, the number of fluorescent probes for selectively detecting reactive oxygen species (ROS) has grown rapidly.^{18,21-26} Compounds such as diphenyl-1-pyrenylphosphine (DPPP, **5.1**)²⁷ and Spy-LHP (**5.2**)¹⁹ have emerged as probes for detection and quantification of lipid hydroperoxides, and we felt that combined with the high-throughput capability of microplate readers, they could be useful in the determination of kinetic parameters for hydrocarbon autoxidation and/or its inhibition by radical-trapping antioxidants.



5.1



5.2



5.3

These probes rely on photoinduced electron transfer (PET) from a phosphine moiety to quench fluorescence of a fluorophore (pyrene or perylene in the previous examples) until the phosphine becomes oxidized via reaction with a hydroperoxide and can no longer serve as a fluorescence quencher. A general scheme depicting PET is shown in figure 5.1.

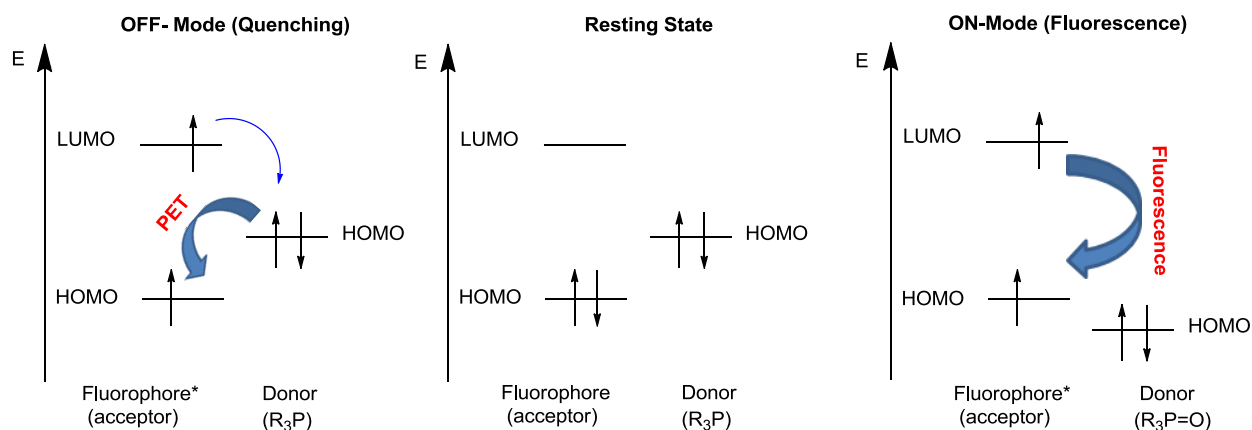


Figure 5.1. Simplified energy diagrams depicting the relative energies of the HOMO/LUMO of the fluorophore and the HOMO energy of the donor involved in a photoinduced electron transfer. An asterisk (*) denotes the fluorophore in an excited state.²⁴

To maximize the efficiency of a PET reaction, the difference in the HOMO energy of the donor and the HOMO energy of the acceptor should be as large as possible (electron-transfer becomes more exergonic). In cases where the redox potentials are favorable, PET occurs very rapidly and irreversibly.

Our initial plans were to utilize Spy-LHP (**5.2**) in a quantitative assay, but we quickly found that the compound suffered from very poor solubility in organic media and was difficult to work with. The same can be said for pyrene-based dyes such as **5.1**. Further survey of the literature revealed that although there are many other scaffolds that have been developed for fluorescence-based detection of reactive oxygen species which can be expected to have better solubilities, many of them are based on alkyl-diarylphosphines. Although these compounds have proven effective sensors for *qualitative* applications (e.g. *in vitro* imaging), their propensity to readily oxidize in air makes them less attractive for *quantitative* assays (e.g. measuring exact hydroperoxide concentrations). For this reason we sought to have a triarylphosphine moiety as

our donor group. Inspired by the work of Bertozzi *et al.*²⁸ and Xian *et al.*,²⁹ and their coumarin-based dyes (**5.3**), which are activated by Staudinger ligation and reaction with S-nitrosothiols respectively, we sought to apply this type of probe in an assay to follow hydrocarbon autoxidations and measure inhibition rate constants for reactions of radical-trapping antioxidants with peroxy radicals.

5.2 Results and Discussion

Using Bertozzi's dye (**5.3**) as a starting point, we replaced the julolidine moiety with a 7-*N,N*-diethylamino group as in **5.4** (Chart 5.1) to ensure the most inexpensive possible synthesis (see Scheme S1). Unfortunately, we found that reactions of **5.4** with hydroperoxides (both tertiary and secondary) were very sluggish, as indicated by a steady increase in fluorescence over intervals greater than 1 hour (20 μM **5.4** with 50-200 μM hydroperoxide). We speculated that the coumarin may impart more steric bulk to the phosphine than that of a typical triarylphosphine used to reduce hydroperoxides (i.e. triphenylphosphine), prompting us to prepare **5.5** (figure 5.2), a compound which incorporated a phenyl spacer between the coumarin and the diphenylphosphine moieties (see Scheme S2). In doing so, we observed an increase in the rate of reaction with hydroperoxides, but the reaction was still far from complete after 15 min in MeOH (20 μM **5.5** with 50-200 μM hydroperoxide).

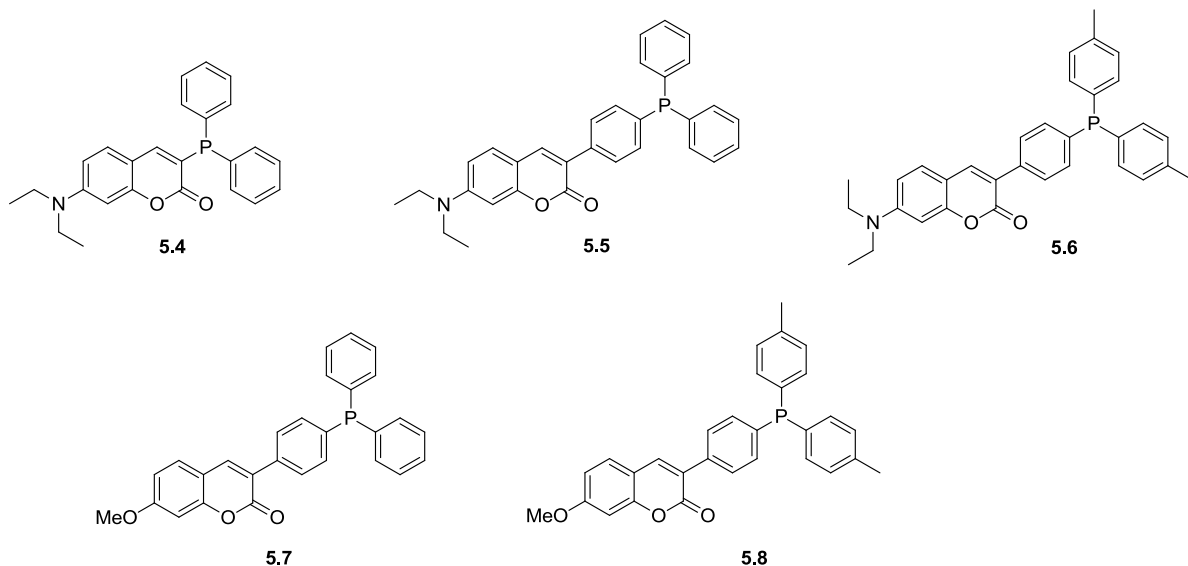


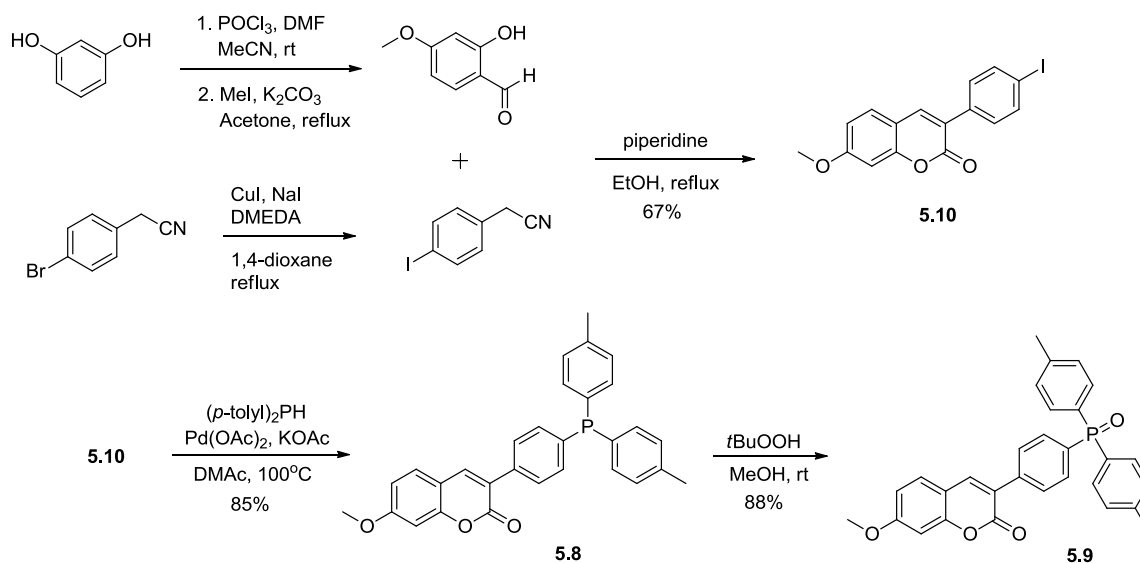
Figure 5.2. Structures synthesized and evaluated for their potential application as fluorescent dyes for the quantitation of hydroperoxides.

Convinced that compound **5.5** would be an effective scaffold for a fluorescent reporter molecule, we set out to optimize the dye by attempting to maximize its rate of reaction with hydroperoxides and at the same time attempting to maximize the fluorescent enhancement between the oxidized and reduced forms of the dye ($\Phi_{\text{ox}}/\Phi_{\text{red}} = 1.2$ for **5.5**). Our first modification was to substitute a di-(*p*-tolyl)phosphine moiety for the diphenylphosphine group of **5.5** to prepare **5.6**, with the electron donating methyl groups serving to raise the HOMO energy of the phosphine moiety (enhancing PET, Figure 5.1) and increasing the nucleophilicity of the phosphine for reaction with hydroperoxides. When **5.6** (see Scheme S3) was treated with tetralin hydroperoxide we did observe faster reaction kinetics than **5.5**, but only a very slight increase in the ratio of quantum yields for fluorescence of the oxidized/reduced forms of the dye ($\Phi_{\text{ox}}/\Phi_{\text{red}} = 1.3$ for **5.6**). The differences in fluorescence quantum yields between oxidized and reduced forms of the dyes (**5.5** and **5.6**) are smaller than expected and may appear suppressed due to the

background oxidation of the reduced dyes in methanol with molecular oxygen. In fact, oxidation products were observed in solid samples of the reduced dyes being stored on the bench under air atmosphere for a few weeks.

As a second-generation modification of compound **5.5**, we replaced the *N,N*-diethylamino-group with a methoxy-group at the 7-position of the coumarin to prepare **5.7** (see Scheme S4) and **5.8**, the rationale being that introduction of a less electron-donating group would lower the HOMO energy of the acceptor moiety (enhancing PET, figure 5.1) – increasing the relative fluorescence quantum yields between oxidized and reduced dyes – as well as diminishing the rate of background oxidation. Indeed, the relative fluorescence quantum yields were increased dramatically ($\Phi_{\text{ox}}/\Phi_{\text{red}} = 2.4$ for **5.7** and $\Phi_{\text{ox}}/\Phi_{\text{red}} = 10.6$ for **5.8**) by lowering the coumarin HOMO energy. Upon lowering the HOMO energy of the acceptor, the effect of replacing the diphenylphosphine (**5.7**) with a di-(*p*-tolyl)phosphine had a much more pronounced effect on the photoinduced electron transfer process, resulting in a 4.4-fold increase in the ratio of oxidized/reduced fluorescence quantum yields. Additionally, the rate of background oxidation was suppressed dramatically – it is minimal in alcoholic solvents and negligible in non-protic solvents (*vide supra*) – and the compounds now appear to be indefinitely bench stable under air atmosphere.

The synthetic route to prepare **5.8** is shown in Scheme 5.1, prepared in 5 steps (see Supporting Information for complete details) from commercially available resorcinol and 4-bromobenzyl nitrile. The oxidized form of the dye (**5.9**), used as a standard for quantifying oxidation of **5.8** was prepared by treating **5.8** with *tert*-butylhydroperoxide in methanol at room temperature.



Scheme 5.1. Preparation of reduced (**5.8**) and oxidized (**5.9**) phosphine dyes.

The excitation and emission spectra of compounds **5.8** and **5.9** are shown in figure 5.3. Both have Stokes shifts of 79 nm but **5.9** shows ca. 10-fold fluorescence enhancement over **5.8** when their absorbances at the excitation maximum (344 nm) are equal. (Spectral characteristics of the other dyes and their corresponding oxidized counterparts are given in the Supporting Information).

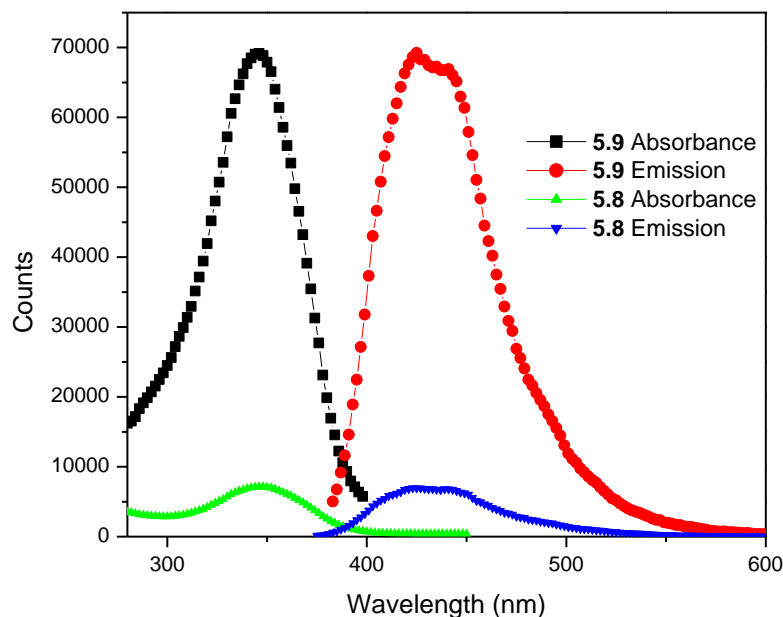


Figure 5.3. Excitation and emission spectra of **5.8** and **5.9** (excitation $\lambda_{\text{max}} = 343$ nm, emission $\lambda_{\text{max}} = 422$ nm) taken in methanol.

The quantum yields of fluorescence were determined using disodium fluorescein ($\Phi_f = 0.92$)³⁰ as a standard and were found to be 0.05 and 0.52 for the reduced (**5.8**) and oxidized form (**5.9**) of the dye respectively ($\Phi_{\text{ox}}/\Phi_{\text{red}} = 10.6$) in methanol. A fluorescence quantum yield of 0.52 for **5.9** is consistent with those reported for other coumarins having substituted alkoxy³¹ or amine groups which are not restricted by substituent linkage (e.g. methoxy- or diethylamino-).³² These compounds have emission yields and lifetimes dramatically lower than their restricted (i.e. cyclized) counterparts (e.g. julolidines) in polar media due to bond rotation-dependent non-radiative decay. In the case of **5.9**, rotation of the methoxy group as well as rotation of the aryl rings appended to the phosphine provide non-radiative relaxation modes.

The reaction of **5.8** with hydroperoxides is still relatively slow (the rate constants for reaction of a secondary hydroperoxide and triarylphosphines are typically $0.3 - 1.6 \text{ M}^{-1}\text{s}^{-1}$, measured by

polarography)³³ and would require lengthy incubation times to ensure an accurate single point measurement. To circumvent the incubation period and to determine hydroperoxide concentrations with much greater precision, a second order rate constant for the reaction between tetralin hydroperoxide and **5.8** was measured. To the best of our knowledge, this is the first time a rate constant has been measured for a fluorescent dye used to detect hydroperoxides and the first use of a second-order rate constant applied towards a quantitative assay for detection of hydroperoxides. Tetralin hydroperoxide was chosen as a representative secondary hydroperoxide (mimicking lipids and other relevant autoxidation substrates) to determine a second-order rate constant because it is crystalline and therefore can be recrystallized to very high purity and can be accurately weighed.³⁴ Figure 5.4 shows the initial observed rates ($k_{\text{obs}} = \text{slope}$) at each hydroperoxide concentration and the plot used to obtain a second order rate constant of $9.5 \text{ M}^{-1}\text{s}^{-1}$ in methanol.

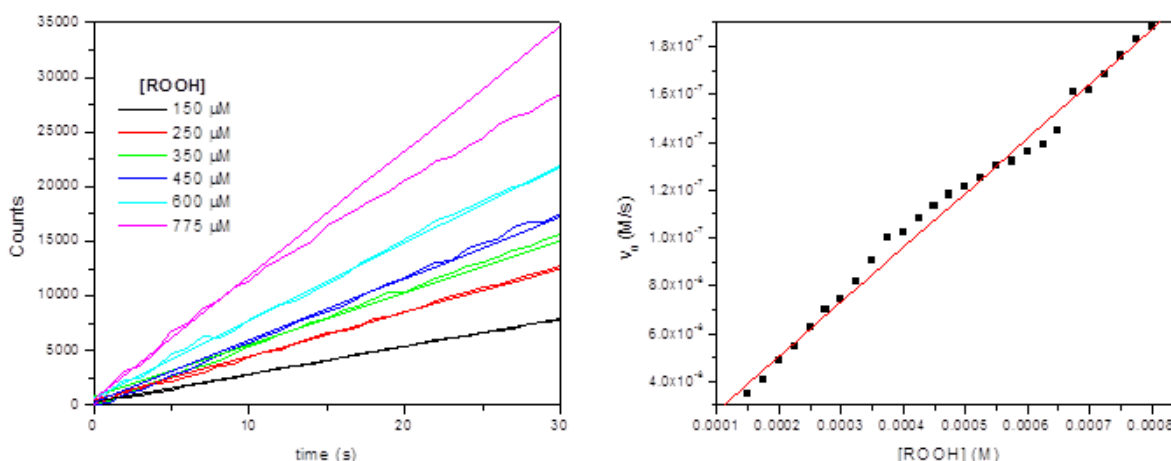


Figure 5.4. Representative initial rates for reactions of **5.8** ($20 \mu\text{M}$) with tetralin hydroperoxide ($150 \mu\text{M} - 775 \mu\text{M}$) in methanol (left) and the resulting plot of the initial rates vs. [ROOH] (right) used to determine the pseudo-first order rate constant, $k_{\text{obs}} = 1.9 \times 10^{-4} \text{ s}^{-1}$ (slope), which was used to obtain the second order rate constant of $k = 9.5 \text{ M}^{-1}\text{s}^{-1}$ ($k_{\text{obs}} = k[\mathbf{5.8}]$, therefore $k = (1.9 \times 10^{-4} \text{ s}^{-1}) / (2 \times 10^{-5} \text{ M}) = 9.5 \text{ M}^{-1}\text{s}^{-1}$).

The choice of solvent proved to be very important, as the desired reaction proceeds fastest in protic media, consistent for the reaction of phosphines with hydroperoxides in general,³⁵ but so too does the background oxidation of **5.8** in solution with molecular oxygen. In fact, in non-protic media the rate of background oxidation becomes negligible, so we found it optimal to prepare stock solutions of dye in acetonitrile and then add this to a solution (in any solvent) containing hydroperoxide, followed by dilution with methanol immediately before recording fluorescence. This procedure becomes trivial when a microplate reader equipped with a reagent dispenser is used for the assay. The choice of solvent for the assay is not limited to methanol (or any alcohol), but rather to those which have dielectric constants high enough to facilitate photoinduced electron transfer – although protic media enhance the rate of reaction between hydroperoxides and the dye dramatically.³⁶

With the second order rate constant for the reaction between **5.8** and tetralin hydroperoxide in hand, secondary hydroperoxide concentrations can accurately be determined in a given solution by measuring the initial rate of dye oxidation and applying $[ROOH] = v_0/(9.5 \text{ M}^{-1}\text{s}^{-1}[\text{dye}])$. When we compare this rate equation to other assays that reportedly quantify hydroperoxides by incubating samples with dyes for several minutes, we can see that quantification is not possible without having a very large excess of one reactant. If concentrations of ROOH and dye are both micromolar (which is the case in most reports), the reaction would need to proceed with a rate constant on the order of diffusion to obtain quantitative reduction of the hydroperoxide for analysis (based on the rate constants determined in the literature, and that which we have determined directly here, all of which are $\sim 1\text{-}10 \text{ M}^{-1}\text{s}^{-1}$, this obviously is not the case). Unfortunately, it is not always possible to have a very large excess of dye (possible photobleaching, excessive background fluorescence, higher rates of

undesired oxidation with molecular oxygen, exceeding the linear dynamic range of the instrument, etc.) and conversely the concentrations of hydroperoxide being detected in a given system may be so low as to preclude it from being a pseudo-first order reactant.

To demonstrate the quantitative utility of this assay, we measured an inhibition rate constant (k_H) for 2,2,5,7,8-pentamethyl-6-chromanol (PMC, **5.10**, a truncated version of α -tocopherol), at 37 °C by following the time course of an inhibited autoxidation of 7-dehydrocholesterol (7-DHC, $k_p = 2260 \text{ M}^{-1}\text{s}^{-1}$)³⁷ in 1,2-dichlorobenzene (Figure 5.5). Although not a common substrate for inhibited autoxidations, Porter *et al.* have recently reported that 7-DHC is the most reactive substrate known that is capable of maintaining a free radical chain reaction,³⁷ which prompted us to explore its use as a substrate for our inhibited autoxidations. The propagation kinetics are much faster than those of styrene ($k_p = 41 \text{ M}^{-1}\text{s}^{-1}$ at 30 °C)⁷ and the oxidation products are hydroperoxides rather than styrene copolymers. Other common substrates for inhibited autoxidation are methyl linoleate ($k_p = 62 \text{ M}^{-1}\text{s}^{-1}$)³⁸ and cumene ($k_p = 0.18 \text{ M}^{-1}\text{s}^{-1}$);³⁹ however, these substrates do not have propagation rates fast enough to conveniently determine inhibition rate constants for very good antioxidants ($k_H > 10^7 \text{ M}^{-1}\text{s}^{-1}$).

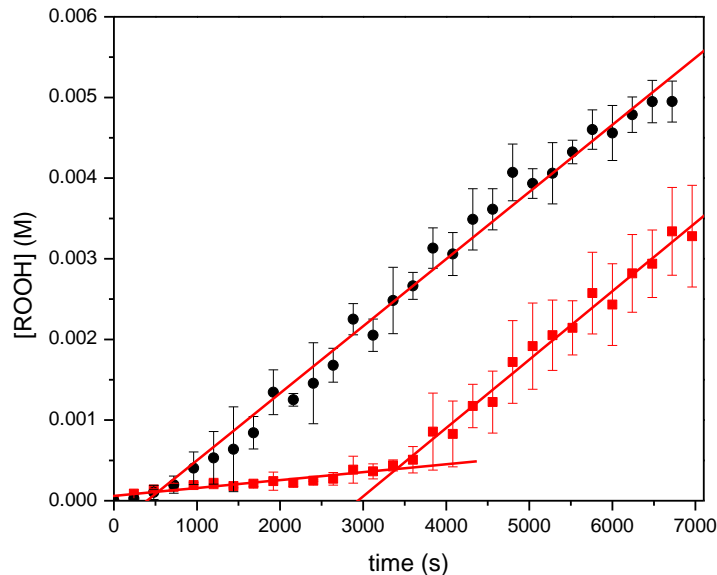


Figure 5.5. Inhibited autoxidation of 7-DHC with 4 μM of **5.10** (■) used to determine $k_{\text{H}} = 1.2 \times 10^6 \text{ M}^{-1}\text{s}^{-1}$ in 1,2-dichlorobenzene. Also shown is the corresponding uninhibited autoxidation of 7-dehydrocholesterol (●).

The reactions were carried out in 96-well plates, using a microplate reader equipped with a reagent dispenser to quench the autoxidation with an excess of 2,6-di-*tert*-butyl-4-methylphenol (BHT) in methanol, and to dispense **5.8** as a solution in acetonitrile to a final concentration of 20 μM at 5 minute intervals. Fluorescence spectra were recorded for 2 min (following a 10 second delay)⁴⁰ after dye addition to accurately measure the hydroperoxide concentration at each time interval and thus obtain $d[\text{ROOH}]/dt$ (Eq. 8). Concentrations of initiator (AIBN, R_i), substrate (7-DHC, k_p) and antioxidant (**5.10**, k_{H}) were adjusted to give a well-defined inhibition period (τ) and chain-lengths >20 so that the kinetic expression shown as Eq. 8 could be applied to determine k_{H} (see experimental section for complete details). Although k_{H} obtained for PMC in Figure 5.5 is a factor of 5 lower than the literature value ($k_{\text{H}} = 6.4 \times 10^6 \text{ M}^{-1}\text{s}^{-1}$), the error may be reflected in the uncertainty of the propagation rate (k_p) for 7-DHC, which has never been used in inhibited autoxidations to determine inhibition rate constants.

Although the assay described above can be expected to be very useful for rapid determination of inhibition rate constants at ambient and/or physiologically-relevant temperatures, its versatility is most obvious from its application to monitor autoxidations carried out at higher temperatures. These are impossible to monitor by oxygen uptake since the solutions must be oxygenated constantly in order to prevent mass transfer of O_2 from being rate-limiting (therefore dramatically changing the kinetics), and are therefore conventionally monitored by iodometry or lengthy GC/HPLC analyses of reaction products. The ability to measure antioxidant activity at high-temperatures is of great industrial importance as it simulates conditions encountered by additives to lubricants and polymers under engine operating conditions or extrusion conditions respectively. Shown in Figure 5.6 are two reaction profiles for inhibited autoxidation of hexadecane at 160 °C in the presence of BHT and 4,4'-diocetyldiphenylamine respectively, obtained by removing aliquots of the reaction mixtures at regular intervals and quantifying their hydroperoxide content using 5.8.

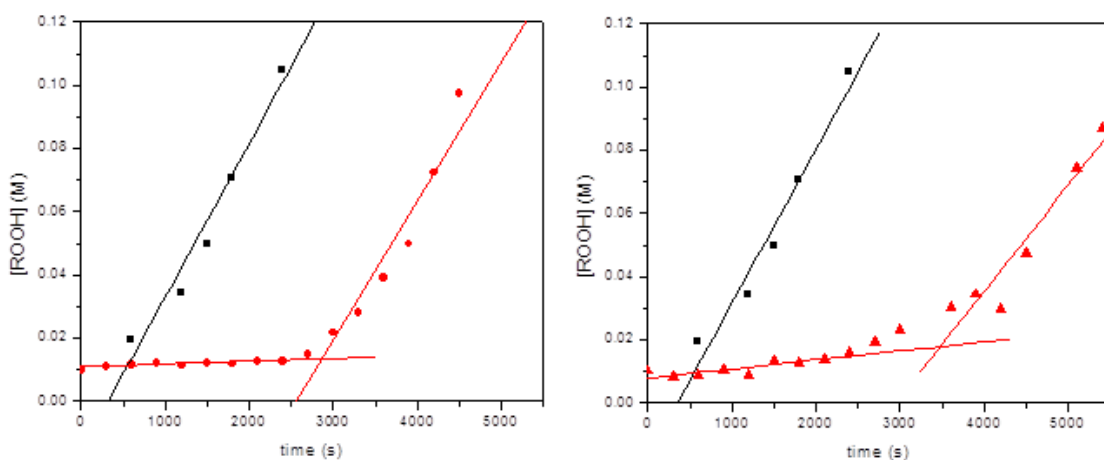
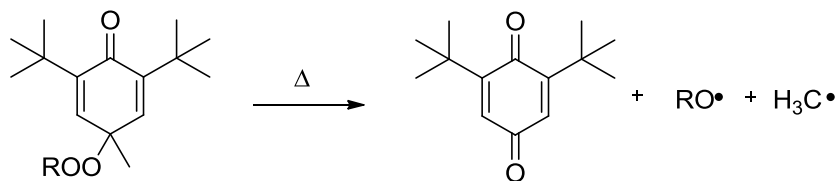
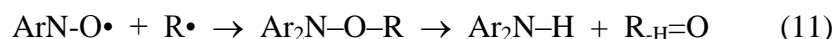


Figure 5.6. (left) Inhibited autoxidation of hexadecane at 160 °C in the presence of 1 mM BHT (●), shown with uninhibited autoxidation (■); (right) Inhibited autoxidation of hexadecane at 160 °C in the presence of 1 mM 4,4'-diocetyldiphenylamine (▲), shown with uninhibited autoxidation (■).

The results of these experiments are in accordance with those published, in that both BHT and 4,4'-dioctyldiphenylamine are effective inhibitors⁴¹ – both have defined inhibition periods (τ) – but the length of inhibition is greater for 4,4'-dioctyldiphenylamine. This implies that BHT has a smaller stoichiometric factor than 4,4'-dioctyldiphenylamine and is consistent with the expected decomposition of BHT-peroxyl (Ar(O)OOR , Eq. 7) compounds to form chain-carrying radicals at elevated temperatures, as shown in Eq. 9 (schematically below)



Additionally, diphenylamines are known to exhibit catalytic radical-trapping antioxidant activity at high temperatures, believed to be the result of reactions of nitroxide intermediates⁴¹ formed in situ from diarylamines (Eq. 10 and 11) that can result in stoichiometric factors as high as $n = 40$.⁴² Thus we can rationalize the results shown in Figure 5.6 – where the inhibition period is longer (and has a less-defined endpoint) for 4,4'-dioctyldiphenylamine than BHT – on the basis that phenolic antioxidants can give rise to chain-carrying radicals at high temperatures, while diphenylamines exhibit catalytic reactivity via nitroxide intermediates at high temperatures.

5.3 Conclusions

In summary, we have prepared a phosphine dye (**5.8**) that has been optimized for enhanced rate of reaction with hydroperoxides and optimized for photoinduced electron transfer (i.e. maximum $\Phi_{\text{ox}}/\Phi_{\text{red}}$). We have determined a second-order rate constant, $k = 9.5 \text{ M}^{-1}\text{s}^{-1}$ for the reaction of **5.8** with secondary hydroperoxides in methanol at 37 °C and have utilized this rate constant as a method of accurately determining hydroperoxide concentrations by measuring observed rate constants as fluorescence vs. time. The assay can be performed using a microplate reader equipped with a reagent dispenser to measure hydroperoxide concentrations in real-time for an inhibited autoxidation of 7-dehydrocholesterol, and thus used to determine rate constants for reactions between antioxidants and peroxy radicals. Additionally, the assay serves as an effective analytical method for determining hydroperoxide concentrations in samples derived from high-temperature inhibited autoxidations of hexadecane – providing a very easy method for studying these highly industrially relevant reactions.

5.4 Supporting Information

5.4.1 Inhibited Autoxidation of 7-dehydrocholesterol

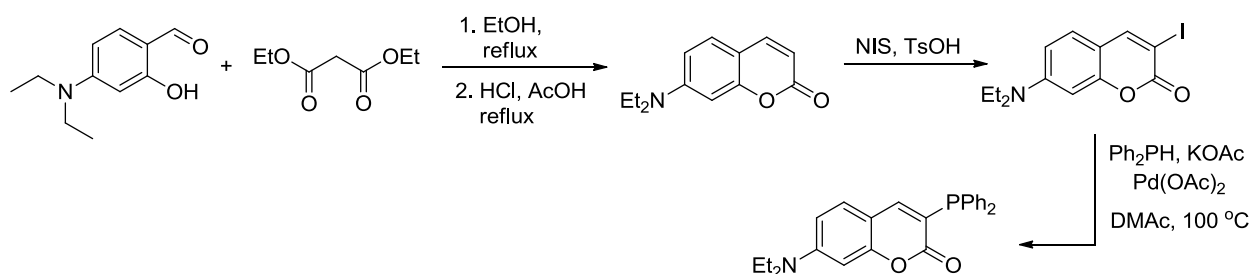
As there was no precedence for measuring inhibition rate constants using 7-dehydrocholesterol (7-DHC), we chose conditions analogous for those in literature using more common autoxidation substrates, such as styrene at 4.3M with propagation $k_p = 41$. We then adjusted 7-DHC concentration (ca. 70-80 mM) to get similar chain lengths (>20) based on the same rate of initiation using MeOAMVN at 37 °C.

For the inhibited autoxidation of 7-DHC with PMC, the conditions were as follows: [7-DHC] = 78 mM, [PMC] = 4 μ M, [MeOAMVN] = 20 μ M in 1,2-dichlorobenzene (chosen to minimize solvent evaporation in open microplate wells) at 37 °C. Samples were quenched at regular intervals with excess BHT (50 mM) and diluted with methanol, followed by addition of **5.8** (20 μ M final concentration) as a solution in acetonitrile. Fluorescence was measured for ca. 2 min (excitation 345 nm, emission 410 nm) to obtain the observed rate constant.

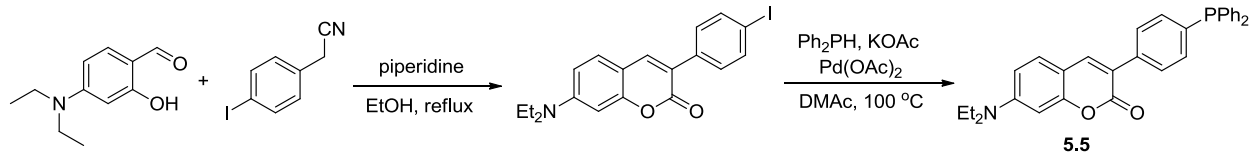
5.4.2 Inhibited Autoxidation of Hexadecane

A solution of hexadecane (purified by passage through silica) containing antioxidant (1-5 mM) was warmed to 160 °C before tetralin hydroperoxide (10 mM) was added (i.e. a known concentration of hydroperoxide initiator) and vigorous bubbling of oxygen was initiated. Samples were removed at regular intervals, quenched with excess BHT and cooled to room temperature prior to fluorescence analysis as described above.

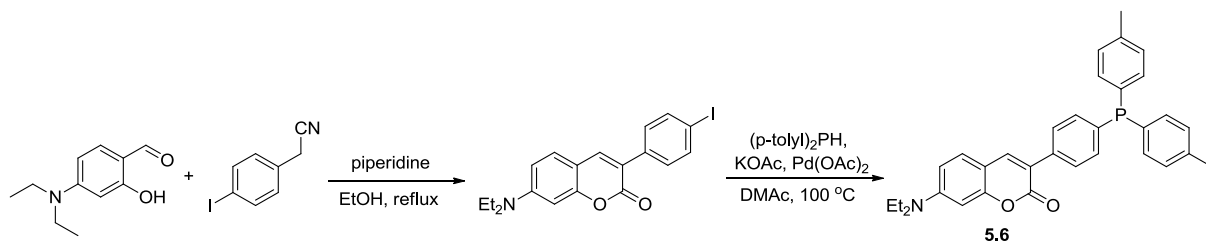
5.4.3 Preparation and characterization of phosphine dyes



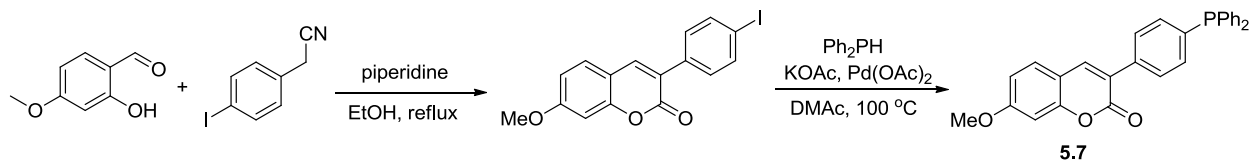
Scheme S1. Preparation of **5.4** using conditions analogous to Bertozzi *et al.*²⁸



Scheme S2. Preparation of **5.5**.



Scheme S3. Preparation of **5.6**.



Scheme S4. Preparation of **5.7**.

Table S1. Excitation and emission maxima for oxidized and reduced forms of dyes **5.4-5.8** along with measured fluorescence quantum yields (determined vs. fluorescein standard, $\Phi = 0.92$).

Compound	λ_{abs} (nm)	λ_{em} (nm)	Quantum Yield
5.4 (red)	405	484	0.003
5.4 (ox)	404	482	0.013
5.5 (red)	408	486	0.17
5.5 (ox)	408	485	0.21
5.6 (red)	406	486	0.15
5.6 (ox)	406	485	0.17
5.7 (red)	345	425	0.20
5.7 (ox)	345	426	0.48
5.8	343	422	0.05
5.9	343	422	0.52

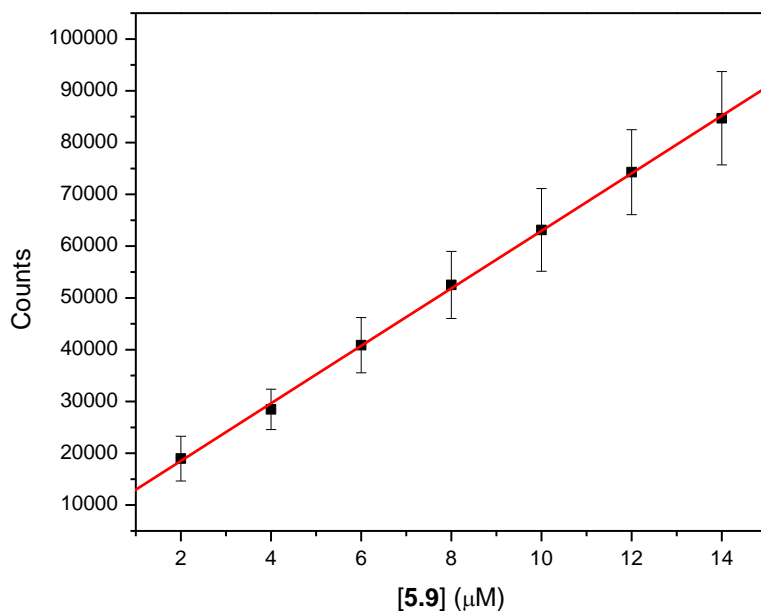
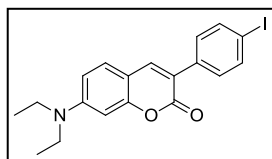


Figure S1. Fluorescence intensity (counts) vs. concentration of oxidized dye **5.9**. The correlation gives: counts = $5.55 \times 10^4[\mathbf{5.9}] + 7411$ ($r^2 = 0.99$).

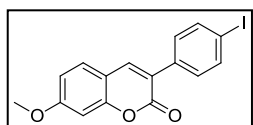
7-(diethylamino)-3-(4-iodophenyl)-2H-chromen-2-one



A solution of 4-iodophenylacetonitrile⁴³ (4.33 g, 17.8 mmol), *p*-(diethylamino)salicylaldehyde (3.38 g, 17.5 mmol) and piperidine (1.52 g, 17.8 mmol) in 35 mL EtOH was heated to reflux until reaction completion, determined by TLC. The reaction was quenched by addition to 150 mL H₂O and extracted 3x with EtOAc. Organics were washed with brine and dried over MgSO₄ to afford a red oil. Purification by column chromatography (EtOAc/Hexanes 1:4) to obtain a yellow solid. Yield: 72 %. ¹H NMR (CDCl₃, 400 MHz) δ ppm 7.72-7.69 (m, 2H), 7.67 (s, 1H), 7.46-7.42 (m, 2H), 7.29 (d, *J* = 8.0 Hz, 1H), 6.58 (dd, *J* = 8.8, 2.4 Hz, 1H), 6.49 (d, *J* = 2.4 Hz, 1H), 3.41 (q, *J* = 7.1 Hz, 4H), 1.21 (t, *J* = 7.1 Hz, 6H). ¹³C NMR (CDCl₃, 100 MHz) δ ppm 161.224, 156.209,

150.653, 140.504, 137.276, 135.269, 129.897, 129.022, 119.302, 109.007, 108.826, 96.935, 93.222, 44.811, 12.414. HRMS (EI) m/z calculated 419.0382, found 419.0369.

3-(4-iodophenyl)-7-methoxy-2*H*-chromen-2-one (5.10)



A solution of 4-iodophenylacetonitrile⁴³ (4.33 g, 17.8 mmol), 2-hydroxy-4-methoxybenzaldehyde⁴⁴ (3.38 g, 17.5 mmol) and piperidine (1.52 g, 17.8 mmol) in 35 mL EtOH was heated to reflux until reaction completion, determined by TLC. The reaction was quenched by addition to 150 mL H₂O and extracted 3x with EtOAc. Organics were washed with brine and dried over MgSO₄ to afford a red oil. Purification by column chromatography (EtOAc/Hexanes 1:4) to obtain a peach-coloured solid. Yield 67 %. ¹H NMR ((CD₃)₂CO, 400 MHz) δ ppm 8.13 (s, 1H), 7.81 (d, $J = 8.5$ Hz, 2H), 7.66 (d, $J = 8.5$ Hz, 1H), 7.58 (d, $J = 8.5$ Hz, 2H), 6.98-6.93 (m, 2H), 3.94 (s, 3H). ¹³C NMR ((CD₃)₂CO, 100 MHz) δ ppm 165.013, 161.516, 157.434, 142.405, 139.172, 137.046, 132.292, 131.517, 124.830, 115.136, 114.550, 102.019, 95.286, 57.394. HRMS (EI) m/z calculated 377.9753, found 377.9767.

General procedure for coupling diarylphosphines

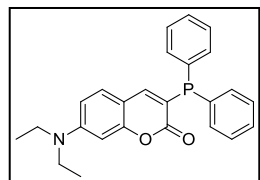
To a solution of aryl iodide (4.0 mmol) in 4.0 mL *N,N*-dimethylacetamide (freshly distilled over BaO) was added Pd(OAc)₂ (2 mg, 4 μ mol), KOAc (471 mg, 4.8 mmol) and Ar₂PH (781 mg, 4.2 mmol). The reaction was stirred at 100 °C until completion, as determined by TLC. Quenched by addition to H₂O and extraction with CH₂Cl₂. Washed with brine and dried over MgSO₄. Purified

by column chromatography, eluting with EtOAc/Hexanes, followed by recrystallization to analytical purity.

General procedure for preparing phosphine oxides

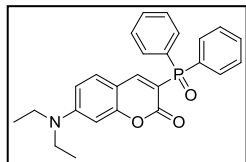
To a solution of phosphine dye (1.0 mmol) in 5 mL MeOH was added *tert*-butylhydroperoxide (1.0 mmol) at room temperature. Once oxidation was complete, the phosphine oxide was passed through a small silica column eluting with EtOAc, followed by recrystallization to analytical purity.

7-(diethylamino)-3-(diphenylphosphino)-2*H*-chromen-2-one (5.4)



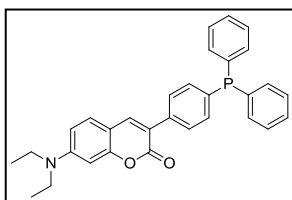
Yield: 90% yellow crystals. ^1H NMR ($(\text{CD}_3)_2\text{CO}$, 400 MHz) δ ppm 7.41-7.38 (m, 10H), 7.19 (d, $J = 8.8$ Hz, 1H), 7.14 (d, $J = 3.6$ Hz, 1H), 6.64 (dd, $J = 8.8, 2.4$ Hz, 1H), 6.50 (d, $J = 2.4$ Hz, 1H), 3.49 (q, $J = 7.0$ Hz, 4H), 1.19 (t, $J = 7.0$ Hz, 6H). ^{13}C NMR ($(\text{CD}_3)_2\text{CO}$, 100 MHz) δ ppm 163.111, 162.898, 158.859, 152.986, 149.430, 149.377, 137.777, 137.662, 135.629, 135.422, 131.139, 130.887, 130.549, 130.487, 120.098, 119.974, 110.653, 110.618, 98.412, 46.274, 13.715. HRMS (EI) m/z calculated 401.1545, found 401.1559.

7-(diethylamino)-3-(diphenylphosphoryl)-2H-chromen-2-one (5.4b)



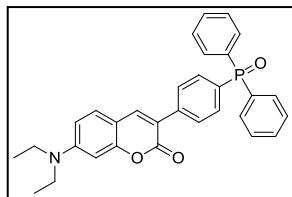
Yield: 80 % yellow solid. ^1H NMR ($(\text{CD}_3)_2\text{CO}$, 400 MHz) δ ppm 8.54 (d, $J = 13.8$ Hz, 1H), 7.89-7.84 (m, 4H), 7.63 (d, $J = 9.0$ Hz, 1H), 7.61-7.48 (m, 6H), 6.81 (dd, $J = 9.0, 2.4$ Hz, 1H), 6.52 (d, $J = 2.4$ Hz, 1H), 3.56 (q, $J = 7.0$ Hz, 4H), 1.23 (t, $J = 7.0$ Hz, 6H). ^{13}C NMR ($(\text{CD}_3)_2\text{CO}$, 100 MHz) δ 160.448, 154.830, 154.772, 154.615, 135.645, 134.566, 133.673, 133.570, 133.519, 133.491, 132.904, 130.093, 129.970, 111.351, 110.119, 110.013, 98.216, 46.482, 13.677. HRMS (EI) m/z calculated 417.1494, found 417.1489.

7-(diethylamino)-3-(4-(diphenylphosphino)phenyl)-2H-chromen-2-one (5.5)



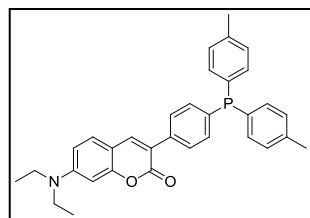
Yield: 60% yellow powder. ^1H NMR (CDCl_3 , 400 MHz) δ ppm 8.01 (s, 1H), 7.78 (dd, $J = 8.4, 1.2$ Hz, 2H), 7.48 (d, $J = 9.0$ Hz, 1H), 7.42-7.30 (m, 12H), 6.75 (dd, $J = 8.8, 2.4$ Hz, 1H), 6.64 (d, $J = 2.4$ Hz, 1H), 3.52 (q, $J = 7.0$ Hz, 4H), 1.22 (t, $J = 7.0$ Hz, 6H). ^{13}C NMR ($(\text{CD}_3)_2\text{CO}$, 100 MHz) δ ppm 162.225, 158.321, 152.833, 142.811, 139.250, 139.134, 138.673, 135.515, 135.319, 135.237, 135.040, 131.438, 130.743, 130.548, 130.479, 130.123, 130.054, 121.050, 110.983, 110.736, 98.308, 46.291, 13.744. HRMS (EI) m/z calculated 477.1858, found 477.1879.

7-(diethylamino)-3-(4-(diphenylphosphoryl)phenyl)-2H-chromen-2-one (5.5b)



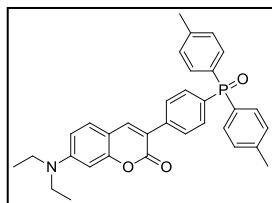
Yield: 90% bright yellow solid. ^1H NMR ($(\text{CD}_3)_2\text{SO}$, 400 MHz) δ ppm 8.19 (s, 1H), 7.88 (dd, $J = 8.0, 2.0$ Hz, 2H), 7.67-7.59 (m, 13H), 7.91 (d, $J = 8.8$ Hz, 1H), 6.74 dd, $J = 8.0, 2.0$ Hz, 1H), 6.56 (d, $J = 2.0$ Hz, 1H), 3.44 (q, $J = 6.8$ Hz, 4H), 1.13 (t, $J = 6.8$ Hz, 6H). ^{13}C NMR ($(\text{CD}_3)_2\text{SO}$, 100 MHz) δ ppm 160.138, 155.983, 150.761, 142.258, 139.161, 133.210, 132.191, 131.974, 131.677, 131.447, 131.350, 131.315, 131.215, 130.649, 129.913, 128.750, 128.633, 128.017, 127.899, 117.197, 109.242, 108.231, 95.993, 44.065, 12.251. HRMS (ESI) m/z calculated 493.1807, found 494.33 (M+H).

3-(4-(di-*p*-tolylphosphino)phenyl)-7-(diethylamino)-2H-chromen-2-one (5.6)



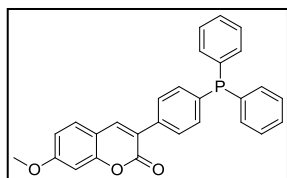
Yield: 77 % yellow solid. ^1H NMR ($(\text{CD}_3)_2\text{CO}$, 300 MHz) δ ppm 7.99 (s, 1H), 7.75 (dd, $J = 8.5, 1.3$ Hz, 2H), 7.47 (d, $J = 9.0$ Hz, 1H), 7.32-7.25 (m, 2H), 7.23-7.22 (m, 8H), 6.74 (dd, $J = 9.0, 2.4$ Hz, 1H), 6.53 (d, $J = 2.4$ Hz, 1H), 3.52 (q, $J = 7.0$ Hz, 4H), 2.34 (s, 6H), 1.22 (t, $J = 7.0$ Hz, 6H). ^{13}C NMR (CDCl_3 , 100 MHz) δ ppm 161.387, 156.102, 150.486, 140.518, 138.559, 137.287, 137.176, 135.811, 133.778, 133.695, 133.582, 133.370, 133.179, 129.227, 129.155, 128.922, 127.949, 127.882, 119.967, 108.910, 96.892, 44.792, 21.191, 12.354. HRMS (EI) m/z calculated 505.2171, found 505.2194.

3-(4-(di-*p*-tolylphosphoryl)phenyl)-7-(diethylamino)-2*H*-chromen-2-one (5.6b)



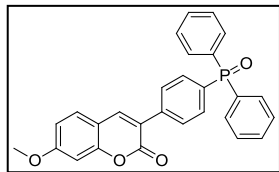
Yield: 56 % yellow solid. ^1H NMR (*d*₆-DMSO, 400 MHz) δ ppm 8.17 (s, 1H), 7.86 (dd, $J = 8.0, 2.0$ Hz, 2H), 7.61 (dd, $J = 11.3, 8.4$ Hz, 2H), 7.53-7.48 (m, 5H), 7.37-7.34 (m, 4H), 6.72 (dd, $J = 8.8, 2.4$ Hz, 2H), 6.55 (d, $J = 2.0$ Hz, 1H), 3.43 (q, $J = 7.0$ Hz, 4H), 2.36 (s, 6H), 1.12 (t, $J = 7.0$ Hz, 6H). ^{13}C NMR (*d*₆-DMSO, 100 MHz) δ ppm 160.131, 155.961, 150.726, 142.167, 141.900 (d, $J = 2.6$ Hz), 138.924 (d, $J = 2.6$ Hz), 132.408, 131.475, 131.341, 131.245, 131.113, 130.399, 129.883, 129.297, 129.136, 129.008, 127.942, 127.786, 117.261, 109.214, 108.227, 95.983, 44.054, 21.007, 12.241. HRMS (EI) m/z calculated 521.2120, found 521.2123.

3-(4-(diphenylphosphino)phenyl)-7-methoxy-2*H*-chromen-2-one (5.7)



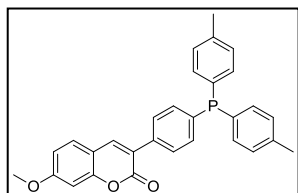
Yield: 80% yellow solid. ^1H NMR ($(\text{CD}_3)_2\text{CO}$, 400 MHz) δ ppm 8.09 (s, 1H), 7.76 (d, $J = 7.1$ Hz, 2H), 7.62 (d, $J = 8.4$ Hz, 1H), 7.40-7.31 (m, 12H), 6.95-6.91 (m, 2H), 3.92 (s, 3H). ^{13}C NMR ($(\text{CD}_3)_2\text{CO}$, 100 MHz) δ ppm 164.861, 161.602, 157.334, 142.399, 139.388, 139.266, 139.038, 138.923, 137.791, 135.538, 135.341, 135.201, 135.005, 131.411, 130.794, 130.559, 130.489, 130.395, 130.327, 125.233, 115.137, 114.464, 101.940, 57.341. HRMS (EI) m/z calculated 436.1228, found 436.1243.

3-(4-(diphenylphosphoryl)phenyl)-7-methoxy-2H-chromen-2-one (5.7b)



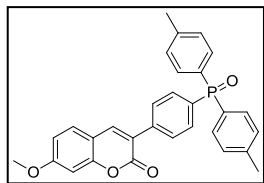
Yield: 92% pale-yellow solid. ^1H NMR ($(\text{CD}_3)_2\text{SO}$, 400 MHz) δ ppm 8.32 (s, 1H), 7.88 (d, $J = 6.8$ Hz, 2H), 7.72-7.57 (m, 14H), 7.05 (s, 1H), 6.99 (d, $J = 8.6$ Hz, 1H), 3.87 (s, 3H). ^{13}C NMR ($(\text{CD}_3)_2\text{CO}$, 100 MHz) δ ppm 165.168, 161.529, 157.561, 143.351, 140.805, 140.775, 135.968, 135.634, 134.945, 134.611, 133.735, 133.708, 133.612, 133.571, 133.473, 131.676, 130.511, 130.392, 130.259, 124.819, 115.081, 114.615, 102.007, 57.407. HRMS (EI) m/z calculated 452.1177, found 452.1182.

3-(4-(di-*p*-tolylphosphino)phenyl)-7-methoxy-2H-chromen-2-one (5.8)



Yield: 85% off-white solid. ^1H NMR ($(\text{CD}_3)_2\text{CO}$, 400 MHz) δ ppm 8.12 (s, 1H), 7.76 (d, $J = 8.0$ Hz, 2H), 7.65 (d, $J = 8.4$ Hz, 1H), 7.32 (m, 2H), 7.23 (m, 8H), 6.94 (m, 2H), 3.94 (s, 3H), 2.34 (s, 6H). ^{13}C NMR (CDCl_3 , 100 MHz) δ ppm 164.913, 161.660, 157.338, 142.334, 140.745, 137.559, 135.768, 135.644, 135.444, 134.971, 134.779, 131.434, 131.277, 131.205, 130.304, 130.238, 125.410, 115.218, 114.488, 102.003, 57.376, 22.260. HRMS (EI) m/z calculated 464.1541, found 464.1540.

3-(4-(di-*p*-tolylphosphoryl)phenyl)-7-methoxy-2*H*-chromen-2-one (5.9)



Yield: 88% off-white solid. ^1H NMR ($(\text{CD}_3)_2\text{CO}$, 400 MHz) δ ppm 8.20 (s, 1H), 7.91 (dd, $J = 8.1, 2.0$ Hz, 2H), 7.76-7.67 (m, 3H), 7.61 (d, $J = 8.0$ Hz, 2H), 7.58 (d, $J = 8.0$ Hz, 2H), 7.37-7.35 (m, 4H), 6.95-6.96 (m, 2H), 3.95 (s, 3H), 2.41 (s, 6H). ^{13}C NMR (CDCl_3 , 100 MHz) δ ppm 165.148, 161.541, 157.547, 144.100 (d, $J = 2.8$ Hz), 143.283, 140.600 (d, $J = 2.8$ Hz), 136.120, 135.097, 133.750, 133.651, 133.518, 133.421, 132.875, 131.828, 131.656, 131.111, 130.989, 130.285, 130.167, 124.873, 115.087, 114.603, 102.003, 57.404, 22.500. HRMS (EI) m/z calculated 480.1490, found 480.1474.

5.5 References

- (1) Sies, H. *Angewandte Chemie-International Edition in English* **1986**, *25*, 1058.
- (2) Maillard, B.; Ingold, K. U.; Scaiano, J. C. *Journal of the American Chemical Society* **1983**, *105*, 5095.
- (3) Pratt, D. A.; Mills, J. H.; Porter, N. A. *Journal of the American Chemical Society* **2003**, *125*, 5801.
- (4) Tallman, K. A.; Roschek, B.; Porter, N. A. *Journal of the American Chemical Society* **2004**, *126*, 9240.
- (5) Ingold, K. U. *Chemical Reviews* **1961**, *61*, 563.
- (6) Mahoney, L. R. *Angewandte Chemie-International Edition* **1969**, *8*, 547.
- (7) Burton, G. W.; Ingold, K. U. *Accounts of Chemical Research* **1986**, *19*, 194.
- (8) Jha, M.; Pratt, D. A. *Chemical Communications* **2008**, 1252.

- (9) Valgimigli, L.; Pratt, D. In *Encyclopedia of Radicals in Chemistry, Biology and Materials*; Chatgillialogu, C., Studer, A., Eds.; Wiley: 2011.
- (10) Burton, G. W.; Doba, T.; Gabe, E. J.; Hughes, L.; Lee, F. L.; Prasad, L.; Ingold, K. U. *Journal of the American Chemical Society* **1985**, *107*, 7053.
- (11) Barclay, L. R. C.; Baskin, K. A.; Locke, S. J.; Schaefer, T. D. *Canadian Journal of Chemistry-Revue Canadienne De Chimie* **1987**, *65*, 2529.
- (12) Pratt, D. A.; Valgimigli, L. In *Encyclopedia of Radicals in Chemistry, Biology and Materials*; John Wiley & Sons, Ltd: 2012.
- (13) Jessup, W.; Dean, R. T.; Gebicki, J. M. *Oxygen Radicals in Biological Systems, Pt C* **1994**, *233*, 289.
- (14) Yagi, K. *Biochemical Medicine* **1976**, *15*, 212.
- (15) Heath, R. L.; Tappel, A. L. *Analytical Biochemistry* **1976**, *76*, 184.
- (16) Zinbo, M.; Jensen, R. K. *Analytical Chemistry* **1985**, *57*, 315.
- (17) Jensen, R. K.; Korcek, S.; Zinbo, M. *International Journal of Chemical Kinetics* **1994**, *26*, 673.
- (18) Gomes, A.; Fernandes, E.; Lima, J. *Journal of Biochemical and Biophysical Methods* **2005**, *65*, 45.
- (19) Soh, N.; Ariyoshi, T.; Fukaminato, T.; Nakajima, H.; Nakano, K.; Imato, T. *Organic & Biomolecular Chemistry* **2007**, *5*, 3762.
- (20) Gray, J. I. *Journal of the American Oil Chemists Society* **1978**, *55*, 539.
- (21) Onoda, M.; Uchiyama, S.; Endo, A.; Tokuyama, H.; Santa, T.; Imal, K. *Organic Letters* **2003**, *5*, 1459.

- (22) Maeda, H.; Futkuyasu, Y.; Yoshida, S.; Fukuda, M.; Saeki, K.; Matsuno, H.; Yamauchi, Y.; Yoshida, K.; Hirata, K.; Miyamoto, K. *Angewandte Chemie-International Edition* **2004**, *43*, 2389.
- (23) Dahlstrom, M.; Forsstrom, D.; Johannesson, M.; Huque-Andersson, Y.; Bjork, M.; Silfverplatz, E.; Sanin, A.; Schaal, W.; Pelcman, B.; Forsell, P. K. A. *Journal of Biomolecular Screening* **2010**, *15*, 671.
- (24) Schaferling, M.; Grogel, D. B. M.; Schreml, S. *Microchimica Acta* **2011**, *174*, 1.
- (25) Koide, Y.; Kawaguchi, M.; Urano, Y.; Hanaoka, K.; Komatsu, T.; Abo, M.; Teraia, T.; Nagano, T. *Chemical Communications* **2012**, *48*, 3091.
- (26) Yuan, L.; Lin, W. Y.; Xie, Y. N.; Chen, B.; Zhu, S. S. *Journal of the American Chemical Society* **2012**, *134*, 1305.
- (27) Okimoto, Y.; Watanabe, A.; Niki, E.; Yamashita, T.; Noguchi, N. *Febs Letters* **2000**, *474*, 137.
- (28) Lemieux, G. A.; de Graffenried, C. L.; Bertozzi, C. R. *Journal of the American Chemical Society* **2003**, *125*, 4708.
- (29) Pan, J.; Downing, J. A.; McHale, J. L.; Xian, M. *Molecular Biosystems* **2009**, *5*, 918.
- (30) Zhang, X. F.; Liu, Q.; Wang, H. B.; Fu, Z.; Zhang, F. S. *Journal of Photochemistry and Photobiology a-Chemistry* **2008**, *200*, 307.
- (31) Farinotti, R.; Siard, P.; Bourson, J.; Kirkiacharian, S.; Valeur, B.; Mahuzier, G. *Journal of Chromatography* **1983**, *269*, 81.
- (32) Jones, G.; Jackson, W. R.; Halpern, A. M. *Chemical Physics Letters* **1980**, *72*, 391.

- (33) Shulman, J. I. *Journal of Organic Chemistry* **1977**, *42*, 3970.
- (34) Knight, H. B.; Swern, D. *Organic Syntheses* **1954**, *34*, 90.
- (35) Hiatt, R.; McColeman, C. *Canadian journal of chemistry* **1971**, *49*, 1712.
- (36) Hiatt, R.; McColeman, C. **1971**, *49*, 1712.
- (37) Korade, Z.; Xu, L. B.; Shelton, R.; Porter, N. A. *Journal of Lipid Research* **2010**, *51*, 3259.
- (38) Howard, J. A. *Absolute Rate Constants for Reactions of Oxyl Radicals*; Logos Press, 1972; Vol. IV.
- (39) Howard, J. A.; Ingold, K. U.; Symonds, M. *Canadian Journal of Chemistry* **1968**, *46*, 1017.
- (40) A 10 second delay was incorporated into the assay due to the near instantaneous electron-transfer reaction that occurs between **5** and the remaining MeOAMVN initiator. The change in concentration of reduced dye is negligible and the initial fluorescence spike does not affect the slope, which reflects the observed reaction rate with the hydroperoxide (41) Jensen, R. K.; Korcek, S.; Zinbo, M.; Gerlock, J. L. *Journal of Organic Chemistry* **1995**, *60*, 5396.
- (42) Bolsman, T.; Blok, A. P.; Frijns, J. H. G. *Recueil Des Travaux Chimiques Des Pays-Bas-Journal of the Royal Netherlands Chemical Society* **1978**, *97*, 310.
- (43) Klapars, A.; Buchwald, S. L. *Journal of the American Chemical Society* **2002**, *124*, 14844.
- (44) Hu, C. Q.; Li, X.; Wang, W. S.; Zhang, L.; Tao, L. L.; Dong, X. W.; Sheng, R.; Yang, B.; Hu, Y. Z. *Bioorganic & Medicinal Chemistry* **2011**, *19*, 5454.

CHAPTER 6: DEVELOPMENT OF A NEW PRECURSOR FOR TRANSIENT ABSORPTION KINETIC STUDIES OF FAST PEROXYL RADICAL REACTIONS

6.1 Reactivity of α -Tocopherol (α -TOH)

α -Tocopherol (α -TOH), the most potent congener of vitamin E, is an important inhibitor of lipid peroxidation both in vivo^{1,2} and in vitro.^{3,4} In fact, α -tocopherol has been identified as the major lipid-soluble, chain breaking antioxidant in human blood^{5,6} and therefore has been the subject of many investigations to understand the mechanisms by which it protects living systems against free-radical damage. Of primary importance in the inhibition of lipid peroxidation is the reaction of α -TOH and other phenolic antioxidants with peroxy radicals⁴ (as discussed in Chapter 1), which have been studied quantitatively in model membrane systems such as micelles,⁷ multilamellar liposomes,⁸ phosphatidylcholine bilayers⁹ as well as in organic¹⁰ and aqueous media.^{11,12} In addition to reactions with peroxy radicals, H-atom transfer kinetics have been measured for reactions with alkoxy, alkyl and hydrazyl radicals. While these reactions are largely irrelevant from a biological perspective (*vide infra*), they were believed to provide insight into the trends in the reactivity of phenols, including α -TOH, towards peroxy radicals. However, in recent years it has come to light that the mechanism of reaction of phenols with peroxy radicals is different than it is with alkyls, alkoxy radicals and hydrazyls.

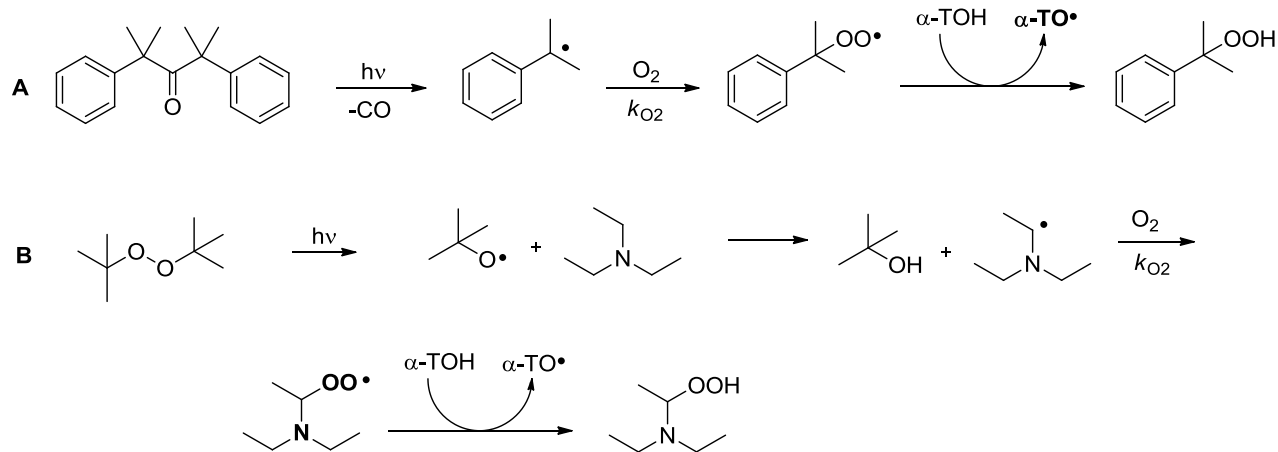
The reaction of phenols with peroxy radicals is best described as a proton-coupled electron transfer (PCET) reaction, where a proton is transferred from the phenol to the peroxy radical via two non-bonding orbitals while an electron moves from the π -HOMO of the phenol to the π -SOMO of the peroxy radical.^{13,14} Reactions between phenols and alkyl radicals are known

to occur via a formal hydrogen-atom transfer (HAT) mechanism where the phenolic proton is transferred with one of its electrons to the unpaired electron on the carbon-centred radical.¹⁵ Similarly, alkoxy radicals react with phenols via a HAT mechanism, but the formation of H-bonded complexes between the phenol and oxygen centred radical affords greatly enhanced reaction rates.¹⁶ The mechanism of reaction between phenols and hydrazyl radicals such as dpph• is not as clear – it has been suggested that the reaction proceeds via a single transition state structure and that the mechanism can best be described as a combination of HAT and PCET.¹⁷

Several methods have been utilized to directly measure rate constants for reactions between α -TOH and peroxy radicals. The rotating sector method (See Chapter 1) has been used to measure rate constants in the range of 10^6 - 10^8 $M^{-1}s^{-1}$ in aqueous and alcoholic media with a variety of peroxy radicals.¹² Ingold and coworkers measured inhibition rate constants for the reaction of α -TOH with poly(peroxystyryl)peroxy radicals (inhibited autoxidation of styrene, see Chapter 1) at 30 °C in the range of $5 \times 10^5 - 5 \times 10^6$ $M^{-1}s^{-1}$.¹⁸ More recently, Valgimigli *et al.* utilized laser flash photolysis (LFP, See Chapter 1) to measure inhibition rate constants with cumylperoxy radicals in a variety of hydrogen-bond accepting solvents to determine kinetic solvent effects on the H-atom transfer kinetics at 30 °C (Scheme 6.1).¹⁰ This method utilizes Norrish fragmentation of dicumylketone in the presence of oxygen to produce cumylperoxy radicals *in situ* and relies on following reaction kinetics by watching the growth of α -tocopheroxy radical at ca. 420 nm, since the cumylperoxy radical does not have absorbance above 300 nm.

An alternative method was put forward by Lalevee *et al.* that allows the reaction kinetics to be followed by measuring the rate of decay of the transient peroxy radical instead of the antioxidant-derived radical (scheme 6.1).¹⁹ The approach relies on formation of α -aminoalkyl-

peroxyl radicals – compounds which have absorbances in the range of 340-420 nm depending on the alkylamine.

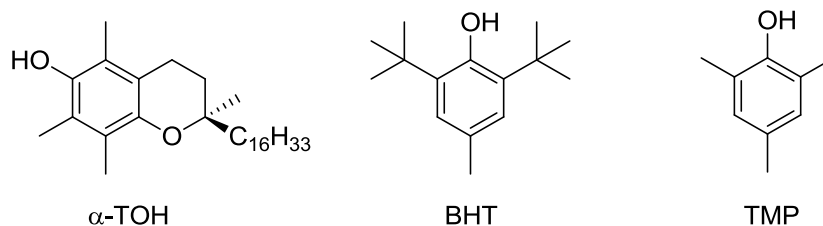


Scheme 6.1. (A) Photolysis of dicumylketone under aerobic conditions to generate cumyl peroxy which is trapped by α -tocopherol. Reaction kinetics are monitored by watching the growth of α -tocopheroxyl radical at 420 nm.¹⁰ (B) Photolysis of di-*tert*-butylperoxide in the presence of a trialkylamine to generate an α -aminoalkyl-peroxy radical that is trapped by α -tocopherol. Reaction kinetics are monitored by watching the decay of the α -aminoalkyl-peroxy radical at ca. 380-420 nm (380 nm for Et₃N as shown).^{19,20}

6.2 Temperature Dependence of Reactions of α -Tocopherol with Radicals

Considering the biological importance of α -TOH and its use as a “gold standard” in radical-trapping reaction kinetics, surprisingly little work has been done to determine the effect of temperature on reactions of radicals with α -TOH. This is likely due to the physiological role of α -TOH, and the corresponding temperature at which its reactions take place in Nature (37 °C). In many instances, the Arrhenius parameters have been measured for the reactions of more industrially relevant phenolic antioxidants with radicals, presumably since they are used in applications outside of the ambient temperatures at which most rate constants are conveniently

determined (e.g. for reactions with alkyl radicals, BHT has $\log A = 6.05$ and $E_a = 3.62$ kcal/mol, while TMP has $\log A = 7.26$ and $E_a = 3.34$ kcal/mol).²¹



6.2.1 Arrhenius Parameters for Reactions of α -TOH and Alkyl Radicals

Typically α -TOH is not used as a chain-terminating antioxidant for reactions with alkyl radicals (the biologically relevant reaction is with peroxy radicals, See Chapter 1), but rate constants have been measured for its reactions with primary and secondary alkyl radicals. Valgimigli *et al.* have most recently measured a rate constant in toluene of $k_H = 6.0 (\pm 1.5) \times 10^5$ $M^{-1}s^{-1}$ using the 5-hexenyl radical clock approach (See Chapter 1).²¹ However, no temperature dependence on this reaction has been measured. Arrhenius parameters have been measured for more industrially relevant phenols such as 2,4,6-trimethylphenol (TMP) and 2,6-di-*tert*-butylphenol using the Neophyl-radical clock²² ($k_r = 1100$ s^{-1} at 25 °C, $\log A = 12.7 \pm 0.3$ and $E_a = 13.8 \pm 0.3$ kcal/mol)²³⁻²⁵ and these compounds can serve as a model for estimating α -TOH reactivity. To estimate the A-factor for α -TOH we can use the value of $\log A = 7.26$ obtained for TMP,²¹ which has similar steric hindrance around the phenolic OH moiety (*ortho* groups = Me). Using $\log A = 7.26$ and a measured rate constant of $6.0 (\pm 1.5) \times 10^5$ $M^{-1}s^{-1}$ in toluene we can estimate an activation energy of 2.7 kcal/mol for the reaction of α -TOH with primary alkyl radicals.

6.2.2 Arrhenius Parameters for Reactions of α -TOH and Aryloxy Radicals

To study the temperature dependence on the rate of reaction between α -TOH and aryloxy radicals, Luszyk *et al.* used laser flash photolysis (355 nm, 40 mJ/pulse) to generate phenoxy radicals (PhO•) (1.4 M of phenol in 2:1 v/v di-*tert*-butylperoxide/MeCN produced ca. 10^{-4} - 10^{-5} M phenoxy) in the presence of several phenolic antioxidants (ArOH, including α -TOH).²⁶ By choosing the right concentrations of phenol/antioxidant, rate constants could be determined by watching the first order growth of ArO•. They found Arrhenius parameters for α -TOH of $\log A = 10.0 \pm 0.2$ and $E_a = 2.0 \pm 0.2$ kcal/mol over a temperature range of 243-328 K. The large pre-exponential factor explains the greater reactivity (ca. 100 fold) of tocopherol (phenols in general) with aryloxy radicals compared to peroxy radicals. An A value of $10^{10} \text{ M}^{-1} \text{ s}^{-1}$ is larger than the “normal” value of $10^{8.5 \pm 0.5} \text{ M}^{-1} \text{ s}^{-1}$ for a simple atom-transfer reaction,²⁷ and can be rationalized by considering that H-atom transfers between two oxygen atoms occurs via equilibrium formation of a hydrogen-bonded complex of the oxygen-centred radical with the phenolic OH group, followed by a rate-controlling atom transfer within the complex.^{4,28,29} If this H-bonded complex dissociates at a rate much slower than the rate of H-atom transfer, the pre-exponential factor will be “high” since in the absence of steric constraints it will be almost equal to the A -factor for a diffusion controlled reaction (i.e. $A \sim 10^{11.5} \text{ M}^{-1} \text{ s}^{-1}$) in solvents of normal viscosity.^{26,30}

6.2.3 Arrhenius Parameters for Reactions of α -TOH and Alkoxy Radicals

At physiological levels, tocopherols cannot efficiently scavenge alkoxy radicals (or hydroxyl radicals) due to the fact that these molecules are extremely reactive towards other

biomolecules and therefore have very fleeting lifetimes. The reactions between α -TOH and alkoxy radicals have been studied in organic media and the reactions are extremely rapid, having rate constants on the order of, $k = 3.1 \times 10^9 \text{ M}^{-1}\text{s}^{-1}$ with $\text{Me}_3\text{CO}\cdot$ at 25 °C in benzene.²¹ However, similar to reactions with alkyl radicals, the lack of biological and industrial relevance has precluded the measurement of the temperature dependence on this specific reaction. In their studies of *tert*-butoxyl radicals reacting with phenols, Scaiano *et al.* measured Arrhenius parameters for 4-methoxyphenol reacting with *tert*-butoxyl radicals in toluene and obtained $\log A = 12.1 \text{ M}^{-1}\text{s}^{-1}$ and $E_a = 4.0 \text{ kcal/mol}$.¹⁶ Such large values of $\log A$ are characteristic of unimolecular reactions so it is likely that H-bonded pre-reaction complexes are formed between phenols and alkoxy radicals, similar to reactions with aryloxy radicals (*vide infra*). Although the A -factor for tocopherol will be lower than 4-methoxyphenol due to steric interaction with the α -TOH *ortho*-methyl groups, this data is the only reasonable estimate available.

6.2.4 Arrhenius Parameters for Reactions of α -TOH and Peroxyl Radicals

The reaction of α -TOH with peroxyl radicals has been extremely well studied in all media, but there has yet to be any Arrhenius parameters measured for these reactions. As previously discussed, the lack of direct biological or industrial relevance may have deterred extensive temperature-reactivity studies; however, since α -TOH is the archetypical phenolic antioxidant, it is surprising that these data are not available in the literature. On several occasions members of our laboratory have lamented this fact, particularly since it would make standardization of our peroxyl radical clocks for use at other temperatures easy *and very useful*. Instead, one has to resort to the general value that an Arrhenius pre-exponential factor for an H-

atom transfer is $10^{8-8.5} \text{ M}^{-1}\text{s}^{-1}$ – a value put forward by Benson in 1976 after a thorough review of H-atom transfer kinetics up to that point in time.²⁷ Over the past 4 decades, few attempts have been made to precisely determine pre-exponential values for reactions between phenols and peroxy radicals. In 1984 Howard measured $\log A$ values of 4.0 - 4.7 $\text{M}^{-1}\text{s}^{-1}$ and corresponding activation energies of 1.0-0.4 kcal/mol for *para*-substituted 2,6-di-*tert*-butylphenols using EPR spectroscopy.

One of the difficulties with measuring Arrhenius parameters using conventional techniques is finding conditions to span a reasonable temperature range – with EPR spectroscopy the experiment requires cryogenic conditions and with LFP it is difficult to conduct low-temperature experiments and difficult to find a source of radicals (e.g. di-*tert*-butylperoxide, diacylperoxide, etc.) that are stable to elevated temperatures in order to span a reasonable temperature range. Additionally, high concentrations of initiator (e.g. di-*tert*-butylperoxide or dicumylketone) are typically required and can yield complicated spectra due to the short wavelengths required for initiation (*vide infra*).

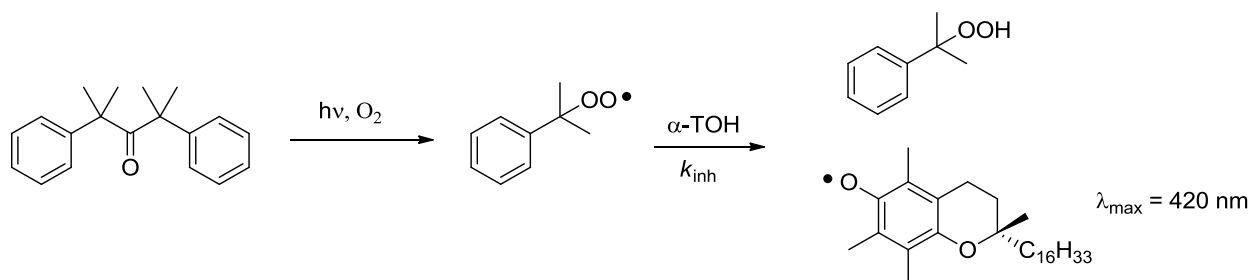
6.3 Project Objectives

To better quantify the temperature dependence of the reaction between peroxy radicals and α -tocopherol (as well as potentially other phenols and diarylamines) we sought to develop a system where peroxy radicals could be generated under LFP conditions using 355 nm light (away from the region where α -TOH has significant absorbance) by decomposition of azocumene. The use of this wavelength will minimize photoionization of α -TOH (*vide infra*) and

should provide clean formation of cumylperoxyl radicals with only molecular nitrogen as a by-product.

6.4 Results and Discussion

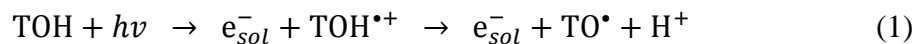
In order to obtain the Arrhenius parameters for the peroxy-radical trapping kinetics of tocopherol we initially envisioned using dicumylketone as a precursor to cumylperoxyl radicals as reported by Valmigli *et al.*,¹⁰ and simply repeat the transient absorption measurements at various temperatures using a thermostatted sample chamber. Upon irradiation with 266 or 308 nm laser light, dicumylketone undergoes a Norrish I fragmentation to yield an acyl radical and a carbon-centred cumyl radical,³¹ and in competition with in-cage recombination is the diffusion-controlled addition of O₂ to the cumyl radical to generate a cumylperoxyl radical. This radical is then trapped by α -tocopherol to give cumyl hydroperoxide and α -tocopheroxyl radical – a compound which has an absorbance maximum at ca. 420 nm.¹² Therefore, by watching the growth of the α -tocopheroxyl radical we can directly obtain an observed second order rate constant for the reaction between α -tocopherol and cumylperoxyl.



Scheme 6.2. Photolysis of dicumylketone to generate cumylperoxyl radicals and their trapping by α -tocopherol.

When we attempted to do the experiment using either a 308 nm XeCl excimer laser or the fourth harmonic of a Nd:YAG laser (266 nm), there was no clean first-order growth corresponding to α -tocopheroxyl formation, but rather a large ‘spike’ in the absorbance at 420 nm, followed by a what appeared to be a first-order growth curve. The spike in absorbance was attributed to the photoionization of α -tocopherol – a problem that is very difficult to avoid using 266 nm or 308 nm laser light – giving rise to an instantaneous growth in the kinetic trace that obscures a significant portion of the tocopheroxyl growth data and makes accurate fitting of the pseudo-first order kinetics impossible.

Photoionization is known to occur when α -tocopherol (TOH) is excited to the S_1 state, usually in a polar medium. It has been suggested that TO^\bullet is formed only as a result of proton release by $TOH^{\bullet+}$, a process which is known to occur in polar solvents on a subnanosecond timescale.³² Bisby and Parker³³ conducted a nanosecond LFP study of TOH in both deaerated methanol and deaerated aqueous micellar solutions and found that the transient absorption spectrum recorded immediately after a 308 nm pulse (10 ns duration) was a superposition of the spectra of a solvated electron (e_{sol}^-) and neutral tocopheroxyl (TO^\bullet). They observed a linear relationship between the TO^\bullet signal and the intensity of the laser pulse, indicating that the formation of TO^\bullet is a monophotonic process. They proposed that photoexcitation of TOH resulted in ejection of an electron, followed by subnanosecond deprotonation of $TOH^{\bullet+}$.³⁴

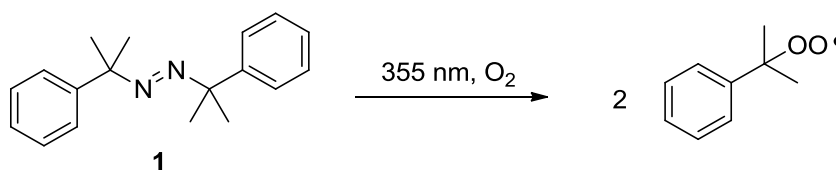


However, later investigations conducted in hexane revealed that TO^\bullet is easily observed, but $TOH^{\bullet+}$ is not detected. In nonpolar media the absence of a signal contributed by $TOH^{\bullet+}$ cannot be explained by a rapid (subnanosecond) deprotonation because the species has a known lifetime of

a few microseconds in hexane. Based on these observations and recent work by Naqvi *et al.*³² it has been determined that as much as 1/3 of TO[•] originates from direct photodissociation.

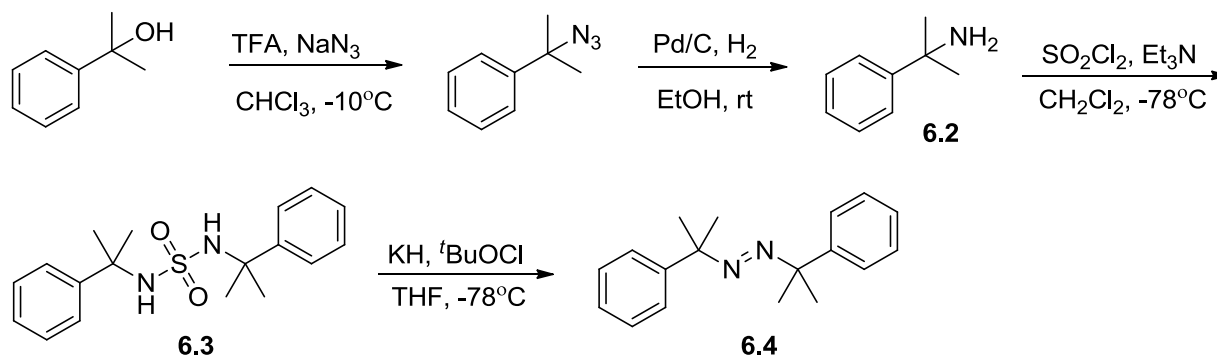


To circumvent the problem of photoionization, we sought to find a method of generating cumylperoxyl radicals using 355 nm laser light, a region of the spectrum where tocopherol has very little absorbance. This led us to pursue azocumene as a radical precursor, a molecule with a reported λ_{max} at 360 nm which upon excitation decomposes to generate two cumyl radicals concurrent with expulsion of nitrogen gas.³⁵ The cumyl radicals will then react with oxygen at diffusion controlled rate to give 2 cumylperoxyl radicals as described above.



Scheme 6.3. Photolysis of azocumene at 355 nm in the presence of oxygen to generate two cumylperoxyl radicals.

The synthesis of azocumene was achieved in 4 steps beginning with commercially available cumyl alcohol. Conversion to cumylamine via an azide intermediate followed by treatment with sulfonyl chloride affords a symmetrical sulfonamide. This compound is then subjected to a strong base and *tert*-butyl hypochlorite to promote a chelotropic elimination of SO₂, providing the desired azocumene.



Scheme 6.4. Synthetic route to prepare azocumene.³⁶

When we attempted to generate cumylperoxyl radicals by photolysis of 5 mM azocumene at 355 nm (Nd:YAG, 4-6 mJ/pulse), we obtained what appeared to be first order growth traces as in Figure 6.1 (at 40 mM and 120 mM α -tocopherol). Although the growth rates of tocopheroxyl radical appear consistent with a higher rate of peroxy trapping at higher α -TOH concentrations, the absolute absorbance values are significantly different. Since both samples contain the same amount of azocumene, it would be expected that the same amount of peroxy radicals would be formed in each sample and thus the same amount of α -tocopheroxyl should be observed regardless of α -TOH concentration. The differences we observe in tocopheroxyl concentration can possibly be accounted for by photoionization of tocopherol – a process that is concentration dependent and that obscures an important region of the growth curve, making accurate curve fitting very difficult. Alternatively, there may be additional decomposition pathways for cumylperoxyl that are unknown/unaccounted for and as a result the higher the tocopherol concentration, the more peroxy radicals are trapped and the higher the observed optical density. It may be a combination of photoionization and alternative decomposition pathways that

contribute to the tocopherol concentration dependent optical densities and does not allow for a confident estimate of the rate of reaction.

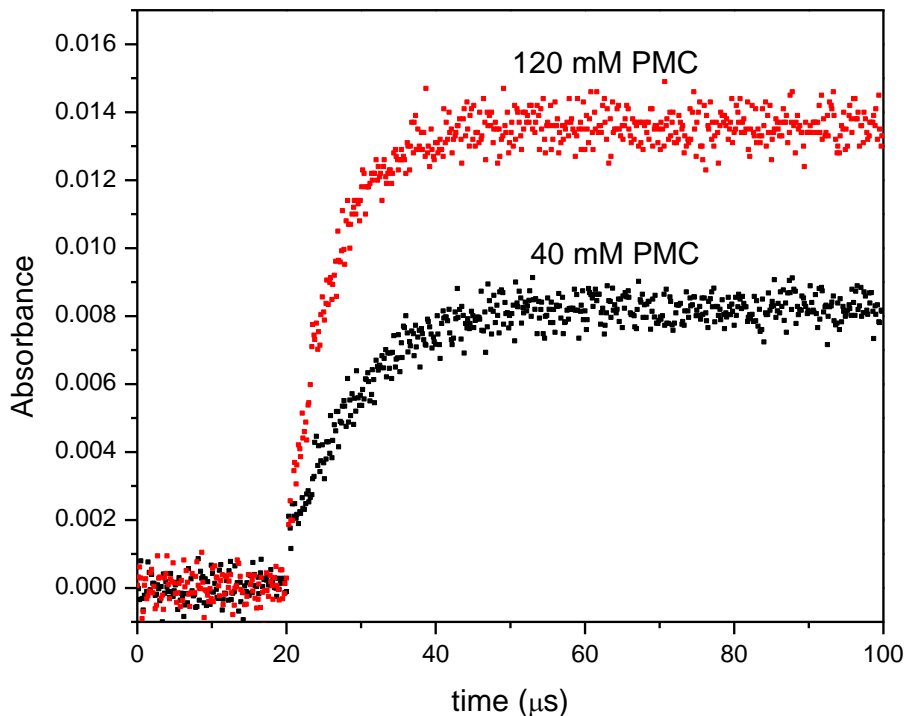
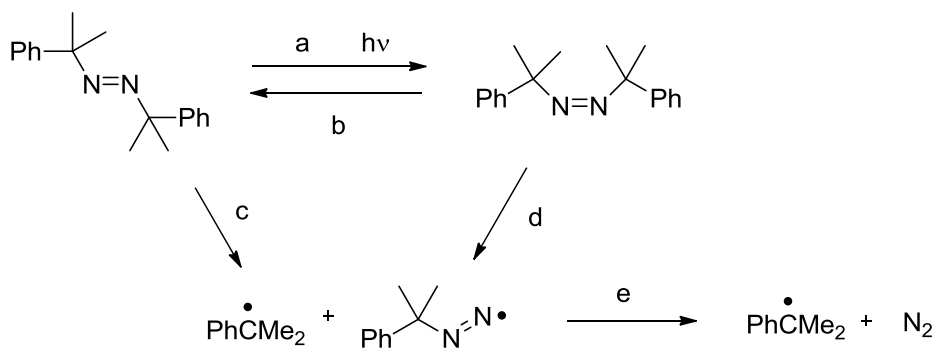


Figure 6.1. LFP traces for growth of α -TOH (recorded at 420 nm), initiated by photolysis of azocumene (5 mM) in oxygenated chlorobenzene in the presence of 40 mM α -TOH (black) and 120 mM α -TOH (red).

However, tocopherol does not have a significant absorbance at 355 nm and the laser power was likely insufficient (ca. 3-6 mJ) to generate significant amounts of TO^\bullet by photoionization. In concert with azocumene decomposition via nitrogen extrusion (Scheme 6.5; c, e), the majority of energy absorbed by azocumene gives rise to a very rapid *cis/trans* isomerization (a) when irradiated at 355 nm, and the *cis*-compound does have a small absorption band at 420 nm. However, the timescale for the *cis*-isomer to decay back to the thermodynamically more favourable *trans*-isomer (b) is extremely short ($t_{1/2} = 5 \mu\text{s}$ at 292 K) and was not expected to obscure the tocopheroxyl growth trace.³⁷



Scheme 6.5. Decomposition and isomerization pathways for azocumene.³⁷

However, even if this process were interfering with our measurement, the absorption coefficient and rate of decay for the cis-isomer are both known and the data could be corrected. Since this process did not appear to be the cause of our absorbance spike, we hypothesized that the azocumene must be acting as a photosensitizer in a process leading to photoionization of α -tocopherol. This would now be a much bigger problem to overcome as it is not possible to photolyze azocumene without some energy transfer to tocopherol and it would be very difficult to quantify the photoionization process.

With respect to our suspected azocumene photosensitized-ionization of tocopherol, we discovered a report by Nau *et al.* where they conclude that photoreactions of excited azoalkanes (DBO and DDBH shown below) can include efficient interactions of the n,π^* -excited states with electrophilic hydrogen atoms – i.e. O-H in alcohols, N-H in amines, and C-H in chlorinated alkanes.³⁸



Compounds such as DBO and DDBH have n,π^* -excited states that are very poor electron-acceptors which do not undergo electron-transfer with amines;³⁸ rather the excited molecules react via hydrogen atom transfer with secondary and primary amines, alcohols and alkanes. This contrasts the general presumption that n,π^* -excited chromophores (e.g. ketones) interact preferentially with nucleophilic α -C-H hydrogens and have very low reactivity with electrophilic hydrogens. The rate constants for abstraction of H-atoms by the n,π^* -excited states of DBO and DDBH have been measured as $k = 1.2 \times 10^9 \text{ M}^{-1}\text{s}^{-1}$ and $k = 6.1 \times 10^7 \text{ M}^{-1}\text{s}^{-1}$ respectively for reactions with diethylamine (determined in neat diethylamine) and a deuterium kinetic isotope effect of $k_{\text{H}}/k_{\text{D}} = 1.3$ was measured for DBO, further supporting a hydrogen-atom transfer process.

Thus a possible explanation for the near-instantaneous growth of tocopheroxyl (and its concentration dependence) could be H-atom abstraction from tocopherol by the n,π^* -excited state of azocumene, as depicted in Eq. 3 (with alkyl groups removed for clarity).

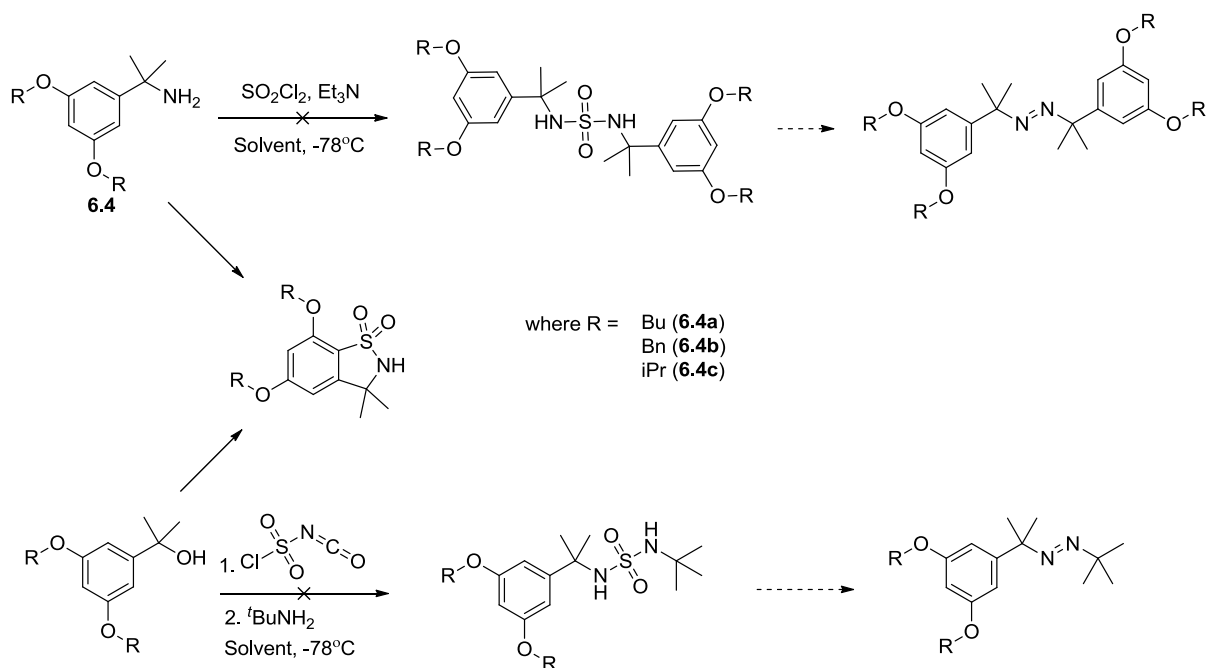


Although these reactions are reported to occur with rate constants on the order of $10^7 \text{ M}^{-1}\text{s}^{-1}$ (for the more sterically-hindered DDBH), it does not seem reasonable to expect that the bimolecular reaction (Eq. 3) between the excited azocumene and tocopherol (mM) could compete with the unimolecular scission of the excited azocumene and unimolecular *cis/trans* isomerization (Scheme 6.5), which reportedly occurs on a timescale $<20 \text{ ns}$ to give cumyl radicals.³⁷ The quantum yield for photocleavage of *trans*-azocumene is reported by Engel to be 0.36,³⁹ incorporating all modes of nitrogen formation (i.e. paths c+e and d+e in Scheme 6.5) and it is known that much of the energy absorbed by *trans*-azocumene is dissipated as a *cis/trans*-

isomerization that follows first-order kinetics with a temperature dependent lifetime on the order of microseconds (5 μ s at 292 K).^{37,40} Based on this evidence we can conclude that H-atom abstraction from the n,π^* -excited state of azocumene is not likely a major contributing pathway towards the instantaneous growth of tocopheroxyl, nor does seem likely that it contributes significantly to the discrepancies in tocopheroxyl concentrations observed in experiments with varying concentrations of α -tocopherol and equal azocumene concentrations (Figure 6.1).

One possible solution to the problem of unaccounted tocopheroxyl formation was to modify our approach of watching tocopheroxyl growth and instead focus on watching a peroxy radical decay. Keeping with our azocumene motif, this would require synthesizing an azo-compound that would decay to give a cumylperoxy radical with a distinct absorbance from the parent molecule. Time-dependent density functional theory (DFT) calculations suggested that a cumylperoxy radical with alkoxy-substitution at the 3- and 5-positions would have a red-shifted absorbance around 450 nm – away from the region where tocopheroxyl absorbs, prompting the preparation of an appropriately-substituted azocumene.

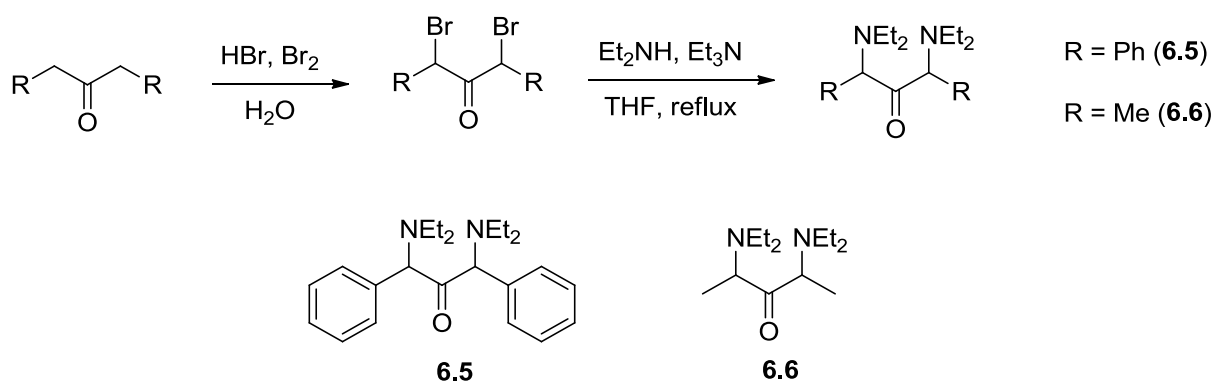
Unfortunately, the synthesis of a 3,5-dialkoxy-substituted compound was not as trivial as that of unsubstituted azocumene. Problems arose when 3,5-dialkoxycumylamines were treated with sulfuryl chloride – the primary isolated products were cyclized sulfonamides after an intramolecular reaction.



Scheme 6.6. Undesired cyclization reaction when preparing symmetrical sulfonamides via sulfonyl chloride or when preparing unsymmetrical sulfonamides using chlorosulfonyl isocyanate and *tert*-butylamine.⁴¹

The intramolecular cyclization was difficult to suppress due to the very poor solubility of the cumylamine derivatives in organic media (THF, DCM, DMF, DMSO and MeCN were all tried) – as increasing the amine concentration would improve the rate of the intermolecular reaction. Alternatively, attempts were made to prepare unsymmetrical sulfonamides by treating the substituted cumyl alcohols (which have much better solubility in organic media) with chlorosulfonyl isocyanate, followed by quenching with *tert*-butylamine (Scheme 6.6).⁴¹ Unfortunately, these reactions did not proceed cleanly and did not afford sulfonamides, with one of the undesired products again appearing to be cyclized sulfonamides formed via intramolecular reaction. Compounds having bulkier alkoxy-side chains (OBn, O*t*Bu, O*t*Pr) were prepared but this did not suppress intramolecular cyclization for either synthetic route.

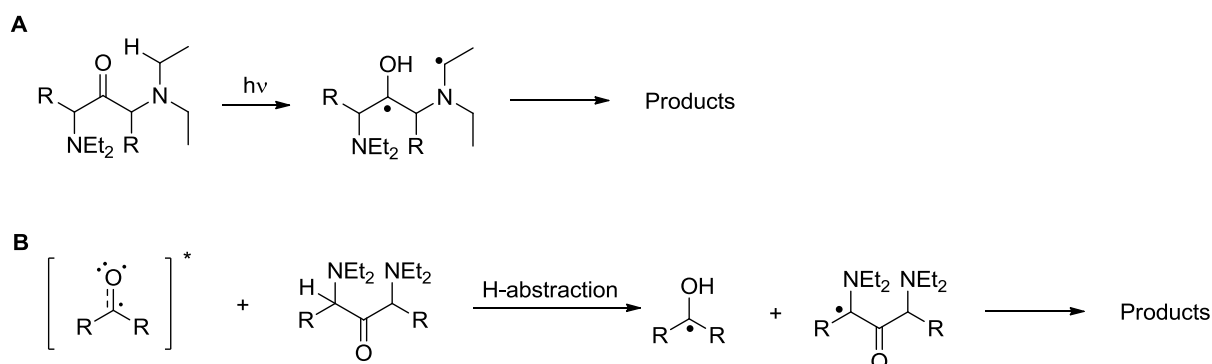
Following the same idea of watching peroxy radical decay, we were inspired by the work of Lalevee, who has developed a triethylamine/di-*tert*-butylperoxide/O₂ system to generate an α -amino-alkylperoxy radical (photolyzed at 308 nm) as in Scheme 6.1B,^{19,20} which has absorbance near 380 nm. Unfortunately this method will not give useful solvent-dependent Arrhenius data due to the very high concentrations of both triethylamine (ca. 1 M) and di-*tert*-butylperoxide (neat) required. We envisioned a system where an α -aminoalkylperoxy radical could be generated without relying on H-atom abstraction by a *tert*-butoxy radical and turned back to Norrish fragmentation as a source of a carbon-centred radical. The β -amino carbonyl compounds shown below were synthesized starting from commercially available ketones.



Scheme 6.7. Synthesis of β -amino carbonyl compounds **6.5** and **6.6**.

When these compounds were subjected to photolysis conditions (either 266 nm Nd:YAG or 308 nm XeCl, 6-14 mJ) in oxygenated chlorobenzene, the resulting traces did not display any transient absorption between 360-420 nm (as predicted by Lalevee).¹⁹ Upon addition of α -tocopherol we did, however, observe instantaneous formation of tocopheroxyl (measured at 420 nm), as was found for azocumene photolysis.

While the appearance of tocopheroxyl is not surprising (tocopherol has a strong absorbance at 266 nm and 308 nm and is known to photoionize readily at these wavelengths),³² the lack of α -aminoalkylperoxyl transient was a bit surprising. There are a few possibilities as to why no transient was observed, the first being that the in-cage recombination of the acyl radical and alkyl radical (or alkyl-alkyl following decarbonylation) was too fast to allow oxygen addition (solutions were under air atmosphere, $[O_2]$ ca. 4 mM) to the alkyl radicals. Another possibility is that there was hydrogen-atom abstraction by excited triplet state of the ketone from an α C-H hydrogen (unlike n,π^* -excited states of azoalkanes, n,π^* -excited ketones react preferentially with *nucleophilic* α C-H hydrogens rather than *electrophilic* O-H or N-H hydrogens) of compounds **6.5** or **6.6** either intramolecularly (Norrish type II, **A**) or intermolecularly (very minor, **B**), as shown below:

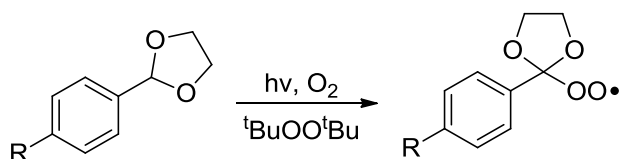


Scheme 6.8. Possible competing reaction pathways from excited ketones **6.5** and **6.6**.

Under the preliminary conditions screened, no transient α -aminoalkylperoxyl radicals were observed. In light of the number of competing reactions available and the limited window with which the α -aminoalkylperoxyl radical can have absorbance to be useful (ca. 370-405 nm or >450 nm), as well as the high-intensity, low-wavelength laser pulses required to

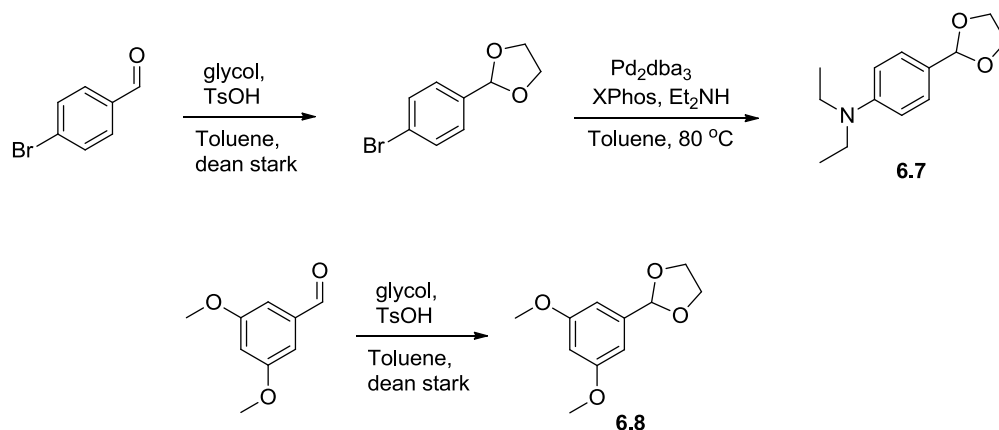
promote Norrish reactions that undoubtedly results in *significant* photoionization of tocopherol, we decided not to pursue this methodology any further.

Instead, we returned back to the idea of *tert*-butoxyl abstracting a hydrogen atom at a position that would give rise to a tertiary peroxy radical having a large enough extinction coefficient to minimize the required concentration of substrate. Again, time-dependent DFT calculations suggested that substituted benzylic acetals could serve as precursors to peroxy radicals having absorbances in the 350-400 nm range and should have readily abstractable hydrogen atoms (scheme 6.9).



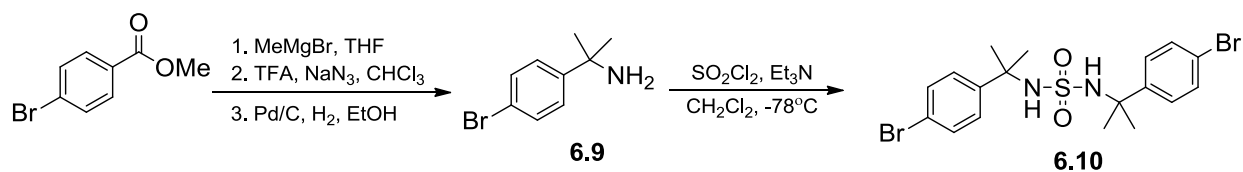
Scheme 6.9. Photolysis of di-*tert*-butylperoxide, followed by H-atom abstraction from a benzylic acetal in the presence of oxygen to produce a peroxy radical having calculated absorbance in the 350-400 nm range.

The acetals shown below were prepared by conventional methods, but unfortunately did not give rise to peroxy radical intermediates having sufficient absorbances to be useful.



Scheme 6.10. Synthesis of acetal compounds 6.7 and 6.8.

After preparing and investigating the utility of ketone and acetal precursors – we inevitably returned back to the azo-compounds, which seemingly are the ultimate precursors for peroxy radicals under the conditions required. To facilitate the synthesis of our target compounds we moved away from 3,5-disubstitution in favour of a single substituent at the *para*-position, which calculations suggested should still have a weak peroxy absorbance that is red-shifted relative to that of tocopheroxy. To minimize undesired cyclization during the sulfonamide forming reaction, it would be preferential that the aromatic ring be as electron-deficient as possible – leading us to a simple arylbromide as our starting material, which could then be functionalized after formation of the sulfonamide. Indeed, starting with methyl 4-bromobenzoate the desired *para*-bromo-substituted sulfonamide was readily obtained.

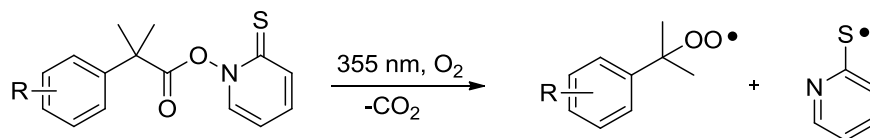


Scheme 6.11. Synthesis of *para*-brominated cumylsulfonamide **6.10**.

Alternatively, the 4-bromocumylamine can be prepared in a single step by methyl cerate addition to 4-bromobenzonitrile at reduced temperatures. With the brominated sulfonamide in hand, two derivatives were desired – a 4-methoxy-sulfonamide and a 4-*N*-methylaniline sulfonamide. However, at this point these compounds were abandoned as it was discovered that the peroxy radicals that would be generated by their decomposition would likely not have sufficient extinction coefficients to be useful (*vide supra*).

As a final strategy for preparing substituted cumylperoxy radicals by flash photolysis we explored PTOC esters as precursors. As exemplified by Barton, these compounds are known to

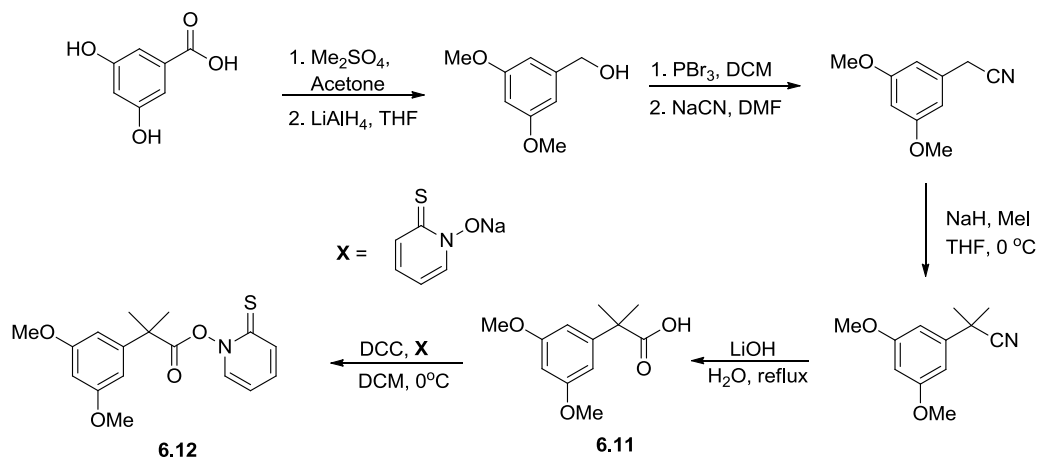
fragment when irradiated at 355 nm via cleavage of the weak O-N bond, yielding an acyloxyl radical (RCO_2^\bullet) and a 2-pyridylthiyl (PyS^\bullet) radical. The acyloxyl radical undergoes a rapid decarboxylation to afford a carbon centred radical that can react with oxygen to make a peroxy radical.



Scheme 6.12. Decomposition of Barton ester to generate a cumylperoxy radical and a 2-thiopyridyl radical.

The primary concern with using a PTOC ester as a source of cumyl radicals is the 2-thiopyridyl radical by-product, which can react with carbon-centred radicals (in cage), peroxy radicals, or the antioxidant and also has a strong, broad absorbance centred near 500 nm. This narrows the window available for monitoring the decay of the peroxy radicals to ca. 430-500 nm, which is within the region calculated for a cumylperoxy having 3,5-dialkoxy-substitution.

The compound was prepared from commercially available 3,5-dihydroxybenzoic acid:



Scheme 6.13. Synthesis of PTOC (Barton) ester **6.12**.

When this compound (5-100 mM in benzene) was subjected to 355 nm laser pulses (ca. 3-4 mJ), the 2-thiopyridyl radical could be detected, but no discernible signal for the peroxy radical (between 380-500 nm) was observed. This suggests that the PTOC ester is decomposing as desired, but that either the peroxy radical formed after decarboxylation is decomposing rapidly or it does not have a significant absorbance to provide a discernible signal. This result, taken with that obtained for substituted acetal derivatives (no discernible peroxy signal) provide quite strong evidence that the extinction coefficient of a derivatized cumylperoxy radical is not large enough to reliably monitor the H-atom transfer kinetics with α -TOH.

6.5 Conclusions and Future Directions

Direct determination of the kinetics of the reaction of ' α '-TOH with peroxy radicals by transient absorption spectroscopy has proven unsuccessful with a number of peroxy radical precursors. Although azocumene appeared to be a very attractive compound for the clean formation of cumylperoxy radicals when photolyzed in the presence of O₂, its possible role in H-atom abstraction from tocopherol (by the n, π^* -excited state of azocumene) complicates the approach – and remains to be resolved. Attempts to synthesize compounds that could lead to peroxy radicals with unique absorbances (outside the range of tocopherol or tocopheroxyl) were unsuccessful. Future work may involve quantification of the photoionization process for tocopherol so that this background reaction may be subtracted from the desired tocopheroxyl trace. Or perhaps it may be easier to return to the system developed by Lalevee²⁰ and accept that it may not be possible to determine solvent effects on Arrhenius parameters, although it seems as

though reproducing Lalevee's experiments has already proven difficult by other members of our laboratory.

6.6 Experimental Section

6.6.1 General

Compounds were prepared according to literature procedures unless otherwise given. Materials and solvents were used as received unless otherwise noted. Column chromatography was carried out using flash silica gel (60 Å, 40-63 μ, 500 m²/g). ¹H and ¹³C NMR spectra were recorded at 25 °C on a Bruker AVANCE spectrometer at 400 MHz and 100 MHz respectively, unless otherwise indicated. High resolution mass spectra were obtained by electron impact ionization on a Kratos Concept Tandem mass spectrometer.

6.6.2 Synthesis

Cumylamine

To a solution of cumyl alcohol (10 mmol) and sodium azide (22 mmol) in 10 mL CHCl₃ cooled to -10 °C was added TFA (55 mmol) dropwise as a solution in 10 mL CHCl₃. The solution was stirred overnight and upon completion was quenched with water. Following extraction with DCM, the organics were washed with brine and dried over MgSO₄. Cumylazide was then dissolved in 50 mL EtOH and ammonium formate (50 mmol) and 10% Pd/C (100 mg) were added. The reaction was stirred at 50 °C overnight. Upon completion, the solution was diluted with ether and filtered through a pad of silica to afford cumylamine as a pale yellow oil. Yield: 80%. Spectral data are consistent with those in the literature.³⁶

***N,N*-bis(1-methyl-1-phenethyl)-sulfamide (6.3)**

To a solution of cumylamine (10 mmol) and dry Et₃N (11 mmol) in dry CH₂Cl₂ (10 mL) cooled to -78 °C was added sulfuryl chloride (5.1 mmol) dropwise. The reaction was maintained at -78 °C until completion, as determined by TLC. The reaction was quenched by addition of water, extracted with CH₂Cl₂ and the organics were washed with brine and dried over MgSO₄. Recrystallization from EtOH afforded white needles. Yield: 90%. Spectral data are consistent with those in the literature.³⁶

Azocumene (6.1)

To a suspension of KH (2.1 mmol) in dry THF cooled to 0 °C was added *N,N*-bis(1-methyl-1-phenethyl)-sulfamide (3, 1.0 mmol) as a solution in THF dropwise. After 2 h, the solution was cooled to -78 °C and tert-butylhypochlorite (1.1 mmol) was added dropwise. The solution was allowed to warm to room temperature and then quenched with water and extracted with Et₂O. Organics were washed with brine and dried over MgSO₄. Purification by column chromatography (Pet Ether/Et₂O) afforded pure azocumene which was then further purified by recrystallization from Hexanes/DCM at -30 °C. Spectral data are consistent with those in the literature.³⁶

General Procedure for the preparation of 2-(3,5-dialkoxyphenyl)propan-2-ols

To a solution of the corresponding methyl 3,5-dialkoxybenzoate (5 mmol) in dry THF (10 mL) cooled to 0 °C was added a solution of MeMgBr (3.0 M, 12 mmol) dropwise. Upon completion the reaction was quenched with water and extracted with Et₂O. The organics were washed with brine, dried over MgSO₄ and passed through a plug of silica. The compounds were carried on without purification or full characterization.

2-(3,5-Butoxyphenyl)propan-2-amine (6.4a)

Prepared as described above for cumylamine starting from 2-(3,5-dibutoxyphenyl)propan-2-ol (see general procedure above; from methyl 3,5-dibutoxybenzoate).⁴² ¹H NMR (CDCl₃, 400 MHz) δ ppm 6.63 (d, *J* = 2.2 Hz, 2H), 6.32 (t, *J* = 2.2 Hz, 1H), 3.95 (t, *J* = 6.5 Hz, 4H), 1.79-1.72 (m, 4H), 1.52-1.48 (m, 4H), 1.46 (s, 6H), 0.97 (t, *J* = 7.4 Hz, 6H). ¹³C NMR (CDCl₃, 100 MHz) δ ppm 160.153, 153.040, 103.752, 98.474, 67.665, 52.575, 32.691, 31.398, 19.271, 13.866.

2-(3,5-Bis(benzyloxy)phenyl)propan-2-amine (6.4b)

(5-(2-azidopropan-2-yl)1,3-phenylene)bis(oxy)bis(methylene)dibenzene was prepared as described above for cumylamine starting from 2-(3,5-bis(benzyloxy)phenyl)propan-2-ol (see general procedure above; from methyl 3,5-dibenzyloxybenzoate)⁴³ and was carried on without any purification. To a solution of (5-(2-azidopropan-2-yl)1,3-phenylene)bis(oxy)bis(methylene)dibenzene (1.0 mmol) in 7 mL dry THF was added LiAlH₄ (1.05 mmol) at room temperature. Upon completion, the reaction was diluted with Et₂O and 1

mL of water was slowly added, followed by 1 mL of 15% NaOH, followed by 3 mL water. After stirring 15 min, a scoop of MgSO₄ was added and stirred another 15 min. The mixture was then filtered and passed through a plug of silica to afford 3,5-dibenzyloxycumylamine as a colorless oil. ¹H NMR (CDCl₃, 400 MHz) δ ppm 7.45-7.31 (m, 10H), 6.77 (d, *J* = 2.2 Hz, 2H), 6.50 (t, *J* = 2.2 Hz, 1H), 5.04 (s, 4H), 1.64 (brs, 2H), 1.46 (s, 6H). ¹³C NMR (CDCl₃, 100 MHz) δ ppm 159.818, 153.097, 136.924, 128.564, 127.970, 127.598, 104.567, 99.349, 70.124, 52.658, 32.656.

1,3-Bis(diethylamino)-1,3-diphenylpropan-2-one (6.5)

To a solution of 1,3-dibromo-1,3-diphenylpropan-2-one (1.0 mmol) in THF (5 mL) was added Et₂NH (2 mmol) and the mixture was heated to 50 °C. Upon consumption of the starting material, the mixture was added to water and extracted with hexanes. Column chromatography with hexanes afforded pure product. Yield: 58 % yellow oil. ¹H NMR (CDCl₃, 400 MHz) δ ppm 7.56-7.50 (m, 4H), 7.41-7.31 (m, 4H), 7.21-7.06 (m, 10 H), 5.69 (d, *J* = 10.8 Hz, 1H), 5.59 (d, *J* = 10.8 Hz, 1H), 4.51 (d, *J* = 10.8 Hz, 1H), 4.42 (d, *J* = 10.8 Hz, 1H), 3.51-2.92 (m, 8H), 1.26 (t, *J* = 7.2 Hz, 3H), 1.12 (t, *J* = 7.2 Hz, 3H), 0.98 (t, *J* = 7.2 Hz, 3H), 0.70 (t, *J* = 7.2 Hz, 3H). ¹³C NMR (CDCl₃, 100 MHz) δ ppm 169.899, 168.908, 141.258, 139.472, 137.970, 136.079, 128.923, 128.847, 128.651, 128.492, 128.430, 128.326, 128.253, 128.172, 128.045, 127.986, 127.941, 127.525, 58.732, 57.712, 56.975, 56.249, 42.168, 42.063, 41.146, 40.557, 14.802, 14.498, 12.903, 12.448. Note: spectral data complicated by mixtures of stereoisomers and tautomers. HRMS (EI) *m/z* calculated 352.2515, found 352.2510.

2,4-Bis(diethylamino)pentan-3-one (6.6)

To a solution of 2,4-dibromopentan-3-one (1 mmol) in THF (5 mL) was added Et₂NH (2 mmol) and the mixture was heated to 50 °C. Upon consumption of the starting material, the mixture was added to water and extracted with hexanes. Column chromatography with hexanes afforded pure product. Yield: 35 % pale yellow oil. ¹H NMR (CDCl₃, 400 MHz) δ ppm 4.07 (q, *J* = 6.7 Hz, 2H), 2.51-2.44 (m, 4H), 2.41-2.34 (m, 4H), 1.04-0.97 (m, 18H). ¹³C NMR (CDCl₃, 100 MHz) δ ppm 212.730, 60.502, 58.319, 44.259, 44.210, 14.310, 13.988, 10.538, 7.549. Note: spectral data may be complicated due to stereoisomers and tautomers. HRMS (EI) *m/z* calculated 228.2202, found 228.2200.

4-(1,3-Dioxolan-2-yl)-*N,N*-diethylbenzeneamine (6.7)

¹H NMR (CDCl₃, 400 MHz) δ ppm 7.30 (d, *J* = 8.8 Hz, 2H), 6.65 (d, *J* = 8.8 Hz, 2H), 5.72 (s, 1H), 4.15-4.11 (m, 2H), 4.01-3.98 (m, 2H), 3.35 (q, *J* = 7.0 Hz, 4H), 1.15 (t, *J* = 7.0 Hz, 6H). ¹³C NMR (CDCl₃, 100 MHz) δ ppm 127.643, 123.988, 120.207, 111.354, 104.352, 65.136, 44.404, 12.509.

2-(3,5-Dimethoxyphenyl)-1,3-dioxolane (6.8)

¹H NMR (CDCl₃, 400 MHz) δ ppm 6.64 (d, *J* = 2.3 Hz, 2H), 6.45 (t, *J* = 2.3 Hz, 1H), 5.77 (s, 1H), 4.14-4.01 (m, 4H), 3.80 (s, 6H). Spectral data are consistent with those in the literature.⁴⁴

5-Bromo- α,α -dimethylbenzenemethanamine (6.9)

Prepared according to literature procedure.⁴⁵ ^1H NMR (CDCl_3 , 400 MHz) δ ppm 7.43 (tt, $J = 8.8, 2.2$ Hz, 2H), 7.39 (tt, $J = 8.8, 2.2$ Hz, 2H), 1.68 (brs, 2H), 1.47 (s, 6H). ^{13}C NMR (CDCl_3 , 100 MHz) δ ppm 149.188, 131.154, 126.706, 120.048, 52.301, 32.784.

***N,N*-Bis(1-methyl-1-(4-bromophenethyl)-sulfamide (6.10)**

To a solution of 9 (2.0 mmol) and Et_3N (2.0 mmol) in 1 mL DCM cooled to -78 °C was added sulfuryl chloride dropwise as solution in 1 mL DCM. Reaction allowed to warm to r.t. and when complete, quenched with water and extracted with DCM. Organics were washed with brine and dried over MgSO_4 . Purified by passing through silica plug with 10% EtOAc/Hex followed by recrystallization from EtOH. Yield: 77 % white needles. ^1H NMR (CDCl_3 , 400 MHz) δ ppm 7.47-7.43 (m, 4H), 7.28-7.24 (m, 4H), 4.24 (brs, 2H), 1.66 (s, 12H). ^{13}C NMR (CDCl_3 , 100 MHz) δ ppm 144.960, 131.460, 127.305, 121.299, 58.264, 29.396. HRMS (EI) m/z calculated 487.9769, found 487.9757.

2-(3,5-Dimethoxyphenyl)-2-methylpropanoic acid (6.11)

To a suspension of 2-(3,5-dimethoxyphenyl)-2-methylpropanenitrile⁴⁶ (1.0 mmol) in water (10 mL) was added LiOH (5 mmol) and the solution heated to reflux overnight. After cooling, the solution was washed with Et_2O , acidified with HCl and extracted with Et_2O . Organics were washed with water and brine before drying over MgSO_4 . No further purification was required. Yield: 75% white solid. ^1H NMR (CDCl_3 , 400 MHz) δ ppm 6.54 (d, $J = 2.2$ Hz, 2H), 6.37 (t, $J =$

2.2 Hz, 1H), 3.79 (s, 6H), 1.57 (s, 6H). ^{13}C NMR (CDCl_3 , 100 MHz) δ ppm 181.605, 160.713, 146.196, 104.461, 98.364, 55.304, 46.322, 26.147. HRMS (EI) m/z calculated 224.1049, found 224.1048.

2-Thioxopyridin-1(2H)-yl 2-(3,5-dimethoxyphenyl)-2-methylpropanoate (6.12)

To a solution of DCC (1.1 mmol) and 3,5-dimethoxy- α,α -dimethylbenzeneacetic acid (1.0 mmol) in DCM (5 mL) cooled to 0 °C was added sodium pyridinethione (1.2 mmol) as a solution in 2 mL DCM dropwise. Once the reaction was complete, water was added and product extracted with DCM. Organics washed with brine, dried over MgSO_4 and purified by very rapid column chromatography using ether as eluent. Yield: 54 % yellow oil. ^1H NMR (CDCl_3 , 400 MHz) δ ppm 7.65 (ddd, $J = 8.8, 1.8, 0.5$ Hz, 1H), 7.49-7.46 (m, 2H), 7.41-7.36 (m, 2H), 7.30-7.23 (m, 2H), 7.13 (ddd, $J = 8.8, 6.8, 1.6$ Hz, 1H), 6.53 (dt, $J = 6.8, 1.8$ Hz, 1H), 1.84 (s, 6H). HRMS (EI) m/z calculated 333.1035, found 333.1028. Note: A reasonable ^{13}C NMR spectrum could not be obtained, presumably due to the rapid decomposition of the material in solution.

General Transient Absorption Spectroscopy Conditions

For all laser flash photolysis experiments, photolyzable substrate concentration (azocumene, cumylketone, etc.) was adjusted to provide sample absorbance between 0.3-0.6 absorbance units at the laser wavelength suitable for substrate photolysis (i.e. 266 nm, 308 nm or 355 nm). For 266 nm and 355 nm photolysis experiments a Nd:YAG laser was used (frequency doubled accordingly) and 308 nm experiments were conducted with a XeCl excimer laser. Laser power was adjusted between 5-10 mJ to ensure a reasonable amount of transient would be produced.

Concentrations of α -tocopherol were varied between 10-500 mM, keeping sure to remain under pseudo first order kinetic conditions.

6.7 References

- (1) de Dure, C.; Hayashi, O. *Tocopherol, Oxygen and Biomembranes*; Elsevier North Holland: Amsterdam, **1978**.
- (2) Tappel, A. L. *Free Radicals and Biology*; Academic Press: New York, **1980**; Vol. 4.
- (3) Burton, G. W.; Ingold, K. U. *Journal of the American Chemical Society* **1981**, *103*, 6472.
- (4) Burton, G. W.; Ingold, K. U. *Accounts of Chemical Research* **1986**, *19*, 194.
- (5) Burton, G. W.; Joyce, A.; Ingold, K. U. *Lancet* **1982**, *2*, 327.
- (6) Ingold, K. U.; Webb, A. C.; Witter, D.; Burton, G. W.; Metcalfe, T. A.; Muller, D. P. R. *Archives of Biochemistry and Biophysics* **1987**, *259*, 224.
- (7) Barclay, L. R. C.; Locke, S. J.; Macneil, J. M.; Vankessel, J.; Burton, G. W.; Ingold, K. U. *Journal of the American Chemical Society* **1984**, *106*, 2479.
- (8) Doba, T.; Burton, G. W.; Ingold, K. U. *Biochimica Et Biophysica Acta* **1985**, *835*, 298.
- (9) Yamamoto, Y.; Niki, E.; Kamiya, Y.; Shimasaki, H. *Biochimica Et Biophysica Acta* **1984**, *795*, 332.
- (10) Valgimigli, L.; Banks, J. T.; Luszyk, J.; Ingold, K. U. *Journal of Organic Chemistry* **1999**, *64*, 3381.

- (11) Valgimigli, L.; Ingold, K. U.; Lusztyk, J. *Journal of the American Chemical Society* **1996**, *118*, 3545.
- (12) Packer, J. E.; Slater, T. F.; Willson, R. L. *Nature* 1979, *278*, 737.
- (13) DiLabio, G. A.; Johnson, E. R. *Journal of the American Chemical Society* **2007**, *129*, 6199.
- (14) Valgimigli, L.; Amorati, R.; Petrucci, S.; Pedulli, G. F.; Hu, D.; Hanthorn, J. J.; Pratt, D. A. *Angewandte Chemie-International Edition* **2009**, *48*, 8348.
- (15) Litwinienko, G.; Ingold, K. U. *Accounts of Chemical Research* **2007**, *40*, 222.
- (16) Evans, C.; Scaiano, J. C.; Ingold, K. U. *Journal of the American Chemical Society* **1992**, *114*, 4589.
- (17) Foti, M. C.; Daquino, C.; Mackie, I. D.; DiLabio, G. A.; Ingold, K. U. *Journal of Organic Chemistry* **2008**, *73*, 9270.
- (18) Burton, G. W.; Doba, T.; Gabe, E. J.; Hughes, L.; Lee, F. L.; Prasad, L.; Ingold, K. U. *Journal of the American Chemical Society* **1985**, *107*, 7053.
- (19) Lalevee, J.; Allonas, X.; Fouassier, J. P.; Ingold, K. U. *Journal of Organic Chemistry* **2008**, *73*, 6489.
- (20) Lalevee, J.; Allonas, X.; Fouassier, J. P. *Chemical Physics Letters* **2007**, *445*, 62.
- (21) Franchi, P.; Lucarini, M.; Pedulli, G. F.; Valgimigli, L.; Lunelli, B. *Journal of the American Chemical Society* **1999**, *121*, 507.
- (22) Griller, D.; Ingold, K. U. *Accounts of Chemical Research* **1980**, *13*, 317.
- (23) Burton, A.; Ingold, K. U.; Walton, J. C. *Journal of Organic Chemistry* **1996**, *61*, 3778.

- (24) Weber, M.; Fischer, H. *Journal of the American Chemical Society* **1999**, *121*, 7381.
- (25) Studer, A.; Bossart, M. *Tetrahedron* **2001**, *57*, 9649.
- (26) Foti, M.; Ingold, K. U.; Luszyk, J. *Journal of the American Chemical Society* **1994**, *116*, 9440.
- (27) Benson, S. W. *Thermochemical Kinetics 2nd Edition*; John Wiley & Sons: New York, **1976**.
- (28) Howard, J. A.; Furimsky, E. *Canadian Journal of Chemistry* **1973**, *51*, 3738.
- (29) Mahoney, L. R.; Weiner, S. A. *Journal of the American Chemical Society* **1972**, *94*, 585.
- (30) Beckwith, A. L. J.; Bowry, V. W.; Ingold, K. U. *Journal of the American Chemical Society* **1992**, *114*, 4983.
- (31) Norrish, R. G. W.; Bamford, C. H. *Nature* **1937**, *140*, 195.
- (32) Zhang, Y.; Yousef, Y. A.; Li, H.; Melo, T. B.; Naqvi, K. R. *Journal of Physical Chemistry A* **2011**, *115*, 8242.
- (33) Bisby, R. H.; Parker, A. W. *Febs Letters* **1991**, *290*, 205.
- (34) Naqvi, K. R.; Li, H.; Melo, T. B.; Webster, R. D. *Journal of Physical Chemistry A* **2010**, *114*, 10795.
- (35) Nelsen, S. F.; Bartlett, P. D. *Journal of the American Chemical Society* **1966**, *88*, 137.
- (36) Ikeda, H.; Hoshi, Y.; Namai, H.; Tanaka, F.; Goodman, J. L.; Mizuno, K. *Chemistry-a European Journal* **2007**, *13*, 9207.
- (37) Boate, D. R.; Scaiano, J. C. *Tetrahedron Letters* **1989**, *30*, 4633.

- (38) Pischel, U.; Nau, W. M. *Photochemical & Photobiological Sciences* **2002**, *1*, 141.
- (39) Engel, P. S.; Steel, C. *Accounts of Chemical Research* **1973**, *6*, 275.
- (40) Engel, P. S.; Bishop, D. J. *Journal of the American Chemical Society* **1975**, *97*, 6754.
- (41) Engel, P. S.; Wang, C. G.; Chen, Y. Q.; Ruchardt, C.; Beckhaus, H. D. *Journal of the American Chemical Society* **1993**, *115*, 65.
- (42) Constable, E. C.; Graber, S.; Hermann, B. A.; Housecroft, C. E.; Malarek, M. S.; Scherer, L. J. *European Journal of Organic Chemistry* **2008**, 2644.
- (43) Srinivasan, M. V.; Kannan, P. *Journal of Materials Science* **2011**, *46*, 5029.
- (44) Bhosale, R. S.; Bhosale, S. V.; Solanke, K. S.; Pawar, R. P.; Chougule, H. S.; Dongare, M. K. *Synthetic Communications* **2006**, *36*, 659.
- (45) Huang, S. L.; Li, R.; Connolly, P. J.; Emanuel, S.; Fuentes-Pesquera, A.; Adams, M.; Gruninger, R. H.; Seraj, J.; Middleton, S. A.; Davis, J. M.; Moffat, D. F. C. *Bioorganic & Medicinal Chemistry Letters* **2007**, *17*, 2179.
- (46) Caron, S.; Vazquez, E.; Wojcik, J. M. *Journal of the American Chemical Society* **2000**, *122*, 712.

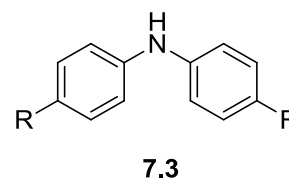
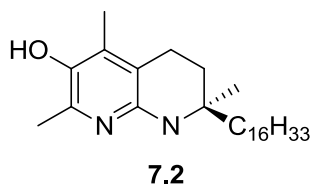
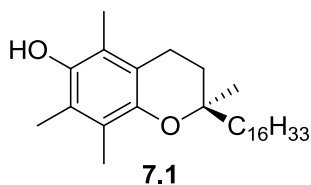
CHAPTER 7: SUMMARY AND PROSPECTIVE

7.1 Summary

Diarylamines (Ar_2NH) and phenols (ArOH) comprise the bulk of radical-trapping antioxidant (RTA) additives to petroleum-derived products owing to their ability to slow hydrocarbon autoxidation through the rate-controlling inhibition reactions:^{1,2}



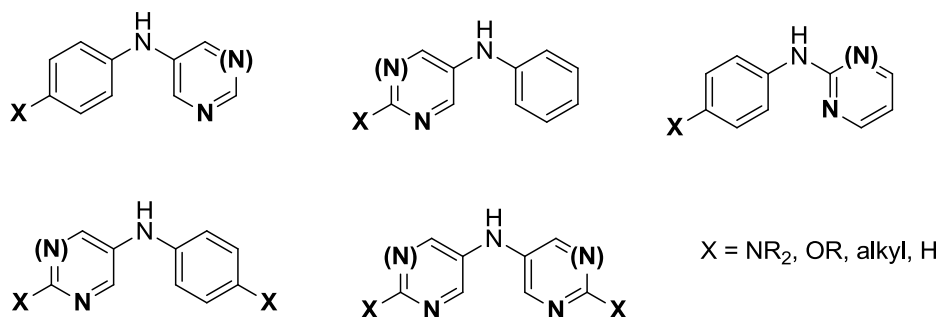
Of the two parent structures, diphenylamine has a weaker N-H bond (84.7 kcal/mol)³ compared to the O-H bond in phenol (87.2 kcal/mol),⁴ which is believed to be responsible for its faster radical-trapping kinetics ($k_{\text{H1}}^5 = 2.0 \times 10^4 \text{ M}^{-1}\text{s}^{-1}$ versus $k_{\text{H2}}^6 = 2.9 \times 10^3 \text{ M}^{-1}\text{s}^{-1}$ in styrene at 65 °C). Regardless, phenols are commonly viewed as the quintessential antioxidants since their reactivities are more easily manipulated. Nature has optimized the substitution of phenol in its evolution of α -tocopherol (α -TOH, **7.1**), the key lipophilic antioxidant *in vivo*, which has an O-H BDE of 77.3 kcal/mol⁷ and $k_{\text{H}} = 3.2 \times 10^6 \text{ M}^{-1}\text{s}^{-1}$.⁸ Furthermore, based on known structure-activity relationships, related synthetic compounds with reactivities up to 90-fold higher than **7.1** have been developed (e.g. **7.2**).⁹⁻¹¹ In contrast, optimization of diarylamines has been difficult.¹² The industry standards are 4,4'-dialkyldiphenylamines (**7.3**), which have N-H BDEs of $\sim 82 \text{ kcal/mol}^3$ and $k_{\text{H}} = 1.8 \times 10^5 \text{ M}^{-1}\text{s}^{-1}$ in PhCl at 37°C.



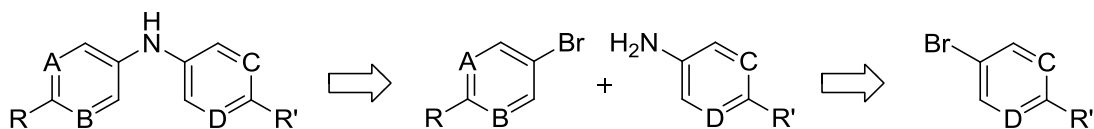
Not long ago, it was shown that when diphenylamine is substituted with increasingly electron-donating groups at the 4- and 4'- positions, the N-H BDE is predictably weakened (e.g. by 4.0 and 6.3 kcal/mol for alkoxy and *N,N*-dialkylamino groups, respectively).³ This suggested that diarylamines with improved RTA activity compared to **7.3** should be accessible. However, 4,4'-(*N,N*-dimethylamino)-diphenylamine and analogous compounds were unstable under typical autoxidation conditions (hydrocarbon, O₂, initiator/light), precluding a determination of their inhibition kinetics (k_H), and implying they would be useless as antioxidants.

Since then, we have found that the incorporation of N-atoms into the aromatic ring of phenols allows them to be substituted with highly electron-donating groups (e.g. **7.2**), substantially weakening their O-H bonds and dramatically accelerating their rates of reactions with radicals, but not at the expense of their stability to oxidation by air or hydroperoxides. Given these results, it was our supposition that this approach could be extended to the development of highly reactive diarylamine RTAs.

In order to properly investigate the structure-reactivity relationships for heterocycle-containing diarylamine antioxidants, we needed a method to prepare a small library of compounds. This library required compounds incorporating N-atoms at a variety of positions within the aryl rings, and each 'scaffold' of N-atom incorporation had to be substituted with a variety of electron-donating groups at the *para*-positions (either symmetrically or unsymmetrically). The desired substitution patterns are shown below.



To accomplish the synthesis of this library, we devised a modular approach that utilized Buchwald-Hartwig type, palladium-catalyzed amination chemistry. The approach was modular in that the aryl bromides used in the construction of the diarylamines also served as precursors to the arylamines as shown in Scheme 7.1.



Scheme 7.1. Synthetic approach to substituted diarylamines (A-D = CH or N; R = H, Alkyl, Alkoxy or *N,N*-dialkylamino).

Additionally, routes were devised to the substituted aryl bromides that could all originate from either 2-aminopyridine or 2-aminopyrimidine – both relatively inexpensive reagents, even on an industrial scale.¹³ To prepare the arylamines used in the construction of the diarylamines, a copper-catalyzed amination reaction protocol was developed where the electronics of the aryl bromide dictated the conditions used. The electron-rich aryl bromides required a two-step sequence involving benzylamine intermediates,¹³ while the electron-poor aryl bromides could be reacted directly with aqueous NH₃.¹⁴

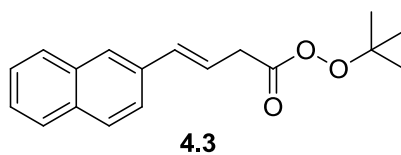
With routes to the aryl bromides and arylamines in hand, Pd-catalyzed C-N couplings were used to prepare the diarylamines. A ligand screen revealed XPhos (2-dicyclohexylphosphino-2',4',6'-triisopropylbiphenyl)¹⁵ as the most general phosphine ligand, showing the least amount of sensitivity to the electronics of the aryl bromides and having the benefit of excellent air-stability for easier handling. Through the course of this work it was discovered that although the Pd₂dba₃/XPhos catalytic system was effective, substituting the little used Pd(η^3 -1-PhC₃H₄)(η^5 -C₅H₅)¹⁶ pre-catalyst for Pd₂dba₃ generally afforded higher reaction yields and shorter reaction times. This observation was further demonstrated through a set of reactions comparing Pd₂dba₃ and Pd(η^3 -1-PhC₃H₄)(η^5 -C₅H₅), where product yield was monitored over time by GC. We surmise that the greater reactivity of Pd(η^3 -1-PhC₃H₄)(η^5 -C₅H₅) is due the fact that it readily undergoes a rapid *irreversible* formation of Pd(XPhos)₂¹⁷ – the catalytically active palladium species – while formation of Pd(XPhos)₂ from Pd₂dba₃ remains in *equilibrium* with inactive coordination complexes. This equilibrium is especially relevant when the substrates contain strongly Lewis-basic heterocycles and likely explains the enhanced reactivity observed with Pd(η^3 -1-PhC₃H₄)(η^5 -C₅H₅).

To confirm that the incorporation of N-atoms would have the desired effect on improving stability to one-electron oxidation, voltammetry was used to quantitatively measure the primary oxidation potentials of the diarylamines. For compounds whose redox properties were reversible or quasi-reversible, cyclic voltammetry was used to determine standard potentials (E°). For those compounds showing non-reversible redox chemistry, differential pulse voltammetry was used to determine anodic peak potentials (E_{pa}). The effect of incorporating N-atoms into the aryl rings was exactly as desired – the one-electron oxidation potentials increased dramatically (~ 5-7 kcal/mol per nitrogen atom, depending on the substituents) with heteroatom incorporation, while

the compounds maintained their facile H-atom transfer chemistry to peroxy radicals (*vide supra*).

With a small library of heterocycle-based diarylamines in hand we could begin to measure their peroxy radical trapping kinetics (k_H). The peroxy radical clock approach is based on the kinetic competition between a unimolecular β -fragmentation of a non-conjugated peroxy radical (occurring with a known rate constant, k_β) and its trapping in a bimolecular reaction with an antioxidant having an unknown rate constant (k_H). With the advent of peroxyester-based peroxy radical clocks, this methodology can now be applied to accurately measure inhibition rate constants and their kinetic solvent effects for a number of phenolic antioxidants.¹⁸

When this methodology was first applied to measuring inhibition rate constants for our diarylamine compounds, the results were inconsistent and the products of the kinetic assay were difficult to resolve from the antioxidant derived products. To improve the analytical component of the peroxy radical clock methodology, a second-generation peroxyester-based clock was synthesized having a naphthalene core, shown below.¹⁹



The higher molecular weight greatly improved chromatographic resolution and *revealed previously unidentified products* in the region of the conjugated and non-conjugated product alcohols. These products were determined to be carbonyl-containing products that originated from the base-promoted dehydration of the product hydroperoxides²⁰ (prior to PPh_3 reduction) in the presence of basic antioxidants. This was confirmed by preparing authentic hydroperoxides

and incubating them with a number of compounds varying in basicity (including Et₃N) and observing a correlation with the amount of carbonyl-containing products formed. The discovery of these products led to the expanded applicability of peroxy clock methodology; enabling the determination of inhibition rate constants for a number of highly reactive pyridinols, pyrimidinols and diarylamines.

In addition to expanding the scope of antioxidants that inhibition rate constants could be obtained for (and the number of solvents in which inhibition rate constants could be obtained), the utility of the peroxy radical clock methodology was expanded by demonstrating that deuterium kinetic isotope effects (DKIEs) could easily be measured to provide important mechanistic information about H-atom transfer reactions. Additionally, the temperature dependence on the rate of β -fragmentation (k_{β}) was determined ($\log A = 12.8 \pm 0.6$ and $E_a = 9.6 \pm 0.9$ kcal/mol), allowing for Arrhenius parameters of H-atom transfer reactions with peroxy radicals to easily be measured.

Unfortunately, the Arrhenius parameters obtained for the rate of secondary-peroxy β -fragmentation only represent (very good) approximate values. Determination of k_{β} and α at higher temperatures required k_H for α -tocopherol (α -TOH) at these temperatures, as α -TOH was the compound used to ‘calibrate’ the clock. To the best of our knowledge, Arrhenius parameters for the reaction of α -TOH with peroxy radicals are not available, but given the typical $\log A \approx 8$ for H-atom transfer reactions as suggested by Benson,²¹ and the inhibition rate constant for α -TOH in chlorobenzene of $7.1 \times 10^6 \text{ M}^{-1} \text{ s}^{-1}$ at 25°C,^{19,22} we calculated $E_a = 1.6$ kcal/mol and were able to estimate the k_H at the required temperatures (37, 45, 50, 60, 70, 80 and 95°C).

Attempts were made to more accurately determine Arrhenius parameters for the reaction between α -TOH and peroxy radicals – data that would provide more accurate Arrhenius parameters for peroxy β -fragmentation and thus Arrhenius parameters for any antioxidants trapping peroxy radicals determined via the peroxy clock methodology. To obtain accurate temperature dependence on the rate constant for peroxy trapping by α -TOH, a direct measurement technique is required, such as laser flash photolysis. Several compounds were tested as peroxy radical precursors, which in the presence of α -TOH would allow detection of the growth of the α -tocopheroxyl radical, including dicumylketone²² and azocumene.^{23,24} To our dismay, it was determined that photoionization of tocopherol²⁵ by the 355 nm laser pulse was skewing the first order growth curve of α -tocopheroxyl, preventing the determination of accurate rate constants. In an effort to render the photoionization of α -TOH irrelevant, we attempted to prepare compounds that would give rise to peroxy radicals having unique absorption maxima. This would allow the reaction kinetics to be followed by watching the decay of the peroxy intermediates, rather than the growth of α -tocopheroxyl. Unfortunately, none of the compounds prepared (various cumyl derivatives substituted with 3,5-OR, 4-OR or 4-NR₂ groups, predicted computationally to have useful absorbance maxima) yielded a peroxy radical species with a large enough extinction coefficient to be useful for reproducibly measuring rate constants. For the time being, the Arrhenius parameters for β -fragmentation ($\log A = 12.8 \pm 0.6$ and $E_a = 9.6 \pm 0.9$ kcal/mol) remain the best estimate available until a more accurate pre-exponential factor is measured than the estimate put forward by Benson of $10^8 \text{ M}^{-1}\text{s}^{-1}$.

Using the peroxy clock method, inhibition rate constants were obtained for nearly all of the diarylamines prepared (a few had very poor solubility in the solvents useful for measuring inhibition rate constants). To our delight, the rate constants for compounds incorporating

heteroatoms (1-4 in total) into the 3 and/or 5 positions of the aryl rings had inhibition rate constants only 2-6 fold slower than the parent diphenylamine, depending on the *para*-substituents. In fact, the *N,N*-dialkylamino substituted compounds were excellent peroxy radical trapping antioxidants, having rate constants ca. 200-fold higher than that of the industry standard (4,4'-dialkyldiphenylamine) and 2-5 fold higher than α -TOH.

To provide a thermodynamic rationale for the observed kinetics, the radical equilibrium electron paramagnetic resonance (EPR) technique was used to determine N-H BDEs for a number of compounds. These measurements were made by Prof. Luca Valgimigli at the University of Bologna. The N-H BDEs of the *N,N*-dialkylamino substituted compounds (symmetrically substituted) were all within experimental error of each other – increasing from 78.4 ± 0.6 kcal/mol to 79.2 ± 0.5 kcal/mol upon going from 0 to 4 N-atoms in the aryl rings. While these results parallel the observed kinetics, the differences in measured N-H BDEs are much smaller than the differences in the E° values. This is consistent with the expectation that incorporation of N-atoms into the aryl rings has a larger destabilizing effect on the diarylamine radical cation formed via one-electron oxidation than it does on the corresponding diarylaminy radical formed via an H-atom transfer reaction. Furthermore, the changes in N-H BDE (and k_H) upon incorporation of N-atoms into the aryl rings are much smaller than those observed in phenolic antioxidants (ca. 1.2-1.5 kcal/mol per N-atom).^{9,10} This likely reflects the fact that the diphenylaminy radical is inherently less electron-poor than the phenoxy radical and therefore is less destabilized by introduction of electronegative N-atoms into the aryl rings.

The forgoing results yielded the unexpected insight that reactions of diarylamines with peroxy radicals are faster than reactions of phenols with peroxy radicals that proceed with comparable thermodynamics. This is best observed in a plot of $\log k_H$ vs. N-H BDE for a series

of diarylamines and $\log k_H$ vs. O-H BDE for a series of *ortho*-substituted phenols (Figure 3.6), where the magnitude of the slope is 1.5-fold greater for the diarylamine correlation. This result seemed to imply that the entropic demand of the reaction of phenols with peroxy radicals is greater than for the reaction of diarylamines with peroxy radicals. However, when Arrhenius parameters were measured for a representative set of diarylamines, it was found that the reactions with peroxy radicals are best described by $\log A = 7.0 \pm 0.1$ (determined using the peroxy clock method, which is calibrated for α -TOH as having $\log A = 8.0$);¹⁹ meaning that the entropic demand is in fact smaller for phenols and the reactivity difference must originate in activation energy (E_a). Indeed, we found that the rate constants for reactions of the most electron-rich diarylamines (*N,N*-dialkylamino-substituted) with peroxy radicals were invariant with temperature – implying a ‘barrier-less’ reaction ($E_a \approx 0$). To rule out that these ‘barrier-less’ reactions did not simply reflect an electron-transfer mechanism, deuterium kinetic isotope effects (DKIEs) and kinetic solvent effects (KSEs) were measured for representative *N,N*-dialkylamino-substituted compounds. Using the peroxy clock methodology a DKIE of $k_H/k_D = 1.4$ was observed – consistent with a primary DKIE and typical for hydrogen atom transfer as rate-determining. When rate constants were measured between *N,N*-dialkylamino-substituted compounds and peroxy radicals in solvents varying in their hydrogen bond accepting (HBA, given by β_2^H)²⁶ abilities (and thus dielectric constants), negative kinetic solvent effects were observed – consistent with a hydrogen atom transfer mechanism²⁷ and again inconsistent with simple electron-transfer.

We surmise that the difference in activation energy between the most reactive phenols and diarylamines can be explained by considering the transition state structures for the formal H-atom transfer reactions with peroxy radicals. As for the reaction of phenols with peroxy radicals, the

calculated transition state structure for the reaction of a diarylamine with a peroxy radical is best described as a proton-coupled electron transfer (PCET) reaction,^{28,29} where a proton is transferred from the amine to the peroxy radical while an electron is transferred from the π -HOMO of the amine to the π -SOMO of the peroxy radical. Therefore, comparing a diarylamine with a given N-H bond strength with a phenol of a similar O-H bond strength, it follows that the amine will have a lower activation energy for reaction with a peroxy radical than the phenol based on the fact that the π -MOs of the diarylamine are higher in energy than those of the phenol.³⁰ This allows for better orbital overlap with the π -SOMO of the peroxy radical and better facilitates electron-transfer.

Rate constants for the abstraction of hydrogen atoms from diarylamines by primary alkyl radicals were also determined by using the 1,2-aryl migration of the 2-methyl-2-(2-naphthyl)-1-propyl (MNP) radical as a clock.³¹ In contrast to peroxy-radical trapping, the abstraction of a hydrogen atom from a diarylamine or phenol by an alkyl radical must occur by a formal hydrogen atom transfer (HAT) mechanism. The rate of H-atom transfer in a HAT reaction is dependent solely on X-H BDEs for compounds having comparable steric crowding around the reaction centre. It was found that the correlation between $\log k_H$ and X-H BDE was larger for diarylamines than for *ortho*-substituted phenols – attributed to the fact that no polar effects can contribute to the HAT transition state for diarylamines as observed with more acidic phenols⁹ due to their larger pK_a values. Thus, the correlation between $\log k_H$ vs. N-H BDE for diarylamines reflects the ‘true’ correlation between the rate of HAT and X-H BDE, and in fact the correlation is identical to that observed for phenoxazines and phenothiazines reacting with primary alkyl radicals.¹² When the N-H BDEs for diarylamines and phenoxazines/phenothiazines were plotted vs. $\log k_H$ for reactions with both alkyl and peroxy radicals (Figure 3.9), two

excellent linear correlations were obtained that parallel each other but differ in the vertical dimension by two orders of magnitude. Therefore, while the thermodynamics favour the reactions with alkyl radicals, the reactions with peroxy radicals proceed with rate constants two orders of magnitude greater – providing strong evidence for a PCET reaction mechanism for the reaction of diarylamines with peroxy radicals.

The diarylamines described in this thesis are extremely efficacious radical trapping antioxidants at ambient temperatures – comparable to or better than the best phenolic antioxidants – but the real utility of diarylamine antioxidants lies in their high temperature applications (>120 °C), such as those commonly attained by the lubricants of operating combustion engines. At these temperatures, diarylamines are known to react with peroxy radicals catalytically, with stoichiometric factors reported as high as $n = 40$ by Korceck *et al.*^{32,33} It is believed that the catalytic activity of diarylamines originates from the *in situ* formation of nitroxide radicals from the diarylamines, via a mechanism that remains unresolved.^{32,34} The diarylamines described in this thesis should provide access to stable but electronically distinct compounds (diarylamines or prepared nitroxide intermediates) to aid in distinguishing which mechanism is responsible for the highly relevant catalytic activity of diarylamine antioxidants.

Typically, high temperature assays to measure inhibition rate constants and stoichiometric factors for high temperature diarylamine peroxy radical trapping are done by inhibited autoxidation of hexadecane at 120-180 °C.³² It has been determined that within the first 1-2 hours of the experiment, measuring the total hydroperoxide concentration is an effective way to determine the rate of oxidation (after ca. 2 hours, the hydroperoxides begin to decompose to acids, alcohols, etc.). The most common analytical techniques used to measure total hydroperoxide content of these complex mixtures are gas chromatography and/or iodometry.³⁵

While these techniques have proven effective, we sought to improve the analytical aspect of the high temperature assays by eliminating the need for lengthy and complicated GC analyses or time-consuming and air-sensitive iodometric titrations by designing a fluorescence-based assay.

The assay relies on a dye (**5.8**) comprised of a fluorescent coumarin core, coupled to a triarylphosphine moiety. In its reduced (phosphine) form, the dye is in its ‘OFF’-state; that is, photoinduced electron transfer from the phosphine moiety quenches the excited state of the coumarin, thereby suppressing its fluorescence.³⁶ When the phosphine reacts with a hydroperoxide – forming a phosphine oxide and the corresponding alcohol – the dye reverts to its ‘ON’-state; that is, the phosphine moiety can no longer transfer an electron to quench the excited coumarin moiety and fluorescence is restored.

The concept of using fluorescent dyes as reporter molecules for *qualitative* detection of reactive oxygen species (ROS) is not new,³⁷⁻³⁹ but their application as a tool for *quantitative* determination of hydroperoxide concentrations in organic media has not been well explored. We prepared a series of coumarin-based dyes and reached an optimized compound that met all of our important criteria: it has excellent solubility in organic media (important for combining with hexadecane autoxidations); it has a negligible rate of background oxidation with molecular oxygen; and it has been optimized to achieve the maximum difference in quantum yields between the oxidized and reduced ($\Phi_{\text{ox}}/\Phi_{\text{red}}$) forms of the dye so as to maximize the signal enhancement upon reaction with a hydroperoxide.

The utility of our fluorescent dye has been successfully demonstrated as the analytical component of inhibited autoxidations (carried out by fellow Pratt group graduate student Evan Haidasz), both at a physiologically relevant temperature on a physiologically-relevant substrate

(37°C, 7-dehydrocholesterol)⁴⁰ and at an industrially relevant temperature on an industrially-relevant substrate (160°C, hexadecane). The assay has been developed with the use of a microplate reader equipped with a reagent dispenser, which enables the *automation* of *quantitative* kinetic measurements on hydrocarbon autoxidations, and their inhibition by radical-trapping antioxidants, at temperatures below 65°C.

7.2 Prospective

The body of work in this thesis has addressed a number of fundamental questions regarding the radical-trapping antioxidant activity of diarylamine antioxidants, and along the way lead to an efficient, modular synthetic procedure for preparing substituted diarylamines and the discovery of a superior palladium precursor (**2.65**) for C-N bond forming reactions used to prepare the compounds. New compounds and methods were developed and used (peroxyester **4.3**)¹⁹ to measure inhibition rate constants, Arrhenius parameters, kinetic solvent effects and deuterium kinetic isotope effects for reactions between diarylamines and peroxy radicals (Chapter 3), information used to infer that the mechanism of reaction between peroxy radicals and diarylamines as a proton-coupled electron transfer (PCET). Additionally, a new fluorescent dye (**5.8**) was developed and used in an assay to accurately quantify hydroperoxide concentrations in solution, and was demonstrated effective as the analytical component of high-temperature autoxidations of hexadecane.

However, many unanswered questions remain to be fully addressed.

Although we have shown that the stability of diarylamines towards one-electron oxidation increases systematically with nitrogen atom incorporation into the aryl rings under

ideal conditions (voltammetry at room temperature) – we do not yet fully understand the relative stabilities and mechanisms of decomposition at industrially relevant temperatures (>150 °C) and/or under non-ideal conditions (in the presence of hydroperoxides). Preliminary measurements have been done by us (Hanthorn *et al. J. Am. Chem. Soc.*, ASAP, DOI: 10.1021/ja300086z) that compare the relative decomposition rates of a series of dialkylamino-substituted diarylamines (**3.13**, **3.16** and **3.18**) incubated at 80 °C with one equivalent of *tert*-butyl hydroperoxide, shown below.⁴¹

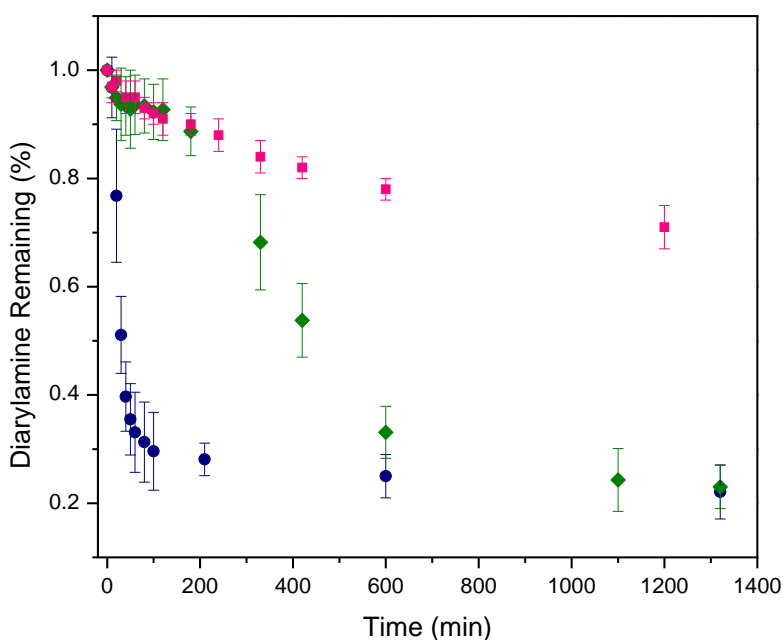


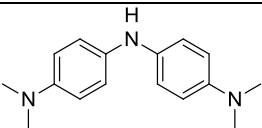
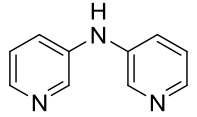
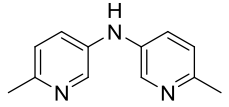
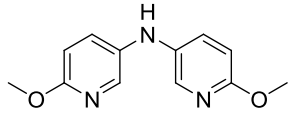
Figure 7.1. Diarylamine decomposition in the presence of a hydroperoxide. Data are presented for diarylamines **3.13** (●), **3.16** (◆) and **3.18** (■) (0.2 M) incubated at 80 °C with one equivalent of *tert*-butylhydroperoxide (0.2 M) in 1,2-dichlorobenzene using biphenyl as an internal standard and analyzed by gas chromatography.⁴¹

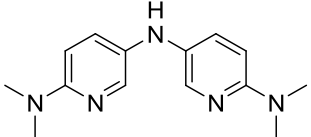
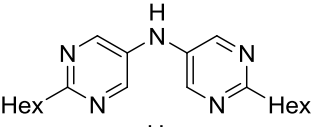
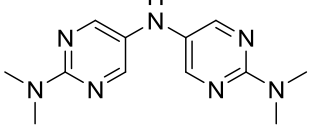
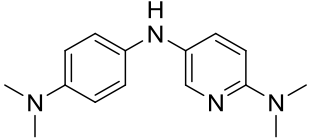
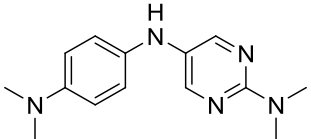
Although the trend is as expected – the compounds with more nitrogen atoms in the aryl rings decompose slower – the decay traces do not fit simple bimolecular kinetics and we do not yet know the decomposition products or their mechanisms of formation.

The oxidative degradation of these compounds might be expected to present itself as a problem via reduced stoichiometric factors in inhibited autoxidations since oxidation products (radical cations of the diarylamines) are unable to trap peroxy radicals and thus the *effective concentration* of amine is lower – resulting in a reduced inhibition period (the amine is consumed faster), which translates into a lower stoichiometric factor ($n = \tau \cdot R_i / [\text{Ar}_2\text{NH}]$).⁴²

In order to complement our kinetic data - which provides inhibition rate constants, but no stoichiometry for the reaction of diarylamines with peroxy radicals - our collaborators, Dr. Luca Valgimigli and Dr. Riccardo Amorati (University of Bologna), have measured inhibition rate constants and stoichiometric factors for a representative (i.e. those for which N-H BDEs were determined) set of diarylamines at 30 °C, summarized in the Table 7.1.

Table 7.1 Inhibition rate constants and stoichiometric factors obtained by inhibited autoxidation of styrene or cumene at 30 °C, shown with corresponding N-H BDEs.

Structure	Compound	k_H ($\text{M}^{-1}\text{s}^{-1}$)	n	N-H BDE (kcal/mol)
	3.13	$(1.5 \pm 0.5) \times 10^7$	2.0	78.4
	-	$(5.5 \pm 0.7) \times 10^3$	3.4	84.7 ± 0.4
	3.10	$(2.2 \pm 0.3) \times 10^4$	2.8	83.1 ± 0.4
	3.22	$(5.0 \pm 0.5) \times 10^5$	2.0	81.6 ± 0.5

	3.16	$(1.0 \pm 0.2) \times 10^7$	2.8	78.8 ± 0.8
	3.12	$(2.0 \pm 0.5) \times 10^4$	2.8	84.1 ± 0.5
	3.18	$(7.4 \pm 0.5) \times 10^6$	2.7	79.2 ± 0.5
	3.14	$(1.0 \pm 0.2) \times 10^7$	2.8	78.8 ± 0.3
	3.15	$(1.7 \pm 0.2) \times 10^7$	3.6	79.0 ± 0.5

The rate constants obtained by inhibited autoxidation of styrene (or cumene) are in good agreement with those obtained by peroxy clock methodology (generally within a factor of 2-3). A factor of 2-3 is a reasonable error given that the peroxy clock is calibrated in chlorobenzene using an inhibition rate constant for α -tocopherol that was extrapolated from previous work,¹⁹ and given that there is some judgement involved in the fitting of oxygen uptake traces. The plot of $\log k_H$ for the rate of peroxy radical trapping obtained by inhibited autoxidation vs. the N-H BDEs of the amines (Figure 7.2) gives an excellent linear correlation with a slope of -0.53 and an intercept of 51.2. This is in very good agreement with the data presented in Figure 3.9, which combines data for the diarylamines described in this thesis, measured by peroxy radical clock methodology, and inhibition rate constants measured for phenothiazines and phenoxazines to obtain a linear correlation with a slope of -0.49 and an intercept of 46.2. Thus the relationship between the inhibition rate constants for peroxy radical trapping ($\log k_H$) and N-HBDEs are the

same obtained by either method, but their different intercepts reflect the fact that the rate constants obtained by inhibited autoxidation are consistently 2-3fold lower than those obtained via peroxy radical clock methods.

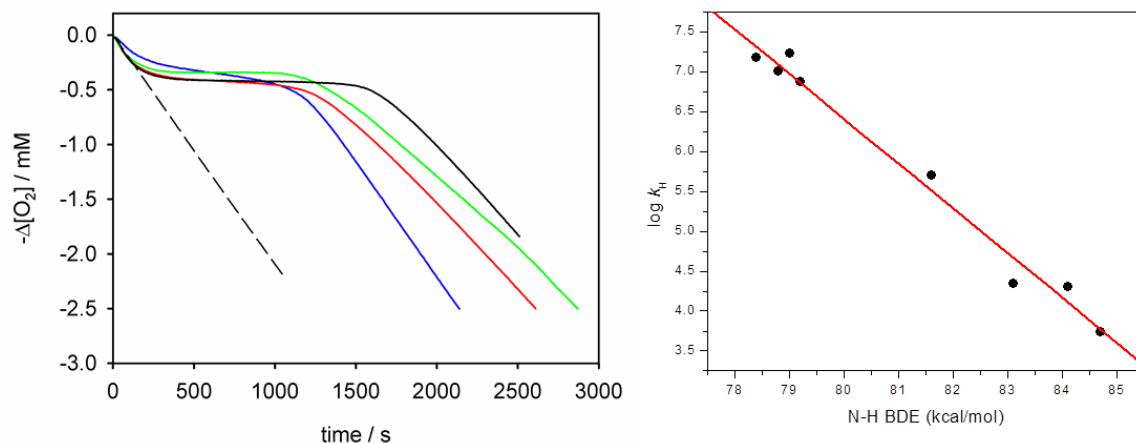
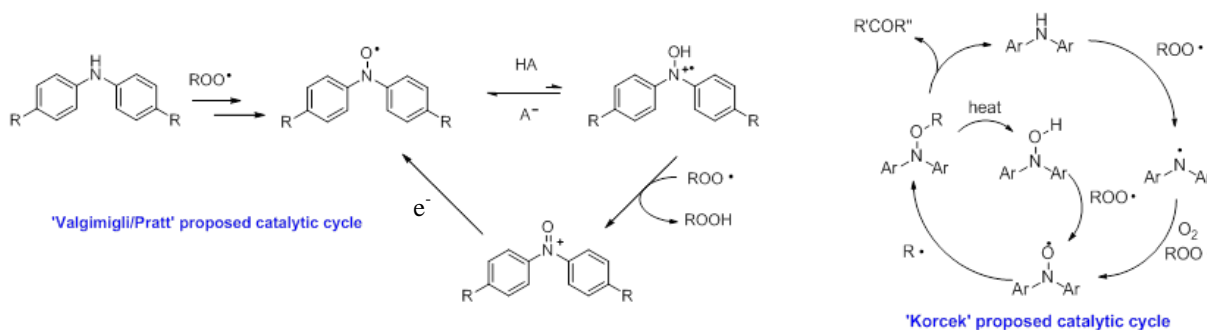


Figure 7.2. (Left) Oxygen consumption during the oxidation of styrene (6.5 M) in chlorobenzene initiated by AIBN (25 mM) at 30°C without inhibitors (dashed line) or in the presence of pentamethylchromanol (PMC, 1.9 μM blue); **3.18** (1.4 μM, red); **3.16** (1.9 μM, black); **3.14** (1.3 μM, green). (Right) Plot of $\log k_H$ obtained by inhibited autoxidation vs. N-H BDEs. Correlation gives: $\log k_H = -0.53(\text{N-H BDE}) + 51.2$ ($r^2 = 0.98$).

From this preliminary data it is apparent that there is no clear trend in the correlation between diarylamine structure and stoichiometric factor. Since the stoichiometric factors for these compounds should be related to their relative stabilities in solution (compounds that oxidize rapidly should have lower stoichiometric factors) the question of ‘stability’ arises once again. Comparing the data presented in Figure 7.1 and in Table 7.1, it seems as though there is a discrepancy between the rate of decomposition of **3.13** observed at 80 °C and the stoichiometric factor obtained at 30 °C. Since diarylamines are generally used at higher temperatures, this discrepancy should be studied in greater detail, by performing inhibited autoxidations at elevated

temperatures (e.g. hexadecane at 160 °C)³³ to obtain proper stoichiometric factors, which are expected to be larger than those observed at 30 °C.

Furthermore, it remains unclear exactly why the stoichiometric factors of amines are higher than $n = 2$ at elevated temperatures. Korcek *et al.*³² have developed a mechanism based on years of high-temperature inhibited autoxidation data that centres on the recycling of a nitroxide intermediate (observed experimentally) as shown in Scheme 7.2. The nitroxide will react with an alkyl radical at or near the diffusion controlled rate to form an alkoxyamine that is thermally cleaved either at the N-O bond or the O-R bond to yield the starting amine or a hydroxylamine respectively, thus continuing the catalytic cycle.

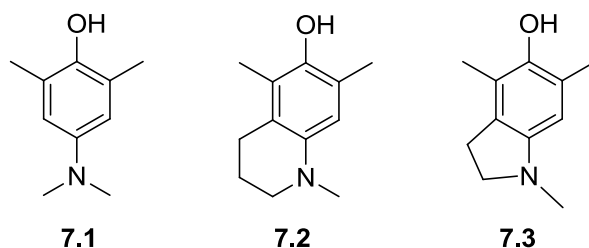


Scheme 7.2. Proposed mechanisms by Valgimigli *et al.*³⁴ and Korcek *et al.*³² to explain the catalytic reactivity (i.e. large stoichiometric factors) observed for diarylamines reacting at high temperatures with peroxy radicals.

Recently a new mechanism was put forth by Valgimigli *et al.*³⁴ (Figure 7.2) suggesting that catalytic activity is achieved by protonation of the nitroxide intermediate, followed by rapid H-atom abstraction by a peroxy radical to give an oxoammonium species that is then reduced back to the nitroxide, thus completing the cycle.

Combining the library of very stable, electronically diverse, fully characterized diarylamine antioxidants described in this thesis with a well-defined fluorescence-based assay as the analytical component of high-temperature inhibited autoxidations of hexadecane should greatly aid in the design of future experiments aimed at distinguishing the mechanism responsible for catalytic activity in diarylamine antioxidants.

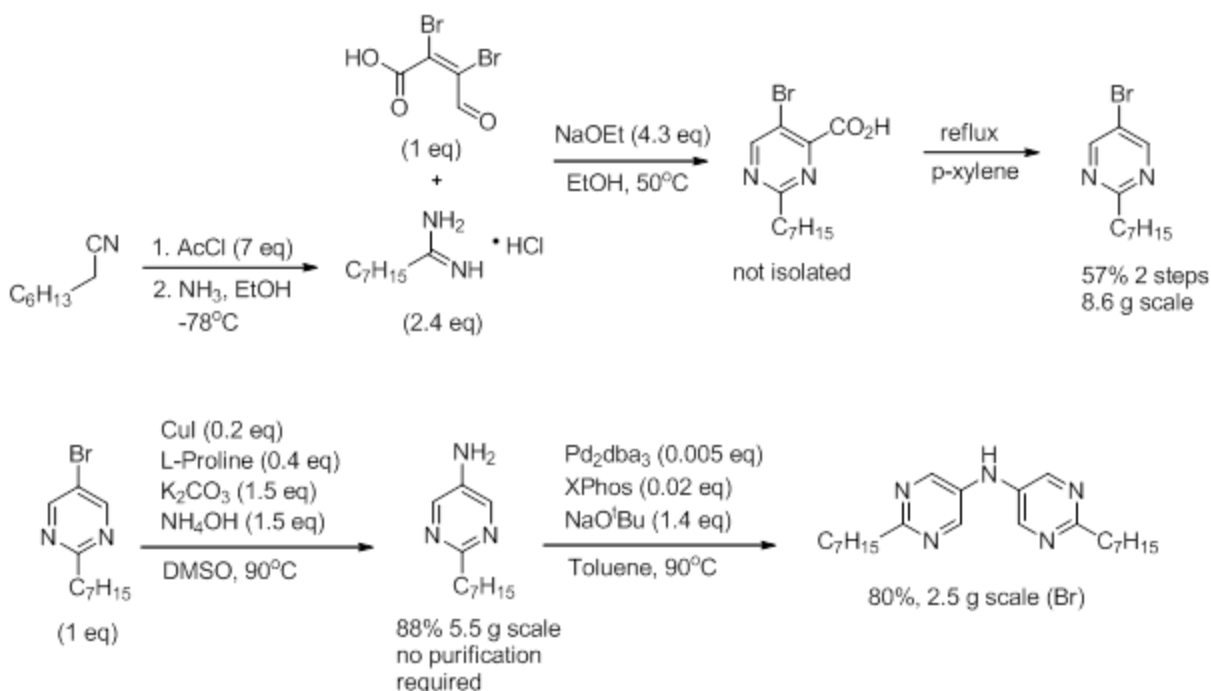
In addition to sorting out the relative rates and mechanisms of decomposition within a series of diarylamines, one of the more fundamental questions that remains unsolved is why the oxidative stability of phenolic antioxidants is considerably lower than what is observed for the diarylamines, even though diarylamines typically have much lower redox potentials than phenols. For instance, in earlier work, the half-lives of pyridinols **7.1**, **7.2** and **7.3** were determined to be >24 h, 30 h and 14 h at 37°C at 0.3 mM in *tert*-butylbenzene⁴³ – indicating that these compounds are substantially more prone to oxidative degradation in solution.



However, the standard potentials of **7.1** and **7.2** are $E^\circ = 0.47$ V and 0.38 V, respectively, when measured under the same conditions on the same instrument in our laboratory. These can be compared to $E^\circ = 0.34$, 0.44 and 0.65 V for diarylamines **3.13**, **3.16** and **3.18**,⁴¹ respectively, whose decompositions at 80°C with 1 equivalent of *tert*-butyl hydroperoxide are shown above in Figure 7.1, and yield approximate half-lives of 30 min, 7 h and 41 h respectively – under *much* harsher conditions. In fact, no significant oxidative degradation of these compounds took place

under the same conditions as the pyridinols were subjected to (above). This enhanced oxidative stability may be attributed to the formation of nitroxides that serve to retard the rate of oxidative decomposition by scavenging the peroxy radicals that result from one-electron oxidation of the diarylamine via reaction with molecular oxygen (oxygen is reduced to superoxide which is protonated by the diarylamine radical cation (diphenylamine radical cation has $pK_a = 3.6$)⁴⁴ to yield a hydroperoxyl radical and a diarylaminy radical, Scheme 1.17). The mechanism of catalytic activity would have to be similar to the mechanism proposed by Valgimigli *et al.*³⁴ (Scheme 7.2), as the mechanism proposed by Korcek *et al.*³² cannot be applied at ambient temperatures. By scavenging the reactive oxygen species produced via the one-electron oxidation of diarylamines, the nitroxide intermediates serve to minimize the ‘damage’ caused by a single oxidation event in a reaction pathway not available to phenolic antioxidants.

The alkylated pyrimidine-based diarylamine **3.12** is a low-melting (103-104 °C) crystalline white solid that has excellent stability to one-electron oxidation ($E^\circ = 1.55$ V);⁴¹ meaning this compound does not readily oxidize in air or organic media and therefore does not colour at an appreciable rate (radical cations of diarylamines, like those derived from phenols, are generally very intensely coloured). The physical properties and oxidative stability of **3.12** make it very attractive for plastics applications where colouring of the plastic is undesired. To be able to test the performance of **3.12** in plastics under extrusion conditions, a cost effective, scalable method needed to be developed to prepare the compound in the quantities required for plastics additives. Thus the synthesis shown in Scheme 7.3 was developed, beginning from feedstock chemicals mucobromic acid and any alkanenitrile to prepare the diarylamine on a multi-gram scale.



Scheme 7.3. Synthetic route to prepare **3.12** cost-effectively on a multi-gram scale.

Although the synthesis of **3.12** inevitably relies on transition-metal catalysis to convert the 5-bromo-2-alkylpyrimidine to the corresponding diarylamine, the amination of the bromide is done using a very inexpensive copper catalyst and ammonia, while the final C-N coupling can be done with very low Pd-catalyst loadings and could very likely be achieved using copper catalysis. With a synthetic route in hand, the next step is to prepare very large quantities of **3.12** (or other alkyl derivatives) to begin testing its performance under extrusion conditions.

Finally, one of the last extensions of this work may be towards the synthesis of pyridine- and pyrimidine-containing phenothiazines and phenoxazines (Chapter 3). These compounds possess comparable reactivity to diarylamines with peroxy radicals (Figure 3.9) and have some of the weakest N-H BDEs known. The reactivity ‘ceiling’ for phenoxazines and phenothiazines

may be higher than it is for diarylamines reacting with peroxy radicals due to potentially larger $\log A$ values, owing to the fact that their locked, highly-planar structures do not require restriction of the rotation of the aryl rings in a PCET transition state, as is required for diarylamines.⁴¹ In addition to the potential for greater radical trapping efficacy, phenothiazines have inherently higher oxidation potentials (phenothiazine has $E^\circ = 0.82$ V vs. NHE and $k_H = 8.8 \times 10^6$ M⁻¹s⁻¹ in benzene at 50 °C)¹² than for diarylamines having similar inhibition rate constants.

Besides having larger $\log A$ values than diarylamines, phenothiazines/phenoxazines also have an additional electron-donating bridging heteroatom (oxygen or sulfur) that facilitates faster PCET reactions with peroxy radicals (inhibition rate constants as large as $k_H = 5.0 \times 10^7$ M⁻¹s⁻¹ have been measured by inhibited autoxidation for substituted phenothiazines); yet the inclusion of the bridging heteroatom does not seem to decrease the ionization potentials of the compounds as much as one might expect. Therefore, preparation of pyridine- and pyrimidine-containing phenothiazines/phenoxazines may provide access to substituted derivatives possessing near-diffusion rate constants for trapping peroxy radicals but yet maintain air stability, and may provide important information about structure/activity relationships with respect to the ionization potentials of these compounds.

7.3 References

- (1) Ingold, K. U. *Chemical Reviews* **1961**, *61*, 563.
- (2) Klemchuk, P. P. In *Ullmann's Encyclopedia of Industrial Chemistry*; Wiley-VCH Verlag GmbH & Co. KGaA: 2000.

- (3) Pratt, D. A.; DiLabio, G. A.; Valgimigli, L.; Pedulli, G. F.; Ingold, K. U. *Journal of the American Chemical Society* **2002**, *124*, 11085.
- (4) Mulder, P.; Korth, H. G.; Pratt, D. A.; DiLabio, G. A.; Valgimigli, L.; Pedulli, G. F.; Ingold, K. U. *Journal of Physical Chemistry A* **2005**, *109*, 2647.
- (5) Brownlie, I. T.; Ingold, K. *Canadian Journal of Chemistry* **1966**, *44*, 861.
- (6) Howard, J. A.; Ingold, K. U. *Canadian Journal of Chemistry-Revue Canadienne De Chimie* **1963**, *41*, 1744.
- (7) Lucarini, M.; Pedrielli, P.; Pedulli, G. F.; Cabiddu, S.; Fattuoni, C. *Journal of Organic Chemistry* **1996**, *61*, 9259.
- (8) Burton, G. W.; Ingold, K. U. *Accounts of Chemical Research* **1986**, *19*, 194.
- (9) Pratt, D. A.; DiLabio, G. A.; Brigati, G.; Pedulli, G. F.; Valgimigli, L. *Journal of the American Chemical Society* **2001**, *123*, 4625.
- (10) Wijtman, M.; Pratt, D. A.; Valgimigli, L.; DiLabio, G. A.; Pedulli, G. F.; Porter, N. A. *Angewandte Chemie-International Edition* **2003**, *42*, 4370.
- (11) Nam, T.-g.; Rector, C. L.; Kim, H.-y.; Sonnen, A. F. P.; Meyer, R.; Nau, W. M.; Atkinson, J.; Rintoul, J.; Pratt, D. A.; Porter, N. A. *Journal of the American Chemical Society* **2007**, *129*, 10211.
- (12) Lucarini, M.; Pedrielli, P.; Pedulli, G. F.; Valgimigli, L.; Giggles, D.; Tordo, P. *Journal of the American Chemical Society* **1999**, *121*, 11546.
- (13) Nara, S. J.; Jha, M.; Brinkhorst, J.; Zemanek, T. J.; Pratt, D. A. *Journal of Organic Chemistry* **2008**, *73*, 9326.
- (14) Kim, J.; Chang, S. *Chemical Communications* **2008**, 3052.

- (15) Anderson, K. W.; Tundel, R. E.; Ikawa, T.; Altman, R. A.; Buchwald, S. L. *Angewandte Chemie-International Edition* **2006**, *45*, 6523.
- (16) Murrall, N. W.; Welch, A. J. *Journal of Organometallic Chemistry* **1986**, *301*, 109.
- (17) Norton, D. M.; Mitchell, E. A.; Botros, N. R.; Jessop, P. G.; Baird, M. C. *Journal of Organic Chemistry* **2009**, *74*, 6674.
- (18) Jha, M.; Pratt, D. A. *Chemical Communications* **2008**, 1252.
- (19) Hanthorn, J.; Pratt, D. A. *Journal of Organic Chemistry* **2012**, *77*, 276.
- (20) Ellam, R. M.; Padbury, J. M. *Journal of the Chemical Society-Chemical Communications* **1972**, 1086.
- (21) Benson, S. W. *Thermochemical Kinetics 2nd Edition*; John Wiley & Sons: New York, 1976.
- (22) Valgimigli, L.; Banks, J. T.; Luszyk, J.; Ingold, K. U. *Journal of Organic Chemistry* **1999**, *64*, 3381.
- (23) Nelsen, S. F.; Bartlett, P. D. *Journal of the American Chemical Society* **1966**, *88*, 137.
- (24) Boate, D. R.; Scaiano, J. C. *Tetrahedron Letters* **1989**, *30*, 4633.
- (25) Zhang, Y.; Yousef, Y. A.; Li, H.; Melo, T. B.; Naqvi, K. R. *Journal of Physical Chemistry A* **2011**, *115*, 8242.
- (26) Abraham, M. H.; Grellier, P. L.; Prior, D. V.; Duce, P. P.; Morris, J. J.; Taylor, P. J. *Journal of the Chemical Society-Perkin Transactions 2* **1989**, 699.
- (27) Litwinienko, G.; Ingold, K. U. *Accounts of Chemical Research* **2007**, *40*, 222.

- (28) DiLabio, G. A.; Johnson, E. R. *Journal of the American Chemical Society* **2007**, *129*, 6199.
- (29) Valgimigli, L.; Amorati, R.; Petrucci, S.; Pedulli, G. F.; Hu, D.; Hanthorn, J. J.; Pratt, D. A. *Angewandte Chemie-International Edition* **2009**, *48*, 8348.
- (30) Lias, S. G.
- (31) Leardini, R.; Lucarini, P.; Pedulli, G. F.; Valgimigli, L. *Journal of Organic Chemistry* **1999**, *64*, 3726.
- (32) Jensen, R. K.; Korcek, S.; Zinbo, M.; Gerlock, J. L. *Journal of Organic Chemistry* **1995**, *60*, 5396.
- (33) Jensen, R. K.; Korcek, S.; Mahoney, L. R.; Zinbo, M. *Journal of the American Chemical Society* **1979**, *101*, 7574.
- (34) Amorati, R.; Pedulli, G. F.; Pratt, D. A.; Valgimigli, L. *Chemical Communications* **2010**, *46*, 5139.
- (35) Jessup, W.; Dean, R. T.; Gebicki, J. M. *Oxygen Radicals in Biological Systems, Pt C* **1994**, *233*, 289.
- (36) Onoda, M.; Uchiyama, S.; Endo, A.; Tokuyama, H.; Santa, T.; Imal, K. *Organic Letters* **2003**, *5*, 1459.
- (37) Schaferling, M.; Grogel, D. B. M.; Schreml, S. *Microchimica Acta* **2011**, *174*, 1.
- (38) Soh, N.; Sakawaki, O.; Makihara, K.; Odo, Y.; Fukaminato, T.; Kawai, T.; Irie, M.; Imato, T. *Bioorganic & Medicinal Chemistry* **2005**, *13*, 1131.
- (39) Soh, N.; Ariyoshi, T.; Fukaminato, T.; Nakajima, H.; Nakano, K.; Imato, T. *Organic & Biomolecular Chemistry* **2007**, *5*, 3762.

- (40) Korade, Z.; Xu, L. B.; Shelton, R.; Porter, N. A. *Journal of Lipid Research* **2010**, *51*, 3259.
- (41) Hanthorn, J. J.; Valgimigli, L.; Pratt, D. A. *Journal of the American Chemical Society* **2012**, *Articles ASAP*.
- (42) Valgimigli, L.; Pratt, D. In *Encyclopedia of Radicals in Chemistry, Biology and Materials*; Chatgillialogu, C., Studer, A., Eds.; Wiley: 2011.
- (43) Wijtmans, M.; Pratt, D. A.; Brinkhorst, J.; Serwa, R.; Valgimigli, L.; Pedulli, G. F.; Porter, N. A. *Journal of Organic Chemistry* **2004**, *69*, 9215.
- (44) Jonsson, M.; Wayner, D. D. M.; Lusztyk, J. *Journal of Physical Chemistry* **1996**, *100*, 17539.